# University of Southampton

Faculty of Engineering and Physical Sciences

School of Engineering

**Energy Management and Sizing of a Dual Energy Storage System for Electric Vehicles**

by

**Tao Zhu**

ORCID ID 0000-0002-2449-4338

Thesis for the degree of Doctor of Philosophy

June 2021

# University of Southampton

## Abstract

Faculty of Engineering and Physical Science

School of Engineering

Thesis for the degree of Doctor of Philosophy

Energy Management and Sizing of a Dual Energy Storage System for Electric Vehicles

by

Tao Zhu

Ambitions of emission reductions have been pushing increasing electrification of the automotive industry. Currently, battery powered electric vehicles (EVs) typically use a Li-ion battery-only energy storage system for propulsion. However, one single energy storage technology is not optimal for all demands of power density, energy density, lifetime and cost. In contrast, dual energy storage system (DESS) paring two energy storage components can decouple EV propulsion demands to each energy storage component.

This work focuses on the optimisation of DESS in EV applications with five inter-related questions: (1) How to model DESS operations with EV propulsion so that the performance metrics of DESS can be simulated. (2) How to control the DESS in real-time so that the DESS can support EV propulsion adaptively and optimally. (3) How to determine the size of DESS so that the DESS can be configured with best-case parameters in long-term usage. (4) What the most critical factor is in controlling and sizing the DESS and how to optimise the factor. (5) Whether the emerging Al-ion battery technologies can replace the conventional Li-ion batteries and supercapacitors in the DESS with better performances. Consequently, five research problems of DESS are divided in terms of modelling, energy management, sizing, battery degradation and Al-ion DESS, and seven performance metrics are adopted as power capability, energy capacity, mass, volume, initial cost, battery degradation and electricity consumption.

With the research problems and performances metrics, this work provides the following deliverables: (1) Hierarchical modelling approaches of EV with DESS. (2) Systematic design flow of the adaptive, optimal energy management strategy. (3) Joint energy management-sizing optimisation framework and general sizing guides. (4) Widely applicable benchmarks to optimise battery degradation. (5) Comparison of Al-ion batteries, Li-ion batteries and supercapacitors for the future development of DESS. By the investigations presented in this work, it is expected to offer optimisation methods and guides to enable the DESS to be robust, compact, economical and long-life in EV applications.

# Table of Contents

# Table of Tables

# Table of Figures

# Research Thesis: Declaration of Authorship

Print name: TAO ZHU

Title of thesis: Energy Management and Sizing of a Dual Energy Storage System for Electric Vehicles

I declare that this thesis and the work presented in it are my own and has been generated by me as the result of my own original research.

I confirm that:

1. This work was done wholly or mainly while in candidature for a research degree at this University;
2. Where any part of this thesis has previously been submitted for a degree or any other qualification at this University or any other institution, this has been clearly stated;
3. Where I have consulted the published work of others, this is always clearly attributed;
4. Where I have quoted from the work of others, the source is always given. With the exception of such quotations, this thesis is entirely my own work;
5. I have acknowledged all main sources of help;
6. Where the thesis is based on work done by myself jointly with others, I have made clear exactly what was done by others and what I have contributed myself;
7. Parts of this work have been published as:

[1] Zhu T, Wills RGA, Lot R. Modelling aluminium energy storage systems comprising ionic liquid and aqueous electrolyte cells: case studies in high-performance electric vehicles. Journal of Energy Storage. 2021;40:102777.

[2] Zhu T, Wills RGA, Lot R, Ruan H, Jiang Z. Adaptive energy management of a battery-supercapacitor energy storage system for electric vehicles based on flexible perception and neural network fitting. Applied Energy. 2021;292:116932.

[3] Zhu T, Wills RGA, Lot R, Kong X, Yan X. Optimal sizing and sensitivity analysis of a battery-supercapacitor energy storage system for electric vehicles. Energy. 2021;221:119851.

[4] Zhu T, Lot R, Wills RGA, Yan X. Sizing a battery-supercapacitor energy storage system with battery degradation consideration for high-performance electric vehicles. Energy. 2020;208:118336.

[5] Zhu T, Lot R, Wills RGA. Optimization of dual energy storage system for high-performance electric vehicles. 2018 IEEE Vehicle Power and Propulsion Conference (VPPC): IEEE; 2018.

Signature: .....Date:.....

# Acknowledgements

First and foremost, I am extremely grateful to my supervisors, Dr Richard Wills and Prof. Roberto Lot, for their continuous support and patience at every stage of my PhD study and the invaluable inputs and feedback on my thesis and paper drafts. I would like to offer my special thanks to Dr Richard Wills for his tremendous supports on the experimental and great inspirations to the thesis and chapter 8 in particular. I would like to express my sincere thanks to Prof. Roberto Lot for his insightful instructions on initialising my PhD project and encouraging my international conference attendance. Immense respect and gratitude to my supervisors for their plentiful knowledge and kind help, which have made my study and life in the UK a wonderful time. I would also like to thank Prof. Andrew Cruden and Prof. Suleiman Sharkh for their thoughtful suggestions for my study.

I would like to express my great gratitude to the China Scholarship Council for the scholarship and subsidy throughout my PhD study. My gratitude extends to the Faculty of Engineering and Physical Sciences, University of Southampton, for the studentship provided. Without their financial supports, it would be impossible for me to complete my PhD study.

I want to thank my officemates and housemates, especially Peng Jiang, who has kept me involved in a great variety of activities outside of my core study and always helps without any hesitation. To every friend I met in the UK, I wish you all the success in your future adventure. Thanks also to the city and the University of Southampton, who have left precious memories in my life.

To my parents, thank you for your unwavering belief in me and being my source of strength, and I am always proud to be your son. I am immensely thankful to every member of the Zhu family for your every effort to help my parents get through the tough times. Xiexie.

# Abbreviations

AC – Alternative Current

ADVISOR – ADvanced VehIcle SimulatOR

AEAIB – Aqueous Electrolyte Aluminium-ion Battery

AIB – Aluminium-ion Battery

Al-ion – Aluminium-ion

DC – Direct Current

DESS – Dual Energy Storage System

DIRECT – DIviding RECTangle (algorithm)

DPR – Drive Pattern Recognition

DOD – Depth-of-Discharge

DP – Dynamic Programming

EM – Energy Management

EMS – Energy Management Strategy

EOL – End-of-Life

EPA – (US) Environmental Protection Agency

ES – Energy Storage

ESS – Energy Storage System

EV – Electric Vehicle

GA – Genetic Algorithm

HPPC – Hybrid Power Pulse Characterisation

HWFET – High Way Fuel Economy Test (drive cycle)

ICE – Internal Combustion Engine

ILAIB – Ionic Liquid Aluminium-ion Battery

Li-ion – Lithium-ion

LIB – Lithium-ion Battery

LP – Linear Programming

MOP – Multi-objective Optimisation

MPC – Model Predictive Control

NN – Neural Network

NSGA – Non-dominated Sorting Genetic Algorithm

NVH – Noise, Vibration and Harshness

OCV – Open-Circuit Voltage

OP – Optimisation Problem

PEF – Power-Energy Function

PMP – Pontryagin's Minimum Principle

PNGV – Partnership for a New Generation of Vehicles

RBS – Regenerative Braking System

RC – Resistance-Capacitor

Rint – Resistance Internal (battery model)

RMSE : Root-mean-square Error

SAE – (US) Society of Automotive Engineers

SC – Supercapacitor

SOA – State-of-Aging

SOC – State-of-Charge

SOE – State-of-Energy

TBS – Thermal Management System

UDDS – Urban Dynamometer Driving Schedule (drive cycle)

# Nomenclature

$A_{veh}$ : Front area of vehicle ($m^2$)

$Ah_{BAT}$ : Nominal capacity of battery (Ah)

$Ah_{put}$ : Ampere-hour throughput (Ah)

$C_D$ : Air drag coefficient

$C_{SC}$ : Nominal capacitance of supercapacitor (F)

$Cycle_{life}$ : Cycle life (cycles)

$E_{BAT}$ : Energy capacity of battery (J)

$E_{BAT,max}$ : Maximum feasible energy capacity of battery (J)

$E_{BAT,min}$ : Minimum feasible energy capacity of battery (J)

$E_{EV}$ : Energy demand of electric vehicle over driving range (J)

$E_{loss}$ : Energy capacity loss of battery (J)

$E_{main}$ : Energy capacity of main energy storage (J)

$E_{main,max}$ : Maximum feasible energy capacity of main energy storage (J)

$E_{main,min}$ : Minimum feasible energy capacity of main energy storage (J)

$E_{SC}$ : Energy capability of supercapacitor (J)

$E_{SC,max}$ : Maximum feasible energy capacity of supercapacitor (J)

$E_{SC,min}$ : Minimum feasible energy capacity of supercapacitor (J)

$E_{second}$ : Energy capacity of second energy storage (J)

$E_{second,max}$ : Maximum feasible energy capacity of second energy storage (J)

$E_{second,min}$ : Minimum feasible energy capacity of second energy storage (J)

$f$ : Rolling resistance coefficient

$F_a$ : Acceleration force of vehicle (N)

$F_d$ : Aerodynamic drag force of vehicle (N)

$F_r$ : Rolling resistance force of vehicle (N)

$F_T$ : Tractive force of vehicle (N)

$g$ : Gravity coefficient (N/kg)

$i$ : Counter

$I$ : Current of battery or supercapacitor (A)

$I_{BAT}$ : Current of battery (A)

$I_{rate}$ : Current rate of battery (C)

$I_{SC}$ : Current of supercapacitor (A)

$j$ : Counter

$J_{all}$ : Overall financial costs of dual energy storage system (USD)

$J_{BAT}$ : Battery degradation costs of dual energy storage system (USD)

$J_{compo}$ : Component costs of dual energy storage system (USD)

$J_{DCDC}$ : Purchase cost of DC/DC converter (USD)

$J_{Degrad}$ : Energy storage degradation costs of dual energy storage system (USD)

$J_{Degrad,main}$ : Degradation costs of main energy storage (USD)

$J_{Degrad,second}$ : Degradation costs of second energy storage (USD)

$J_{Elec}$ : Electricity consumption costs of dual energy storage system (USD)

$J_{fixed}$ : Fixed costs of dual energy storage system (USD)

$J_{initial}$ : Initial cost of dual energy storage system (USD)

$J_{long}$ : Long-term costs of dual energy storage system (USD)

$J_{main}$ : Initial cost of main energy storage (USD)

$J_{SC}$ : Purchase cost of supercapacitor (USD)

$J_{second}$ : Initial cost of second energy storage (USD)

$k$ : Execution stage number in dynamic programming

$l_1$ : Slope of Region I in curve fitting

$l_2$ : Slope of Region II in curve fitting

$l_3$ : Slope of Region III in curve fitting

$M_{BAT}$ : Mass of battery (kg)

$M_{DCDC}$ : Mass of DC/DC converter (kg)

$M_{DESS}$ : Mass of dual energy storage system (kg)

$M_{main}$ : Mass of main energy storage (kg)

$M_{SC}$ : Mass of supercapacitor (kg)

$M_{second}$ : Mass of second energy storage (kg)

$M_{veh}$ : Mass of vehicle (kg)

$N$ : Times of battery replacements

$P_{BAT}$ : Power of battery (W)

$P_{BAT,max}$ : Maximum power of battery (W)

$\bar{P}_{BAT}$ : Mean power of battery (kW)

$P_{bus}$ : Power of power bus (W)

$\bar{P}_{bus}$ : Mean power of power bus (W)

$P_{DCDC}$ : Power of DC/DC converter (W)

$P_{DCDC,max}$ : Maximum power of DC/DC converter (W)

$P_{EV}$ : Power demand of electric vehicle (W)

$P^{I}_{EV}$ : Power demand of electric vehicle in Region I (W)

$P^{III}_{EV}$ : Power demand of electric vehicle in Region III (W)

$P_{EV,bound}$ : Boundary for battery-supercapacitor power splitting (W)

$P_{EV,max}$: Maximum power demand of electric vehicle (W)

$P^{+}_{EV,mean}$ : Mean positive power demand of electric vehicle (W)

$P^{-}_{EV,mean}$ : Mean negative power demand of electric vehicle (W)

$P^{I}_{EV,mean}$ : Mean power demand of electric vehicle in Region I (W)

$P^{III}_{EV,mean}$ : Mean power demand of electric vehicle in Region III (W)

$P^{+}_{EV,std}$ : Standard derivation of positive power demand of electric vehicle

$P_{main}$ : Power of main energy storage (W)

$P_{main,max}$ : Maximum power of main energy storage (W)

$P_{SC}$ : Power of supercapacitor (W)

$P_{SC,max}$ : Maximum power of supercapacitor (W)

$P^{I}_{SC}$ : Power of supercapacitor in Region I (W)

$P^{II}_{SC}$ : Power of supercapacitor in Region II (W)

$P^{III}_{SC}$ : Power of supercapacitor in Region III (W)

$P_{second}$ : Power of second energy storage (W)

$P_{second,max}$ : Maximum power of second energy storage (W)

$Price_{BAT}$ : Price of battery (USD/kWh)

$Price_{DCDC}$ : Price of DC/DC converter (USD/kWh)

$Price_{Elec}$ : Price of electricity (USD/kWh)

$Price_{main}$ : Price of main energy storage (USD/kWh)

$Price_{SC}$ : Price of supercapacitor (USD/kWh)

$Price_{second}$ : Price of second energy storage (USD/kWh)

$O$ : Objective function

$Q_{BAT}$ : Electricity consumption of battery (J)

$Q_{DESS}$ : Electricity consumption of dual energy storage system (J)

$Q_{main}$ : Electricity consumption of main energy storage (J)

$Q_{SC}$ : Electricity consumption of supercapacitor (J)

$Q^{+}_{SC}$ : Positive electricity consumption of supercapacitor (J)

$Q^{-}_{SC}$ : Negative electricity consumption of supercapacitor (J)

$Q_{second}$ : Electricity consumption of second energy storage (J)

$R_{BAT}$ : Equivalent internal resistance of battery (Ohm)

$R_{SC}$ : Equivalent internal resistance of supercapacitor (Ohm)

$R^2$ : Coefficient of determination in curve fitting

$Range_{EVcycle}$ : Driving range of electric vehicle over one drive cycle (km)

$Range_{EVlife}$ : Driving range of electric vehicle over vehicle lifetime (km)

*RMSE* : Root-mean-square error

*SOC* : State-of-charge of battery or supercapacitor (%)

$SOC_{BAT}$ : State-of-charge of battery (%)

$SOC_{BAT,0}$ : Initial state-of-charge of battery (%)

$SOC_{main}$ : State-of-charge of main energy storage (%)

$SOC_{SC}$ : State-of-charge of supercapacitor (%)

$SOC_{second}$ : State-of-charge of second energy storage (%)

$SOC_{second,min}$ : Minimum allowable state-of-charge of second energy storage (%)

*SOE* : State-of-energy of supercapacitor (%)

$SOE_{high}$ : High threshold of state-of-energy of supercapacitor (%)

$SOE_{low}$ : Low threshold of state-of-energy of supercapacitor (%)

$SOE_{min}$ : Minimum allowable state-of-energy of supercapacitor (%)

$SOE_{second}$ : State-of-energy of second energy storage (%)

$SOE_{second,min}$ : Minimum allowable state-of-energy of second energy storage (%)

*t* : Time (s)

$t_{end}$ : End time of drive cycle or micro-trip (s)

$t_{start}$ : Start time of drive cycle or micro-trip (s)

*T* : Temperature (K)

*u*: Decision variable in dynamic programming

$U_{BAT}$ : Voltage of battery (V)

$U_{BAT,nom}$ : Nominal voltage of battery (V)

$U_{oc,BAT}$ : Open circuit voltage of battery (V)

$U_{oc,SC}$ : Open circuit voltage of supercapacitor (V)

$U_{SC}$ : Voltage of supercapacitor (V)

$U_{SC,max}$ : Maximum voltage of supercapacitor (V)

$v$ : Velocity of vehicle (km/h)

$V_{BAT}$ : Volume of battery ($m^3$)

$V_{DCDC}$ : Volume of DC/DC converter ($m^3$)

$V_{DESS}$ : Volume of dual energy storage system ($m^3$)

$V_{main}$ : Volume of main energy storage ($m^3$)

$V_{SC}$ : Volume of supercapacitor ($m^3$)

$V_{second}$ : Volume of second energy storage ($m^3$)

$x$: State variable in dynamic programming

$z$: State transfer function in dynamic programming

$\alpha$ : Degradation coefficient of battery (%)

$\alpha_{main}$ : Degradation coefficient of main energy storage (%)

$\alpha_{second}$ : Degradation coefficient of second energy storage (%)

$\delta$: Correction coefficient of vehicle rotating mass

$\eta_{BAT}$ : Coulombic efficiency of battery (%)

$\eta_{DCDC}$ : Conversion efficiency of DC/DC converter (%)

$\rho_{BAT,E/M}$ : Energy to mass density of battery (J/kg)

$\rho_{BAT,E/V}$ : Energy to volume density of battery ($J/m^3$)

$\rho_{BAT,P/E}$ : Power to energy density of battery (W/J)

$\rho_{DCDC,P/C}$ : Power to cost density of DC/DC converter (W/USD)

$\rho_{DCDC,P/M}$ : Power to mass density of DC/DC converter (W/kg)

$\rho_{DCDC,P/V}$ : Power to volume density of DC/DC converter ($W/m^3$)

$\rho_{main,E/C}$ : Energy to cost density of main energy storage (J/USD)

$\rho_{main,E/M}$ : Energy to mass density of main energy storage (J/kg)

$\rho_{main,E/V}$ : Energy to volume density of main energy storage ($J/m^3$)

$\rho_{main,P/E}$ : Power to energy density of main energy storage (W/J)

$\rho_{SC,E/M}$ : Energy to mass density of supercapacitor (J/kg)

$\rho_{SC,E/V}$ : Energy to volume density of supercapacitor ($J/m^3$)

$\rho_{SC,P/E}$ : Power to energy density of supercapacitor (W/J)

$\rho_{second,E/C}$ : Energy to cost density of second energy storage (J/USD)

$\rho_{second,E/M}$ : Energy to mass density of second energy storage (J/kg)

$\rho_{second,E/V}$ : Energy to volume density of second energy storage ($J/m^3$)

$\rho_{second,P/E}$ : Power to energy density of second energy storage (W/J)

$\tau$ : Cost optimisation rate (%)

# Chapter 1 Introduction

## 1.1 Background and motivation

### 1.1.1 Electric vehicle and energy storage system

Reducing private and public transportation's environmental impact is pushing increasing electrification of vehicle drivetrains [1]. Electric vehicles (EVs), as clean transport agents powered by electricity, have been identified as critical for satisfying the long-term ambitions of emission reductions in the UK, which is still true at the international level [2]. The prosperity of EVs can be reflected by the historical and predicted global EV sales in Figure 1 [3], which demonstrates an increasingly fast growth. By the year 2040, EV sales are predicted to reach 400 million worldwide, representing more than one-third of new vehicle sales.

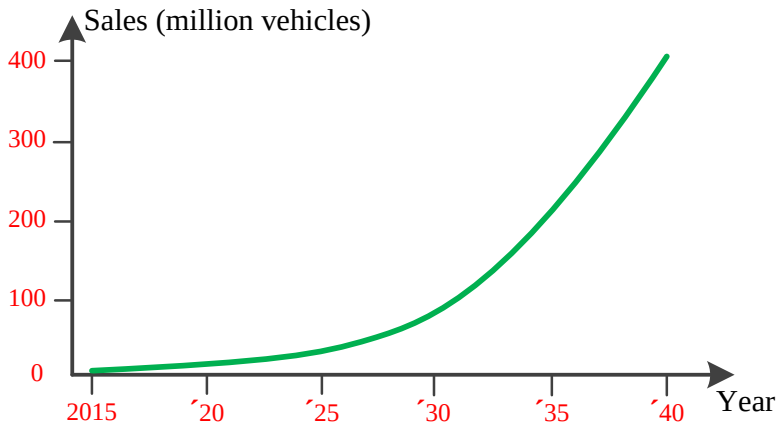


Figure 1 Historical (2015-2020) and predicted (2021-2040) global EV sales adapted from [3].

As the heart of an EV, the energy storage system (ESS) delivers the power and energy for EV propulsion and auxiliary systems and occupies more than one-quarter of total vehicle manufacturing costs [4]. The past few decades have witnessed various attempts on the choice of vehicle-mounted energy storage units, including electrochemical batteries, supercapacitors (SCs) and fuel cells, while batteries represent the most popular ones because they are the best compromise between power and energy density [5], as shown in Figure 2. Among different kinds of batteries, Li-ion batteries, thanks to their high energy density (>100 Wh/kg) and steady voltage output [6], are the most commonly used energy storage units in practical engineering. The battery-only ESS, which employs hundreds or thousands of Li-ion batteries into a battery pack with dozens of kWh capacity, is the most popular ESS practice for the time being [7]. However, the battery-only ESS is not quite a perfect power source and energy storage for EV propulsion due to the limitations summarised below:

(1) EV propulsion requires the onboard ESS to possess a high power capability (>100 kW) for rapid acceleration, as well as a sufficient energy capacity (dozens of kWh) for long-range driving [8].

However, battery-only ESS uses one single energy storage technology and can hardly be optimal for both power and energy without significantly increasing costs [9], which obliges EV designers to make a compromise between dynamic performance and driving range.

(2) EV driving usually involves periods of high-speed cruising producted by acceleration/deceleration periods, proposing bursts of power demand as 100 kW high in the seconds' timeframe over thousands of cycles [8]. However, batteries are not well suited to satisfy the short-term power pulses experienced over the EV lifetime. The bursts of power demand significantly accelerate battery degradation in an exponential manner, resulting in battery replacements and considerable financial costs during EV service term [10].

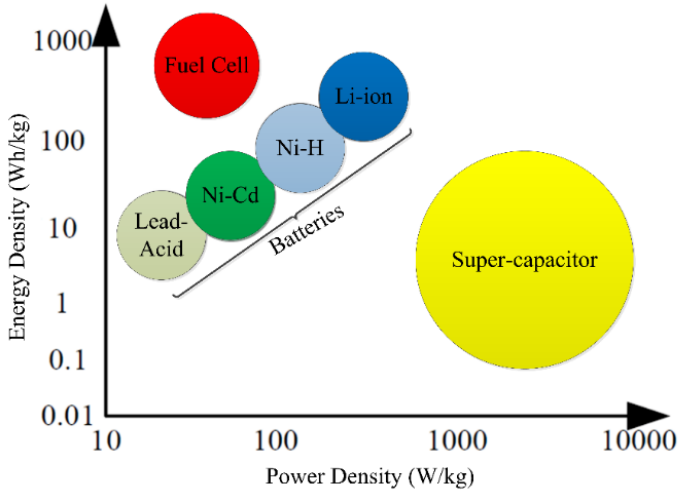


Figure 2 Power and energy density of different energy storage devices [5].

Targeted the limitations of battery-only ESS, researchers make tremendous efforts to develop novel batteries with hopes of improving battery performances. Published work [5] has reported the batteries of new chemistries and manufacturing techniques, with performance improvements in power/energy density, gravimetric/volumetric density, factory costs, energy efficiency or lifespan. However, these batteries always claim improvements of certain performances at the expense of sacrificing the other performances. For example, batteries with a long lifespan tend to be excessively expensive [7], and the power density and energy density are usually contradictory [11]. Overall, it would be difficult to see a breakthrough in battery performances in all aspects.

### 1.1.2 Dual energy storage system

Another solution to supplementing batteries' performance limitations is to deploy a second kind of energy storage with the batteries, forming a dual energy storage system (DESS) [3]. DESS refers to an ESS pairing two kinds of complementary energy storage units so that the advantages of each can compensate for the disadvantages of the other [3]; in combination, the benefits should outweigh the performances of either energy storage technology acting alone. Typically, the DESS comprises a main storage with high specific energy (usually batteries) and a second storage with high specific

power [3]. The main storage is mainly responsible for delivering energy for long-term driving, while the second storage is specifically used for peaking short-term bursts of power [3]. In this way, the energy and power demands of EV propulsion can be decoupled. Moreover, the second storage essentially unloads the high power transients from the batteries, lowering battery degradation and prolonging battery life [12].

The working principles of DESS are shown in Figure 3 [3]. When the EV calls for high-power propulsion (e.g., sharp acceleration or hill climbing), both kinds of energy storage will deliver power to the EV drivetrain (the load), as Figure 3 (a). In the case of low-power demands (e.g., low-speed cruise), only the main storage with high specific energy will feed the load, but in some cases, there is also a power flow from the main to the second storage, recovering the charge of the second storage, as Figure 3 (b). In the case of negative power demands (e.g., regenerative braking), the recovered power is expected to be absorbed all by the second storage, whereas one exception is when the second storage is almost full of charge, part of the recovered power will have to be accepted by the main storage, as Figure 3 (c). Normally, the DESS has no power flow from the second to the main energy storage, as seen in Figure 3. This is because the second storage usually has a very small energy capacity (e.g., the SC pack in a battery-SC DESS only has hundreds of Wh capacity [13]), which means that the second storage can be easily depleted under high power operations. Therefore, the second storage is expected to reserve its energy for peaking the power demands from the load rather than wasting its energy charging the main storage.

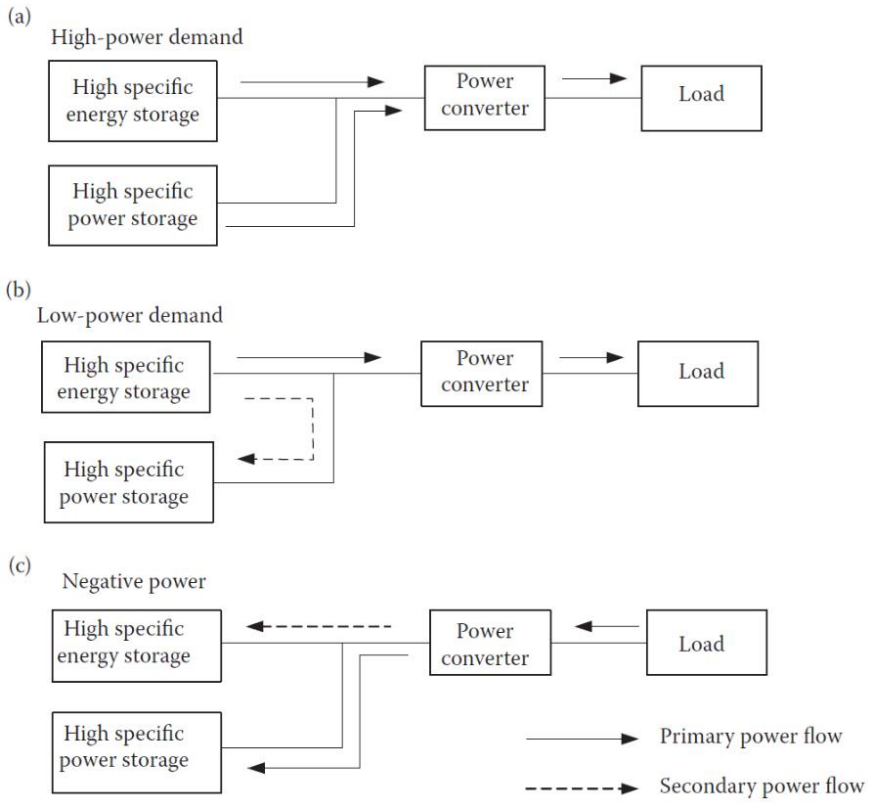


Figure 3 Working principles of DESS: (a) hybrid powering, (b) power split, (c) hybrid charging adapted from [3].

By pairing energy-intense batteries with power-intense SCs, the battery-SC DESS is the most popular in EV applications [14]. Compared with batteries, the reason for acceptance of SCs in an onboard DESS is their high-pulse power capability, fast and efficient discharge and re-charging, plus full-charge cycling over 500,000 cycles, a lifespan comparable to vehicle lifetime [10]. Figure 4 shows the typical deployment of battery-SC DESS fit with the EV drivetrain. Except for the battery pack and SC pack, the DESS also includes the DC/DC converter(s). Since the battery pack and SC pack have different voltage/power outputs, the DC/DC converter plays an important role in coordinating both packs [15]. The whole DESS is connected to the EV drivetrain via the power bus. It has been reported that the battery-SC DESS can reduce battery degradation rate by more than half compared to the battery-only ESS [16].

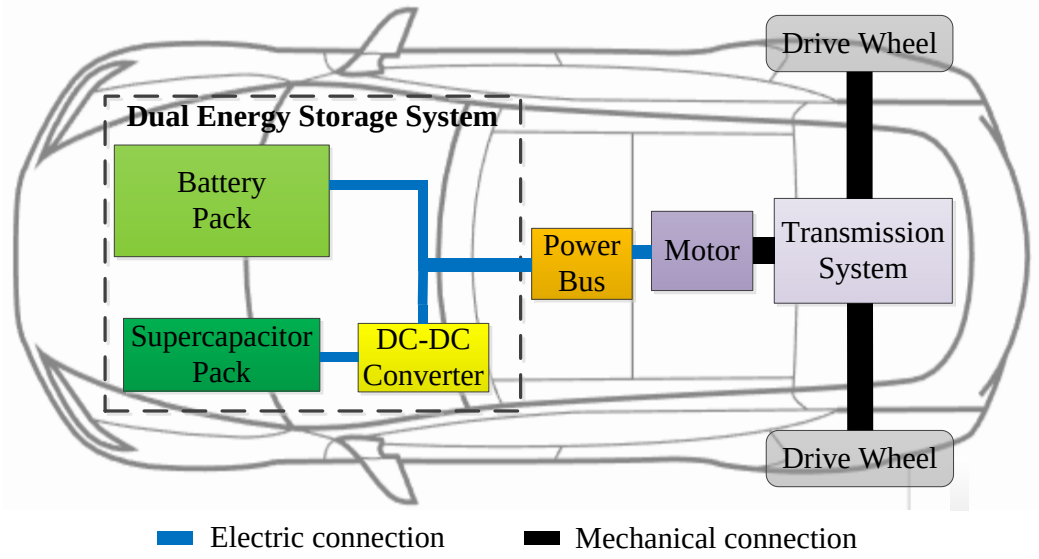


Figure 4 Deployment of the battery-SC DESS fit with the EV drivetrain.

## 1.2 Research problems and objectives

This work investigates the optimisation of DESS in EV applications with five divided research problems and seven independent objectives. Before introducing the problems and objectives, the hypotheses used in this work are described as follows.

- Concept definition: “EV” refers to the all-electric car with a serial drivetrain (no torque coupling). “DESS”, unless otherwise defined, refers to the battery-SC DESS with a Li-ion battery pack being the main energy storage, a SC pack being the second energy storage, and a DC/DC converter interfacing the SC pack.
- Given condition: EV parameters (i.e., design parameters and drivetrain parameters) and energy storage unit parameters (i.e., parameters of the battery cell and SC cell) are known.

### 1.2.1 Research problems

Five research problems of the DESS are investigated:

(1) Modelling of DESS. This research problem aims to model EV operation with DESS and then use this to investigate the research problems of energy management and sizing with simulated impacts on DESS performance metrics. This work develops an EV model composed of the DESS module and electric drivetrain module and adapts the ADvanced VehIcle SimulatOR (ADVISOR, a vehicle simulation platform within MATLAB/Simulink) to successfully run the EV model.

(2) Energy management (EM) of DESS. This research problem aims to split the power demands from the EV to the battery pack and SC pack so that the total power delivery of DESS can satisfy EV propulsion; meanwhile, the EM is expected to optimise the electricity consumption and battery degradation of DESS and maintain adaptiveness to unpredicted EV driving conditions. This work proposes an energy management strategy (EMS) that minimises the financial costs caused by both electricity consumption and battery degradation and can be adaptive to real-time EV driving conditions.

(3) Sizing of DESS. This research problem aims to determine the size of DESS components reflected by the metrics of power capability, energy capacity, mass, volume or initial cost so that the configured DESS and its EM can be the best match and, as such, optimally sustain EV propulsion. This work develops a joint EM-sizing optimisation framework to minimise the overall financial costs of DESS over EV lifetime and analyses how and why the DESS sizing is sensitive to different influence factors.

(4) Battery degradation with EM and sizing of DESS. This research problem is inspired by the conclusion from Chapter 6 that battery degradation causes more than 75% of DESS financial costs throughout EV lifetime, even if the battery price can be low as 100 USD/kWh. Therefore, this research problem aims at the deep optimisation of battery degradation through the efforts of both EM and sizing of the DESS. This work deduces and validates the best-case EM and sizing benchmarks for general cases to optimally reduce battery degradation.

(5) Aluminium DESS. This research problem is inspired by the fact that Al-ion batteries are being developed as emerging alternatives to the existing Li-ion battery and SC technologies, since Al-ion chemistries can be tailored for either high energy (e.g., ionic liquid cells) or high power (e.g., aqueous electrolyte cells) with low costs [17]. This research problem aims at modelling the performances of the DESS composed of Al-ion batteries and expanding the generic modelling methodology to DESSs using novel energy storage technologies. This work substitutes one of or both Li-ion batteries and SCs with Al-ion batteries and proposes three Aluminium DESSs compared to the conventional Li-ion battery-SC DESS.

The connections among the research problems are illustrated as follows. The development of DESS models is the bedrock of this work because the modelled, simulated DESS performances have significant implications for the EM and sizing investigations. EM and sizing are two highly coupled research problems. The EM is investigated under a fixed DESS size, and the investigation of sizing is performed with optimal offline EM. The research problem of battery degradation involves both EM and sizing efforts, and the research problem of Aluminium DESS reuses/adapts the methodology of modelling, EM and sizing.

### 1.2.2 Objectives

This work adopts seven performance metrics of DESS as the objectives assessing how well the research problems are solved:

(1) Power capability. The power capability of DESS should be competent to satisfy any transient power demands proposed by EV propulsion. This is a mandatory precondition for the DESS and is used as a constraint for any research problem. Specifically, the maximum power demand of EV is the touchstone for DESS power capability.

(2) Energy capacity. The energy capacity of DESS should be competent to satisfy the accumulated energy demands specified by the EV driving range. This is another mandatory precondition for the DESS and is also used as a constraint.

(3) Electricity consumption. The electricity consumption of DESS is expected to be as low as possible since it determines the electricity costs of EV operation. This is used as an optimisation problem embedded in the research problem of EM. The DESS electricity consumption is equivalent to DESS efficiency since an efficient DESS would generate fewer energy losses and lead to less electricity consumption.

(4) Battery degradation. The battery degradation of DESS is expected to be as low as possible since it determines the occurrence of battery replacement and leads to battery degradation costs. This is used as another optimisation problem embedded in the research problem of EM. Battery degradation is the most crucial objective in this work because it is proved (in Chapter 6) as the dominating cause of DESS financial costs.

(5) Mass. The mass of DESS is related to vehicle dynamics as a heavy DESS brings down vehicle acceleration capability and top speed, which matters much, especially for high-performance EVs. This is used as one optimisation problem embedded in the research problem of sizing.

(6) Volume. The volume of DESS influences the chassis layout as a bulky DESS restricts the flexibility to arrange vehicle components, which matters much, especially for light passenger EVs

because the room for the component arrangement is always insufficient. This is used as one optimisation problem embedded in the research problem of sizing.

(7) Initial cost. The initial cost of DESS is the one-off costs to purchase DESS components, which assesses the start-up costs of deploying a DESS. This is used as one optimisation problem embedded in the research problem of sizing.

## 1.3 Thesis structure, contributions and publications

The division of chapters is illustrated in the following. The contributions and publications attached to each chapter, if any, are also reported.

Chapter 1 introduces the research backgrounds and problems of the thesis.

Chapter 2 presents a literature review of energy storage and DESS and the sizing and EM approaches for the DESS in EV applications.

Chapter 3 illustrates the methodology of the following chapters.

Chapter 4 offers the modelling approaches developed for EVs deploying DESS along with adapting and matching the models. The modelling approaches have led to the following publication:

- *T. Zhu, R. Lot and R. Wills, "Optimization of Dual Energy Storage System for High-performance Electric Vehicles", in IEEE Vehicle Power and Propulsion Conference, 2018.*

Chapter 5 proposes an online real-time EMS that optimises the long-term operating costs of DESS and can be adaptive to real-time EV driving conditions. The contributions are that 1) the designed online EMS features reduced complexity, flexible perception and intelligent rulemaking compared with the existing studies, and 2) the online performance of the proposed EMS is comparable with the optimal offline benchmarks. The contributions have been identified as the following publication:

- *T. Zhu, R. Wills, R. Lot, H, Ruan and Z. Jiang. "Adaptive Energy Management of a Battery-Supercapacitor Energy Storage System for Electric Vehicles Based on Flexible Perception and Neural Network Fitting", Applied Energy, vol. 292, p. 116932, 2021.*

Chapter 6 provides an optimal sizing method with sensitivity analysis for the DESS to minimise financial costs over EV lifetime. The contributions are that 1) a joint EM-sizing framework is proposed to minimise the overall financial costs of DESS over EV lifetime, and 2) The influence of different factors on DESS sizing is analysed, and the relative importance of each factor is quantified. The contributions have been identified as the following publication:

- *T. Zhu, R. Wills, R. Lot, X. Kong and X. Yan, "Optimal Sizing and Sensitivity Analysis of a Battery-supercapacitor Energy Storage System for Electric Vehicles", Energy, vol. 221, p. 119851, 2021.*

Chapter 7 targets the deep optimisation of DESS battery degradation and presents the general EM and sizing benchmarks to best reduce battery degradation. The contributions are that 1) the benchmarks are independent of EM techniques or sizing formulations and as such can be general guides, and 2) the benchmarks apply to broad cases using different parameters of EV and DESS, rather than merely working for specific case studies. The contributions have been identified as the following publication:

- *T. Zhu, R. Lot, R. Wills and X. Yan, "Sizing a Battery-Supercapacitor Energy Storage System with Battery Degradation Consideration for High Performance Electric Vehicles", Energy, vol. 208, p. 118336, 2020.*

Chapter 8 proposes three novel DESSs comprising Aluminium batteries, simulating and comparing their performances with the conventional battery-SC DESS. The contributions are that 1) the ionic liquid Al-ion battery is found not a strong competitor of the Li-ion battery because of its inferior volumetric attributes, but the aqueous Al-ion battery can be a promising substitute of the SC, and 2) considering both financial costs and deployment feasibility, the DESS composed of Li-ion batteries and aqueous Al-ion batteries is the most viable hybrid combination of Li-ion, Al-ion, and SC technologies for future development. The contributions have been identified as the following publication:

- *T. Zhu, R. Wills and R. Lot, "Modelling Aluminium Energy Storage Systems Comprising Ionic Liquid and Aqueous Electrolyte Cells: Case Studies in High-performance Electric Vehicles", Journal of Energy Storage, vol. 40, p. 102777, 2021.*

Chapter 9 concludes the thesis and offers suggestions for configuring a DESS of EV in real-life engineering. Further improvements to the presented work are proposed in future work.

# Chapter 2 Literature review

Following the title of the thesis, as Figure 5, this chapter performs a literature review expanded from four keywords: electric vehicle (EV, Section 2.1), dual energy storage system (DESS, Section 2.2), energy management (EM, Section 2.3) and sizing (Section 2.4).

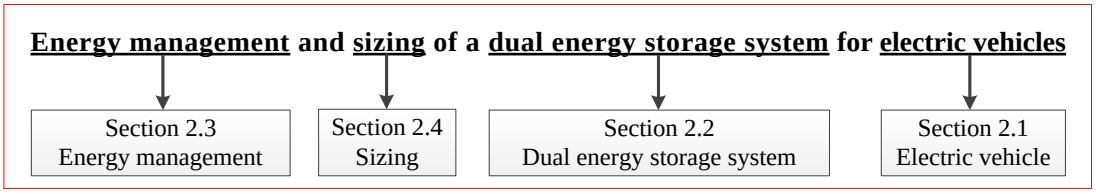


Figure 5 Structure of the chapter.

## 2.1 Electric vehicle

In this work, "EV" refers to the all-electric vehicle, in which the electric energy storage is the only power/energy source providing vehicle propulsion [18]. EVs came into existence in the mid 19th century but were soon replaced by the internal combustion engine (ICE) vehicles because, at that time, ICE technology noticeably surpassed the electric drive technology in terms of tractive force, convenience and sustainability [3]. With novel electric drive, storage and control technologies emerging, the past few decades saw a resurgence of EVs in research and development, and it is widely recognised that the EV market will witness prosperity in the coming few decades [19]. Recent research on EVs mainly follows two technical routes. One route focuses on making the EV "greener" by environmentally friendly electrification technologies, including electric energy storage, electric control strategy and electric motor [20]. The other route aims to make the EV "smarter" with interconnected networking and artificial intelligence assistance, and autonomous driving is a typical practice of the route [21].

### 2.1.1 Electric drivetrain

Compared with ICE vehicles, the most distinguishing feature of EVs is the electric drivetrain deployed instead of the mechanical drivetrain. Figure 6 shows the simplified electric drivetrain of a representative EV – Tesla Model S P85, a rear-wheel-drive, high-performance EV with a driving range of 426km and 0-100km/h acceleration time within 4.5 seconds [22]. Electric power from the battery pack goes into the synchronous motor via a DC/AC inverter. The synchronous motor completes the energy conversion from electric to kinetic and outputs torque and rotation to the transmission system [23]. Different from ICE vehicles, the transmission system in EVs is usually a single-speed gearbox without the clutch, while recent studies report that introducing a tailored clutch into the drivetrain can improve EV acceleration performances at high speeds [19]. Finally, the driven wheels take up the kinetic energy from the transmission and enable EV mobility.

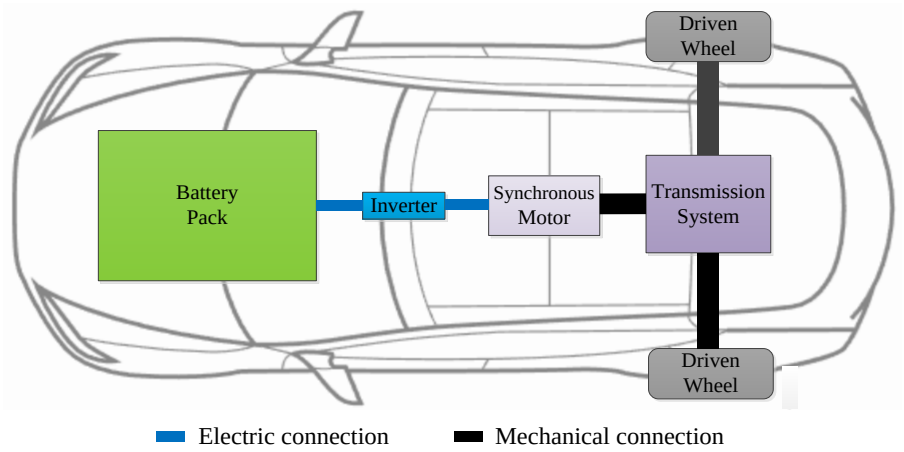


Figure 6 Electric drivetrain of Tesla Model S P85 adapted from [22].

From the drivetrain point of view, the most significant difference between EVs and ICE vehicles is that the power plant of an EV is a motor rather than an engine. For example, the Tesla Model S P85 adopts a synchronous motor, while in other cases, such as Tesla Model S P100D and Model X P100D, the induction motor is used [24]. The choice of synchronous or induction motor for EV mobility is still debated; however, the current consensus is moving towards the synchronous motor [24]. For either kind of motor, the attention of development has been paid to improving its peak power, torque and rotate speed, as well as higher efficiency and smaller size [25]. The motor map is a significant motor performance metric that exhibits motor efficiency as a function of rotation speed and torque [26]. Figure 7 shows the motor map of the Tesla Model S P85. It can be seen from Figure 7 that the peak rotate speed and torque are about 1600 rad/s and 600 Nm, respectively, and the motor gets its optimal efficiency at intermediate speeds and torques. Besides, the power density and torque density are also significant motor performance metrics, e.g., the motor used by Tesla Model S P85 has a power density of 3.9 kW/kg and a torque density of 7.5 Nm/kg, respectively [27].

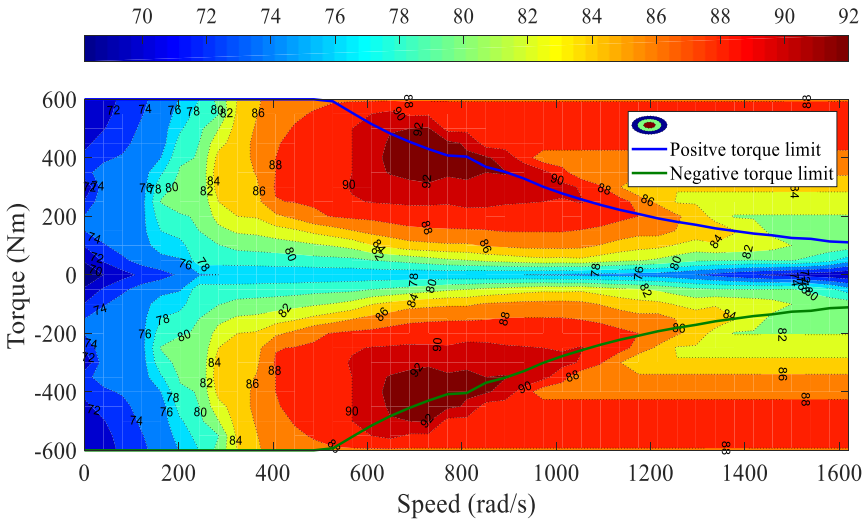


Figure 7 Motor MAP of Tesla Model S P85 adapted from [22].

### 2.1.2 Advantages and limitations

EVs are commonly considered a promising substitute for ICE vehicles, with the following advantages: (1) Environmentally friendly. The EVs themselves are almost zero-emission, despite the argument that EVs' electric power mostly comes from fossil fuels so that the emission is not eliminated but transferred from EVs to the power plants [28-30]. Also, there are growing concerns about battery manufacturing and recycling environmental impacts. (2) Better noise, vibration and harshness (NVH) performance. The electric motor works more smoothly than ICE, leading to fewer NVH issues [3]. (3) High efficiency. The electric drivetrain components – battery, supercapacitor (SC), motor and inverter – have an average efficiency of around 90% or even higher. In contrast, the engine typically has an efficiency between 25% and 50% [23]. (4) Regenerative braking. The EV usually has a regenerative braking system (RBS) that can transform the motor into a generator while EV brakes, absorbing EV kinetic energy and recharging the battery pack [31].

Despite those advantages, EVs cannot replace ICE vehicles overnight. The most crucial reason that limits the widespread of EVs is energy storage technology. Compared to the increasingly ambitious driving range of newly produced EVs, batteries' energy density experiences relatively slow progress [32]. Besides, the onboard battery pack costs are still high, representing more than one-quarter of EV production costs [7]. Apart from energy storage technology, the infrastructure also imposes restrictions on the popularity of EVs, as there have not been sufficient public charging points en-route to sustain EVs' distant travelling. Besides, existing power grids can hardly tolerate the loading of many EVs being charged simultaneously [33].

## 2.2 Dual energy storage system (DESS)

The DESS is typically composed of batteries and SCs plus DC/DC converter(s). Therefore, the literature review of DESS is broken down into a review of each component and system topology, from the standpoint of numerical modelling in particular. The battery and SC are reviewed in Sections 2.2.1 and 2.2.2, respectively, with emphasis on their electrical and degradation characteristics. The DC/DC converter is reviewed together with the system topology in Section 2.2.3.

### 2.2.1 Battery

Li-ion batteries are currently the most popular batteries in the automotive sector because of their balance between power density, energy density, efficiency, thermal safety and price [34]. Hence, the review of batteries takes the characteristics of Li-ion batteries, for instance. So far, there have been three mainstream Li-ion batteries: lithium iron phosphate ($LiFePO_4$), ternary lithium ($LiNiCoMnO_2$ mainly) and lithium manganite ($LiMn_2O_4$). Table I compares the these batteries [35].

Table I Comparison of $LiFePO_4$, $LiNiCoMnO_2$ and $LiMn_2O_4$ batteries [35].

| | **$LiFePO_4$** | **$LiNiCoMnO_2$** | **$LiMn_2O_4$** |
|---|---|---|---|
| **Nominal voltage (V)** | 3.3 | 3.6 | 3.8 |
| **Energy density (Wh/kg)** | 150 | 160 | 120 |
| **Maximum current rate** | ★★ | ★ | ★★★ |
| **Price** | ★★ | ★★★ | ★ |
| **Lifespan** | ★★★ | ★ | ★★ |
| **Environmental impacts** | ★★★ | ★ | ★★ |
| **Thermal safety** | ★★ | ★ | ★★★ |

It can be seen from Table I that $LiNiCoMnO_2$ batteries have the highest energy density, which is a beneficial characteristic for onboard energy storage. However, when deploying the $LiNiCoMnO_2$ batteries onboard as an energy storage system, their poor thermal safety call for careful protection measures implemented in the battery thermal management system (TMS). Moreover, their price and lifespan are inferior to the $LiFePO_4$ and $LiMn_2O_4$ batteries. In practise, $LiFePO_4$ batteries are currently the most popular Li-ion battery used in mass-produced EVs, occupying more than half of EV battery market share, followed by $LiNiCoMnO_2$ batteries, while $LiMn_2O_4$ batteries only make up for less than 10% [35].

#### 2.2.1.1 Battery electrical characteristics

A battery comprises the anode, cathode, separator, electrolyte and two current collectors (positive and negative). The anode and cathode store the lithium. The electrolyte carries positively charged Li-ions from the anode to the cathode and vice versa via the separator. The movement of Li-ions creates free electrons in the anode, which creates a charge at the positive current collector. The electrical current then flows from the current collector via a device being powered to the negative current collector. The separator blocks the flow of electrons inside the battery [36].

Although batteries seem to act like simple electrical energy storage devices, they actually undergo thermally-dependent electrochemical processes when they deliver and accept energy [37]. However, battery thermal effects, including battery heat generation and temperature variation, are not involved in this work. This is because battery thermal effects must be considered jointly with battery TMS, but battery TMS is a complicated research problem that needs particular development rather than arbitrary configuration [38]. For example, there are many factors to be carefully considered for the battery TMS, such as the thermal medium, pipelines, power source of the system, control strategies of the system and also their interactions with the sizing and EM of DESS [39]. All these factors, if considered in this work, could not be exhaustively discussed, as this work focuses on the EM and sizing of DESS. Hence, this work does not investigate the battery thermal effects/TMS and considers that the temperature can be invariant at 20℃. Targeted the engineering aspects of batteries in EV applications, this work gets rid of the material-related parameters and dimension-related governing

equations in the electrochemical processes and focuses on the electrical characteristics (i.e., power, energy, voltage, current, resistance) that directly connect with EV propulsion. As a reduced-order modelling approach with convenient characterisation and fast computation, the equivalent circuit modelling is widely used for the representation of battery electrical characteristics in the control-based areas [40]. Using equivalent electrical components (e.g., voltage source, current source, resistance and capacitor) to compose the battery circuit, the battery equivalent circuit model can be expressed by state equations and combined with modern control theories. In this way, the battery's electrical behaviour is considered a nonlinear function of a variety of constantly changing parameters [39].

The literature has reported three typical kinds of battery equivalent circuit models: Resistance INTernal (Rint) model, Partnership for a New Generation of Vehicles (PNGV, was a cooperative research program led by the US government) model and second-order Resistance-Capacitor (RC) model, as shown in Figure 8 [41]. Figure 8 (a) shows the fundamental but most commonly used battery model – the Rint model, which characterises the battery with a perfect voltage source and an effective internal resistance. Its advantage is the easiness of characterisation while ensuring enough accuracy, while the disadvantage is that it cannot represent the circuit transients caused by polarisation reactions [42]. Evolved from the Rint model, as Figure 8 (b), the PNGV model adds a RC circuit to represent the polarisation reactions inside the battery and an additional capacitor to compensate for the change of open-circuit voltage (OCV). The PNGV model takes into account battery polarisation, but it is reported that the accuracy decreases dramatically with battery cycles increasing [43]. Figure 8 (c) shows the more complicated battery model – the second-order RC model. It uses two RC circuits to divide the concentration polarisation and electrochemical polarisation and thus is the most accurate model compared with the other two. However, this model needs a large number of testing data to characterise and has a high computation complexity [42].

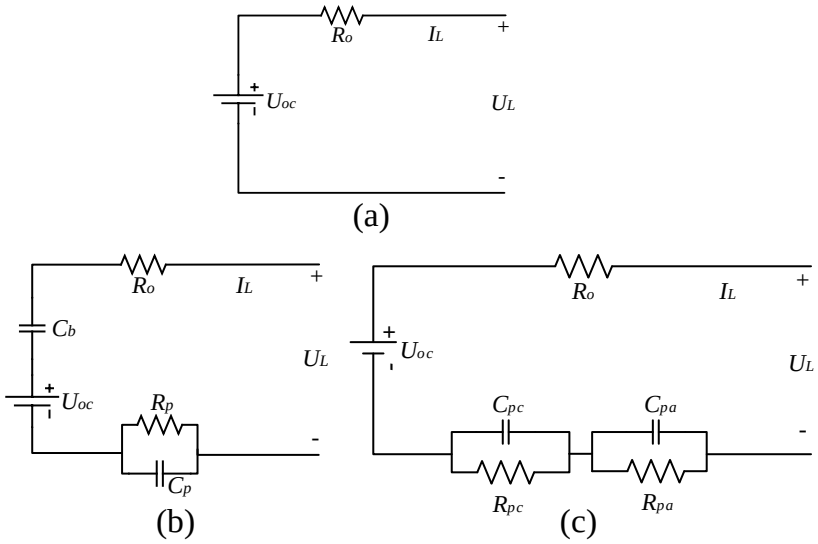


Figure 8 Typical equivalent circuit models for the battery: (a) Rint, (b) PNGV, (c) second-order RC model.

Considering the demands of battery modelling in this work, the Rint model is chosen as the basis for battery modelling. Reasons follow: (1) Compared with the Rint model, the primary benefit of either the PNGV or second-order RC model is the representation of battery polarisation. By considering battery polarisation, the voltage and current transients of the battery can be dynamically reflected. However, this work focuses on the DESS with EM and sizing problems rather than battery dynamic response, in which case the battery transients are less concerned. With DESS EM and sizing, the battery model is used for working out the steady-state power, energy, voltage, current and resistance of the battery so that combining the outputs of the SC model, the steady-state status of the DESS can be then analysed. The consideration of battery transients contributes little to this work; thus, the PNGV model or second-order RC model is not adopted [44]. (2) Despite its simplicity, the Rint model has enough accuracy and has been widely used in recent studies. For example, Song [45] uses the Rint model to look into the heating demands of DESS at sub-zero temperatures and points out "the Rint model has sufficient accuracy"; Zhang [46] uses the Rint model to investigate the EM of DESS, considering inaccurate terrain information; Wieczorek [47] uses the Rint model to develop a mathematical representation of an EM strategy along with real-time optimisation using genetic algorithm; Golchoubian [48] uses the Rint model to design a real-time nonlinear model predictive controller for the DESS in EVs. The above studies indicate successful applications of the Rint model in the recent studies of DESS.

#### 2.2.1.2 Battery degradation characteristics

Currently, the price of automotive batteries is still high, and the whole battery pack represents more than one-quarter of the total EV price [3]. In this case, battery degradation has been a worrying concern because it leads to a noteworthy reduction in battery service time and high battery replacement costs (as the battery degrades to end-of-life (EOL), the onboard battery pack has to be replaced by a new one; consequently, corresponding replacement costs occur) [49]. Battery degradation can be categorised into cycle degradation that happens with battery cycling and calendar degradation that happens within battery shelf life [49]. In this work, calendar degradation is not considered because it is spontaneous degradation that cannot be optimised by the efforts of EM or sizing [49]. According to the research by Lawrence Berkeley National Laboratory, USA, battery degradation usually results in battery impedance increase, voltage decrease, capacity loss (reflected by ampere-hour or watt-hour loss) and power loss [43, 50]. However, battery power loss does not significantly impact the EV's driveability performance, even with substantial power loss down to 30% remaining power capability. Hence, EV battery replacement is driven by capacity loss rather than power loss [51]. In most cases, the battery degradation rate is strongly influenced by battery operating conditions such as the temperature, current rate, depth-of-discharge (DOD) and state-of-charge (SOC) region [52]. Furthermore, evidence also exhibits that higher charge cut-off voltage can also aggravate battery degradation [53]. By investigating the influence factors of battery degradation rate, it is found that the mechanisms of battery degradation can be sorted into three groups: (1) Loss of active

electrode materials. (2) Loss of cyclable Li-ion (i.e., Li plating), (3) Loss of conductivity in electrode or electrolyte [54]. Rather than going far in the electrochemical mechanisms, this work focuses on the numerical formulation and battery degradation modelling.

The formulation of battery degradation is usually fitted from a large volume of testing data. This work adopts a fitting formula proposed by Wang [55, 56] to calculate the battery degradation coefficient ($\alpha$), which is defined as the percentage of battery capacity loss to the original battery capacity. It is widely recognised that the battery gets EOL when the battery degradation coefficient reaches 20% [44]. As (1), this formula follows Arrhenius Law [55] and uses battery current rate ($I_{rate}$, unit: C, defined as the ratio between battery current and battery ampere-hour capacity), ampere-hour throughput ($Ah_{put}$, unit: ampere-hour) and temperature ($T$, unit: Kelvin) as independent variables, and $a, b, c, d, e$ are five constant coefficients that are characterised by testing. In this work, battery thermal issues are not considered so that the temperature is fixed at 293 K (i.e., 20°C). This formula has been widely adopted to perform battery degradation calculation in the literature [57].

$$\alpha = \left(aT^2 + bT + c\right) \cdot exp\left[\left(dT + e\right) I_{rate}\right] \cdot Ah_{put} \tag{1}$$

### 2.2.2 Supercapacitor

The SC is an energy storage device similar to the battery in many respects (electrodes, liquid electrolyte, and separator are main components) [58]. SCs have found plenty of applications in vehicle propulsion systems: Honda IMA and Toyota ES are production vehicles that incorporate SCs as high-power energy storage devices in the drivetrains [3]. Compared with batteries, the most remarkable features of SCs are the ten times higher power density, 50 times lower energy density and a much longer lifespan comparable to vehicle lifetime [59]. These features can be reflected in Table II, where the specifications of mass-produced SCs by Maxwell Technologies are collected. The SC is reviewed in terms of electrical and degradation characteristics with emphasis on its differences from the battery.

#### 2.2.2.1 SC electrical characteristics

Compared with batteries, SCs have unique characteristics that make them competent to be onboard energy storage devices, as follows reviewed.

(1) Internal voltage drop. Compared to batteries, SCs have significantly lower internal resistance (this can be reflected by Table IX) and much relieved polarisations (i.e., electrochemical polarisation and concentration polarisation), making SCs have rare memory effects and small internal voltage drop. Theoretically, SCs can operate between their rated voltage and zero [59]. A complicated voltage balancing circuitry is often used in battery systems; in contrast, a SC management system can be simple with the focus on preventing SCs from exceeding their rated voltage [59]. The usable

energy stored in the SC ($E_{SC,\ usable}$) is a quadratic function of SC OCV ($U_{oc,SC}$), as (2), where $C_{SC}$ is the nominal capacitance of the SC [60, 61].

$$E_{SC,usable} = \frac{1}{2} C_{SC} U_{oc,SC}^{2} \tag{2}$$

Table II Mass-produced SCs for automotive use by Maxwell Technologies* [62].

| | **BCAP 0650** | **BCAP 1200** | **BCAP 1500** | **BCAP 2000** | **BCAP 3000** |
|---|---|---|---|---|---|
| **Capacitance (F)** | 650 | 1200 | 1500 | 2000 | 3000 |
| **Nominal voltage (V)** | 2.7 | 2.7 | 2.7 | 2.7 | 2.7 |
| **Resistance (mΩ)** | 0.8 | 0.58 | 0.47 | 0.35 | 0.29 |
| **Power density (W/kg)** | 6800 | 5800 | 6600 | 6900 | 5900 |
| **Energy density (Wh/kg)** | 4.1 | 4.7 | 5.4 | 5.6 | 6.0 |
| **Mass (g)** | 160 | 260 | 280 | 360 | 510 |
| **Volume (L)** | 0.211 | 0.294 | 0.325 | 0.373 | 0.475 |
| **Price (£)** | 8 | 19 | 22 | 28 | 40 |
| **Worked calendar life** | 10 years | | | | |
| **Worked cycle life** | 1,000,000 cycles | | | | |

*: Data reported at 20℃.

(2) Current capability. The continuous current density recommended maximum for reliable long-life operations of SCs is 500mA per Farad, which makes SCs capable of dealing with high-rate charging and discharging, something no battery can tolerate [59]. Moreover, SCs have a typical time constant of approximately one second (the time constant is the time necessary to charge a capacitor to 63.2% of full-charge or discharge to 36.8% of full-charge [63]). In this case, SCs can be charged to 95% capacity within seconds, making them well suited for regenerative braking applications and other quick-charge scenarios [64].

(3) Detection of SOC. Determining battery SOC is a significant factor in designing robust battery systems, requiring sophisticated data acquisition, complex algorithms and long-term data integration. In comparison, it is very simple to determine the SOC of SC. Since the usable energy stored in a capacitor is a function only of capacitance and voltage, as (2), and the capacitance is constant, a simple OCV measurement defines SOC [59].

(4) Coulombic efficiency. SC coulombic efficiency for most uses is greater than 98%, and the typical efficiency under high-current pulses is still greater than 90% [59], which means that little charge is lost when charging and discharging the SC. The only coulombic efficiency losses associated with SCs are attributed to the internal resistance resulting in voltage drop during cycling (i.e., the $I^2R$ losses) [59].

#### 2.2.2.2 SC degradation characteristics

The SC has a much longer lifespan and less severe degradation than the battery because the SC's energy storage mechanism is a highly reversible process that moves charge and ions only and does not make or break chemical bonds [65]. Like battery degradation, SC degradation can be categorised into cycle degradation and calendar degradation, while calendar degradation is not considered in this section. Existing research points out that factors like temperature, voltage, current and DOD may greatly influence SC degradation [66]. In general, SC degradation reflects in the capacitance reduction, resistance increase and leakage current increase. According to Maxwell Technologies [67], the SC gets EOL if one of the following criteria is reached: (1) A reduction in capacitance of 20%. (2) An increase in resistance of 100%. It is typical that before the resistance rises by 100%, the capacitance does decay by 20% [68]. Thus, the capacitance criterion is often used as the metric to reflect SC degradation.

Focusing on the numerical formulation of SC degradation, Pascal [69] puts forward a fitting differential formula to model SC degradation with temperature, voltage and current as independent variables. He defines the "state-of-ageing (SOA)" as the metric of SC degradation, which equals zero for brand new SC and reaches 100% as the SC goes EOL, as (3) [69].

$$\frac{d(SOA)}{dt} = \frac{1}{t_{life}^{ref}} \cdot exp\left( \ln 2 \cdot \frac{\theta - \theta^{ref}}{\theta_0} \right) \cdot \left[ exp\left( \ln 2 \cdot \frac{U_{SC} - U_{SC}^{ref}}{U_{SC,0}} \right) + K \right] \cdot exp\left( k_{RMS} \cdot \frac{I_{RMS}}{C_{SC}} \right) \quad (3)$$

Where, $t^{ref}_{life}$ is the reference lifetime (1470h). $\theta$ is SC temperature. $\theta^{ref}$ is the reference temperature (65℃). $\theta_0$ is a constant parameter (7.7K). $U_{SC}$ is SC voltage. $U^{ref}_{SC}$ is the reference voltage (2.7V). $U_{SC,0}$ is a constant parameter (89mV). $K$ is a constant parameter (0.0029). $k_{RMS}$ is a constant parameter ($68s \cdot V^{-1}$). $C_{SC}$ is SC nominal capacitance. $I_{RMS}$ is the root-mean-square current flowing through the SC and can be calculated by a three-step procedure [69]:

(1) Compute the square current, as (4).

$$x(t) = I(t)^2 \quad (4)$$

(2) Filter it with a first-order low-pass filter and time constant $\tau_{filter}$, as (5).

$$Y(s) = \frac{X(s)}{1 + \tau_{filter} \cdot s} \quad (5)$$

(3) Take the root square of the result, as (6).

$$I_{RMS}(t) = \sqrt{y(t)} \quad (6)$$

This work uses the above formulations to calculate SC degradation but finds that SC degradation is too small to be considered over EV lifetime. For example, with the case study configuration in Section 5.1.1, UDDS drive cycle and 150000km mileage (the European Automobile Manufacturers Association considers EV lifetime mileage as 150000km [70]), the SOA of SC only reaches 17%. This indicates that the SC does not reach EOL over EV lifetime, resulting in no replacements nor degradation costs. Similarly, the literature assumes that the SC has an infinite lifecycle that neglects SC degradation [71]. It is also believed that SC can be cycled 100~500 thousand times at room temperature with minimal change in performance [10]. In this case, the SC degradation is not considered in the EM and sizing problems of DESS.

### 2.2.3 DESS topology

The DESS contains a battery pack and a SC pack, and each pack has specific electrical characteristics so that they cannot be directly connected via a simple switch. The DC/DC converter(s) is usually deployed to connect both packs and to coordinate their power, voltage and current. In a DESS, the DC/DC converter(s) determines the relative contributions of the dynamic (SC) and sustained (battery) power levels by generating buck-boost converter gating signals, offering much flexibility to EM implementation [72]. The DESS topologies can be categorised by the number and usage of DC/DC converters, and there are three primary types of topologies in the literature: passive, full-active and semi-active [73]. The most commonly adopted DESS topology is the semi-active topology with one bidirectional buck-boost DC/DC converter [74], whereas the other topologies also witness plenty of applications.

#### 2.2.3.1 Passive topology

Figure 9 shows the passive DESS topology. This is the simplest topology in which the battery pack and SC pack are connected in parallel and coupled directly to the DC bus, and no DC/DC converter is used. The most significant deficiency is that power/energy flows cannot be actively controlled [75]. The SC pack's voltage has to stay the same as the battery pack; thus, the SC capacity cannot be made full use of, and the regenerative braking energy cannot be well absorbed by the SC [76]. The SC pack only works as a low-pass filter for the battery pack. Despite the advantage of easy implementation, the passive DESS topology is not favoured in practical engineering.

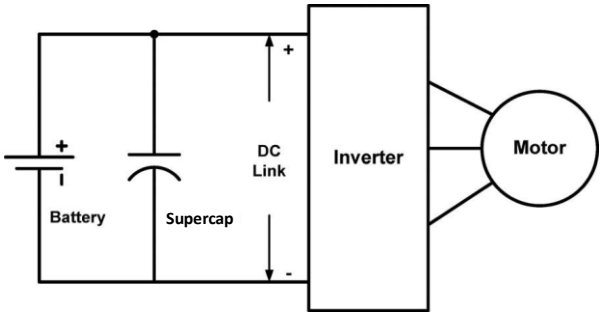


Figure 9 Passive DESS topology [77].

### 2.2.3.2 Full-active topology

Compared to the passive topology, the full-active topology can realise full-scale control on the DESS by adopting multiple DC/DC converters (or a multiple-input DC/DC converter) [77], as shown in Figure 10. The most significant disadvantage of full-active topology is the complex electrical architecture, which greatly increases DESS implementation cost. This topology is barely used in mass production but is an excellent approach for the early-stage development of DESS. The full-active topology can be further divided into cascaded, parallel and multiple-input configurations [78]. Explanations of each configuration are given below.

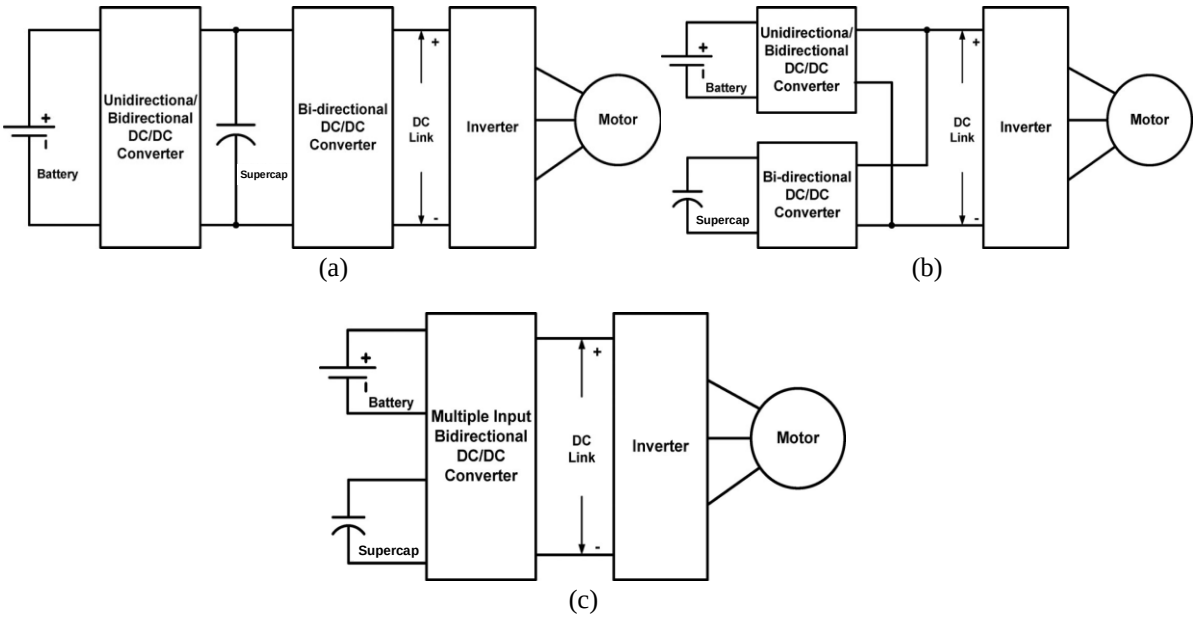


Figure 10 Full-active DESS topologies, with: (a) cascaded multiple converters, (b) parallel multiple converters, (c) single multiple-input converter [77].

(1) To make a better voltage range of both the battery pack and SC pack, two bidirectional DC/DC converters are placed with one between the SC pack and battery pack and the other between the SC pack and SC bus [79]. This forms a cascaded topology, as can be seen in Figure 10 (a).

(2) Figure 10 (b) shows the diagram of the parallel topology. Instead of the cascaded connection with two converters, the parallel topology parallels the outputs of two converters. Voltages of both the battery and SC can be maintained lower than the DC bus voltage, less voltage balancing problem so as incurred [80]. The voltage of the SC can vary in a wide range so that the SC can be fully used. The disadvantage of this topology is that two full-size converters are necessary.

(3) The cost of either the cascaded or parallel topology is high because either requires two full-size bidirectional converters to interface both the battery pack and SC pack. Multiple-input topology [81, 82] is so as proposed to reduce the overall system's cost. The diagram of the multiple-input topology is shown in Figure 10 (c).

2.2.3.3 Semi-active topology

As a trade-off between the passive and full-active topologies, the semi-active topology employs one single DC/DC converter to realise the control on DESS. Being a good balance between system cost and control realisation, this topology is the most popular in the literature and practical applications [83]. Semi-active topology can be further divided into Battery/SC and SC/Battery topologies, as shown in Figure 11 (a) and (b), respectively [77], and explanations follow:

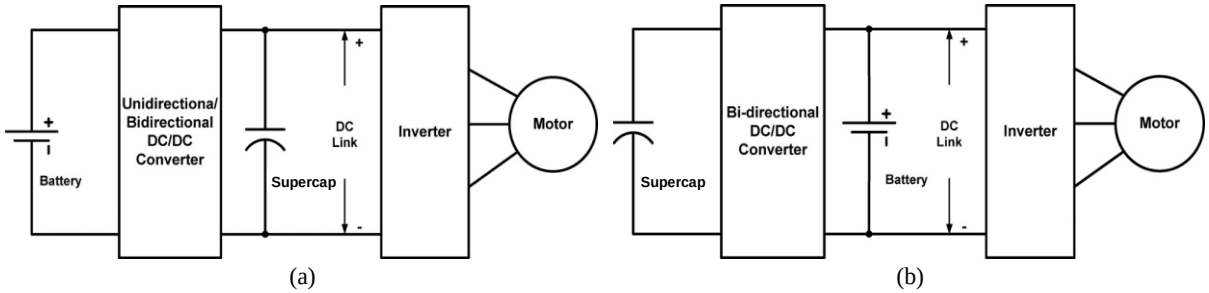


Figure 11 Semi-active DESS topologies: (a) Battery/SC topology, (b) SC/Battery topology [77].

(1) In Battery/SC topology, the SC pack is directly connected to the DC bus; thus, the SC pack is the main energy storage. However, due to the low energy capacity of SC pack, the battery pack is still responsible for fulfilling the energy demands from the DC bus [84]. In this topology, battery pack voltage can be maintained lower or higher than the SC pack voltage. The control strategy applied to this topology allows the DC bus voltage to vary within a wide range so that the SC pack energy can be more effectively used. The most significant advantage is that this topology can significantly reduce battery use, which directly relieves battery degradation. However, compared to the battery pack that is interfaced by the DC/DC converter, the SC pack is directly connected to the DC bus and thus can not be proactively controlled, which requires the EM to have high robustness and adaptiveness [85].

(2) In SC/Battery topology, the battery pack is the main energy storage, and the SC pack compensates for the power gap when the battery cannot cover the high power demands individually. Using a bidirectional DC/ DC converter to interface the SC pack, the SC pack voltage can be used in a wide range. The battery pack is directly connected to the DC bus; thus, the DC bus voltage cannot be varied too much. Compared to the Battery/SC topology, this topology can ease the burden of EM [84]. However, to handle the SC pack's power, the DC/DC converter in this topology is usually larger than that in the Battery/SC topology [86].

Research [82] compares the Battery/SC and SC/Battery topologies in terms of power and energy capabilities, battery lifespan, and system efficiency by simulation and bench tests. It is concluded that: (1) Both kinds of topologies can realise the same power and energy capabilities without too much difference in mass, volume and cost. (2) Battery/SC topology has a better performance in improving battery life, while the SC/Battery topology has a better system efficiency.

Since the SC/Battery topology is more popular in practice than the Battery/SC topology [77], this work adopts the SC/Battery topology for the DESS. With this topology, the typical work modes of DESS are presented in Figure 12. Explanations follow [77]:

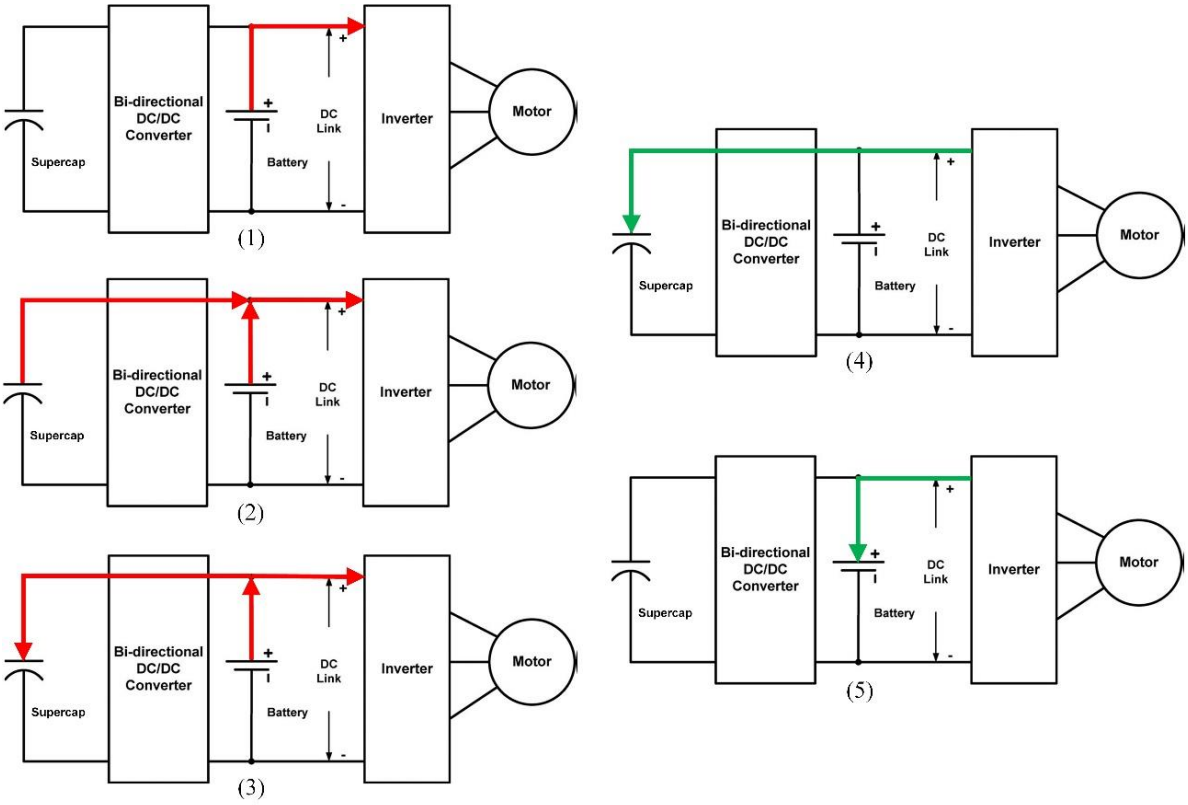


Figure 12 Typical work modes of the DESS with SC/battery topology.

(1) Mode 1 represents that the battery pack powers the motor individually. This requires the DC/DC converter to shut down so that the DESS can operate like a battery-only ESS.

(2) Mode 2 represents that the battery pack and SC pack drive the motor together. This mode requires the DC/DC converter to boost the SC pack voltage onto the same level as the battery pack.

(3) Mode 3 represents that the battery pack drives the motor while charges the SC pack. This mode requires the DC/DC converter to work at buck pattern so that the battery power can go into the SC.

(4) Mode 4 represents that the motor recharges the SC pack. This mode requires the DC/DC converter to work at buck pattern; simultaneously, to make this mode effective, the motor inverter needs to coordinate motor voltage and battery voltage so that the regenerative braking power would not go into the battery pack.

(5) Mode 5 represents that the motor recharges the battery pack. This mode requires the DC/DC converter to shut down so that the regenerative braking power can only go into the battery pack.

## 2.3 Energy management of DESS

The literature has provided tremendous energy management strategies (EMSs) for the DESS. This section enumerates the typical EMSs as an overview and dissects one of them as a case study.

### 2.3.1 Overview of energy management strategy

Existing studies of the EMS of DESS can be classified as either "objective-oriented" or "technique-oriented" ones. The "objective-oriented" studies target various engineering requirements that are the objectives of the EMS and can be formulated as the cost functions to be optimised [87]. For example, the electricity consumption of DESS is the most frequently used cost function in the literature [47] since electricity consumption determines the electricity costs of vehicle operations. Battery degradation is another common cost function since it determines battery replacement [88] and leads to battery degradation costs [89]. Besides, additional objectives can be formulated as penalty functions along with main cost functions. For example, considering the battery pack's thermal safety, the battery pack's temperature can be formulated as a penalty [90]. The SOC of SC pack can also be used as a penalty [91] to prevent the SC pack from being depleted or overcharged. Despite various objectives being adopted, the formulation of cost functions needs to take into account practical engineering requirements.

The "technique-oriented" studies provide specific control schemes or algorithms to solve the formulated cost functions [87]. The current literature in the past few decades shows that studies of EMS evolve with the progress of novel control techniques. For example, the rule-based technique is early but also the most robust control technique that has long been used [92]. It sets up thresholds for certain control variables and decides control actions based on rules associated with the thresholds [93]. Later, the fuzzy logic control technique appears, updating the rule-based technique. The fuzzy technique also uses prescribed rules, but these rules are no longer related to thresholds but are defined by membership functions [19]. Both rule-based and fuzzy techniques are empirical techniques that need applied experiences to formulate accurate rules [94]. In comparison, control algorithms such as genetic algorithm (GA), dynamic programming (DP) and Pontryagin's minimum principle (PMP) arise as less judgemental techniques that follow normative optimisation policies [95]. With these algorithms being widely applied, some modified algorithms are proposed to overcome the original algorithms' shortcoming. For example, the non-dominated sorting GA II has an improved computation efficiency with a simplified iteration process [96]; the stochastic DP and adaptive PMP can be suboptimal online implementable algorithms, while the original DP and PMP can only be used to obtain optimal offline benchmarks [87]. The EMS should perform online to fit real-time driving conditions, but real-life driving always has a degree of "future uncertainty" [97]. With this regard, more prediction-based control schemes are proposed, such as the Markov chain and model predictive control (MPC) techniques [61]. For example, the MPC technique uses an EV model and

historical driving states (e.g., vehicle velocity and acceleration) within a specific perception horizon to make predictions about future driving states [98]. Both historical and predicted driving states are imported into an online algorithm, and the algorithm works out the control strategies to be used in the coming control horizon [99]. With the development of artificial intelligence, recent years see the machine learning techniques like the neural network (NN) being increasingly applied to the field of EMS [100]. Machine learning is a broad discipline with many branches such as supervised learning, unsupervised learning, deep learning and reinforcement learning, while the state-of-art turns to deep reinforcement learning [101]. Compared with the MPC technique, the machine learning techniques do not need explicit models or representations to make predictions [102], and the transformation from control inputs to outputs is hidden behind artificial intelligence [103]. It should be noted that the control techniques reviewed above are not mutually exclusive; instead, some practice of EMS, such as the drive pattern recognition (DPR) based EMS, adopts a combination of more than one control techniques [104]. The DPR-based EMS defines a few typical drive patterns and works out the optimal offline control strategies for each drive pattern. The online efforts of DPR-based EMS are to sense the historical and real-time driving states, then in some cases to predict the future driving states. They recognise similar drive patterns to recall the appropriate control strategies, exploiting the fact that the EMSs are similar for drive cycles with similar statistical properties [104]. Implementing such an EMS needs the cooperation of several control techniques; for example, the reference [61] uses the combination of DP, MPC and NN, plus a PID controller.

### 2.3.2 Case study: rule-based energy management strategy

The rule-based strategy is the most fundamental EMS and evolves to various, advanced EMSs [96]. Therefore, this section reviews the rule-based strategy as the EMS of DESS. The rule-based strategy uses a set of thresholds as the entry conditions of different working modes; once specific entry conditions are satisfied, the corresponding working mode will engage, and the power split strategies within that working mode will be executed [85]. The key points to implement the rule-based strategy are selecting thresholds and designing working modes [85]. The thresholds are used to estimate the status of the EV or energy storage so as to guide the entry of the proper working mode, and the working modes determine the power delivered by the battery pack and SC pack, respectively. Figure 13 presents an example [105] of the rule-based strategy as the EMS of DESS. Combining Figure 13, the implementation of rule-based EMS is explained in terms of the selection of thresholds and design of working modes, as follows.

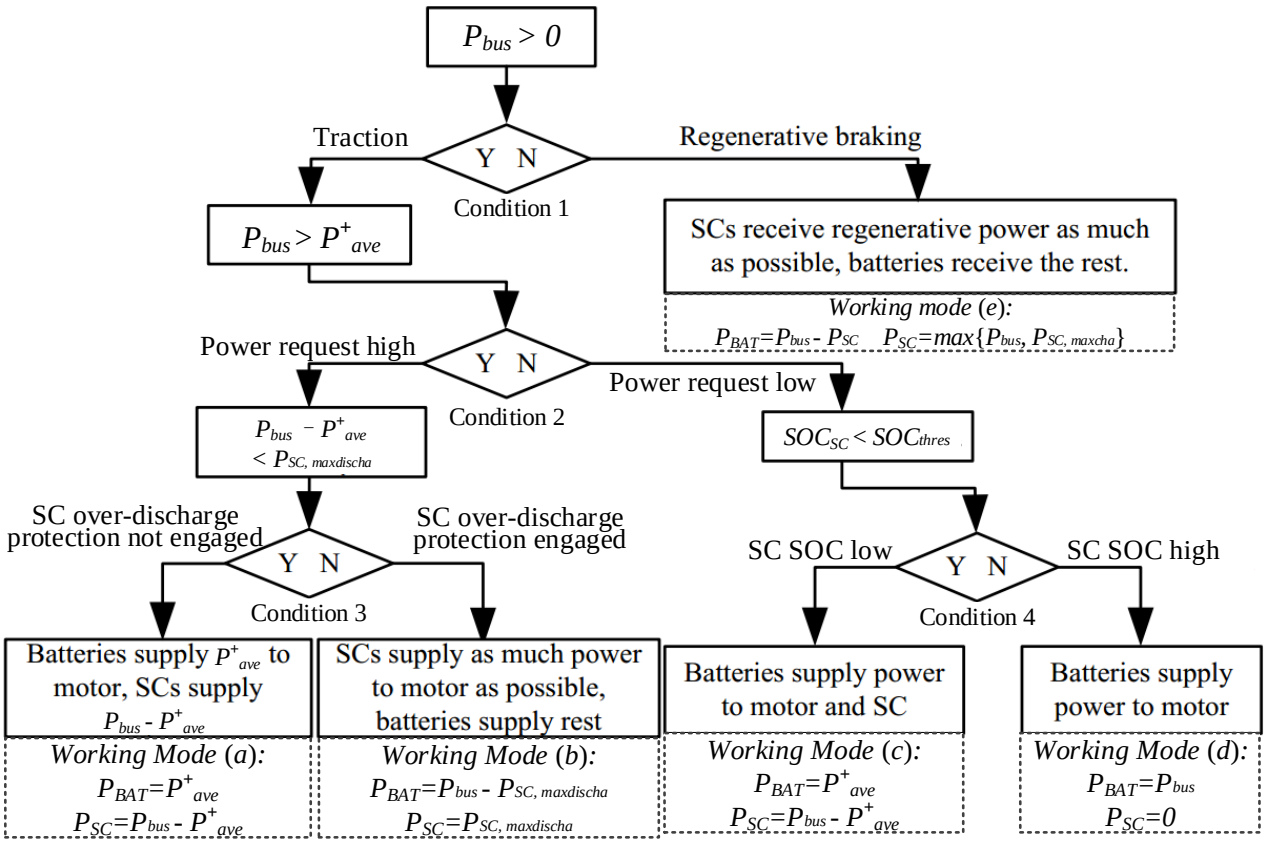


Figure 13 An example of the rule-based strategy as the energy management strategy of DESS.

2.3.2.1 Selection of thresholds

The example in Figure 13 selects four thresholds: three thresholds (0, $P^{+}_{ave}$, $P_{SC,maxdischa}$) for the power requests of the bus ($P_{bus}$) and one threshold ($SOC_{thres}$=0.5) for the SOC of SC pack ($SOC_{SC}$) [105]. These thresholds make up the entry conditions of different working modes. The four thresholds are explained with Conditions 1, 2, 3, and 4 in Figure 13, as follows.

(1) Condition 1. "0" is compared with $P_{bus}$, defining whether the vehicle is under traction or regenerative braking, which further indicates whether the DESS as a whole needs to deliver power or receive power.

(2) Condition 2. "$P^{+}_{ave}$" is the average positive power request from the bus. Its value is predefined by simulation and depends on the drive cycle used. "$P^{+}_{ave}$" is used as the soft constraint for battery working power. It is compared with $P_{bus}$, defining whether the bus's power request is more than the battery can take alone. If yes, the SC would be expected to perform power peaking; if no, the battery would power the motor alone.

(3) Condition 3. "$P_{SC,maxdischa}$" is the SC's maximum discharge power, which represents the real-time power peaking capability of the SC. The value of $P_{SC,maxdischa}$ changes with the SOC of SC and can be acquired from either the SC model (in the case of simulation) or the SC management system (in the case of real-life vehicle operation). "$P_{SC,maxdischa}$" is compared with the expected power output of

the SC ($P_{bus}$ - $P^{+}_{ave}$), defining whether the SC can deliver the power as much as ($P_{bus}$ - $P^{+}_{ave}$). If yes, the SC would deliver power as expected; if no, which means that the expected power output is more than the SC can deliver, the SC's over-discharge protection would engage. In this case, the SC can only deliver power as much as $P_{SC,maxdischa}$, and the battery would have to violate the soft constraint for its working power and deliver power at ($P_{bus}$ - $P_{SC,maxdischa}$).

(4) Condition 4. "$SOC_{thres}$" is compared with $SOC_{SC}$, defining whether $SOC_{SC}$ is low. If yes, the battery would need to charge the SC while powering the motor; if no, the SC would not need to be charged. The value of $SOC_{thres}$ is often determined by the "trial-and-error" method or even by the designer's experience; in other words, the determination of $SOC_{thres}$ is a quite empirical process [57]. The thumb rules to determine $SOC_{thres}$ are: (1) A high $SOC_{thres}$ would make $SOC_{SC}$ stay high; however, the SC would frequently be charged by the battery and thus impose a heavy burden on the battery. (2) A low $SOC_{thres}$ would make $SOC_{SC}$ stay low, and in the worst case, the SC would drain all its available energy and thus cannot perform any power peaking.

#### 2.3.2.2 Design of working modes

The working modes are responsible for determining how much power should be provided by the battery and SC, respectively [105]. Besides, they are also responsible for performing over-discharge/-charge protection for the SC in case that the expected power output/input is more than the SC can take [106]. Combining the Working Modes (a), (b), (c), (d) and (e) in Figure 13, the design of working modes are explained as follows.

(1) Mode (a) is the most representative working mode of DESS in which the battery and SC would work together, performing hybrid powering. This mode would engage if both of the following conditions are satisfied: (1) The power request is defined as high ($P_{bus} > P^{+}_{ave}$) so that the hybrid powering is expected. (2) The power gap is less than the maximum discharge power of SC ($P_{bus}$ - $P^{+}_{ave} < P_{SC,\ maxdischa}$) so that SC can compensate for the whole power gap. In this mode, the battery would obey the soft constraint for its working power and deliver power at $P^{+}_{ave}$; meanwhile, the SC would perform power peaking and compensate the power gap ($P_{bus}$ - $P^{+}_{ave}$).

(2) Mode (b) can be regarded as the adaptation of Mode (a), and the difference in Mode (b) is that the power gap ($P_{bus}$ - $P^{+}_{ave}$) is more than the SC can cover ($P_{SC,\ maxdischa}$). In this case, the SC can only deliver power as much as $P_{SC,maxdischa}$, even though the expected power output is more at ($P_{bus}$ - $P^{+}_{ave}$). The battery would have to violate the soft constraint for its working power and deliver power at ($P_{bus}$ - $P_{SC,maxdischa}$). This mode is a compromise between hybrid powering and SC over-discharge protection.

(3) Mode (c) represents that the battery powers the motor while charges the SC. This mode is engaged if both of the following conditions are satisfied: (1) $SOC_{SC}$ is defined as low ($SOC_{SC} < SOC_{thres}$) so that the SC would need to be charged. (2) The power request is defined as low ($P_{bus} < P^{+}_{ave}$) so that

the battery can have surplus power ($P^{+}_{ave}$ - $P_{bus}$) to charge the dying SC. In this mode, the battery would work at the soft constraint ($P^{+}_{ave}$). One part of battery power would be used to drive the motor as expected at ($P_{bus}$), while the other part of battery power would charge the SC at ($P^{+}_{ave}$ - $P_{bus}$). This mode aims to maintain SC's energy status so that the SC can be well prepared for possible power peaking operations in the future.

(4) Mode (d) represents that the battery powers the motor individually. This mode is engaged if both of the following conditions are satisfied: (1) $SOC_{SC}$ is defined as high ($SOC_{SC} > SOC_{thres}$) so that the SC would not need to be charged. (2) The power request is defined as low ($P_{bus} < P^{+}_{ave}$) so that the battery can handle the power request on its own. In this mode, the DESS works like a battery-only ESS.

(5) Mode (e) is tailored for regenerative braking in which the power request is below zero ($P_{bus} < 0$). In this case, the SC is expected to receive as much regenerative power as possible, but the maximum charge power of SC ($P_{SC,\ maxcha}$, below zero) should be checked in advance. Considering SC over-charge protection, the SC would work at either $P_{bus}$ or $P_{SC,\ maxcha}$, whichever is larger, and this is fulfilled by "$max[P_{bus}, P_{SC,maxcha}]$". Since both $P_{bus}$ and $P_{SC,\ maxcha}$ are below zero, "$max[P_{bus}, P_{SC,maxcha}]$" is actually choosing the minimum absolute value to be used as the charge power for the SC. The battery would accept the remaining regenerative power ($P_{bus}$ - $P_{SC}$) that is more than the SC can take.

## 2.4 Sizing of DESS

The literature has provided tremendous sizing methods for the DESS. This section enumerates the typical sizing methods as an overview and dissects two of them as a case studies.

### 2.4.1 Overview of sizing methods

Existing studies of DESS sizing can be classified as "objective-oriented", "problem-oriented" and "objective-problem-oriented" ones. The "objective-oriented" studies consider that the sizing problem is usually coupled with the EM problem, sharing overlapped objectives. For example, battery degradation or electricity consumption is known as a combined result of both sizing and EM [107]. Targeted the common objectives, the sizing problem can be solved along with the EM problem by formulating an "objective-oriented" integrated framework. For example, Mamun [108] develops a mathematical framework for joint sizing-EM optimisation of a series hybrid EV with a DESS. By finding the optimal sizes of the battery pack and SC pack as well as the optimal EMS of DESS, the objective of energy consumption is minimised. Masih-Tehrani [109] develops a formulation for EM and sizing of a DESS in a series hybrid electric bus. With the objective of optimising the 10-years battery degradation costs, the EM and sizing problems are solved by the DP and GA. Song [13] proposes an integrated optimisation problem to solve the life cycle costs of a DESS in an electric city

bus, in which the DP approach is responsible for searching the optimal DESS size while a rule-based controller is tuned to represent the near-optimal EMS.

The "problem-oriented" studies aim to investigate a few objectives with the individual sizing problem at a time, performing multi-objective optimisation (MOP) to optimise the co-existing objectives. For example, Eldeeb [107] develops a MOP formulation to optimally size a DESS for a plug-in EV, where the four objectives of mass, volume, initial cost and battery degradation are minimised simultaneously. Song [110] adopts the NSGA-II to size a DESS for use in an electric bus, and the DESS initial cost and battery capacity loss are formulated as two conflicting objectives. Zhang [111] investigates the sizing problem of a DESS in an example EV and solves three objectives of battery state-of-health, DESS weight and initial cost by using the wavelet-transform-based algorithm and NSGA-II. Aiming at optimising DESS mass and battery cycle life simultaneously, Shen [112] proposes a formulation for sizing a DESS deployed in an electric passenger car, where the DIviding RECTangles (DIRECT) algorithm solves the optimal size.

Combining the integrated sizing-EM framework and MOP, the best practice of DESS study demonstrates the "objective-problem-oriented" investigations. For example, Song [91] uses the PMP to determine the optimal EMS and the best-case size for a DESS equipped with a plug-in EV and the objectives of battery degradation, fuel consumption, and electricity consumption are optimised all together. Using the DP, Song [113] formulates the optimisation of battery degradation and electricity consumption of a DESS in EV applications, and the optimisation problems are solved through the efforts of both EM and sizing; furthermore, sensitivity analysis is performed towards various temperatures and battery prices.

### 2.4.2 Case studies: power-energy function and multi-objective optimisation based sizing methods

#### 2.4.2.1 Power-energy function based sizing methods

Power-energy function (PEF) was put forward [114] targeted the energy and power capabilities of the DESS. It formulates the SC pack size as a function of the battery pack size [115]. Considering the battery is an energy-intense storage whose weakness is power capability, the battery pack size is represented by its power capability. Similarly, SC is a power-intense storage whose weakness is energy capability so that the SC pack size is represented by its energy capability [116]. To this end, the PEF actually formulates the energy capability of SC pack as a function of the power capability of battery pack, and the sizing results given by PEF are a solution set of all possible combinations of battery pack power capability and SC pack energy capability [57].

The significance of PEF can be explained as follows [109]. Under high-power EV propulsion, the SC pack would peak the power demands that are more than the battery pack can take alone. The

power peaking operations of SC pack are accompanied by certain SC energy delivery. The SC pack is expected to have a sufficient energy capability so that it would run out of energy during its power peaking operations. However, the energy capability of SC pack depends on the power capability of battery pack, since a battery pack with lower power capability would require more power peaking operations as well as more energy delivery from the SC pack so that the energy capability of SC pack need to be enlarged. In this way, the PEF formulates the energy capability of SC pack as a function of the power capability of battery pack, and its mathematical representation is explained in the following.

Assume that the EV is running under a random drive cycle and the power bus proposes certain power demands ($P_{bus}$) that would be fulfilled by the battery pack and SC pack jointly, as shown in Figure 14 (a). The battery pack has a maximum power capability ($P_{BAT,max}$), above which the SC pack would perform power peaking. As the bus power demands $P_{bus}$ exceed $P_{BAT,max}$, the SC would have to work at ($P_{bus}$ - $P_{BAT,max}$) to bridge the power gaps. Based on Figure 14 (a), the energy delivery of SC pack ($E_1$, $E_2$,…, $E_n$) during power peaking operations are expressed as (7).

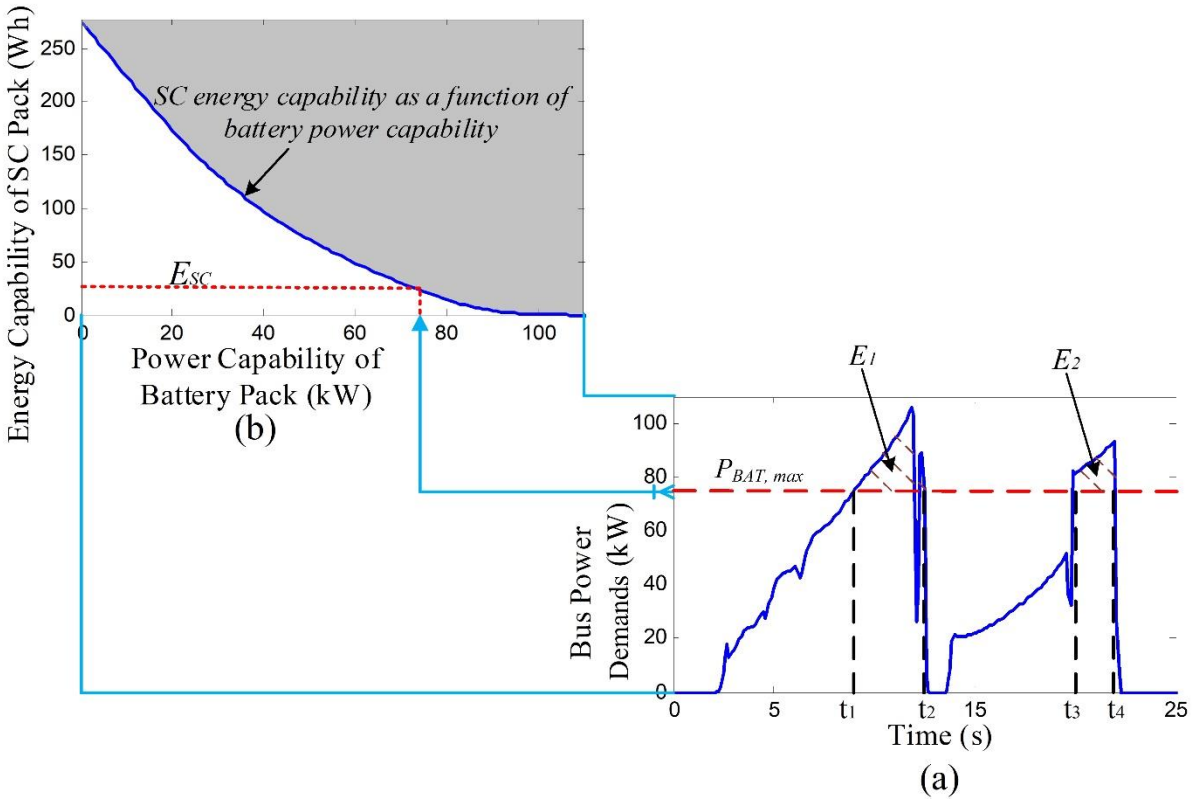


Figure 14 Power-energy function based sizing methods: (a) bus power demands with time; (b) energy capability of SC pack as a function of power capability of battery pack.

$$\begin{cases} E_1 = \int_{t_1}^{t_2} (P_{bus} - P_{BAT,\,max})dt, \\ E_2 = \int_{t_3}^{t_4} (P_{bus} - P_{BAT,\,max})dt, \\ \quad \cdots\cdots \\ E_n = \int_{t_{2n-1}}^{t_{2n}} (P_{bus} - P_{BAT,\,max})dt \end{cases} \tag{7}$$

To fulfil power peaking operations, the energy capability of SC pack ($E_{SC}$) should be larger than any energy delivery expressed in (7). This relationship is then expressed as (8). Furthermore, if the power capability of battery pack $P_{BAT,\,max}$ is considered as a variable, then the energy capability of SC pack $E_{SC}$ can be considered as a function of $P_{BAT,max}$. Based on this, Figure 14 (b) shows the $E_{SC}$ as a function of $P_{BAT,max}$ varying from 0 to 100kW, where the solution set of battery pack size (represented by power capability) and SC pack size (represented by energy capability) is constrained by (8).

$$E_{SC} \geq max(E_i) = max\left[\int_{t_{2i-1}}^{t_{2i}} (P_{bus} - P_{BAT,\,max})dt\right] \quad i = 1,2,...,n \tag{8}$$

2.4.2.2 Multi-objective optimisation based sizing methods

The MOP is the most popular DESS sizing method and has been widely applied in the literature [2]. Therefore, this section reviews the MOP-based sizing method of DESS. MOP is an area of multiple criteria decision making involving more than one objectives to be optimised simultaneously. The outcome of MOP is usually a trade-off between two or more conflicting objectives [117]. In terms of DESS sizing, the MOP is typically applied with objectives of mass, volume, power capability, energy capability, initial cost, battery degradation and energy efficiency [44, 89], and the optimisation results can be obtained by solving a particular algorithm. The key point of implementing MOP is to formulate the sizing problem with selected objectives. With this, an example of the MOP-based sizing method is reviewed as follows.

Shen [112] formulates a two-objective optimisation problem for sizing the DESS deployed in an electric passenger car under the UDDS drive cycle. In that work, the EMS of DESS is predefined as a rule-based strategy since the MOP-based sizing method requires the EMS to be totally/partially defined before solving the sizing problem. In the sizing formulation, one objective is the DESS mass, and the other objective is the battery degradation reflected by watt-hour loss. The proposed formulation uses three design variables of the DESS: the number of batteries in the battery pack ($N_{BAT}$), the number of SCs in the SC pack ($N_{SC}$), and one threshold ($P_{thres}$) to define whether the bus power request is high. Connecting the design variables with the two objectives, the first objective ($J_1$)

is the DESS mass ($M_{DESS}$) as a function of $N_{BAT}$ and $N_{SC}$, and the second objective ($J_2$) is the battery watt-hour loss ($E_{loss}$) as a function of $P_{thres}$, as (9).

$$\begin{cases} J_1 = M_{DESS}(N_{BAT}, N_{SC}) \\ J_2 = E_{loss}(P_{thres}) \end{cases} \tag{9}$$

Combining $J_1$ and $J_2$, the overall objective ($J$) is expressed as (10). In (10), $J_1$ is used as the main function because the primary purpose of the sizing problem is to optimise the DESS mass; in contrast, $J_2$ is a penalty function with a weight factor $\gamma$.

$$Min\ J = Min\{J_1 + \gamma J_2\} = Min\{M_{DESS}(N_{BAT}, N_{SC}) + \gamma \cdot E_{loss}(P_{thres})\} \tag{10}$$

The DIRECT algorithm is applied to solve the formulated MOP-based sizing problem, and the Pareto Frontier (a set of nondominated solutions, being chosen as optimal if no objective can be improved without sacrificing at least one other objective) is acquired with different $\gamma$ used in the penalty function. It is found that a larger $\gamma$ results in lower battery watt-hour loss in a trade-off with larger DESS mass. By setting $\gamma$ to 2, it is said that the DESS mass can be reduced by 230 kg in comparison with the battery-only ESS, and a 76% reduction of battery degradation costs can also be achieved.

# Chapter 3 Methodology

This chapter presents the methods/techniques used for the research problems tackled in each research chapter. The methods/techniques are summarised in Table III and then discussed in the sections that follow.

Table III Methods and techniques used for each research problem.

| Chapter No. | Research problem | Methods/Techniques |
|---|---|---|
| Chapter 4 | Modelling | Semiempirical modelling, Formula derivation, Experimental, Simulation. |
| Chapter 5 | Energy management | Dynamic programming algorithm, Curve fitting, Statistical analysis, Regression analysis, Neural network, Rule-based control strategy, Graphic method. |
| Chapter 6 | Sizing | Dynamic programming algorithm, Sensitivity analysis, Fuzzy logic algorithm. |
| Chapter 7 | Battery degradation | Graphic method, Formula derivation. |
| Chapter 8 | Aluminium DESS | Semiempirical modelling, Dynamic programming algorithm. |

## 3.1 Methodology of modelling

The modelling chapter presents the semiempirical modelling approach developed for electric vehicles (EVs) with a dual energy storage system (DESS). The input/output relationships are represented through formula derivations. The core components, battery and supercapacitor (SC), are modelled and validated by experiments, while the other components are validated by simulation. More details follow:

(1) Semiempirical modelling. Empirical modelling relies entirely on looking up the datasheet collected beforehand and benefits from immediate processing but suffers from insufficient accuracy, while nonempirical modelling relies entirely on the formulated input/output relationships and benefits from an in-depth understanding of the physical/chemical mechanisms but suffers from slow computation [118]. In contrast, semiempirical modelling is a compromised modelling approach that relies on the input/output relationships using empirical data collected in steady-state tests and then correcting them for transient effects [10, 31]. This work uses the semiempirical modelling approach to model the EV and DESS. For battery electrical modelling (Section 4.1.1.1), the empirical look-up tables account for the open-circuit voltage and internal resistance, while the equivalent circuit representations account for the terminal voltage, current and power.

(2) Formula derivation. Most of the derivations in this work are concerned with continuous transformations, while the other concern the discretisation of continuous functions. One example with modelling exists in Section 4.1.1.2, where a battery degradation model is proposed by discretising a continuous formula from literature.

(3) Experimental. This work is mainly based on modelling and numerical simulation, while the experimental is involved to a small extent in Section 4.3.1, where the battery model and SC model are experimentally validated.

(4) Simulation. Compared with the experimental, simulation enables a fast, convenient estimate of the performance metrics of large-scale systems such as the EV with DESS. Chapters 4 to 8 largely use the simulated outcomes of the EV with DESS to analyse the energy management (EM) and sizing problems proposed in this work.

## 3.2 Methodology of energy management

The EM chapter proposes an offline energy management strategy (EMS) as the optimal benchmark and designs an online EMS that can be adaptive to real-time driving conditions. The offline EMS aims to optimise the DESS operating costs and is solved by the dynamic programming algorithm. The solved offline EMS is analysed using methods of curve fitting and statistical analysis with the goal to inspire online EMS design. The online EMS is tuned through regression analysis and implemented by the combination of variable perception horizon, neural network (NN) and rule-based strategy. The variable perception horizon is demonstrated by the graphic method.

(1) Dynamic programming (DP) algorithm. DP is an optimisation algorithm that breaks down a complicated problem into simpler sub-problems. These sub-problems are strongly associated with each other because the solution to the former sub-problem would influence that to the later one. By achieving optimisation for each sub-problem, the overall problem can get a best-case solution [16]. Chapters 5, 6 and 8 tailor the DP algorithm into different forms to fit different problems. With the EM problem in Chapter 5, the DP is implemented with a one-dimensional form in Section 5.2.1 to find out the optimal offline energy management strategy (EMS).

(2) Curve fitting. Curve fitting is performed in Section 5.2.2, where the optimal offline EMS is analysed. Specifically, this work adopts the Shape Language Modeling [119] toolbox to perform the piecewise linear fitting.

(3) Statistical analysis. To characterise the optimal offline EMS, Section 5.2.2 sorts out the statistics under different driving conditions and analyses the similarities and differences hidden behind the statistics.

(4) Regression analysis. To find out the influence factors of online EMS, two groups of linear regression analysis are performed in Section 5.3.2, with each group estimating the relationships between one dependent variable and two independent variables.

(5) NN. The development of artificial intelligence in recent years leads to the NN techniques being growingly applied to the area of EM. Basically, the NN techniques can be exploited in terms of data clustering, data fitting, pattern recognition, and time series [120]. This work applies the NN data fitting to make predictions and assist in designing an online EMS in Section 5.3.2.

(6) Rule-based control strategy. The rule-based strategy has been reviewed in Section 2.3.2, and it is used as a framework to integrate the whole online EMS in Section 5.3.3.

(7) Graphic method. This work involves quite a few graphic representations to assist the understanding of texts or formulas. With the EM problem, Section 5.3.1 provides a timing chart to explain the variable perception horizon, Section 5.3.2 offers a schematic diagram to assist formula derivations, and Section 5.3.3 gives a flow chart to demonstrate the whole online EMS.

## 3.3 Methodology of sizing

The sizing chapter proposes the sizing approach based on dynamic programming algorithm to determine the optimal size of battery pack and SC pack. Furthermore, this chapter sorts out different factors and analyses how and why DESS sizing is sensitive to these factors, i.e., sensitivity analysis. Specifically, EV drive cycle is one of the factors, and its analysis involves the use of fuzzy logic algorithm.

(1) Dynamic programming algorithm. Based on the one-dimensional DP algorithm implemented for EM optimisation in Section 5.2.1, Section 6.2.2 expands the DP algorithm with two more dimensions accounting for DESS size, forming a joint EM-sizing optimisation framework.

(2) Sensitivity analysis. This work performs sensitivity analysis to determine how DESS sizing is affected by changes in different input factors. Specifically, Section 6.3 adopts the one-at-a-time technique [121], analysing the influence of one varying factor on DESS sizing at a time while keeping the other factors invariant.

(3) Fuzzy logic algorithm. The fuzzy logic algorithm can be regarded as an improved version of the rule-based strategy. Like the rule-based strategy, the fuzzy logic algorithm also uses prescribed rules, but these rules are defined by the membership functions [19]. This work applies the fuzzy logic algorithm in Section 6.3.1.1 to recognise the intensity of driving conditions by accepting the power and energy demands.

## 3.4 Methodology of battery degradation

The battery degradation chapter aims at the EM and sizing benchmarks to minimise battery degradation. The benchmarks are expected to be widely applicable to different cases using various EV, battery, and SC parameters. Therefore, this chapter starts with general assumptions and uses the graphic method and formula derivations to obtain general benchmarks.

(1) Graphic method. Section 7.2 uses two schematic diagrams and formula derivations to demonstrate the EM benchmarks for a DESS to minimise battery degradation.

(2) Formula derivation. Section 7.3 performs formula derivations specifically in partial derivatives to work out the general trends of battery degradation with DESS component size.

## 3.5 Methodology of Aluminium DESS

The Aluminium DESS chapter generalises the modelling, EM and sizing methodologies and applies the generalised methodologies to the DESSs using Aluminium batteries. The semiempirical modelling approach proposed in Chapter 4 is adapted to fit the Aluminium DESSs. The dynamic programming algorithm is also adapted to solve the joint EM-sizing optimisation of Aluminium DESSs.

(1) Semiempirical modelling. Section 8.2 reuses and modifies the modelling methodology of Li-ion battery and SC to fit for the modelling of Al-ion battery and Aluminium DESS.

(2) Dynamic programming algorithm. The DP algorithm developed in Section 6.2.2 is adapted in Section 8.3.3.3, solving the joint EM-sizing optimisation of Aluminium DESSs.

# Chapter 4 Modelling and validation

This work develops improvements to electric vehicle (EV) operation via investigation of energy management (EM) and sizing of a dual energy storage system (DESS). The research area of EV with DESS is complex, and experimental tests of the whole system are time-intensive and costly [122]. In contrast, simulation tests enable a fast, convenient estimate of the performance metrics of the EV and DESS, so as to assist the optimisation of EM and sizing [123]. The efficacy of simulation tests relies on robust modelling of the system; therefore, this chapter presents the modelling approach developed for EVs deploying DESS along with adapting ADvanced VehIcle SimulatOR (ADVISOR, a platform for vehicle simulation within MATLAB) to match and run the models, into which specific case studies are then introduced.

This chapter divides the whole EV model into DESS module (components: battery pack, SC pack, DC/DC converter, energy management strategy) and drivetrain module (components: motor and controller, drive cycle and vehicle dynamics, wheel and axle, final drive and gearbox, electrical accessory, power bus), while each module is further divided into different components, as Figure 15. With this hierarchical division, this chapter adopts a bottom-up modelling approach, i.e., each component is modelled separately, after which these components are grouped into modules, and finally into the combined EV model. The components and modules are validated by either simulation or experimental tests. The component of energy management strategy (EMS) is specifically studied in Chapter 5. The remainder of this chapter first introduces component modelling, followed by the integration of the whole EV model, and finally by the validation of the models.

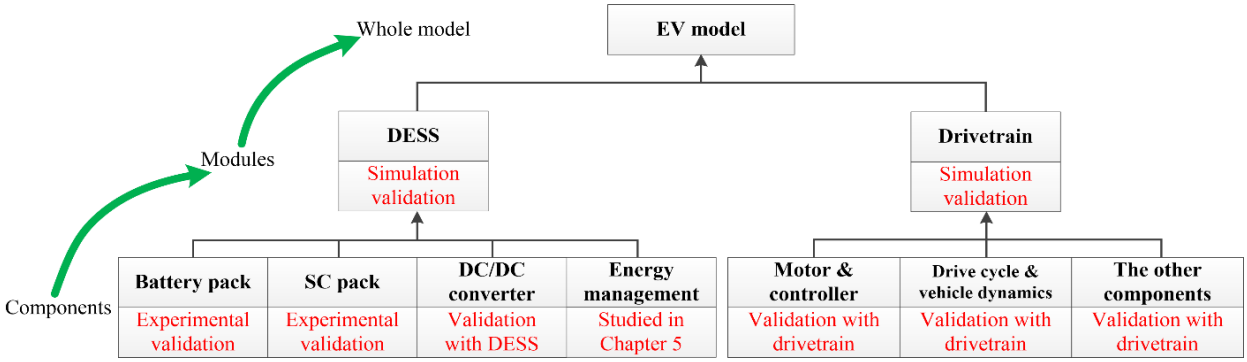


Figure 15 Hierarchical division of EV model and validation methods.

## 4.1 Modelling of components

ADVISOR requires numerical models that rely on component input/output relationships using empirical data collected in steady-state tests and then correcting them for transient effects [124, 125]. Therefore, this section focuses on explaining the assumptions and equations to formulate the input/output relationships. In this work, bespoke models of the core DESS components (the battery,

SC and DC/DC converter) are developed and explained. In contrast, the other components are modelled using existing templates within ADVISOR.

### 4.1.1 Battery model

As discussed in Section 2.2.1.1, the Rint equivalent circuit model (Figure 16) is adopted to represent electrical characteristics (power, voltage, current, resistance, state of charge) of the battery. Besides, battery degradation is expected to be estimated, so that battery degradation is also modelled on the basis of the Rint model.

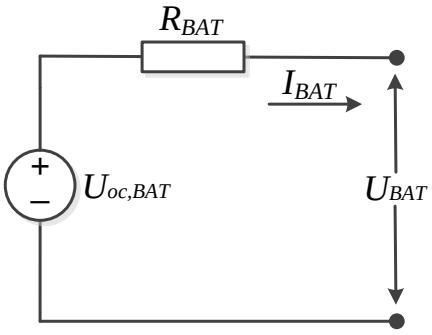


Figure 16 Rint equivalent circuit model for battery modelling.

#### 4.1.1.1 Battery electrical modelling

Based on the Rint model in Figure 16, battery electrical modelling follows the assumptions below. The battery is a charge reservoir and an equivalent circuit whose parameters are a function of the state of charge (SOC) and ambient temperature. The equivalent circuit accounts for the battery's circuit parameters as if it were a perfect open-circuit voltage source in series with the internal resistance. The amount of charge that the battery can hold is taken as constant. The amount of charge that is required to replenish the battery after discharge is affected by coulombic efficiency. The charging of the battery is limited by the maximum battery voltage. Power delivered by the battery is limited to the maximum that the equivalent circuit can deliver or the maximum that the motor controller can accept, given its minimum voltage requirement. Power loss is computed as $I^2R$ losses plus losses due to coulombic efficiency [126].

The input/output relationships of the battery are expressed as follows.

1) Battery open-circuit voltage ($U_{oc,BAT}$) and internal resistance ($R_{BAT}$) are computed as piecewise linear functions of the SOC. The functions are defined by empirical data, while the general case is that $U_{oc,BAT}$ increases with growing SOC while $R_{BAT}$ increases with declining SOC [43]. If given battery current ($I_{BAT}$), battery terminal voltage ($U_{BAT}$, also known as battery voltage) can be expressed as:

$$U_{BAT} = U_{oc,BAT} - I_{BAT} R_{BAT} \tag{11}$$

2) If given $U_{BAT}$ and $I_{BAT}$, battery power ($P_{BAT}$) can be calculated as:

$$P_{BAT} = U_{BAT} I_{BAT} \tag{12}$$

3) If given $P_{BAT}$, $I_{BAT}$ can be calculated by solving the equation set of (11) and (12), as:

$$I_{BAT} = \frac{U_{oc,BAT} - \sqrt{U_{oc,BAT}^{\ 2} - 4R_{BAT}P_{BAT}}}{2R_{BAT}} \tag{13}$$

4) If given $I_{BAT}$, battery SOC ($SOC_{BAT}$) can be updated as (14). Where $SOC_{BAT,0}$ is the initial SOC of the battery. $I$ is the current in ampere-hour integration, and its value equals $I_{BAT}$ if the battery discharges or needs to multiply battery coulombic efficiency ($\eta_{BAT}$) if the battery charges [11].

$$\begin{cases} SOC_{BAT} = SOC_{BAT,0} - \dfrac{1}{3600}\displaystyle\int \frac{I}{Ah_{BAT}}\, dt \\ I = \begin{cases} I_{BAT}, & I_{BAT} \geq 0 \\ \eta_{BAT} I_{BAT}, & I_{BAT} < 0 \end{cases} \end{cases} \tag{14}$$

#### 4.1.1.2 Battery degradation modelling

As discussed in Section 2.2.1.2, this project adopts the expressions in (15) to model battery degradation. This returns battery the degradation coefficient ($\alpha$, in %, defined as the ratio between degraded battery capacity and original battery capacity) by accepting ambient temperature ($T$, in Kelvin), battery current rate ($I_{rate}$, in C, expressed as the ratio between absolute battery current $|I_{BAT}|$ and battery ampere-hour capacity $Ah_{BAT}$) and battery ampere-hour throughput ($Ah_{put}$, expressed as the product of absolute battery current $|I_{BAT}|$ and time $t$). $a$, $b$, $c$, $d$, $e$ are constants specific to the battery type and need to be identified. It can be seen from (15) that a high $I_{rate}$ can significantly enlarge $\alpha$ because $I_{rate}$ has an exponential correlation with $\alpha$ as well as a liner correlation with $Ah_{put}$.

$$\begin{cases} \alpha = \left(aT^2 + bT + c\right) exp\left[\left(dT + e\right) I_{rate}\right] Ah_{put} \\ I_{rate} = \left|I_{BAT}\right| / Ah_{BAT} \\ Ah_{put} = \left|I_{BAT}\right| t \end{cases} \tag{15}$$

Equations (15) are mainly applicable to current-invariant conditions [57]; however, DESS operation requires the battery current to fluctuate to satisfy changing power demands. Thus, for modelling battery degradation with variant battery current, this equation should be transformed into a discrete equation, and the procedure follows.

1) Assume that $I_{rate}$ is unchanged within each discrete step (if only the step can be short enough) [49]. The partial derivative of $\alpha$ to $Ah_{put}$ can be then expressed as (16).

$$\frac{\partial(\alpha)}{\partial(Ah_{put})} = \frac{\Delta\alpha}{\Delta Ah_{put}} = (aT^2 + bT + c)exp[(dT + e)I_{rate}] \tag{16}$$

2) Based on (16), the delta battery degradation coefficient within step i ($\Delta\alpha i$) can be transformed into a discrete equation, as (17), where $I_{rate,i-1}$ and $\Delta Ah_{put,i-1}$ are the current rate and delta ampere-hour throughput within step i-1.

$$\Delta\alpha_i = (aT^2 + bT + c)exp[(dT + e)I_{rate,i-1}]\Delta Ah_{put,\,i-1} \tag{17}$$

3）Following (17), $\alpha$ can be expressed as the accumulation of $\Delta\alpha_i$ over all steps, as below:

$$\alpha = \sum_{i=1}^{n}(\Delta\alpha_i) \tag{18}$$

### 4.1.2 SC model

Similar to the battery model, the Rint equivalent circuit approach (Figure 17) is adopted to represent electrical characteristics (power, voltage, current, capacitance, resistance, SOC, state of energy) of the SC. The assumptions for SC modelling are as follows. The SC is a charge reservoir and an equivalent circuit whose parameters are a function of ambient temperature. The equivalent circuit accounts for the SC's circuit parameters as if it were a perfect capacitance in series with the internal resistance. The amount of charge that the SC can hold is taken as constant. The amount of charge that is required to replenish the SC after discharge is affected by coulombic efficiency. The charging of the SC is limited by the maximum SC voltage. Power delivered by the SC is limited to the maximum that the equivalent circuit can deliver or the maximum that the motor controller can accept, given its minimum voltage requirement. Power loss is computed as $I^2R$ losses plus losses due to coulombic efficiency [126].

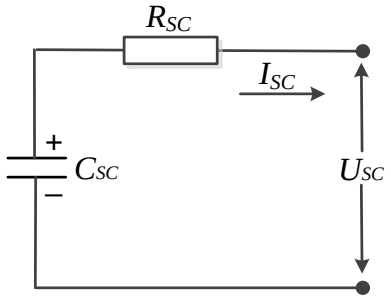


Figure 17 Rint equivalent circuit model for SC modelling.

The input/output relationships of the SC are expressed as follows.

1) SC capacitance ($C_{SC}$) and internal resistance ($R_{SC}$) are computed as piecewise linear functions of ambient temperature, which are defined by empirical data. If given SC current ($I_{SC}$), SC open-circuit voltage ($U_{oc,SC}$) and SC terminal voltage ($U_{SC}$, also known as SC voltage) can be expressed as:

$$\begin{cases} U_{oc,SC} = \dfrac{\int I_{SC} dt}{C_{SC}} \\ U_{SC} = U_{oc,SC} - I_{SC} R_{SC} \end{cases} \tag{19}$$

2) If given $U_{SC}$ and $I_{SC}$, SC power ($P_{SC}$) can be calculated as:

$$P_{SC} = U_{SC} I_{SC} \tag{20}$$

3) If given $P_{SC}$, $I_{SC}$ can be calculated as:

$$I_{SC} = \frac{U_{oc,SC} - \sqrt{U_{oc,SC}^{\ 2} - 4R_{SC}P_{SC}}}{2R_{SC}} \tag{21}$$

4) If given $U_{oc,SC}$, SC SOC ($SOC_{SC}$) can be calculated as (22) [102], where $U_{SC,max}$ is the maximum voltage (equal to nominal voltage) of SC.

$$SOC_{SC} = \frac{U_{oc,SC}}{U_{SC,max}} \tag{22}$$

5) Apart from $SOC_{SC}$, the state of energy (*SOE*, defined as the ratio between available energy and nominal energy capacity) of the SC is formulated using (23). The significance of *SOE* exists in the perspective of EM. Compared with $SOC_{SC}$, *SOE* is more sensitive to the change of voltage and thus fluctuates more dramatically. Therefore, *SOE* is more used as the control variable in EM of SC [127].

$$SOE = SOC_{SC}^{\ 2} = \frac{U_{oc,SC}^{\ 2}}{U_{SC,\max}^{\ 2}} \tag{23}$$

6) Different from batteries, SCs may undergo significant self-discharge, reflected by the leakage current or open-circuit voltage drop at non-service status [9]. This work performs experiments to characterise SC self-discharge. The Maxwell BCAP0650 2.7V SC is used, whose parameters can be found in Table II. In experiments, the SC is firstly held at a sustaining voltage for more than 2 hours and then cut off as an open circuit. The open-circuit voltage of SC is recorded with standing time, and the experiments repeat with different sustaining voltage. The experimental results are listed in Table IV, where the first row represents a series of sustaining voltage; the first column represents standing time, which ends at 30 minutes because all the vehicle drive cycles involved in this thesis

are less than 30 minutes; the other cells in Table IV represent the open-circuit voltage of SC at given sustaining voltage and standing time.

Table IV SC open-circuit voltage with sustaining voltage and standing time.

| | **2.7V** | **2.6V** | **2.5V** | **2.4V** | **2.3V** | **2.2V** | **2.1V** | **2.0V** |
|---|---|---|---|---|---|---|---|---|
| **0** | 2.700V | 2.600V | 2.500V | 2.400V | 2.300V | 2.200V | 2.100V | 2.000V |
| **5 min** | 2.699V | 2.599V | 2.499V | 2.399V | 2.299V | 2.199V | 2.099V | 1.999V |
| **10 min** | 2.698V | 2.599V | 2.498V | 2.399V | 2.299V | 2.199V | 2.099V | 1.999V |
| **15 min** | 2.698V | 2.598V | 2.498V | 2.399V | 2.298V | 2.198V | 2.099V | 1.999V |
| **20 min** | 2.698V | 2.598V | 2.498V | 2.398V | 2.298V | 2.198V | 2.098V | 1.998V |
| **25 min** | 2.698V | 2.598V | 2.498V | 2.398V | 2.298V | 2.198V | 2.098V | 1.998V |
| **30 min** | 2.698V | 2.598V | 2.498V | 2.398V | 2.298V | 2.198V | 2.098V | 1.998V |

Table IV indicates that the voltage change caused by SC self-discharge over 30 minutes is only 0.002V. According to (22) and (23), the change of SOE caused by SC self-discharge over 30 minutes is about $5.5*10^{-5}$%, which is too subtle to be considered in SC modelling. Hence, this work does not consider SC self-discharge due to its tiny impacts on SC modelling.

### 4.1.3 DC/DC converter model

The DC/DC converter plays a vital role in coordinating the power, voltage and current between the battery pack and SC pack [72]. This project focuses on modelling the conversion efficiency of DC/DC converter because it directly impacts energy losses and energy consumption of DESS, which further affects the EM and sizing of DESS [125]. In contrast, the design of power electronic circuits or the implementation of gating signals is less concerned because they have little contribution to EM or sizing [128]. The assumptions in DC/DC converter modelling are as follows. The DC/DC converter adopts a hypothetical half-bridge bidirectional buck-boost architecture [125] as if it had no lag in frequency response and were capable of accomplishing any power conversion requirement, given the target step-up/down ratio [129]. The DC/DC converter model accepts the power converted and the voltage ratio between the battery pack and SC pack and returns a conversion efficiency [74]. The voltage of battery pack is considered the same as that of bus so that the voltage ratio is equivalent to the SC pack voltage divided by bus voltage. As a general case, Figure 18 shows the DC/DC conversion efficiency as a piecewise linear function of power and voltage ratio [129].

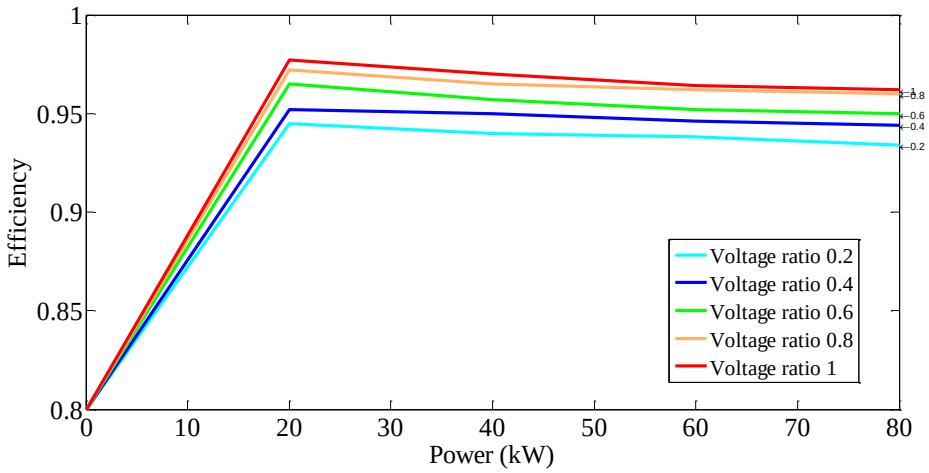


Figure 18 DC/DC conversion efficiency as a function of power and voltage ratio adapted from [31].

### 4.1.4 Models of the other components

#### 4.1.4.1 EMS

The EMS of DESS is responsible for splitting total energy/power demands from the bus to the battery pack and SC pack [130]. Once the bus proposes an energy/power request, the EMS will determine how much power/energy should be provided by the battery and SC, respectively, so that the total energy/power can satisfy vehicle propulsion. The development of EMS is a complicated process because optimisation problems (e.g., minimising battery degradation) are usually considered along with designing the EMS. In this case, the designing and modelling of EMS are specifically studied in Chapter 5. For running the whole EV model, this chapter provisionally uses the rule-based EMS reviewed in Section 2.3.2.

#### 4.1.4.2 Motor and controller

The motor and controller is the drivetrain terminal, where electric inputs are transformed into mechanical outputs [131]. This project duplicates the motor and controller templates in ADVISOR. The motor template includes the relationships between electric power and mechanical speed/torque, as well as the loss data and rotational inertia [32]. The controller template implements the inverter's control functions, which prevents the motor from requesting more current than it can handle and shuts the motor off if the EV is not moving [132]. This project considers motor efficiency as a function of rotor speed and torque. As a general case, Figure 19 shows the motor efficiency map of the AC induction motor of Tesla Model S P85 [1, 133].

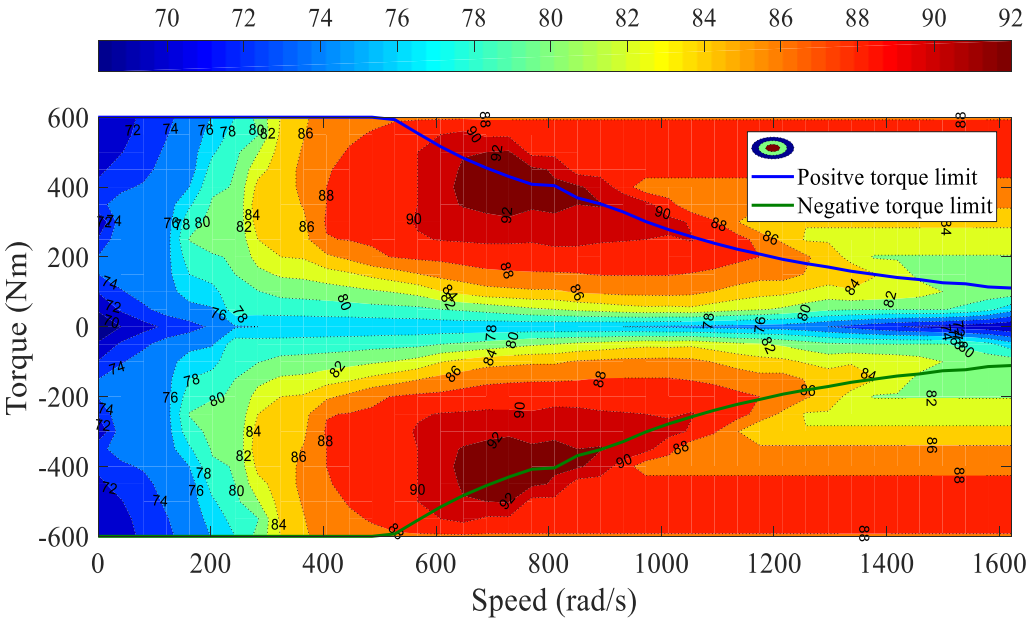


Figure 19 Motor efficiency as a function of rotor speed and torque (from the AC induction motor of Tesla Model S P85) [1, 133].

#### 4.1.4.3 Drive cycle and vehicle dynamics

The drive cycle defines the longitudinal speed with time for the EV to follow. The Society of Automotive Engineers (SAE) has formulated various drive cycles for vehicle tests [134]. As a general case, this project adopts three standard drive cycles that are recommended for measurement of (equivalent) fuel consumption by the US Environmental Protection Agency (EPA) [135]: UDDS (Urban Dynamometer Driving Schedule), HWFET (Highway Fuel Economy Test) and US06 (an aggressive, high-speed and rapid-acceleration drive cycle), as Figure 20. However, the standard drive cycles have different durations and diverse statistic characteristics, making it difficult to distinguish the difference among these cycles and tell which cycle is more challenging than the other [136]. To better compare the influence of different drive cycles on the EM and sizing of DESS, this project also customises the "Strengthened-US06 (S-US06)" and "Weakened-US06 (W-US06)" drive cycles, as Figure 21. Using the US06 cycle as the baseline, the S-US06 and W-US06 drive cycles are derived from the US06 cycle via a multiplication/division coefficient. The S-US06 cycle comes from the product of the US06 cycle and a coefficient of 1.45 (this coefficient is determined to fit for the top speed of the studied Tesla EV), while the W-US06 cycle comes from the US06 cycle divided by 1.45. The three cycles have the same timelines and tendencies; thus, it is evident that S-US06 is the most challenging drive cycle, while W-US06 is the least challenging one.

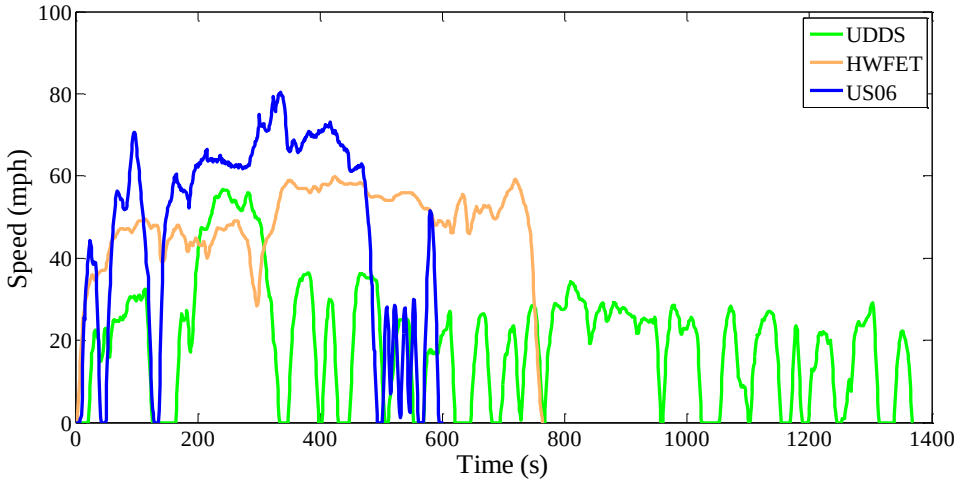


Figure 20 Typical drive cycles for vehicle tests: UDDS, HWFET and US06.

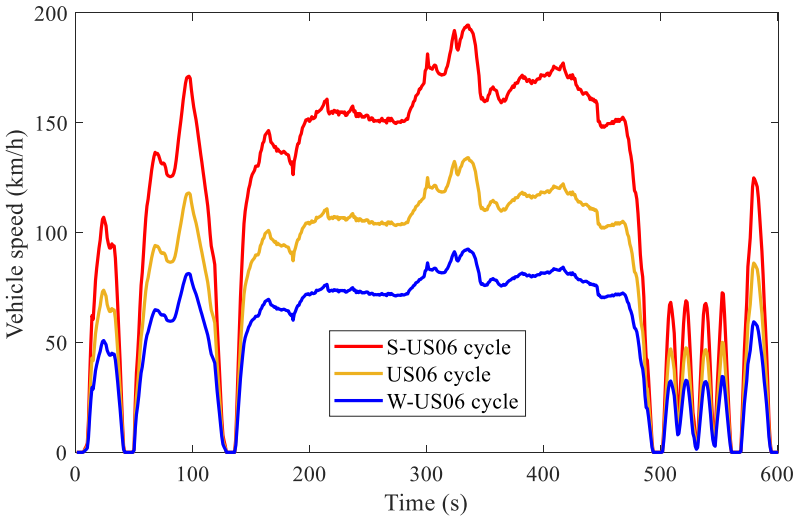


Figure 21 S-US06, US06 and W-US06 drive cycles.

The vehicle dynamics is responsible for longitudinal force balance. Given the prescribed drive cycle, vehicle tractive force ($F_T$) can be worked out as (24). Where $F_r$ is rolling resistance force. $F_d$ is aerodynamic drag force. $F_a$ is the acceleration force. $M_{veh}$ is vehicle mass. $g$ is the gravity coefficient. $f$ is the rolling resistance coefficient. $C_D$ is air drag coefficient. $A_{veh}$ is the vehicle front area, $v$ is vehicle speed. $\delta$ is the correction coefficient of rotating mass [3].

$$F_T = F_r + F_d + F_a = M_{veh} g f + 0.613 C_D A_{veh} v^2 + \delta M_{veh} \frac{dv}{dt} = 0 \quad (24)$$

4.1.4.4 The other drivetrain components

The wheel, axle, final drive and gearbox constitute the vehicle transmission system that transmits speed/torque between the motor and the wheel. The change of rotate speed via the transmission system is affected by the transmission ratio, while the torque loss via the system is affected by transmission efficiency [137].

The electrical accessory represents the dedicated auxiliary load systems powered by an electrical source. This project considers no auxiliary loads in the EV. The power bus collects the power requests from both the motor and the electrical accessory loads and then requires power from the DESS. With no accessory loads, the power correlation between the power bus and DESS should satisfy (25), where $P_{bus}$, $P_{BAT}$, $P_{SC}$ are the power of bus, battery pack and SC pack, respectively, $\eta_{DCDC}$ is DC/DC conversion efficiency [138].

$$P_{bus} = \begin{cases} P_{BAT} + P_{SC} \cdot \eta_{DCDC}, & P_{SC} > 0 \\ P_{BAT} + P_{SC} / \eta_{DCDC}, & P_{SC} \le 0 \end{cases} \tag{25}$$

## 4.2 Integration of EV model

The component models are integrated into the DESS module and drivetrain module, respectively, and further into an EV model specific to ADVISOR. The integration and workflow of the EV model are described. Besides, solutions to adapt ADVISOR for running the EV model are provided.

### 4.2.1 Integration and workflow

Figure 22 shows the integrated EV model composed of the drivetrain module and DESS module. The drivetrain module contains drive cycle, vehicle dynamics, wheel and axle, final drive, gearbox, motor and controller, electric accessory, power bus. The DESS module adopts the SC/battery topology (reviewed in Section 2.2.3.3) and contains EMS, battery pack, SC pack and DC/DC converter. With ADVISOR, the EV model runs in a "backwards-facing" manner [139], which means that the simulation starts with prescribed vehicle speed versus time trace, and each component performs in reverse to meet the required trace from the drive cycle to DESS. The workflow of the EV model with ADVISOR is explained as follows.

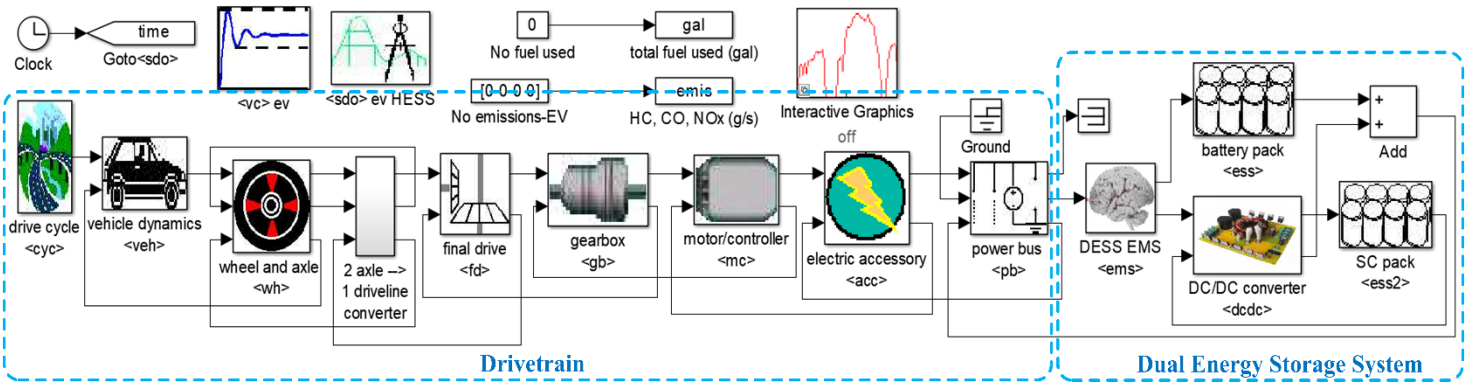


Figure 22 The integrated EV model in ADVISOR.

1) The simulation of EV begins with the drive cycle, where vehicle speed with time is specified and passed to the vehicle dynamics. The vehicle dynamics works out the required tractive force in response to the given drive cycle and then transmits the requirement to the wheel and axle.

2) The wheel and axle convert the required vehicle speed and tractive force into rotate speed and tractive torque, respectively. The rotate speed and torque requirements are transmitted through the wheel and axle, final drive and gearbox to the motor. In the meanwhile, the transmission ratio and efficiency of each component are taken into account.

3) The motor accepts the rotate speed and torque requirements and returns a power request for traction. The electrical accessory also proposes a power request. After adding up both power requests, the total power request is transmitted through the power bus to the DESS EMS.

4) The EMS distributes the total power request to the battery pack and SC pack, respectively, based on offline/online rules or algorithms. Details of EMS are presented in Chapter 5.

5) The battery pack accepts its power share, using which to calculate battery electrical and degradation characteristics. After checking performance limits, the battery pack returns an achieved power output back to the power bus.

6) The power share distributed to the SC pack first goes into the DC/DC converter. By considering DC/DC conversion efficiency, the DC/DC converter works out the actual power that should be provided by the SC pack and passes the actual power request to the SC pack.

7) The SC pack accepts the actual power request, using which to calculate SC electrical characteristics. After checking performance limits, the SC pack returns an achieved power output via DC/DC converter to the power bus.

8) The power bus collects the achieved power from both the battery pack and SC pack and then transmit the achieved total power frontwards along the drivetrain. Finally, the vehicle dynamics works out the achieved vehicle speed and tractive force.

### 4.2.2 Adaptation of ADVISOR

For successfully running the EV model with ADVISOR, some more adaptations are presented below.

(1) ADVISOR allows the user to select drivetrain type among front/rear/full -wheel drive in the vehicle input interface. However, the rear-wheel drive for EV seems to be broken, in which case the power loss of wheels and axle loss goes negative. ADVISOR developers have reported this bug in [140]. To fix this bug, the rear-wheel drive for EV is implemented by the methodology in [141].

(2) To activate the SC pack as the second energy storage in ADVISOR, specific codes must be added into the load file [123], as follows:

```
vinf.energy_storage2.name='ESS2_UCPro_Maxwell'; % locate the file defining variables of SC %
vinf.energy_storage2.ver='saber';          % version of SC must be ‘saber’ %
vinf.energy_storage2.type='pb';            % type of SC must be ‘pb’ %
```

(3) The variables of SC can only be named with the prefix “ess2” [141]. Otherwise, ADVISOR cannot recognise the variables of SC.

(4) ADVISOR initialises any newly added vehicle model as an internal combustion engine (ICE) vehicle model and thus declares some components that do not exist in EVs, such as the engine and exhaust system. The following line should be added into the “InputFig.m” file to remove unnecessary component declarations:

```
fields2remove={'fuel_converter','generator','exhaust_aftertreat','torque_coupling';

% remove the engine, generator, exhaust system and torque coupling off EV drivetrain %
```

(5) For ADVISOR to transform the EV electricity consumption into the equivalent fuel (petrol) consumption, two properties of the petrol must be declared in addition [125], as follows:

```
fc_fuel_lhv=749;          % lower heating value of petrol, J/g %
fc_fuel_den=42600;        % density of pertrol, g/L %
```

## 4.3 Validation of models

This section validates the models of components and modules depicted in Figure 15. Regarding component models, the battery model and the SC model are validated in particular, respectively, by experiments on the cell level. The other component models do not have standalone validation since they are modelled based on ADVISOR templates [40]. Regarding module models, the drivetrain model and DESS model are validated, respectively, by analysing the simulation results from a case-study EV, Tesla Model S P85 [1, 131, 133]. Results demonstrate that the models have high accuracy (detailed in the following) so that they are capable of assisting further study in the following chapters.

### 4.3.1 Validation of battery model and SC model

The validation of the battery/SC model follows the procedure set out in Figure 23. Explanations follow.

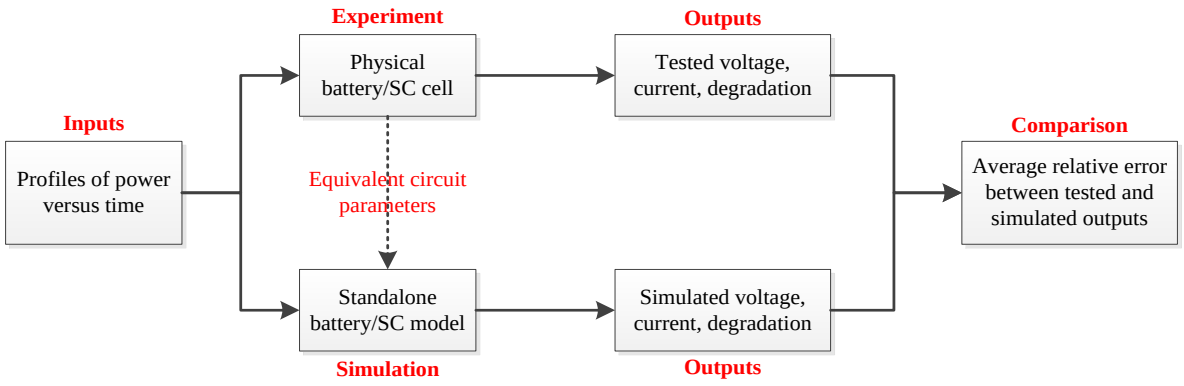


Figure 23 Procedure to validate battery/SC model.

1) Inputs. The profiles of power versus time are designed as the inputs for validation. Targeted at challenging the robustness of the battery/SC model, the profiles have high power amplitude approaching the maximum power capability of the battery/SC and intense variations fluctuating within the maximum power capability. Considering the battery and SC have different characteristics (e.g., the SC is power-intense while the battery is energy-intense), the profiles for the battery and SC are tailored, respectively.

2) Experiment. A battery/SC cell is used for testing under the prescribed power profiles. The testing for battery/SC aims at the voltage and current with time. Besides, the battery testing also acquires battery degradation with power cycling, and the testing methods are described in Section 4.3.1.1. All the testing is performed with the Maccor battery analyser [142] at 20℃, and the battery/SC is brand new and is fully charged to 100% SOC before any testing.

3) Equivalent circuit parameters. Apart from the testing under power profiles, another group of testing is performed to characterise the equivalent circuit parameters of the battery/SC, which are then used to initialise the battery/SC model for simulation. The parameters characterised for the battery are open-circuit voltage with SOC, equivalent resistance with SOC and coulombic efficiency, while for the SC, they are capacitance, equivalent resistance and coulombic efficiency. These parameters are tested according to the hybrid power pulse characterisation (HPPC) procedure issued in [143].

4) Simulation. Rather than using the whole EV model for simulation, the standalone battery/SC model is extracted and simulated. The characterised equivalent circuit parameters and the same power profiles for experiments are used as the inputs for the standalone simulation of the battery/SC.

5) Outputs and comparison. The tested and simulated voltage, current and degradation (degradation is only for the battery) are then acquired from experiment and simulation, respectively. The accuracy of the battery/SC model is assessed by the average relative error between tested and simulated outputs.

#### 4.3.1.1 Validation of battery model

1) Inputs. The power profile for validating the battery model is shown in Figure 24, designed based on the power demands for each battery cell of Tesla Model S P85 under the S-US06 drive cycle (presented in Figure 21). The battery energy throughput with time is also shown in Figure 24.

2) Experiment. The experiment uses EFEST IMR 18650 3500mAh battery, whose specifications are listed in Table V [144].

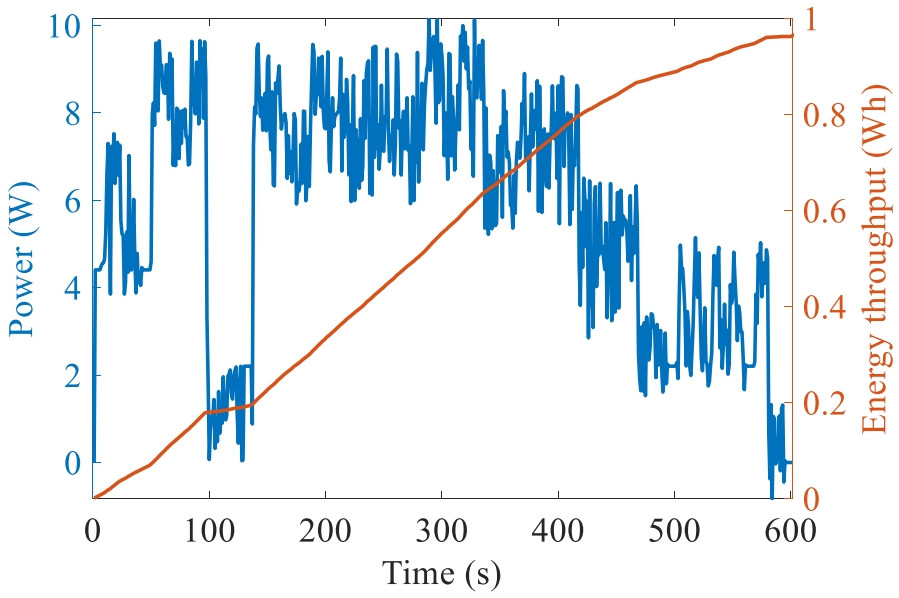


Figure 24 Profile of power versus time for validation of battery model.

Table V Specifications of EFEST IMR 18650 3500mAh battery [144].

| | |
|---|---|
| Nominal capacity | 3.5 Ah, 13 Wh |
| Voltage range | 2.5 V – 4.2 V |
| Nominal voltage | 3.7 V |
| Maximum charge/discharge current | 4 A / 10 A |
| Maximum power | 37 W |

The testing methods for battery degradation with power cycling are presented as a flowchart in Figure 25, and explanations follow. As the battery fulfils a one-off operation following the power profile in Figure 24, it is considered that the battery has completed one power cycle. The battery repeats more power cycles until the number of completed cycles reaches 10, in which case battery SOC drops to around 20%, and the battery will be fully charged following HPPC procedure [143]. After charging, the battery performs more power cycles until 200 cycles completed, in which case, the battery capacity test will be conducted, and the battery degradation coefficient can be then calculated as a function of the total cycle number. After the battery is fully charged again, the loop continues so that more battery degradation coefficient data with the total cycle number can be acquired.

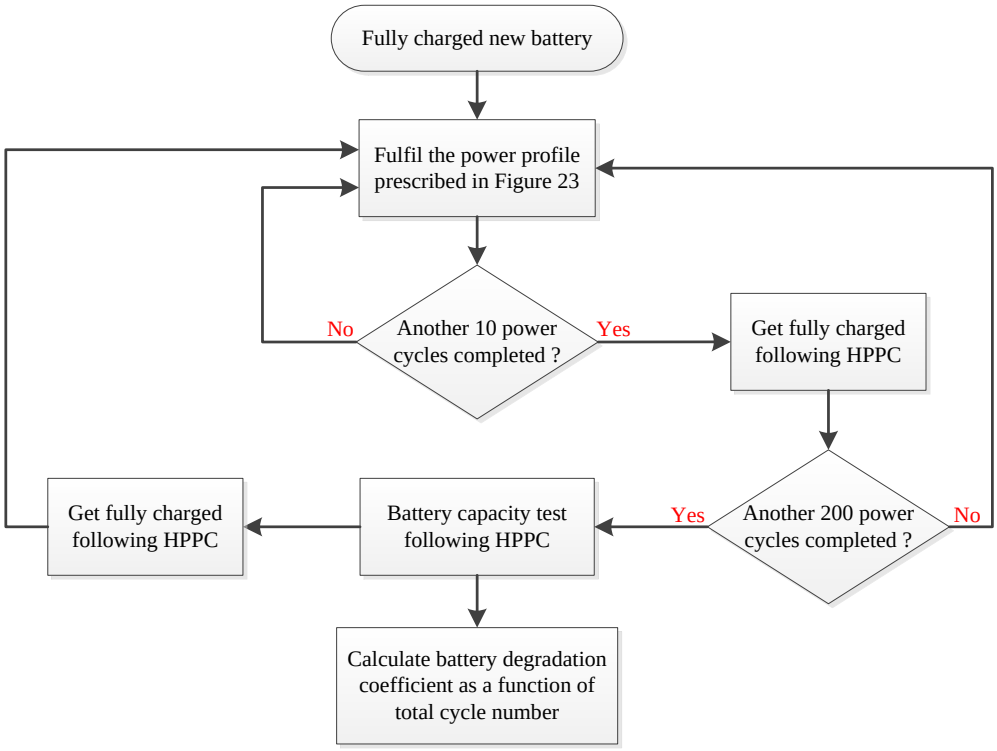


Figure 25 Flowchart of testing battery degradation with power cycling.

3) Equivalent circuit parameters. Battery open-circuit voltage and equivalent resistance with SOC are tested using HPPC procedure [143], as Figure 26. The coulombic efficiency of the battery is tested as 96%.

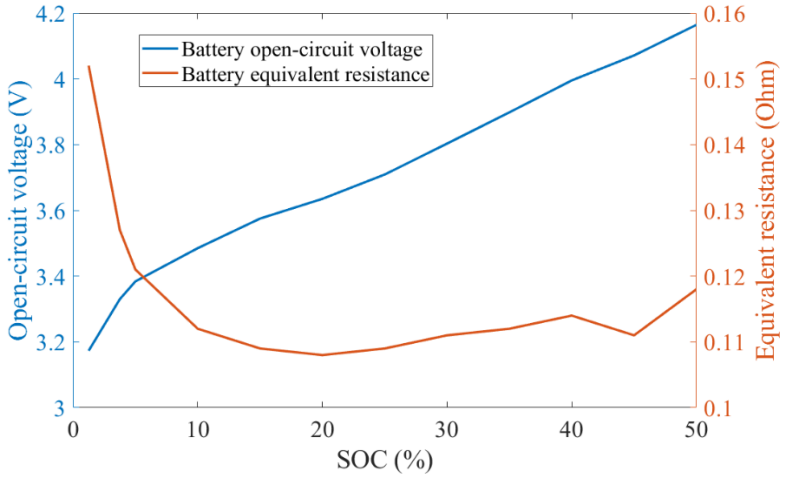


Figure 26 Battery open-circuit voltage and equivalent resistance with SOC.

4) Simulation. The battery model in Section 4.1.1 is used for standalone simulation.

5) Outputs and comparison. Figure 27 (a) and (b) plot the simulated battery voltage and current compared to the tested ones, respectively. The simulated voltage and current are very close to the tested ones, and the average relative error (relative error is the absolute error divided by the magnitude of the tested value; average relative error is the relative errors over the datasheet being

averaged) for voltage and current are 0.20% and 2.05%, respectively, which indicates that the battery model has high accuracy for emulating battery electrical characteristics. Figure 28 compares the simulated battery degradation coefficient with the tested one. The simulated battery degradation is near-linear and is obtained by equations (15) to (18), where *a*, *b*, *c*, *d*, *e* are tuned as $8.9*10^{-7}$, $5.3*10^{-4}$, $.7.9*10^{-2}$, $-6.7*10^{-3}$ and 2.35. Specifically, the coefficients are tuned by finding the least square error between the simulated and tested battery degradation data. The testing of battery degradation ends at 6000 cycles because battery degradation almost reaches 20% at this point, in which case the battery is usually considered end-of-life [44]. The average relative error for battery degradation is 3.69%, which indicates that the battery model can emulate battery degradation characteristics with high accuracy. Compared with the simulated battery degradation, the tested battery degradation grows faster at the beginning of the whole cycling test and slows down at the end, which is the primary cause of errors.

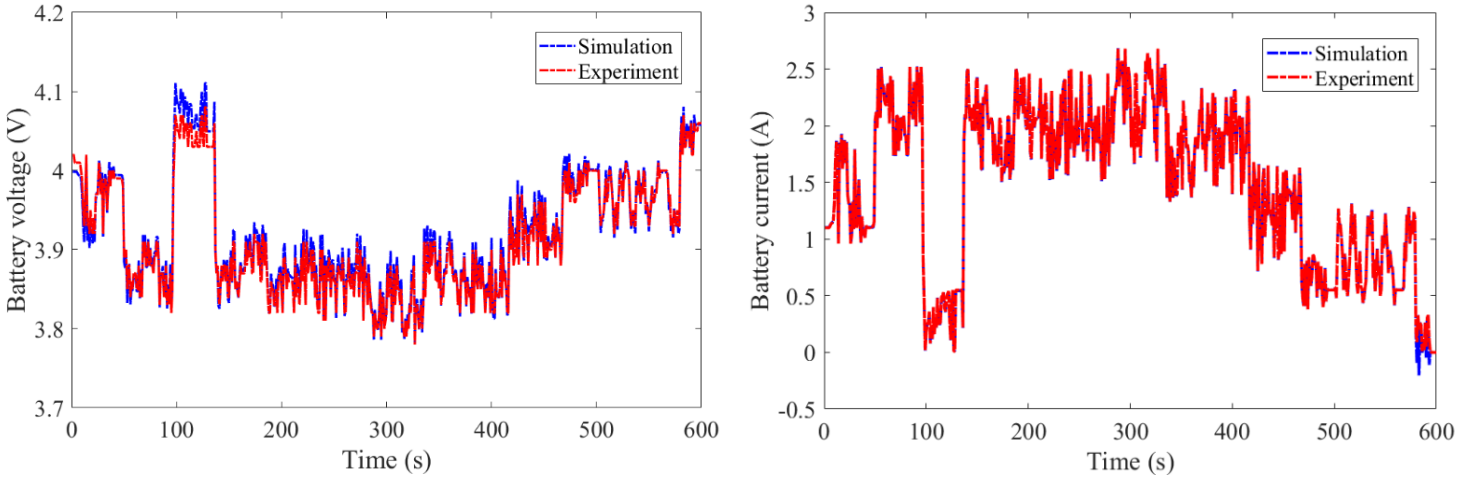


Figure 27 Simulation versus experiment: (a) battery voltage; (b) battery current.

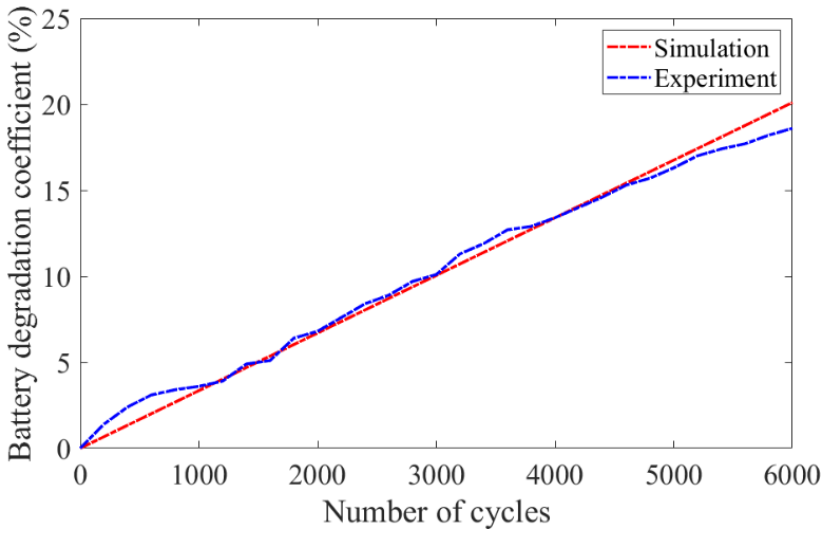


Figure 28 Simulation versus experiment: battery degradation coefficient.

4.3.1.2 Validation of SC model

1) Inputs. Figure 29 shows the power profile for validating the SC model. This profile is designed with the following considerations. Firstly, since the SC is good at handling power pulses, this profile involves rapid, dramatical shifts between positive and negative power to validate the SC model's accuracy in the case of power burst. Secondly, this profile also involves gradual slopes of power, representing the case of mild change of power. Lastly, since SC has a small energy capacity (0.658 Wh, as Table III), this profile alternates positive and negative power to avoid depleting or overcharging the SC.

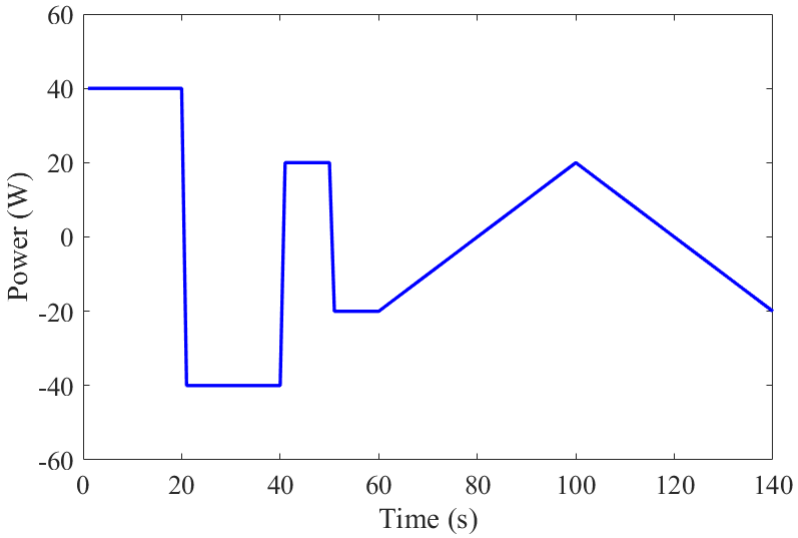


Figure 29 Profile of power versus time for validation of SC model.

2) Experiment. Maxwell BCAP0650 2.7V SC is used, and its specifications are in Table II [62]. It should be noted that a maximum limit for SC voltage (2.7V) is enforced in the experiment, aiming to prevent the SC from being charged by a voltage beyond its tolerance. In other words, the maximum charge voltage for the SC is controlled as 2.7V.

Table VI Specifications of Maxwell BCAP0650 2.7V SC [62].

| | |
|---|---|
| Nominal capacity | 650 F, 0.658 Wh |
| Voltage range | 0 – 2.7 V |
| Nominal voltage | 2.7 V |
| Maximum charge/discharge current | 680 A |
| Maximum power | 1088 W |

3) Equivalent circuit parameters. The capacitance, equivalent resistance and coulombic efficiency of SC at 20℃ are tested as 650F, 0.018 Ohm and 99% using HPPC procedure [143], respectively.

4) Simulation. The SC model in Section 4.1.2 is used for standalone simulation.

5) Outputs and comparison. The simulated SC voltage and current are compared with the tested ones in Figure 30 (a) and (b), respectively. In Figure 30 (a), the initial SC voltage is set at 2.4V rather than at the maximum voltage (2.7V), because the SC is expected to be charged during experiments and a lower initial voltage can give more flexibility to SC charging. Figure 30 (a) shows that the SC is charged to the maximum voltage (2.7V) at around 40 seconds and then the SC voltage is limited at the maximum voltage. The limitation of SC voltage leads to a sudden limitation of SC current, reflected by a sharp slope in Figure 30 (b) at around 40 seconds. The simulated and tested outputs have small gaps between each other. The average relative error for SC voltage is 1.09%, while that for SC current is 1.55%. This indicates that the SC model is capable of emulating SC electrical characteristics.

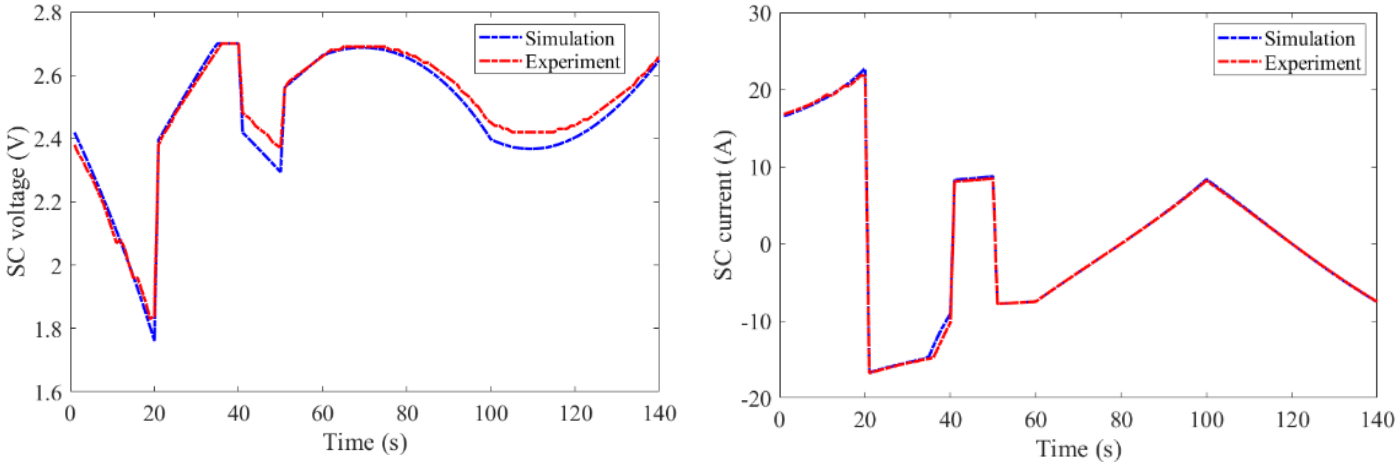


(a) (b)

Figure 30 Simulation versus experiment: (a) SC voltage; (b) SC current.

### 4.3.2 Validation of drivetrain module and DESS module

The drivetrain module and DESS module are validated by using them to simulate the performances of Tesla Model S P85 EV as a case study, and the procedure follows.

1) Drivetrain module validation. The original Tesla EV deploys a battery-only ESS. Using design parameters of the drivetrain and ESS of the original Tesla EV, EV performances can be simulated in terms of acceleration ability and equivalent fuel economy. The drivetrain module can be validated by checking the relative errors between the simulated performances and the official performance statements.

2) DESS module validation. Substituting the battery-only ESS with a DESS, the performances of hypothetical DESS Tesla EV can be simulated. The DESS Tesla EV can be regarded as an extension of the original Tesla EV by incorporating a DC/DC converter and a SC pack, while the drivetrain is identical for both EVs. By analysing the difference between the original and DESS Tesla EVs, the

DESS module can be validated if the performances of DESS Tesla EV demonstrate reasonable evolutions from those of the original Tesla EV.

The drivetrain and motor parameters of the Tesla EV, which are used in the simulation, are listed in Table VII and Table VIII. The original Tesla EV adopts Panasonic NCR 18650B battery in its battery-only ESS, and parameters of the battery are presented in Table IX. This project adopts Maxwell BCAP3400 2.7V SC in the hypothetical DESS Tesla because it is a high-capacitance SC widely applied in automotive applications [145], and its parameters are also shown in Table IX. The DC/DC converter parameters used in modelling are listed in Table X [13]. The ESS configurations of the original and DESS Tesla EVs are compared in Table XI. Lastly, the UDDS drive cycle is used in the simulation of both EVs.

Table VII Drivetrain parameters of Tesla Model S P85 EV [1, 131, 133].

| | |
|---|---|
| Drivetrain type | Rear-wheel drive |
| Vehicle mass | 2146 kg |
| Top speed | 250 km/h |
| Acceleration (0-100 km/h) | 4.4 s |
| Driving range | 426 km (EPA) |
| Rolling resistance coefficient | 0.0089 |
| Air drag coefficient | 0.24 |
| Front area | 2.838 $m^2$ |
| Correction coefficient of rotating mass | 1.1 |
| Transmission ratio | 9.73 : 1 |
| Transmission efficiency | 85% |
| Wheel/Tyre type | 245/45 R19 98V |

Table VIII Motor parameters of Tesla Model S P85 EV [1, 133].

| | |
|---|---|
| Motor type | AC Induction |
| Voltage range | 240V - 350V |
| Maximum power | 310 kW |
| Maximum rotate speed | 15480 rad/s |
| Maximum torque | 600 Nm |
| Over torque factor | 1.8 |
| Rotor inertia | 0.0433 $kgm^2$ |
| Mass | 80 kg |
| Efficiency | Figure 19; 88% average |

Table IX Parameters of Panasonic NCR18650B battery [146, 147] and Maxwell BCAP3400 2.7V SC [145].

| | **Panasonic NCR18650B battery** | **Maxwell BCAP3400 2.7V SC** |
|---|---|---|
| Nominal voltage (V) | 3.6 | 2.7 |
| Voltage range (V) | 2.5 – 4.2 | 0 – 2.7 |
| Maximum current (A) | 6.50 | 2600 |
| Maximum power (W) | 23.40 | 3800 |
| Capacity (Ah) | 3.25 | 1.27 |
| Energy (Wh) | 11.70 | 3.44 |
| Mass (g) | 76 | 513 |
| Volume (mL) | 16.54 | 390 |
| Coulombic efficiency (%) | 95 | 99 |
| Resistance (Ohm) | 0.036 | $2.2*10^{-4}$ |
| Price (USD/kWh) | 300 | 15000 |

Table X Parameters of the DC/DC converter used in modelling [13].

| Gravimetric power density | Volumetric power density | Unit Price | Conversion efficiency |
|---|---|---|---|
| 3.81 kW/kg | 1.74 kW/L | 20 USD/kW | Figure 18; 92% average |

Table XI ESS configurations of the original and DESS Tesla EVs.

| | **Original Tesla EV** | **Hypothetical DESS Tesla EV** |
|---|---|---|
| ESS connection | 96s 74p [a](battery pack) | 96s 74p (battery pack) 40s [b](SC pack) |
| ESS maximum power | 332kW [c](battery pack) | 166kW [d](battery pack) + 152kW [e](SC pack) |
| ESS energy capacity | 83.12kWh [f] | 85kWh (battery) + 0.14kWh [g](SC) |
| ESS initial conditions | Battery SOC=100% [h] Temperature=20°C [j] | Battery SOC=100%, SC SOE=50% [i] Temperature=20°C |
| ESS EMS | Battery-only strategy | Rule-based controller [k] |

a: 96s 74p means that the pack has 96 cells in series and 74 cells in parallel. This connection follows the original battery pack connection of Tesla Model S P85 [1, 131, 133].
b: This SC pack connection is associated with DESS sizing, which is determined later in Section 6.2.3.
c: This maximum power is confirmed in response to the original maximum current rate of battery cell (4C).
d: This maximum power is confirmed in response to a reduced maximum current rate of battery cell (2C).
e: This maximum power is confirmed in response to the maximum power of SC cell (3.8kW).
f: This energy capacity is confirmed in response to the energy capacity of battery cell (11.7Wh).
g: This energy capacity is confirmed in response to the energy capacity of the SC cell (3.44Wh).
h: The battery pack is initially full of charge, which is the common practice in most research [49, 148].
i: The SC pack is initially half of charge following the charge-sustaining principle [87].
j: The initial temperature is set at the common temperature used in most research [45].
k: The rule-based controller adopts the one reviewed in Section 2.3.2.

#### 4.3.2.1 Validation of drivetrain module

The simulated EV performances are compared with the official performance statements of Tesla Model S P85, as Table XII. It can be seen that the relative error of top speed exceeds 10%. However, the top speed in official statements is not necessarily the maximum speed that can be achieved by vehicle dynamics. The determination of practical top speed involves other considerations such as safety and vehicle bodywork tolerance, which limits the officially stated top speed to below the simulated one [3]. Except for the top speed, the other relative errors are all below 7%. For the simulation of a complex system such as the EV, these errors are within the confidence interval [134]; therefore, the drivetrain module is considered precise and is consequently validated.

Table XII Comparison of official performance statements and simulated performances for the original Tesla Model S P85 [1, 131, 133].

| | **Official statements** | **Simulation results** | **Relative error** |
|---|---|---|---|
| 0 - 100 km/h time (s) | 4.4 | 4.1 | 6.8 % |
| Maximum acceleration ($m/s^2$) | 7.0 | 6.9 | 1.4 % |
| Top speed (km/h) | 250 | 277 | 10.8 % |
| Equivalent fuel consumption (L/100km) | 2.67 | 2.60 | 2.6 % |

#### 4.3.2.2 Validation of DESS module

The simulated performances of the original and DESS Tesla EVs are compared in terms of equivalent fuel economy and acceleration ability, as Table XIII. The overall vehicle efficiency is the product of drivetrain efficiency and ESS efficiency. It can be seen that the DESS Tesla EV has a lower overall efficiency than the original Tesla EV; since both EVs use the same drivetrain module, this means the efficiency of DESS is lower than that of battery-only ESS. This can be explained by considering the DC/DC conversion efficiency: the energy into/out of the SC pack has to pass through the DC/DC converter, in which case extra energy loss happens because of the DC/DC conversion efficiency [13]. Another reason is that the EMS used in the DESS Tesla EV is a preliminary rule-based controller rather than an optimal EMS targeting improving DESS efficiency. The observation of equivalent fuel consumption indicates that the DESS consumes more energy than the battery-only ESS. This observation can be attributed to the overall vehicle efficiency, as well as the truth that DESS Tesla EV is a bit heavier than the original Tesla EV due to the incorporation of DC/DC converter and SC pack. In terms of 0-100km/h time and maximum acceleration, both EVs witness no much difference from each other. However, the DESS Tesla EV needs a bit more time to accelerate from 0 to 250km/h and has a slightly lower top speed because it is a bit heavier than the original Tesla EV. The simulated performances of the DESS Tesla EV show reasonable evolutions from those of the original Tesla EV so that the DESS module is validated.

Table XIII Comparison of the original and DESS Tesla EVs in terms of equivalent fuel economy and acceleration ability.

| | | **Original Tesla EV** | **Hypothetical DESS Tesla EV** |
|---|---|---|---|
| Equivalent fuel economy | Overall vehicle efficiency (%) | 39.5 | 36.2 |
| | Equivalent fuel consumption (L/100km) | 2.6 | 3.1 |
| Acceleration ability | 0 - 100km/h time (s) | 4.1 | 4.1 |
| | 0 - 250km/h time (s) | 17.9 | 18.4 |
| | Maximum acceleration ($m/s^2$) | 6.9 | 6.9 |
| | Top speed (km/h) | 277.2 | 277.1 |

By respective validation of components and modules, the whole EV model is equivalently validated.

### 4.3.3 Summary

In summary, this chapter models an EV with a DESS. The core components of DESS (battery, SC and DC/DC converter) are tailored and modelled in particular. By adapting the ADVISOR program, the combined EV model is integrated for simulating the performance of the DESS and EV. The whole EV model is validated by combining experiments and simulation and will be used for assisting the EM and sizing of DESS in the following chapters.

# Chapter 5 Energy management

The dual energy storage system (DESS) can be regarded as a plant with two controlled objects – battery pack and supercapacitor (SC) pack, plus an actuator – DC/DC converter. The control strategy of DESS, which has also named the energy management strategy (EMS), is responsible for splitting the power demands from the electric vehicle (EV) to the battery pack and SC pack [47]. The fundamental requirement for the EMS is to sustain EV propulsion: as the EV proposes a power demand with time, the EMS will instruct the battery pack and SC pack to deliver respective power. In combination, the total power delivery should exactly meet EV power demand [96]. Beyond this point, there are two further requirements for the EMS, optimality and adaptiveness. The requirement of optimality aims to solve optimisation problems (OPs) such as minimising electricity consumption and battery degradation while sustaining EV propulsion [87]. The requirement of adaptiveness considers that real-life driving always has a degree of "future uncertainty", leading to unpredicted power demands, so that the EMS should be adaptive to real-time power demands [37].

Following the above requirements, this chapter designs an online EMS that minimises the long-term operating costs of DESS and can be adaptive to real-time EV driving conditions. This is broken down into four subsections, as explained below and shown in Figure 15:

1) Section 5.1 introduces the case-study EV, DESS and ten drive cycles for which the EMS is designed. The specification of EV and size of DESS must be placed before designing the EMS since the EMS is specific to EV specification and DESS size [149]. Ten different drive cycles typical of three kinds of driving conditions are adopted for EV operations. Moreover, the OPs embedded in the EMS are formulated as the long-term operating costs of DESS, which is defined as the financial costs caused by electricity consumption and battery degradation.

2) Section 5.2 targets the requirement of optimality for the EMS and tailors the dynamic programming (DP) approach to solve the optimal DESS long-term costs under ten different drive cycles. The DP optimally distributes the power demands from the EV to the battery pack and SC pack, with the overreaching goal of minimising DESS long-term costs, and the optimal EMS is thus obtained. It should be noted that DP requires prior knowledge of the entire drive cycle before performing optimisation; hence, the optimal EMS solved by DP can only be used as an offline benchmark but cannot be an online implementable EMS. However, the significance of optimal offline EMS lies in its inspiration to online EMS design since the optimal offline EMS may have specific characteristics that can be imitated and implemented into the online EMS, and this is analysed in Section 5.2.

3) Section 5.3 targets the requirement of adaptiveness for the EMS and proposes the adaptive online EMS. The proposed EMS has three components: (1) the variable perception horizon to capture

consistent driving behaviour. (2) the neural network (NN) to predict the threshold for battery-SC power splitting. (3) the rule-based strategy to imitate the optimal offline EMS. Compared with existing studies, the proposed EMS features flexible perception, intelligent rulemaking and reduced complexity.

4) Section 5.4 demonstrates the control performances of the proposed EMS under two extra drive cycles, compared with two comparative online EMSs and the offline optimal EMS. Specifically, the control performances are sorted out into cost optimisation performance, perception performance, prediction performance and imitation performance. Results show that the performances of the proposed EMS are comparable with the optimal offline EMS.

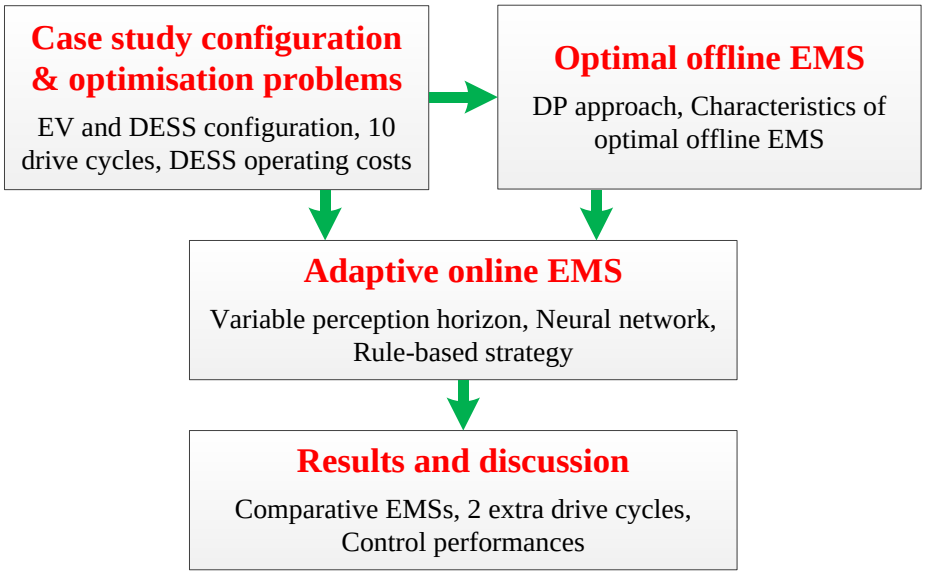


Figure 31 Structure of the chapter.

## 5.1 Case study configuration and optimisation problems

This section introduces the case-study EV, DESS and ten drive cycles and formulates the DESS long-term costs as the sum of electricity consumption costs and battery degradation costs.

### 5.1.1 Case study configuration

The EV uses Tesla Model S P85 (Table VII, Table VIII), and the DESS adopts SC/battery topology (Figure 11) with Panasonic NCR 18650B battery (Table IX), Maxwell BCAP3400 2.7V SC (Table IX) and a hypothetical DC/DC converter (Table X). The size and initial conditions of DESS follow Table XI, which is determined by the optimal sizing in Section 6.2.3. Ten different drive cycles are used, and their vehicle velocity and EV power demands are plotted in Figure 32.

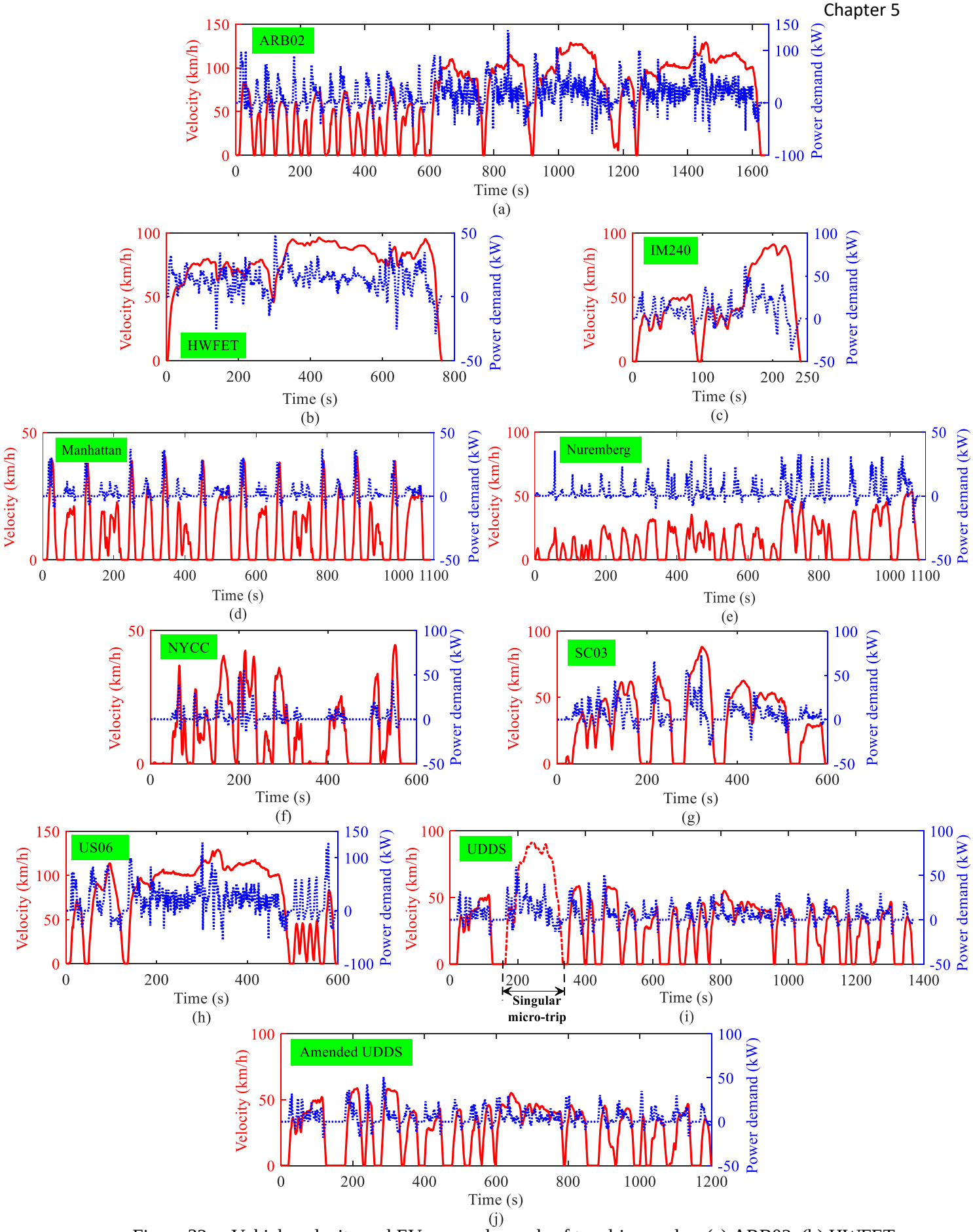


Figure 32 Vehicle velocity and EV power demands of ten drive cycles: (a) ARB02, (b) HWFET, (c) IM240, (d) Manhattan, (e) Nuremberg, (f) NYCC, (g) SC03, (h) US06, (i) UDDS, (j) Amended UDDS.

The ten drive cycles include nine standard drive cycles that are close to real-life driving behaviour (ARB02, HWFET, IM240, Manhattan, Nuremberg, NYCC, SC03, US06, UDDS) and one amended drive cycle (Amended UDDS). These drive cycles are typical of three kinds of driving behaviour: urban (Manhattan, Nuremberg, NYCC, UDDS and Amended UDDS), suburban (IM240 and SC03) and highway (ARB02, HWFET and US06) [150]. As shown in Figure 32 (i) and (j), the Amended UDDS is transformed from UDDS by removing the "singular micro-trip" that is plotted by a dashed red curve. The micro-trip is defined as an excursion between two successive time points at which a vehicle is stopped [151], while the singular micro-trip refers to the micro-trip that is significantly different from the others in terms of velocity and power. It can be seen from Figure 32 (i) that the singular micro-trip is considerably different from the other micro-trips in UDDS and breaks the consistency of driving behaviour. Its maximum vehicle velocity and EV power demand are much higher than those of the other micro-trips and may thus influence the EMS. The Amended UDDS in Figure 32 (j) is tailored to investigate whether one singular micro-trip can make a big difference to the optimal offline EMS.

### 5.1.2 Optimisation problems

The optimisation problems are unified as the long-term operating costs of DESS, which are the financial costs accumulated with the DESS service [152]. In this regard, electricity consumption and battery degradation with EV driving are considered two causes of DESS long-term costs. The corresponding costs are electricity consumption costs ($J_{Elec}$) and battery degradation costs ($J_{BAT}$).

As (26), $J_{Elec}$ is calculated as the product of DESS electricity consumption ($Q_{DESS}$) and electricity price ($Price_{Elec}$, considered as 0.1 USD/kWh [45]), where $Q_{BAT}$ and $Q_{SC}$ are the electricity consumption of the battery pack and SC pack. $E_{BAT}$ and $E_{SC}$ are the energy capacity of the battery pack and SC pack. $\Delta SOC$ and $\Delta SOE$ are the delta state-of-charge of the battery pack and delta state-of-energy (SOE, defined as the remaining energy divided by the rated energy capacity) of the SC pack.

$$\begin{cases} J_{Elec} = Q_{DESS}\, Price_{Elec} = (Q_{BAT} + Q_{SC})\, Price_{Elec} \\ Q_{BAT} = E_{BAT}\Delta SOC \\ Q_{SC} = E_{SC}\Delta SOE \end{cases} \tag{26}$$

As (27), $J_{BAT}$ is calculated as the product of battery energy capacity loss ($E_{loss}$, the lost energy capacity caused by battery degradation) and battery price ($Price_{BAT}$, considered as 300 USD/kWh [14]). Besides, a divisor of 20% is used because the battery pack reaches end-of-life and loses all values when $E_{loss}$ becomes 20% of the original battery energy capacity [153]. $E_{loss}$ is further calculated as the product of the original battery energy capacity ($E_{BAT}$) and battery degradation coefficient ($\alpha$, defined as $E_{loss}$ divided by $E_{BAT}$). $\alpha$ is calculated as a function of battery current rate ($I_{rate}$) and battery ampere-hour throughput ($Ah_{put}$), based on the representations formulated in Section 4.1.1.2, where

the temperature ($T$) is considered invariant at 293K (20℃) and the other coefficients ($a$, $b$, $c$, $d$, $e$) are tuned by the least square error method described in Section 4.3.1.1.

$$\begin{cases} J_{BAT} = E_{loss}\, Price_{BAT} / 20\% \\ E_{loss} = E_{BAT}\alpha \\ \alpha = \dfrac{1}{2364} exp\left(\dfrac{I_{rate}}{2525}\right) Ah_{put} \end{cases} \tag{27}$$

The DESS long-term costs ($J_{long}$) are the sum of electricity consumption costs and battery degradation costs, as (28). It should be noted that $J_{Elec}$, $J_{BAT}$ and $J_{long}$ keep growing with EV driving, and the unit for each is USD/100km in this chapter. However, in Chapters 6, 7 and 8, the unit is USD (/150000km) because in those chapters, the $J_{Elec}$, $J_{BAT}$ and $J_{long}$ are assessed throughout EV lifetime while EV lifetime mileage is considered as 150000km [70].

$$J_{long} = J_{Elec} + J_{BAT} \tag{28}$$

## 5.2 Optimal offline EMS

Before designing the online EMS, this section works out and analyses the optimal offline EMS for the ten known drive cycles. The DP approach is exploited to solve the optimal offline EMS. By analysing the optimal offline EMS, both general and specific control rules are extracted to guide online EMS design.

### 5.2.1 Design of DP approach for solving optimal offline EMS

The DP approach is to split the EV power demands between the battery pack and SC pack, while its objective is to minimise $J_{long}$. It accepts the case-study parameters as inputs, and then calculates the electrical characteristics of the battery pack, SC pack and DC/DC converter with time, using which to feed the objective function of $J_{long}$ and finally find out the optimal battery operating power and SC operating power (i.e., the optimal offline EMS). Its formulation is as follows.

(1) Execution stage ($k$), represents the timeline in the solving process. Given that the drive cycle duration is from zero to $t_{end}$ seconds, $t_{end}$ stages can be established with one second time step. A smaller time step can increase solving accuracy but lower solving efficiency; one second time step is thus determined as a compromise between accuracy and efficiency.

$$k = 0,1,2,...,t_{end} \tag{29}$$

(2) Decision variable ($u$), is the controllable parameter which finding its values is the purpose of the optimisation efforts. Battery operating power $P_{BAT}$ is adopted as the decision variable, and it is constrained by the maximum power capability of battery pack $P_{BAT,\,max}$, as (30). Given the EV power

demands $P_{EV}$, the SC operating power $P_{SC}$ can be determined and constrained by (31), where $\eta_{DCDC}$ is DC/DC conversion efficiency. $P_{SC,\,max}$ is the rated power capability of the SC pack.

$$\begin{cases} u(k)=P_{BAT}(k) \\ \left|P_{BAT}(k)\right| \le P_{BAT,max} \end{cases} \tag{30}$$

$$\begin{cases} P_{SC}(k)=\begin{cases} \left[P_{EV}(k)-P_{BAT}(k)\right]/\eta_{DCDC}, & P_{EV}(k)-P_{BAT}(k)>0 \\ \left[P_{EV}(k)-P_{BAT}(k)\right]\eta_{DCDC}, & P_{EV}(k)-P_{BAT}(k)\le 0 \end{cases} \\ \left|P_{SC}(k)\right| \le P_{SC,max} \end{cases} \tag{31}$$

(3) State variable ($x$), is the variable used to describe the mathematical "state" of the DESS. The SOE of SC is used as the state variable, and it is constrained from 4% to 100% with a 1% interval. Namely, the minimum allowable SOE of SC is 4%, which corresponds to the minimum SOC of SC being 20% [154]. Following the charge-sustaining principle [87], the final stage SOE is set the same as the initial stage SOE at 50%, as (32). The charge-sustaining principle requires the SOE of SC pack to be controlled the same before/after the EV undertakes a drive cycle. This is because the SC pack is charged during driving rather than from an external power supply so that maintaining the SOE can enable the SC pack to better sustain the proceeding drive cycles in the future. The charge-sustaining principle can be realised in offline EM but should also be fulfilled as much as possible in online EM.

$$\begin{cases} 4\% \le x(k)=SOE(k) \le 100\% \\ SOE(t_{end})=SOE(1)=50\% \end{cases} \tag{32}$$

(4) State transfer function ($z$), is the function connecting the state variables in adjacent stages; it represents how the iteration evolves and is a function of the control variable. Since the time step is one second, the state transfer function can be expressed as (33).

$$z(k)=x(k)-x(k+1)=P_{SC}(k)/E_{SC}/3.6 \tag{33}$$

(5) The objective is ($O$) to minimise $J_{long}$ over the drive cycle. Based on (28), the objective function can be expressed as (34).

$$O=Min\sum_{k=1}^{t_{end}} J_{long}(k) \tag{34}$$

### 5.2.2 Analysis of optimal offline EMS and inspiration to online EMS

The DP solves the optimal DESS long-term operating costs ($J_{long}$) and the corresponding offline EMS for each drive cycle. The optimal $J_{long}$ is compared in Figure 33, while the optimal offline EMS is

presented in Figure 34, where the optimal operating power of the SC pack ($P_{SC}$, represented by hollow blue circles) is plotted as a function of EV power demands ($P_{EV}$). For every single $P_{EV}$, the DP determines the optimal $P_{SC}$ while the battery pack takes the residual power demand. Figure 34 also presents the best fit curve of $P_{SC}$, as represented by the red polyline. The best fit curve is acquired by using the piecewise linear fitting method of the Shape Language Modeling [119] toolbox, and the freedom of curve fitting is constrained by three preconditions: (1) The best fit curve can be divided into three linear regions, as represented by Regions I, II and III in Figure 34. (2) The boundary between Regions I and II is $P_{EV}$ =0. (3) The slope of Region II ($l_{II}$) is zero. These preconditions are determined by a rough observation of $P_{SC}$ distribution with $P_{EV}$; however, the preconditions can be validated as rational by the coefficient of determination for the best fit curve in Table XIV. Table XIV collects the statistics of the best fit curve under each drive cycle. Based on Figure 34 and Table XIV, the optimal offline EMS along with the curve fitting results under the ten drive cycles are discussed in terms of similarities and differences, as follows.

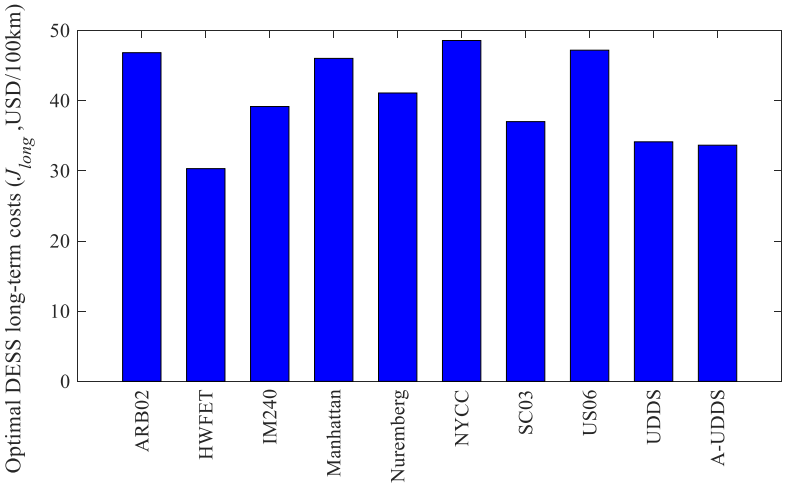


Figure 33 Optimal DESS long-term operating costs ($J_{long}$) under ten drive cycles.

Table XIV Statistics of the best fit curve under each drive cycle.

| | **Coefficient of determination $R^2$** | **Slope of Region I $l_I$** | **Slope of Region III $l_{III}$** | **Boundary between Regions II and III $P_{EV,\,bound}$** |
|---|---|---|---|---|
| **ARB02** | 0.9007 | 1.1496 | 0.9313 | 30.6 kW |
| **HWFET** | 0.9304 | 1.0105 | 1.0361 | 24.5 kW |
| **IM240** | 0.9811 | 0.9384 | 1.0804 | 22.8 kW |
| **Manhattan** | 0.9452 | 1.0009 | 1.0704 | 12.4 kW |
| **Nuremberg** | 0.9452 | 1.0072 | 1.0746 | 13.5 kW |
| **NYCC** | 0.9698 | 0.9908 | 1.0866 | 14.3 kW |
| **SC03** | 0.9620 | 0.9957 | 1.0171 | 21.0 kW |
| **US06** | 0.9152 | 1.1243 | 0.9827 | 34.6 kW |
| **UDDS** | 0.9196 | 0.9586 | 0.8536 | 17.2 kW |
| **Amended UDDS** | 0.9604 | 0.9745 | 1.0331 | 15.6 kW |

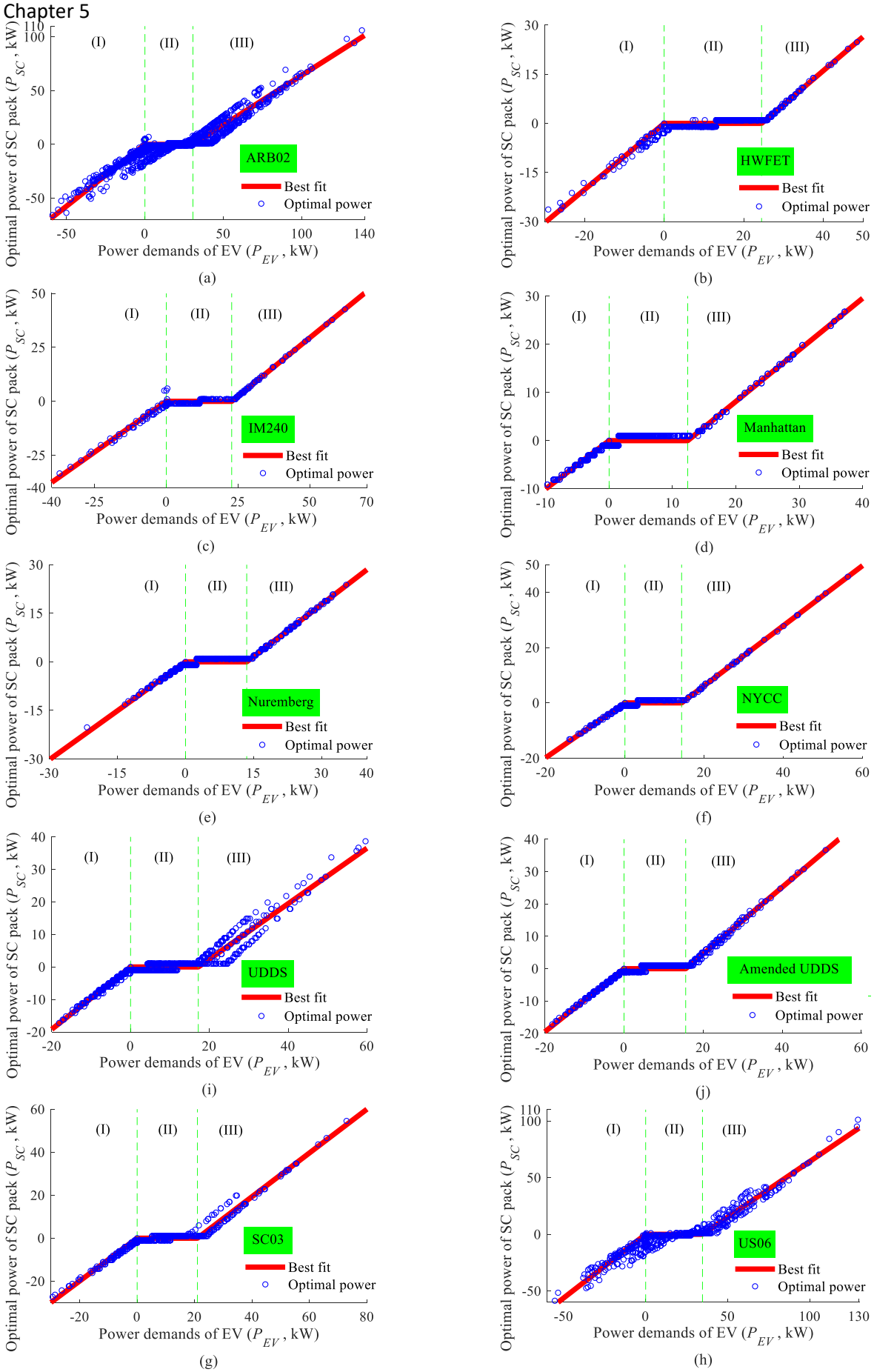


Figure 34 Optimal operating power of SC pack as a function of EV power demands, plus the best fit polyline under ten drive cycles: (a) ARB02, (b) HWFET (c) IM240, (d) Manhattan, (e) Nuremberg, (f) NYCC, (g) SC03, (h) US06, (i) UDDS, (j) Amended UDDS.

From the perspective of similarities, firstly, $P_{SC}$ can always be fitted as an "N-shape" function of $P_{EV}$, and the coefficient of determination ($R^2$) is always greater than 0.9, which indicates the "N-shape" curve fitting has high precision. Secondly, the slope of Region I ($l_I$) is always very close to 1, which means when $P_{EV}$ is below zero, $P_{SC}$ is approximately equal to $P_{EV}$. Thirdly, the slope of Region II ($l_{II}$) is zero, which means when $P_{EV}$ is between zero and the power boundary ($P_{EV,\,bound}$), $P_{SC}$ equals zero. Lastly, the slope of Region III ($l_{III}$) is always around 1, which means when $P_{EV}$ is greater than $P_{EV,\,bound}$, $P_{SC}$ approximately equals ($P_{EV}$ - $P_{EV,\,bound}$). These similarities imply that under the ideal EMS, the SC pack should absorb all the negative power demands and perform power peaking only if the positive power demands exceed $P_{EV,\,bound}$. The above similarities are summarised from ten standard drive cycles and thus can be general control rules for general driving conditions, which can be imitated by the online EMS and are realised in Section 5.3.3.

From the perspective of differences, firstly, the ARB02, US06 and UDDS have more divergent $P_{SC}$ distribution and thus are worse fitted, compared with the other drive cycles. This can be reflected by the evident outliers in Figure 34 or the $R^2$ in Table XIV, while can be explained by the comparison between UDDS and Amended UDDS. The UDDS has one singular micro-trip that breaks the consistency of driving behaviour, which obliges the optimal offline EMS to fit for mixed driving behaviour. As a result, the UDDS has a relatively divergent $P_{SC}$ distribution and a low $R^2$ at 0.9196. In comparison, the Amended UDDS only removes the singular micro-trip but consequently has less divergent $P_{SC}$ distribution and a significantly improved $R^2$ at 0.9604. Hence, even one singular micro-trip can dramatically impact the optimal offline EMS of the whole drive cycle. Inspired by this, when implementing the online EMS, every micro-trip should be taken into account separately; the perception horizon should not cover more than one micro-trip in case the singular micro-trips are averaged with the other micro-trips. This concern is realised by a variable perception horizon, which is illustrated in Section 5.3.1. Secondly, the $l_I$ and $l_{III}$ of ARB02, US06 and UDDS are more deviated from 1 than the other drive cycles. This can also be attributed to the consistency of driving behaviour. As can be seen from Figure 32, Figure 34 and Table XIV, the drive cycles with more consistent driving behaviour can have more congregate $P_{SC}$ distribution and more precise fit curve and thus enable the $l_I$ and $l_{III}$ to be closer to 1. Thirdly, the $P_{EV,\,bound}$ of each drive cycle varies considerably from 12.4 kW to 30.6 kW. As the boundary between Regions II and III, $P_{EV,\,bound}$ is a significant parameter determining whether the SC pack should output power. Inspired by this, when implementing the online EMS, the $P_{EV,\,bound}$ needs to be predicted accurately, and this is realised in Section 5.3.2. The above differences provide guides for tailoring the online EMS adaptive to different driving conditions.

Inspired by the above similarities and differences of the optimal offline EMS, the online EMS can be implemented by imitating the "N-shape" distribution of $P_{SC}$ with $P_{EV}$, while adjusting the perception horizon and predicting the $P_{EV,\,bound}$ in real-time. In other words, the real-time workloads

of the online EMS are only adapting the perception horizon and the $P_{EV,\ bound}$, which enables the online EMS to have low complexity of processing and fast response.

## 5.3 Adaptive online EMS

The online EMS is expected to optimise DESS long-term operating costs while offering battery-SC hybrid powering strategies for unforeseen driving conditions. Existing studies offer various approaches to design the expected online EMS successfully; however, there are limitations as summarised below. Firstly, existing studies rely too much on the collection and prediction of velocity-related driving states (e.g., average/standard deviation of positive/negative vehicle velocity [128]) but neglect the power-related ones. Using the collected velocity-related driving states, existing studies tend first to predict future vehicle velocity, based on which future vehicle power is then estimated [61]. Finally, the control strategies are determined by referring to the estimated power other than the predicted velocity, and the control actions are to manage future power other than future velocity. Therefore, the predicted velocity is actually an intermediate variable that has no direct impact on the control strategies, but the velocity-related intermediate transformations may retard the fast response of EMS [155]. In other words, the aim of EMS should come back to power management rather than velocity prediction. Secondly, most studies adopt a constant perception horizon to sense and process driving states [156] regardless of the singularity of micro-trips. The constant perception horizon may subdivide one micro-trip with consistent driving behaviour or group several micro-trips with very different driving behaviour. Consequently, control strategies are determined based on incomplete or mixed driving behaviour and thus have inferior optimality. Thirdly, most studies adopt redundant driving states to make predictions; for example, Ref. [157] uses as many as 17 driving states. However, these driving states are not always the necessary and efficient ones that can contribute much to accurate predictions. The adopted driving states should be proved helpful; otherwise, the unnecessary driving states can increase the onboard processors' computation loads. Lastly, some studies use offline control strategies of known driving conditions to fit for online new driving conditions [104] but fail to generate intelligent control strategies specifically adaptive to the new driving conditions. Targeted the above limitations, this section proposes an adaptive online EMS that optimises long-term operating costs of DESS in EVs, with the following contributions:

(1) Section 5.2.2 performs a deep analysis of the optimal offline benchmark to guide online EMS design. This refines effective control rules from the offline benchmark and exploits the control rules to enable a concise yet efficient online EMS.

(2) Section 5.3.1 proposes the variable perception horizon that can break down real-time driving conditions into successive driving behaviours. The consistent driving behaviours can be clustered as a whole to feed the online prediction, consequently improving the EMS optimality. In other words,

this work achieves better EMS optimality through adapting the perception horizon, something no existing literature has reported.

(3) Section 5.3.2 adopts a NN with significantly lowered complexity to realise the online prediction. The NN technique is chosen because this technique can decouple a great volume of computational loads from online calculations and pre-process them by offline training, something no other techniques can be comparable. The complexity of NN is reduced by only accepting the necessary inputs, which are refined through analytical deductions and regression analysis.

(4) The overall EMS in Section 5.3.3 can be easily implemented using simple hardware configurations. A workflow is suggested as one implementable hardware scheme to realise the proposed EMS. Simulation results indicate that the proposed EMS can achieve more than 97% cost optimisation efficacy of the offline benchmark.

Based on the analysis in Section 5.2.2, the EMS can leap from optimal offline to adaptive online by realising the following functions: (1) Capture the driving behaviour of every micro-trip; (2) Predict and update the power boundary $P_{EV,\,bound}$ in real-time; (3) Imitate the "N-shape" relationship between SC operating power and EV power demands. These functions are realised by the variable perception horizon, the NN fitting and the rule-based strategy, respectively. The graphical representation of the proposed online EMS is shown in Figure 35 and are explained in the following subsections.

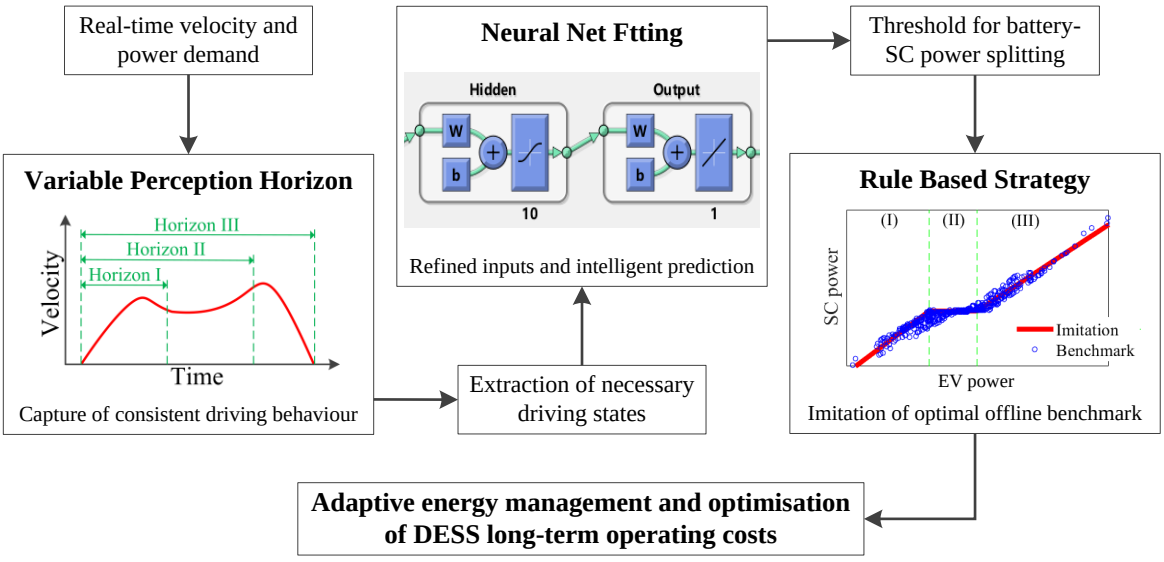


Figure 35 Graphical representation of the proposed adaptive online EMS.

### 5.3.1 Variable perception horizon to capture every micro-trip

This section designs a variable perception horizon, which divides the real-time driving conditions into successive micro-trips based on the consistency of driving behaviours. The consistent driving behaviours can be then captured to feed the prediction of $P_{EV,bound}$. In this section, the variable

perception horizon is described in terms of working principle, while the detailed implementation will be illustrated with the whole online EMS in Section 5.3.3.

The working principle of the variable perception horizon can be explained with Figure 36, where the velocity with time of a random drive cycle is depicted in red while the variable perception horizon is green. In general, each horizon is supposed to exactly contain one micro-trip, as Horizons I and II in Figure 36. Velocity sensing is needed to determine the horizon length since every micro-trip starts when the velocity grows from zero and ends when the velocity drops to zero. One exception is when the micro-trip is longer than 200 seconds, the horizon will end every 200 seconds until the micro-trip ends, and the length of the horizon is from the micro-trip start to the current end, as Horizons III, IV and V. Namely, the minimum update frequency of EMS is limited as once every 200 seconds, and this limit is in case the EV performs long cruises with no stops, in which case the EMS should be updated at set intervals. The minimum update frequency is inspired by the fact that most micro-trips end within 200 seconds except for the ones with long cruises, as shown in Figure 32. As each horizon ends, the driving behaviour of the current horizon will be extracted to enforce the prediction of $P_{EV,bound}$, as Predictions I to V. Each prediction returns a $P_{EV,bound}$ that will be used immediately until being updated by the next prediction, as $P^{I}_{EV,bound}$ to $P^{V}_{EV,bound}$ in Figure 36. Namely, the $P_{EV,bound}$ predicted by the current horizon will be used in the next horizon, with the hypothesis that the two adjacent horizons are probable to have similar driving behaviour [87] so that the driving behaviour of the current horizon can be used to determine the EMS for the next horizon. $P^{0}_{EV,bound}$ is the initial $P_{EV,bound}$ and set as 20.7 kW (the mean of the data in Table XII).

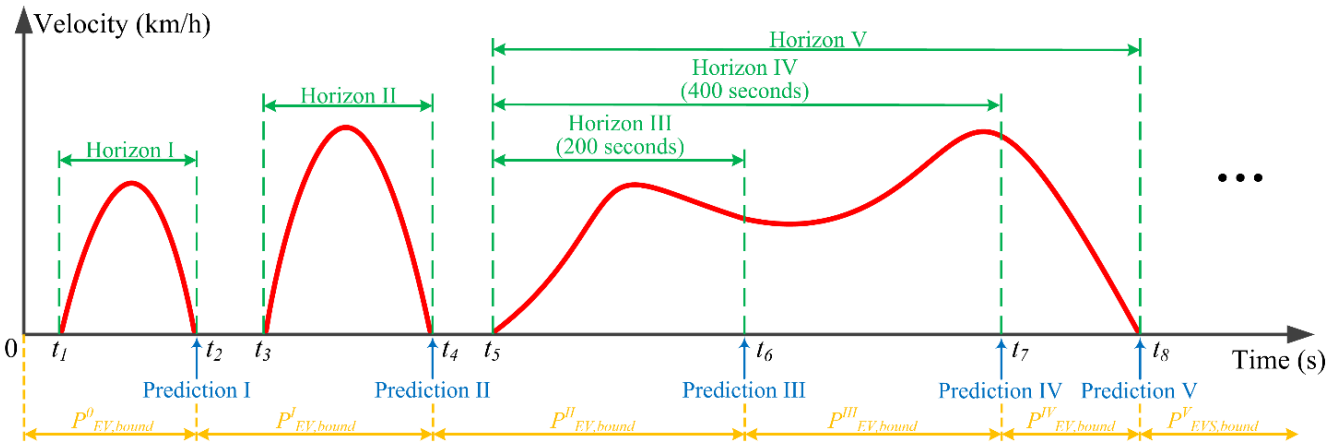


Figure 36 Explanation of the variable perception horizon with a random drive cycle.

Compared with the conventional constant perception horizon, the proposed variable perception horizon does not necessarily result in more horizons, which depends on the drive cycle used and will be demonstrated in Table XIX. In other words, the computational complexity of the variable perception horizon is subject to the specific drive cycle, while in general, the computational complexity of the variable perception horizon is close to that of the constant perception horizon.

### 5.3.2 Prediction of power boundary based on NN fitting

This section implements the NN fitting technique to realise the prediction of $P_{EV,bound}$. The implemented NN has a low complexity because it only accepts three necessary driving states refined through analytical deductions and regression analysis, as follows.

The analytical deduction follows on from the "N-shape" relationship discussed in Section 5.2.2. To make the deduction transparent, Figure 37 is plotted as a general schematic diagram derived from Figure 34, showing the optimal distribution of $P_{SC}$ with $P_{EV}$ under a random drive cycle. Similar to Figure 34, the optimal $P_{SC}$ in Figure 37 can be fitted into an "N-shape" polyline with three linear regions, and the slope of Regions I, II and III is 1, 0 and 1, respectively. It is assumed that the global $P_{EV}$ comprises a number of discrete power demands, and the number of discrete power demands lying in Regions I and III is $m$ and $n$, respectively, as denoted in Figure 37. According to Figure 37, the relationship between $P_{SC}$ and $P_{EV}$ in Regions I, II and III can be expressed as (35), (36) and (37). Where. $P^{I}_{SC}$, $P^{II}_{SC}$ and $P^{III}_{SC}$ are the optimal operating power of SC pack in Region I, II and III, respectively. $P^{I}_{EV}$, $P^{II}_{EV}$ and $P^{III}_{EV}$ are the total power demands of EV in Region I, II and III, respectively.

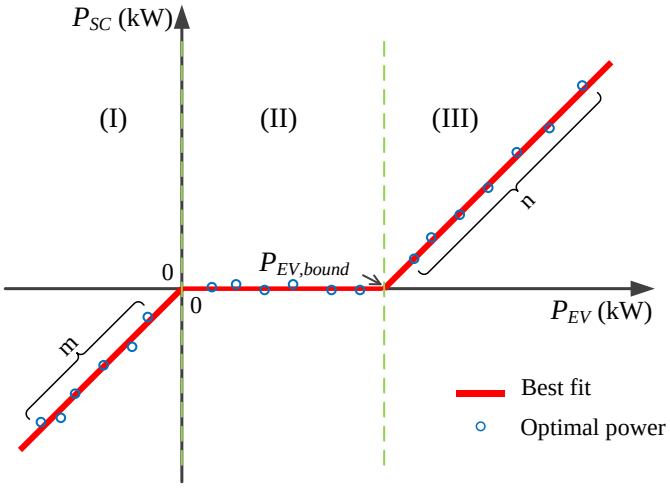


Figure 37 General schematic diagram showing the optimal distribution of SC pack operating power with EV power demands under a random drive cycle.

$$\text{Region I: } P^{I}_{SC} = P^{I}_{EV} \tag{35}$$

$$\text{Region II: } P^{II}_{SC} = 0 \tag{36}$$

$$\text{Region III: } P^{III}_{SC} = P^{III}_{EV} - P_{EV,bound} \tag{37}$$

Further considering the "charge-sustaining principle" [87], before/after a drive cycle, the net energy consumption of SC pack ($Q_{SC}$) should be zero, while $Q_{SC}$ can be further expressed as the sum of the negative ($Q^{-}_{SC}$) and positive ($Q^{+}_{SC}$) electricity consumption of SC pack, as (38).

$$Q_{SC} = Q_{SC}^{-} + Q_{SC}^{+} = 0 \tag{38}$$

According to Figure 37, the SC pack's negative power comes from the $P^{I}_{SC}$ in Region I, and the positive power of the SC pack comes from the $P^{III}_{SC}$ in Region III. Also, considering (35) and (37), $Q^{-}_{SC}$ and $Q^{+}_{SC}$ can be then expressed as (39), where $\Delta t$ is the time step of the drive cycle. $P^{I}_{EV,mean}$ and $P^{III}_{EV,mean}$ are the mean power demand of EV in Regions I and III, respectively. $P^{-}_{EV,mean}$ is the mean negative power demand of EV and equals $P^{I}_{EV,mean}$.

$$\begin{cases} Q_{SC}^{-} = \sum_{i=1}^{m} P_{SC}^{I}\Big|_i \cdot \Delta t = \sum_{i=1}^{m} P_{EV}^{I}\Big|_i \cdot \Delta t = m \cdot P_{EV,mean}^{I} \cdot \Delta t = m \cdot P_{EV,mean}^{-} \cdot \Delta t \\ Q_{SC}^{+} = \sum_{i=1}^{n} P_{SC}^{III}\Big|_i \cdot \Delta t = \sum_{i=1}^{n} \left( P_{EV}^{III}\Big|_i - P_{EV,bound} \right) \cdot \Delta t = n \cdot \left( P_{EV,mean}^{III} - P_{EV,bound} \right) \cdot \Delta t \end{cases} \tag{39}$$

Combining (38) and (39), $P_{EV,bound}$ can be solved as (40). It can be seen that $P_{EV,bound}$ is likely to be influenced by four factors: $m$, $n$, $P^{-}_{EV,mean}$ and $P^{III}_{EV,mean}$. $m$ and $P^{-}_{EV,mean}$ are online sensible, but $n$ and $P^{III}_{EV,mean}$ are dependent on $P_{EV,bound}$ and can only be sensed after $P_{EV,bound}$ is confirmed. To further relate the four factors with $P_{EV,bound}$, Table XV lists the four factors with $P_{EV,bound}$ under ten different drive cycles. Besides, the mean positive power demand of EV ($P^{+}_{EV,mean}$) and the standard derivation of positive power demands of EV ($P^{+}_{EV,std}$) are also presented in Table XV and will be discussed later.

$$P_{EV,bound} = \frac{m}{n} P_{EV,mean}^{-} + P_{EV,mean}^{III} \tag{40}$$

Table XV Possible influence factors of the power boundary ($P_{EV,bound}$) under ten drive cycles *

| | $m$ | $n$ | $P^{-}_{EV,mean}$ | $P^{III}_{EV,mean}$ | $P^{+}_{EV,mean}$ | $P^{+}_{EV,std}$ | $P_{EV,bound}$ |
|---|---|---|---|---|---|---|---|
| **ARB02** | 366 | 449 | -12.6 kW | 49.5 kW | 27.5 kW | 21.9 | 30.6 kW |
| **HWFET** | 67 | 84 | -7.3 kW | 30.0 kW | 15.5 kW | 9.4 | 24.5 kW |
| **IM240** | 52 | 54 | -9.3 kW | 31.6 kW | 16.1 kW | 10.5 | 22.8 kW |
| **Manhattan** | 164 | 88 | -3.3 kW | 21.0 kW | 6.5 kW | 7.6 | 12.4 kW |
| **Nuremberg** | 209 | 104 | -2.6 kW | 21.5 kW | 7.2 kW | 8.0 | 13.5 kW |
| **NYCC** | 102 | 47 | -3.4 kW | 25.9 kW | 7.1 kW | 11.4 | 14.3 kW |
| **SC03** | 115 | 84 | -6.9 kW | 32.9 kW | 13.4 kW | 12.2 | 21.0 kW |
| **US06** | 135 | 157 | -14.6 kW | 55.6 kW | 31.4 kW | 20.4 | 34.6 kW |
| **UDDS** | 235 | 182 | -5.2 kW | 26.1 kW | 10.8 kW | 9.7 | 17.2 kW |
| **Amended UDDS** | 194 | 153 | -5.1 kW | 22.7 kW | 8.2 kW | 8.4 | 15.6 kW |

* *m:* Number of EV power demands in Region I; *n*: Number of EV power demands in Region III; $P^{-}_{EV,mean}$: Mean negative power demand of EV; $P^{III}_{EV,mean}$: Mean power demand of EV in Region III; $P^{+}_{EV,mean}$: Mean positive power demand of EV; $P^{+}_{EV,std}$: Standard derivation of positive power demands of EV; $P_{EV,bound}$: Power boundary between Regions II and III.

Using the data in Table XV, regression analysis is performed with the possible influence factors. The ratio between $m$ and $n$ ($m/n$) is found having a linear regression relationship with $P^{-}_{EV,mean}$ and $P^{III}_{EV,mean}$, as Figure 38 (a). This regression relationship has an $R^2$ at 0.8558 and a root-mean-square error (RMSE) at 0.2206, which means $m/n$ is highly dependent on $P^{-}_{EV,mean}$ and $P^{III}_{EV,mean}$. Therefore, $m/n$ can be dismissed from (40) while $P^{-}_{EV,mean}$ and $P^{III}_{EV,mean}$ are sufficient factors to predict $P_{EV,bound}$. However, as mentioned previously, $P^{-}_{EV,mean}$ is online sensible but $P^{III}_{EV,mean}$ can only be sensed with a known $P_{EV,bound}$. Namely, $P^{III}_{EV,mean}$ is not an online implementable factor to predict $P_{EV,bound}$ and should be substituted by the online implementable ones. Considering $P^{III}_{EV,mean}$ represents the local positive power demands in Region III and is thus dependent on $P_{EV,bound}$, the substitutes of $P^{III}_{EV,mean}$ should represent the global positive power demands in both Regions II and III so that they can be independent on $P_{EV,bound}$, such as the mean positive power demand ($P^{+}_{EV,mean}$) and standard derivation of positive power demands ($P^{+}_{EV,std}$) [158]. According to the regression analysis in Figure 38 (b), $P^{+}_{EV,mean}$ and $P^{+}_{EV,std}$ can significantly determine $P^{III}_{EV,mean}$ with an $R^2$ at 0.9891 and an RMSE at 1.399, which means $P^{III}_{EV,mean}$ can be substituted by $P^{+}_{EV,mean}$ and $P^{+}_{EV,std}$. Based on the above, the online implementable factors to predict $P_{EV,bound}$ are confirmed as three power-related driving states: $P^{-}_{EV,mean}$, $P^{+}_{EV,mean}$ and $P^{+}_{EV,std}$. These driving states are refined using the data under ten different drive cycles; hence, they are the necessary driving states for predicting the $P_{EV,bound}$ under general drive cycles.

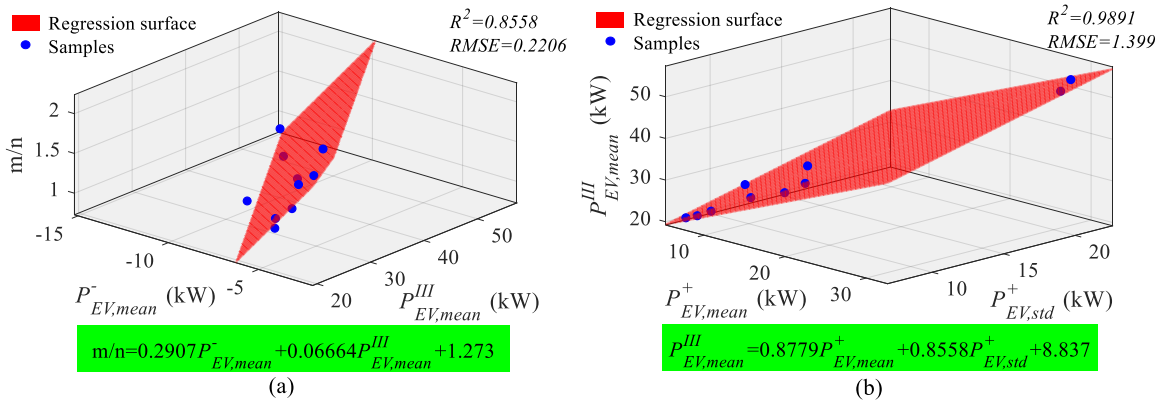


Figure 38 Linear regression analysis: (a) $m/n$ with $P^{-}_{EV,mean}$ and $P^{III}_{EV,mean}$; (b) $P^{III}_{EV,mean}$ with $P^{+}_{EV,mean}$ and $P^{+}_{EV,std}$.

Combining (40) and the fitting equations in Figure 38, $P_{EV,bound}$ can be numerically fitted as a polynomial function of $P^{-}_{EV,mean}$, $P^{+}_{EV,mean}$ and $P^{+}_{EV,std}$, as (41). This function can be a rough method to predict $P_{EV,bound}$ with an overall $R^2$ at 0.9463 and RMSE at 18.2421, while the NN fitting can realise the more accurate method. Compared with NN fitting, the numerical fitting has to customise the fitting equations' type and degree, which makes the prediction accuracy subject to the custom fitting equations. In contrast, we adopt the NN fitting because it does not need custom equations to predefine the relationship between prediction inputs and outputs, improving the prediction accuracy and control performances. The control performances of numerical and NN fitting will be compared in Section 5.4.2.

$$P_{EV,bound} = \left(0.29P^{-}_{EV,mean} + 0.06P^{+}_{EV,mean} + 0.06P^{+}_{EV,std}\right) \cdot P^{-}_{EV,mean} + \\ + 0.88P^{+}_{EV,mean} + 0.86P^{+}_{EV,std} + 8.84 \quad (41)$$

The NN is created as a feed-forward network with ten sigmoid neurons in the hidden layer and one linear neuron in the output layer, as in Figure 39, where *w* and *b* represent the weight vector and bias vector, respectively [61]. The hidden layer translates the nonlinear relationship between the input and output, while the output layer enables a linear target as the predicted outcome [128]. The number of sigmoid neurons is determined as ten by trial and error since more neurons can improve the fitting accuracy, but excessive neurons can lead to overfitting. The input of NN is $P^{-}_{EV,mean}$, $P^{+}_{EV,mean}$ and $P^{+}_{EV,std}$, while the output is $P_{EV,bound}$. The data of the ten drive cycles in Table XV is used to train and validate the NN. The ten drive cycles provide ten samples in two groups. One group of eight samples is for training, which uses the Levenberg-Marquardt backpropagation algorithm to adjust the NN according to the $R^2$. The other group of two is for validation, which measures the network generalisation and halts training when an increase occurs in the RMSE. The training group and validation group are randomly divided as each time the NN is trained and validated. The NN is trained until the $R^2$ of both training and validation approaches 1. In our case, the training and validation are halted with the status in Table XVI. It can be seen that the NN can achieve very high regression with an $R^2$ at 0.99 and very high accuracy with an RMSE at below 1.

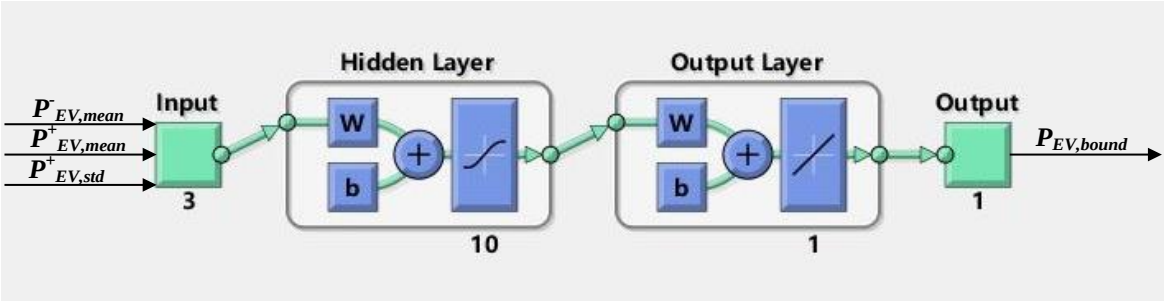


Figure 39 Structure of the two-layer feed-forward neural network for prediction making.

Table XVI Status of the neural network when training and validation are halted.

| | **Training** | **Validation** |
|---|---|---|
| $R^2$ | 0.99 | 0.99 |
| **RMSE** | $1.05*10^{-21}$ | 0.84 |

Noted that the training and validation are performed offline, but after trained and validated, the NN can be deployed to make online predictions and generate new $P_{EV,bound}$, given the sensed driving states. When deployed online, the NN simply performs like a three-inputs-single-output system, and the system's correlations are predefined through offline training and validation. In other words, the online NN can have low computational complexity since the primary complexity has been decoupled by offline training and validation.

### 5.3.3 The whole online EMS with rule-based strategy

Based on the aforementioned variable perception horizon and NN, the whole online EMS can be accomplished by further imitating the "N-shape" relationship between SC power and EV power, and this is realised by the rule-based strategy. Moreover, the rule-based strategy is also responsible for constraining the SOE of SC pack, considering the SC pack has a small energy capacity and thus can easily get over-charged/-discharged in practical engineering. In this section, the rule-based strategy is described together with the variable perception horizon and NN as parts of the whole online EMS. From an engineering viewpoint, the whole online EMS can be implemented with simple hardware of timer, sensor, memory and microprocessor. The flow chart in Figure 40 shows one implementable hardware scheme to realise the proposed EMS, and the workflow is explained as follows.

As the trip starts, the timer will reset and then accumulate every second, offering index ($j$) to memorise the velocity and power. The velocity sensor detects the current vehicle velocity ($v_j$), which is memorised along with the previous vehicle velocity ($v_{j-1}$). The $v_j$ and $v_{j-1}$ are then passed to the microprocessor to diagnose whether a new micro-trip just gets started, in which case $v_{j-1}$ is zero and $v_j$ is nonzero. If yes, a new horizon will be considered starting at time $t_{start}=j-1$, and the EV power demand ($P_{EV,j}$) will begin being memorised with time until the new micro-trip ends. Meanwhile, the prediction and update of $P_{EV,bound}$ is skipped, and the previous $P_{EV,bound}$ is adopted in the following rule-based strategy. If the micro-trip start is not triggered, the microprocessor will further diagnose whether the current micro-trip comes to an end, in which case $v_{j-1}$ is nonzero and $v_j$ is zero. If yes, the memory of $P_{EV,j}$ with time will stop, and the current horizon will be considered ending at time $t_{end}=j$ so that current horizon length is from $t_{start}$ to $t_{end}$. If the micro-trip end is not triggered, the microprocessor will further diagnose whether the EMS minimum update frequency is reached. The *Mod* function [159] can realise this diagnosis by identifying whether the duration from $t_{start}$ to current time can be dividable by 200. If yes, the current horizon will also be considered ending at time $t_{end}=j$ so that the current horizon length is from $t_{start}$ to $t_{end}$, but $P_{EV,j}$ will continue being memorised with time because the current micro-trip has not yet ended. Once the current horizon length is confirmed, the $P_{EV,j}$ memorised within the current horizon will be extracted to calculate the $P^{-}_{EV,mean}$, $P^{+}_{EV,mean}$ and $P^{+}_{EV,std}$, which will be further passed to the NN trained in Section 5.3.2. Subsequently, a new $P_{EV,bound}$ is predicted and updated into the rule-based strategy.

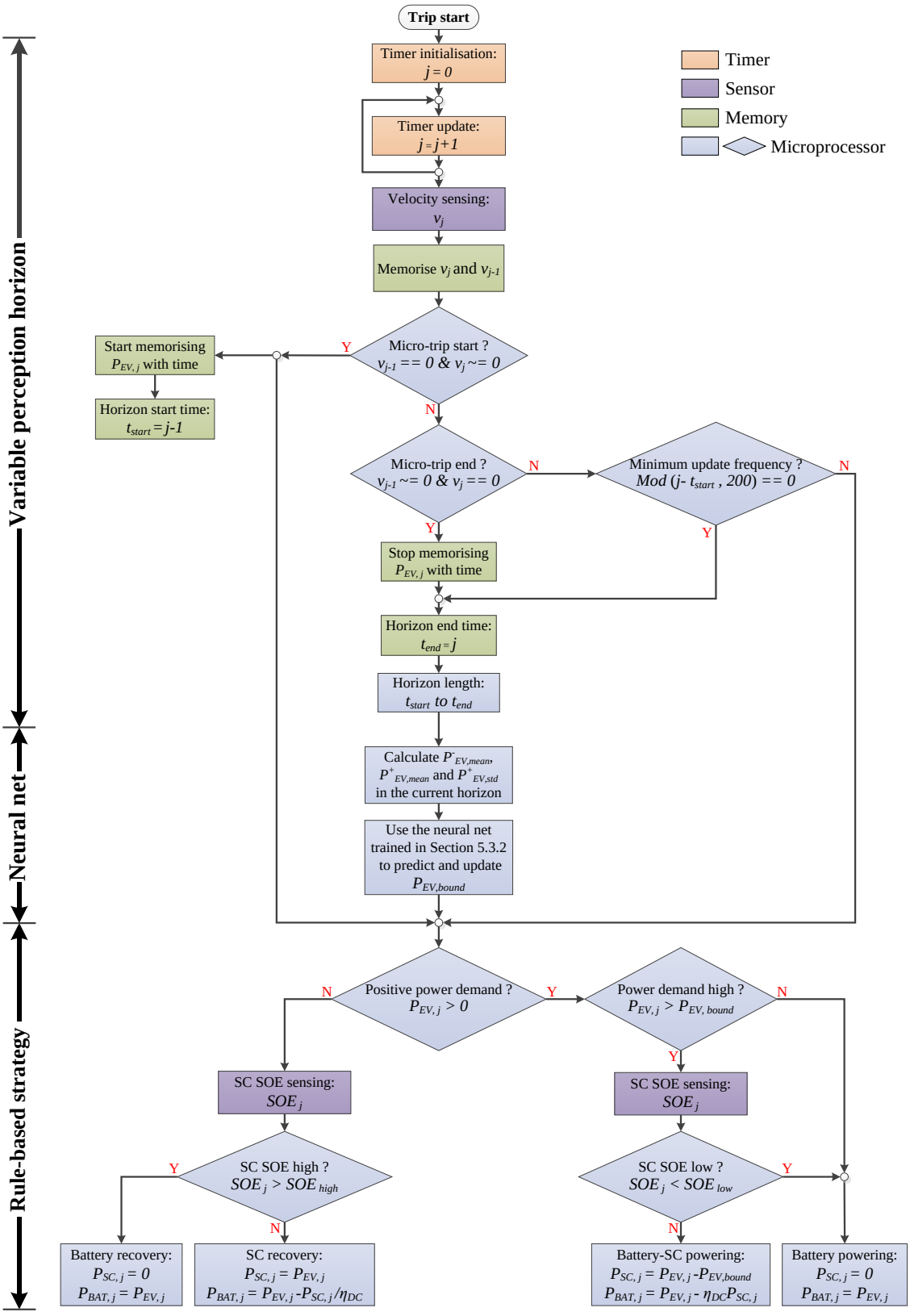


Figure 40 Flow chart of the implementation of the whole online EMS.

As the workflow proceeds to the rule-based strategy, the microprocessor will first diagnose whether the current $P_{EV,j}$ is positive or negative. If negative, the SC pack is expected to take advantage of the negative $P_{EV,j}$ to recover its charge. However, the SOE of SC pack ($SOE_j$) should be detected and compared with $SOE_{high}$ (set at 0.99 in this section), which is the threshold indicating whether the SC

pack is nearly full of charge and cannot be charged any more. If yes, the battery pack will accept the negative $P_{EV,j}$ while the SC pack idle. Otherwise, the SC pack will be charged with its operating power ($P_{SC,j}$) equal to $P_{EV,j}$, and the value of $P_{SC,j}$ is determined by the "N-shape" relationship discussed in Section 5.2.2. Consequently, the operating power of battery pack ($P_{BAT,j}$) can be calculated according to (31). If $P_{EV,j}$ is positive, it will be compared with the $P_{EV,bound}$, which is passed from the NN previously and is the threshold indicating whether $P_{EV,bound}$ is high and SC power assistance is needed. If no, the battery pack will work alone while the SC pack idle. If yes, the SC pack is expected to perform power peaking and work together with the battery pack. However, the $SOE_j$ should be detected and compared with $SOE_{low}$ (set at 0.05 in this section), which is the threshold indicating whether the SC pack is nearly depleted and cannot provide positive power any more. If yes, the battery pack will have to load the entire $P_{EV,j}$ while the SC pack idle. If no, the SC pack will offer positive power at ($P_{EV,j}$- $P_{EV,bound}$), which is determined by imitating the "N-shape" relationship, and $P_{BAT,j}$ can be then confirmed by (31).

This rule-based strategy only adopts four decision conditions, and its outputs simply reflect the linear relationships between $P_{EV,j}$ and $P_{SC,j}$. Therefore, the rule-based strategy can have low complexity. The whole online EMS, as the combination of the variable perception horizon, NN and rule-based strategy, is not computationally complex since each component has low complexity.

## 5.4 Results and discussion

This section presents the control performances of the proposed online EMS in comparison with other EMSs. The follows first introduces the comparative EMSs and the drive cycles used in the comparison, and then discuss the performances of different EMSs.

### 5.4.1 Comparative EMSs and drive cycles in the comparison

Three comparative EMSs are selected to be compared with the proposed EMS. The first EMS is the DP-based EMS mentioned in Section 5.2.1, which provides the optimal offline EMS. The proposed EMS can validate its optimality by comparing itself with the optimal offline EMS. The second and third EMSs keep the other characteristics the same with the proposed EMS, but the second EMS substitutes the variable perception horizon with a constant perception horizon of 100 seconds (the value does not directly determine EMS optimality, which will be explained by Table XIX), and the third EMS substitutes the NN fitting with the numerical fitting using the fitting equation in (41). The second and third EMSs are used to validate the control performances with the variable perception horizon and NN fitting, which are the features of the proposed EMS. To distinguish these EMSs in the following presentation, the three comparative and the proposed EMSs are numbered with features listed in Table XVII.

Table XVII Four EMSs implemented in the comparison and their features.

| EMS No. | Online/offline | Features |
|---|---|---|
| EMS 1 | Offline | Globally optimal benchmark |
| EMS 2 | Online | Constant perception + Neural fitting |
| EMS 3 | Online | Variable perception + Numerical fitting |
| EMS 4 (The proposed EMS) | Online | Variable perception +Neural fitting |

The drive cycles used in the comparison are LA92 and REP05, as Figure 41. The micro-trips of LA92 differ from each other noticeably in terms of velocity and power demands so that LA92 is selected to test the EMSs in terms of adaptiveness to changing driving conditions. REP05 has continuously high velocity and dramatically fluctuating power demands with the maximum power demand at around 130 kW so that REP05 is selected to challenge the EMSs at aggressive driving conditions. Although the global velocity and power demands are presented, the online EMSs can only read the current and historical velocity and power demands but cannot know the future ones in advance.

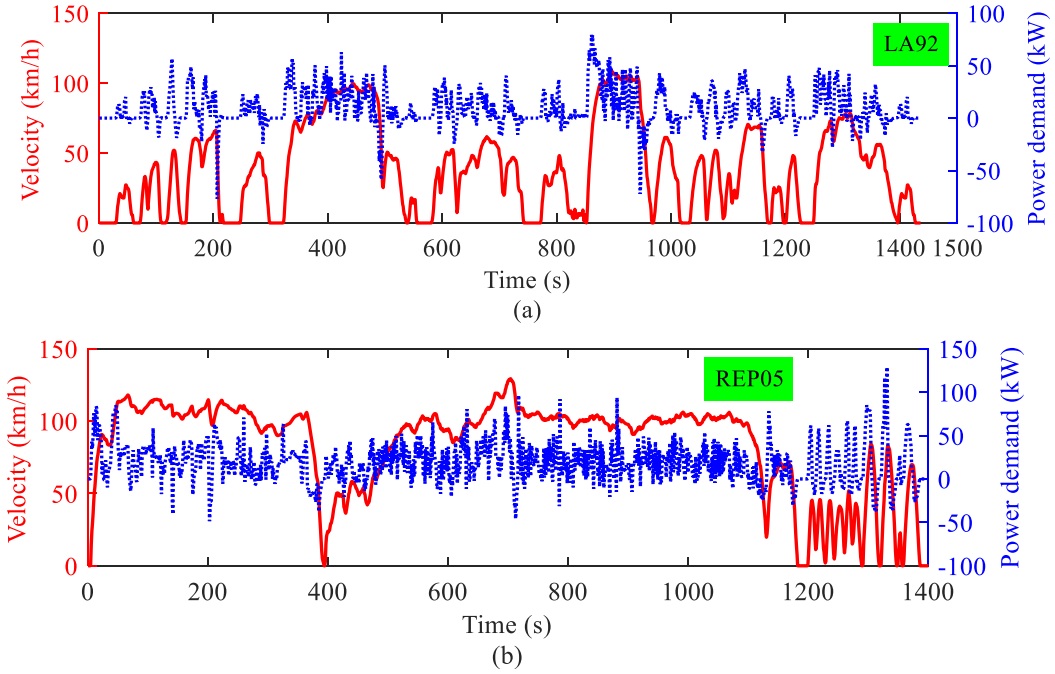


Figure 41 Vehicle velocity and EV power demands of the drive cycles used in the comparison: (a) LA92, (b) REP05.

### 5.4.2 Control performances of different EMSs

The control performances of the four EMSs are compared from four aspects: (1) Cost optimisation performances, which reflect the four EMSs' optimality of reducing DESS long-term operating costs. (2) Perception performances, which compare the constant and variable perception horizon in terms of horizon statistics. (3) Prediction performances, which demonstrate the online EMSs' accuracy of predicting $P_{EV,bound}$, compared with the optimal offline EMS. (4) Imitation performances, which focuses on the proposed EMS's capability of imitating the optimal offline EMS.

(1) Cost optimisation performances.

Table XVIII presents the $Q_{DESS}$, $E_{loss}$ and $J_{long}$, which are formulated in Section 5.1.2, of four EMSs under two drive cycles. The $Q_{DESS}$ and $E_{loss}$ of three online EMSs are all higher than those of EMS 1, while the difference of $Q_{DESS}$ among three online EMSs is less than 1%, but the difference of $E_{loss}$ can be more than 6%, which means that the electricity consumption of DESS is not significantly affected by EMSs, but the battery degradation is. The $J_{long}$ of three online EMSs indicates that EMS 4 is the best online EMS with the smallest $J_{long}$, followed by EMS 2 with a slightly higher $J_{long}$, while EMS 3 has a noticeable gap with the other EMSs. Considering EMS 3 adopts the numerical fitting while EMSs 2 and 4 adopt the neural fitting, it means that the neural fitting technique can enable the EMS to realise much better optimality. Table XVIII also presents the cost optimisation rate ($\tau$), which is defined as (42), where $J_{long,EMS1}$ is the DESS operating costs of EMS 1 (optimal benchmark), $J_{long,EMSX}$ is the DESS operating costs of EMS 2 or 3 or 4. EMS 2 can realise a very high $\tau$ at more than 97%, but EMS 4 is even more elevated. Considering the only difference between EMS 2 and EMS 4 is the implementation of either constant or variable perception horizon, the variable perception horizon can enable the EMS to further improve optimality.

$$\tau = 100\% - \left| \frac{J_{long,EMS1} - J_{long,EMSX}}{J_{long,EMS1}} \right| \tag{42}$$

Table XVIII Cost optimisation performances of four EMSs under two drive cycles.

| **Drive cycle** | **EMS No.** | **DESS electricity consumption** ($Q_{DESS}$, Wh) | **Battery capacity loss** ($E_{loss}$, Wh) | **DESS operating costs** ($J_{long}$, USD/100km) | **Cost optimisation rate** ($\tau$) |
|---|---|---|---|---|---|
| LA92 | EMS 1 | 3671 | 4.207 | 42.26 | 100% |
| | EMS 2 | 3731 | 4.318 | 43.35 | 97.4% |
| | EMS 3 | 3702 | 4.881 | 48.68 | 84.8% |
| | EMS 4 | 3733 | 4.286 | 43.06 | 98.1% |
| REP05 | EMS 1 | 7238 | 8.492 | 41.88 | 100% |
| | EMS 2 | 7321 | 8.753 | 43.05 | 97.2% |
| | EMS 3 | 7294 | 9.263 | 45.41 | 91.6% |
| | EMS 4 | 7324 | 8.734 | 42.96 | 97.4% |

(2) Perception performances.

To excavate the influence of constant/variable perception horizon on EMS optimality, the horizon statistics of EMS 2 and EMS 4 are compared in Table XIX. EMS 3 adopts the same variable perception horizon as EMS 4 does and is not presented in Table XIX. The mean horizon length reflects the mean timespan of driving behaviour being captured, while the number of horizons reflects how many predictions are made and updated into the EMS. In general, the mean horizon length and number of horizons have a negative correlation, as more horizons can be divided by each horizon

being shorter. Existing studies have debated whether a long or short horizon length and more or fewer horizons can improve EMS optimality, as follows. On the one hand, existing studies [128] tend to conclude that either a long or short horizon length can improve EMS optimality. For those in favour of the long horizon length, their argument is that a long horizon can collect more comprehensive driving behaviour to feed the prediction; for the short horizon length, the argument is that a short horizon can better capture the fast-changing driving behaviour. However, Table XIX indicates that the horizon length does not necessarily impact EMS optimality, as explained below. Under LA92 drive cycle, EMS 4 has a longer horizon length than EMS 2, while under REP05 drive cycle, EMS 4 has a shorter horizon length than EMS 2. However, under whichever drive cycle, EMS 4 can always achieve a higher cost optimisation rate than EMS 2 (Table XVIII). Therefore, the horizon length does not directly determine EMS optimality. On the other hand, there are also debates [48] on whether more or fewer horizons can improve EMS optimality. The former argues that more horizons can enable the predictions to be made and updated more frequently so that the EMS can be adaptive to instantaneous driving behaviour, while the latter considers that excessive horizons can result in the DESS being overcontrolled. However, Table XIX indicates that the number of horizons does not necessarily impact EMS optimality, as explained below. As shown in Table XIX, EMS 4 has more horizons than EMS 2 under LA92, but fewer horizons under REP05. However, EMS 4 always has better optimality than EMS 2 under whichever drive cycle (Table XVIII). Therefore, the number of horizons does not directly determine EMS optimality. Based on the above analysis and that in Section 5.2.2, this work holds the view that neither horizon length nor the number of horizons necessarily matters with EMS optimality; what matters is whether the horizon can capture the consistent driving behaviour within every micro-trip. By changing the horizon length adaptively, the proposed variable perception horizon aims to recognise every micro-trip and extract the consistent driving behaviour to feed prediction making, something no constant perception horizon can realise. As a result, EMS 4 with the variable perception horizon realises better optimality than EMS 2 with the constant perception horizon.

Table XIX Perception performances of two online EMSs under two drive cycles.

| **Drive cycle** | **EMS No.** | **Mean horizon length** (seconds) | **Number of horizons (i.e., number of predictions)** | **Cost optimisation rate** ($\boldsymbol{\tau}$) |
|---|---|---|---|---|
| LA92 | EMS 2 | 100 | 14 | 97.4% |
| | EMS 4 | 84.4 | 17 | 98.1% |
| REP05 | EMS 2 | 100 | 14 | 97.2% |
| | EMS 4 | 251.6 | 11 | 97.4% |

(3) Prediction performances.

The predicted $P_{EV,bound}$ of three online EMSs is compared with the $P_{EV,bound}$ of EMS 1, as Figure 42. The $P_{EV,bound}$ of EMS 1 is solved offline and remains unchanged globally, while the $P_{EV,bound}$ of each online EMS is predicted online and varies with time. The $P_{EV,bound}$ of EMS 3 stays far above that of

EMS 1 and thus is not well predicted. In contrast, the $P_{EV,bound}$ of EMS 2 and EMS 4 fluctuates closely around that of EMS 1 and is much better predicted. Considering the only difference between EMS 3 and EMS 4 is either numerical fitting or neural fitting, it means that neural fitting can realise much higher prediction accuracy than numerical fitting. The only difference between EMS 2 and EMS 4 is the implementation of either constant or variable perception horizon, while the predicted $P_{EV,bound}$ of EMS 2 is quite different from that of EMS 4, which indicates that the constant/variable perception horizon also has an evident impact on the prediction. However, it is difficult to tell from Figure 42 whether EMS 2 or EMS 4 can better predict $P_{EV,bound}$. In this case, Table XX compares the prediction statistics of EMS 2 and EMS 4. Firstly, the mean $P_{EV,bound}$ of EMS 4 is closer to the $P_{EV,bound}$ of EMS 1, which indicates that the $P_{EV,bound}$ of EMS 4 is more accurate in general. Secondly, the standard deviation of EMS 2 is smaller, which means the $P_{EV,bound}$ of EMS 2 is more stable with smaller shifts. Lastly, the mean relative error of EMS 4 is smaller than that of EMS 2, which confirms that EMS 4 has higher overall accuracy than EMS 2. Namely, variable perception horizon can better assist the prediction of $P_{EV,bound}$ than constant perception horizon.

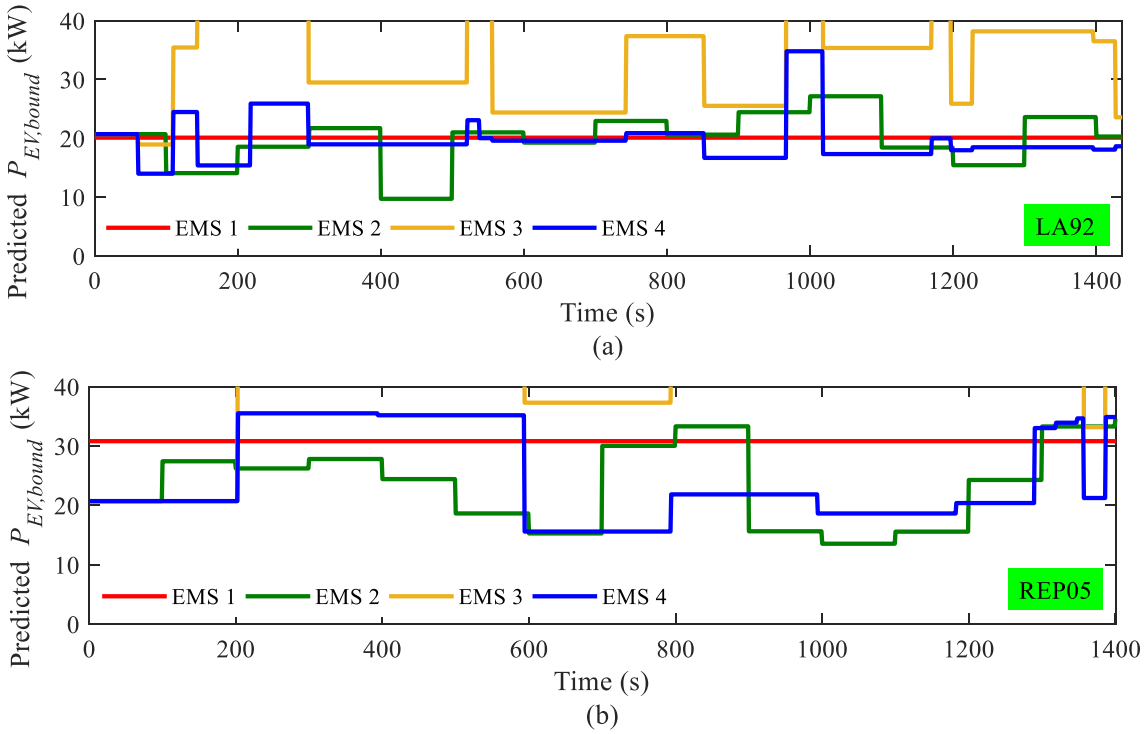


Figure 42 Predicted $P_{EV,bound}$ of four EMSs under two drive cycles: (a) LA92, (b) REP05.

Table XX Prediction performances of two online EMSs under two drive cycles.

| Drive cycle | EMS No. | Mean $P_{EV,bound}$ | Standard deviation of $P_{EV,bound}$ | Mean relative error with the $P_{EV,bound}$ of EMS 1* |
|---|---|---|---|---|
| LA92 | EMS 2 | 19.80 | 4.50 | 16.38% |
| | EMS 4 | 20.28 | 4.85 | 16.21% |
| REP05 | EMS 2 | 24.28 | 7.38 | 25.24% |
| | EMS 4 | 27.7 | 8.01 | 23.2% |

*: The $P_{EV,bound}$ of EMS 1 under LA92 and REP05 are 20.1kW and 30.8kW, respectively.

(4) Imitation performances.

To validate whether the proposed online EMS can perform like the optimal offline EMS, the power and SOE of the SC pack are compared between EMS 4 and EMS 1, as Figure 43. It should be noted that this is a very rigorous comparison since the online EMS cannot know the global driving conditions in advance but the offline EMS can, so that the online EMS can mostly be locally optimal and is bound to have a gap with the globally optimal offline EMS. It can be seen from Figure 43 (a) that under LA92, the SC power of EMS 4 substantially overlaps with that of EMS 1, except at around 400 and 900 seconds. This is because, as shown in Figure 43 (b), the SOE of EMS 4 stays low at around 400 and 900 seconds; as a result, the SC pack of EMS 4 cannot continuously provide high power output as the SC pack of EMS 1 can. In contrast, under REP05, the SC power of EMS 4 does not coincide well with that of EMS 1, as Figure 43 (c). The best match of SC power occurs from 380 to 650 seconds and from 1100 to 1400 seconds, during which the SC pack of EMS 4 has sufficient SOE to support continuous high power output, as shown in Figure 43 (d). Figure 43 (d) also shows that the SOE of EMS 4 keeps low-level operating in most the time of REP05. This is because REP05 is a very aggressive drive cycle with continuously high power demands (Figure 41 (b)), making the SC pack almost depleted most of the time. Based on the above, EMS 4 accords well with EMS 1 under LA92, but does not imitate EMS 1 very well under REP05 because REP05 is a very aggressive drive cycle that depletes the SC pack. Despite this, the proposed EMS 4 is more capable than the referenced online EMSs and has proved its optimality by the cost optimisation rate in Table XVIII.

### 5.4.3 Summary

This chapter presents an adaptive EMS that optimises the operating costs of EV-mounted battery-SC DESS and can be implemented with simple hardware. The proposed EMS has three components: the variable perception horizon to capture consistent driving behaviour, the neural network to predict the threshold for battery-SC power splitting, and the rule-based strategy to imitate the optimal offline benchmark. Compared with existing studies, the proposed EMS has the following advantages: (1) Rather than using a complicated framework to integrate the whole EMS, the proposed EMS is integrated with low complexity using the rule-based strategy, which is designed based on careful analysis of optimal offline benchmark. It is found that the optimal operating power of SC is highly piecewise linear with DESS power demand, which enables the whole EMS to be integrated with significantly reduced complexity. (2) Rather than perceiving mixed driving behaviours, the proposed variable perception horizon can accurately cluster consistent driving behaviours by breaking down real-time driving conditions into successive micro-trips. By accepting the consistent driving behaviours, the accuracy of online prediction can be improved, and consequently, the EMS optimality is also improved. (3) Rather than burdening the neural network with many unsubstantiated inputs, the proposed neural network only accepts three necessary inputs that are refined based on analytical deductions and regression analysis. In this way, the complexity of the neural network is

significantly lowered. Benefiting from the above advantages, the proposed online EMS shows high control effectiveness, with the cost optimisation rate being more than 97% under LA92 and REP05 drive cycles. Apart from demonstrating the optimisation results, statistical analysis is performed to explain why the proposed variable perception horizon and neural network techniques can improve EMS optimality.

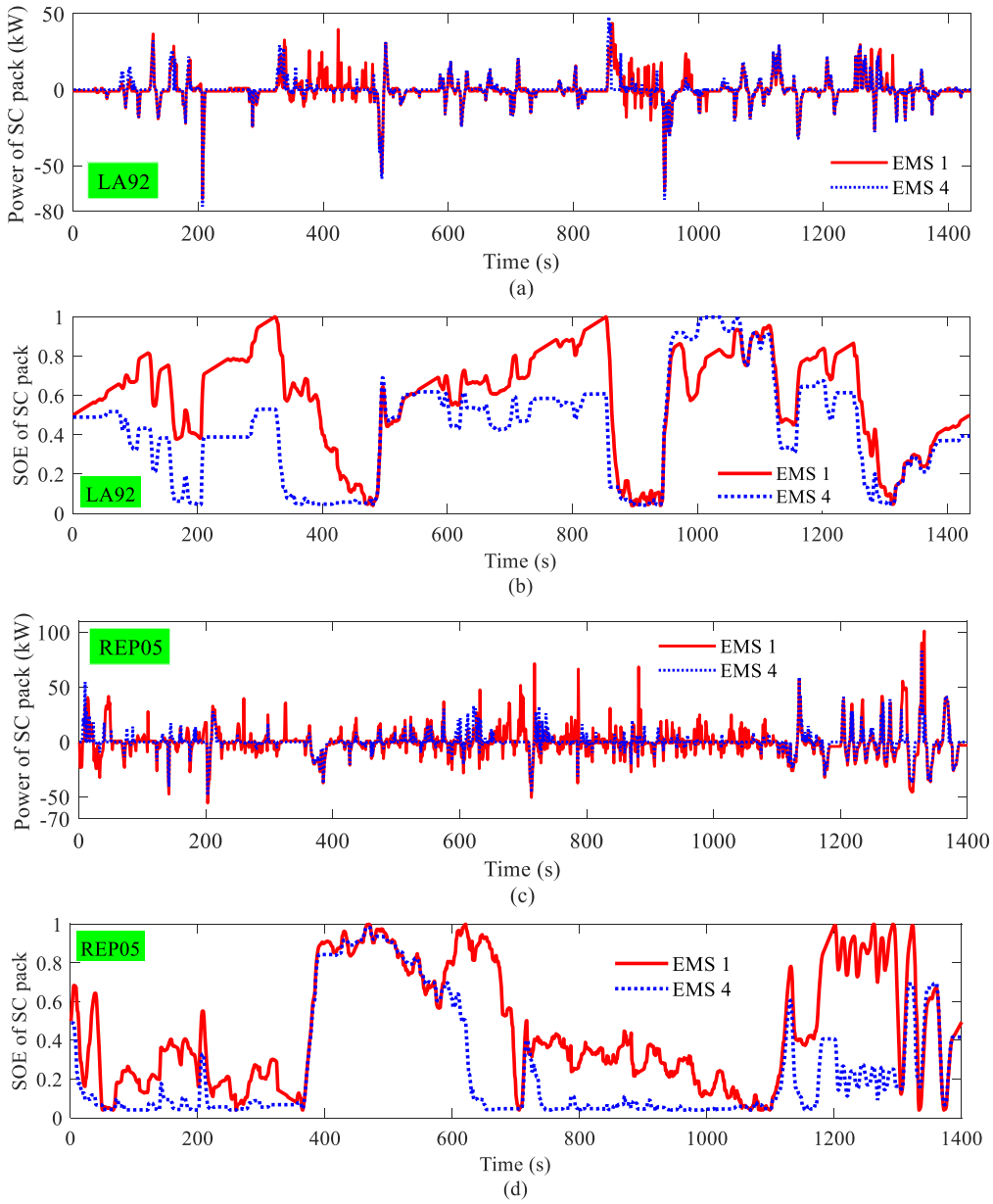


Figure 43 Comparison between the optimal offline EMS (EMS 1) and the proposed online EMS (EMS 4): (a) operating power of SC pack under LA92, (b) SOC of SC pack under LA92, (c) operating power of SC pack under REP05, (d) SOC of SC pack under REP05.

# Chapter 6 Sizing

For a dual energy storage system (DESS) to fit an electric vehicle (EV) drivetrain and as such provide propulsion, one research problem is to determine the size of DESS, that is, sizing [112]. In this work, the DESS is considered to comprise a battery pack, a supercapacitor (SC) pack and a DC/DC converter; thus, the size of DESS can be determined by solving that of each component [116]. Specifically, this chapter uses the battery pack size and SC pack size as two design variables to represent DESS size. The DC/DC converter size is not considered as a design variable because it is subject to and can be determined by the SC pack size [160]. Various metrics can reflect the size of battery pack or SC pack: mass (kg), volume (L), energy capacity (kWh or Wh), power capability (kW), electrical configuration and financial costs (USD) [109]. This chapter uses energy capacity as the main metric for the convenience of solving but also involves the other metrics for adapting various engineering demands. Although DESS sizing is the topic of this chapter, the energy management (EM) of DESS is inevitably engaged due to the strong coupling of EM and sizing. To dismiss the influence of EM and focus on sizing, the EM of DESS is controlled as optimal all through this chapter; namely, the sizing methodology and results are studied under the optimal EM.

The sizing problem can be expressed as: on satisfying the constraints, determine the size of battery pack and SC pack via solving the proposed optimisation problems (OPs). Furthermore, analyse how and why the DESS sizing is sensitive to different influence factors. This is shown in Figure 15 and can be broken down into three components:

1) Constraints (boundary conditions). Given EV design parameters, the energy and power demands from EV propulsion can be raised as the hard constraints for DESS sizing. The hard constraints must be satisfied because fulfilling EV propulsion is the fundamental duty of DESS [16]. Optionally, the mass and volume of DESS, if considered, can be raised as the soft constraints that can be violated to some extent [161].

2) OPs and solving methods. On satisfying the constraints, OPs can be embedded with DESS sizing. This chapter considers three OPs - the fixed costs, battery degradation and electricity consumption. By adding up the financial costs caused by each OP, this chapter emphasises the optimisation of overall costs. A systematic solving framework is proposed to minimise the overall costs throughout EV lifetime along with finding the optimal DESS size.

3) Sensitivity analysis. Considering a small change in one of the EV parameters can lead to very different sizing results [113], this chapter sorts out eight EV parameters as sensitive factors and analyses how and why DESS sizing is sensitive to these factors. Specifically, the trends of optimal DESS size and overall costs with varying factor values are revealed, and the relative importance of each factor is quantified and discussed for guiding practical engineering.

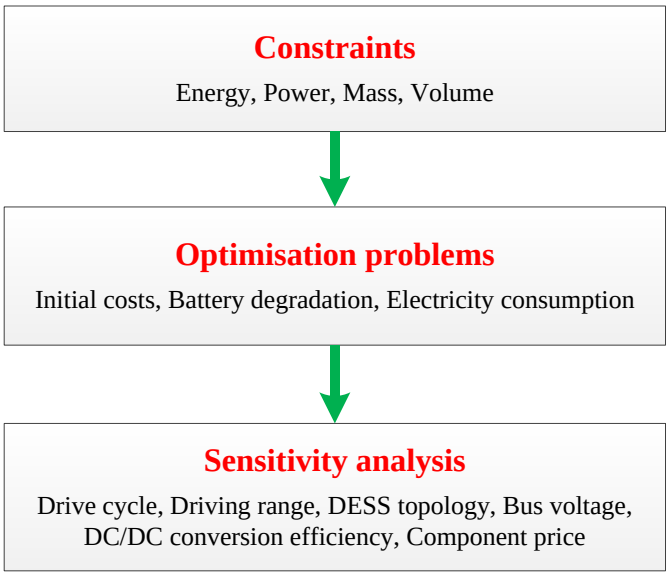


Figure 44 Structure of the chapter.

## 6.1 Constraints

This section formulates the constraints for sizing in terms of energy, power, mass and volume. These constraints are applied to a case study in Section 7.4.1 (not in this chapter to avoid repetition).

### 6.1.1 Energy and power

EVs usually have a finite driving range that accords with the onboard ESS's energy capacity [111]. To secure this driving range, the whole DESS's energy capacity (battery pack + SC pack) must satisfy the energy demands over the EV driving range, as (43). Where $E_{BAT}$ and $E_{SC}$ are the energy capacity of the battery pack and SC pack, respectively. $E_{EV}$ is the energy demands over EV driving range and can be obtained via simulation using the EV model. $\eta_{DCDC}$ is DC/DC conversion efficiency and accounts for the conversion loss that happens when the DC/DC converter interfaces the SC pack.

$$E_{BAT} + E_{SC} \cdot \eta_{DCDC} \geq E_{EV} \tag{43}$$

Considering the SC pack is a power peaking device with a relatively small (compared to the battery pack whose energy capacity is normally dozens of kWh, the SC pack is only hundreds of Wh) [13], $E_{SC}$ can be approximated to zero in (43). $E_{BAT}$ alone is expected to cover $E_{EV}$, as (44), which is the energy constraint for DESS sizing.

$$E_{BAT} \geq E_{EV} \tag{44}$$

EVs sometimes require high power to boost sharp accelerations or maintain high-speed cruise [162]. To secure high-power operations, the power capability of the whole DESS (battery pack + SC pack)

must satisfy the maximum EV power demand, as (45). Where $P_{BAT,max}$ and $P_{SC,max}$ are the maximum power capability of the battery pack and SC pack, respectively. $\rho_{BAT,P/E}$ and $\rho_{SC,P/E}$ are the power to energy density of the battery pack and SC pack, respectively. $P_{EV,max}$ is the maximum EV power demand and can be obtained via simulation. Equation (45) is the power constraint for DESS sizing. Combining (44) and (45), DESS size can be constrained within a feasible set of $E_{BAT}$ and $E_{SC}$.

$$P_{BAT,max} + P_{SC,max} \cdot \eta_{DCDC} = E_{BAT}\rho_{BAT,P/E} + E_{SC}\rho_{SC,P/E} \cdot \eta_{DCDC} \geq P_{EV,max} \tag{45}$$

### 6.1.2 Mass and volume

The mass is a metric relevant to vehicle dynamics since a heavy DESS reduces the EV acceleration capability and driving range, while the volume matters for chassis layout as a bulky DESS restricts the flexibility to arrange EV components [163]. The mass ($M_{DESS}$) and volume ($V_{DESS}$) of DESS can be formulated as (46) and (47). These equations consider the total mass and volume of DESS as the accumulation of each component. Where $\rho_{BAT,E/M}$ and $\rho_{BAT,E/V}$ are the energy to mass and to volume density of the battery pack, respectively. $\rho_{SC,E/M}$ and $\rho_{SC,E/V}$ are the energy to mass and to volume density of the SC pack, respectively. $\rho_{DCDC,P/M}$ and $\rho_{DCDC,P/V}$ are the power to mass and to volume density of the DC/DC converter, respectively. $P_{DCDC,max}$ is the maximum power capability of the DC/DC converter, and it is subject to the maximum power capability of the SC pack [77], as expressed in (48).

$$M_{DESS} = M_{BAT} + M_{SC} + M_{DCDC} = \frac{E_{BAT}}{\rho_{BAT,E/M}} + \frac{E_{SC}}{\rho_{SC,E/M}} + \frac{P_{DCDC,max}}{\rho_{DCDC,P/M}} \tag{46}$$

$$V_{DESS} = V_{BAT} + V_{SC} + V_{DCDC} = \frac{E_{BAT}}{\rho_{BAT,E/V}} + \frac{E_{SC}}{\rho_{SC,E/V}} + \frac{P_{DCDC,max}}{\rho_{DCDC,P/V}} \tag{47}$$

$$P_{DCDC,max} = P_{SC,max} = E_{SC}\rho_{SC,P/E} \tag{48}$$

Equations (46), (47) and (48) offer the methods to calculate the mass and volume as linear functions of $E_{BAT}$ and $E_{SC}$, but do not set up constraints for $E_{BAT}$ and $E_{SC}$ from the perspectives of mass and volume. However, the constraints can be set up conveniently if only specific engineering demands are proposed otherwise. For example, given the demand that "the mass of DESS must not exceed 80 kg", a feasible set of $E_{BAT}$ and $E_{SC}$ can be obtained using (46) and (48). This chapter does not introduce specific engineering demands for the mass or volume of DESS, while (46), (47) and (48) are used to calculate the mass and volume of different DESS designs.

## 6.2 Optimisation problems and solving methods

The fixed costs, battery degradation and electricity consumption of DESS are formulated as the OPs of DESS sizing. The OPs are unified into the same metric – financial costs and the final objective is to minimise the overall costs caused by all the OPs throughout the EV lifetime. To solve the optimal overall costs and find the corresponding DESS size, a joint sizing-EM optimisation framework is tailored based on the dynamic programming (DP) approach. Finally, a case study is investigated with the OPs and solving methods.

### 6.2.1 Optimisation problems

The overall financial costs of DESS should cover the costs from initial deployment to long-term service until the EV lifetime expires. The costs that happen only once with DESS initial deployment are the fixed costs; in this chapter, the fixed costs are considered as the money to purchase each DESS component. The costs that accumulate with DESS long-term service are the long-term costs; this chapter considers that the long-term costs come from the component replacements caused by component degradation and the energy consumption by DESS operations. Among DESS components, the SC pack and DC/DC converter are regarded as having a long enough lifespan and no replacements over EV lifetime [9]; thus, they have one-off purchase costs but no degradation cost. For the battery pack, it has the purchase cost and the degradation cost because battery lifespan can be shorter than EV lifetime, and the battery pack may be replaced several times over EV lifetime [6]. In this chapter, the battery purchase cost is regarded as equivalent to the battery degradation cost that happens with first-time battery replacement. Therefore, the battery purchase cost is merged into battery degradation cost and counted into long-term costs. Besides, DESS operations consume an amount of energy, and the corresponding energy cost over EV lifetime is counted into long-term costs. Based on the above, Figure 45 shows the overall costs composed of four kinds of sub-costs.

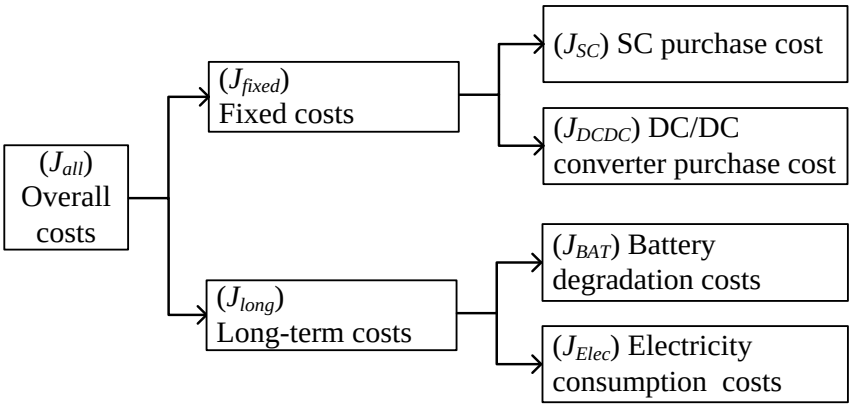


Figure 45 DESS overall costs composed of the SC purchase cost, DC/DC converter purchase cost, battery degradation cost and electricity consumption cost.

The formulations of battery degradation costs ($J_{BAT}$) and electricity consumption costs ($J_{Elec}$) have been given in Section 5.1.2, respectively, while the formulations of SC and DC/DC converter purchase cost are as follows. The SC purchase cost ($J_{SC}$) is calculated as directly proportional to the energy capacity of SC pack ($E_{SC}$), as (49). Where $Price_{SC}$ is the SC unit price in USD/Wh. The DC/DC converter purchase cost ($J_{DCDC}$) is calculated as directly proportional to the maximum power capability of DC/DC converter ($P_{DCDC,max}$), as (50). Where $Price_{DCDC}$ is the DC/DC converter unit price in USD/kW. Finally, the overall costs of DESS throughout EV lifetime can be expressed as (51).

$$J_{SC} = Price_{SC} E_{SC} \tag{49}$$

$$J_{DCDC} = Price_{DCDC} P_{DCDC,max} \tag{50}$$

$$J_{all} = J_{fixed} + J_{long} = J_{SC} + J_{DCDC} + J_{BAT} + J_{Elec} \tag{51}$$

### 6.2.2 Solving methods

Combining equations (26), (27) and (48) to (51), it can be seen that the overall costs $J_{all}$ is actually a nonlinear function of the current, voltage and energy capacity of the battery pack and SC pack. As mentioned in Chapter 5, the current and voltage are the results of DESS EM, while the energy capacity is a result of DESS sizing. Therefore, solving $J_{all}$ requires a joint sizing-EM optimisation. Based on the DP approach, a joint sizing-EM framework is tailored to solve the optimal DESS size and EM that can minimise $J_{all}$. The joint sizing-EM optimisation is necessary because the DESS can have different overall costs, depending on its specific size and EM [136]. The optimisation aims at working out the minimum overall costs, which reflects the greatest potential of the DESS under best-case size and EM conditions. The DP approach has been implemented for EM optimisation in Section 5.2, but it has only one dimension accounting for DESS EM. In comparison, the joint sizing-EM framework in this section is an enhancement with two more dimensions accounting for DESS sizing (one dimension for the energy capacity of battery pack $E_{BAT}$, while the other one for that of SC pack $E_{SC}$) [13]. DP is an offline technique that requires prior knowledge of all the input profiles, due to which DP can hardly be implemented as real-time EM algorithms [164]. However, this chapter does not aim at designing a real-time EM strategy that can be used online but focuses on the sizing problem. In this case, the input profiles for DESS sizing can be known beforehand so that DESS sizing optimisation can be fulfilled by the DP-based framework offline. With this joint sizing-EM framework, the optimisation of $J_{all}$ is a six-step process, as described below.

1) Import profiles. The sizing-EM framework accepts prescribed EV parameters (e.g., driving range), DESS architecture (e.g., DESS topology), and DESS component parameters (e.g., battery price) as inputs. These inputs are also sensitive factors to be investigated in Section 6.3.

2) Traverse DESS size within the feasible set. The feasible set is acquired by following the energy and power constraints in Section 6.1.1. It constrains the upper and lower limits of $E_{BAT}$ and $E_{SC}$ as $E_{BAT,max}$, $E_{BAT,min}$ and $E_{SC,max}$, $E_{SC,min}$, respectively. Each feasible $E_{BAT}$ and $E_{SC}$ within limits will be traversed in ascending order.

3) Traverse EM strategy with time. With each DESS size traversed in the previous step, the optimisation process further traverses the possible EM strategy of DESS. The EM strategy is time-dependent, and the timeline ($k$) of the EM strategy is also the timeline of the input drive cycle [97]. Given that the input drive cycle's duration is from 0 to $t_{end}$ seconds, the EM strategy can be regulated to perform every one second; thus, $k$ can be expressed as (52). At each time point of $k$, the EM strategy determines the working power of battery pack ($P_{BAT}$) and SC pack ($P_{SC}$), based on the constraints in (53) and the correlation in (54).

$$k = 0,1,2,...,t_{end} \tag{52}$$

$$\begin{cases} \left|P_{BAT}(k)\right| \le P_{BAT,max} \\ \left|P_{SC}(k)\right| \le P_{SC,max} \end{cases} \tag{53}$$

$$P_{BAT}(k) = \begin{cases} P_{EV}(k) - P_{SC}(k)\eta_{DCDC}, & P_{SC}(k) > 0 \\ P_{EV}(k) - P_{SC}(k)/\eta_{DCDC}, & P_{SC}(k) \le 0 \end{cases} \tag{54}$$

4) Calculate the electrical states of DESS components. As $P_{BAT}$ and $P_{SC}$ change with time, the electrical states (e.g., voltage, current, SOC, SOE) of DESS components would change as a result. The equivalent circuit models proposed in Chapter 4 account for the change of electrical states. In particular, the SOC of the battery pack and SOE of the SC pack are constrained as (55). Where the battery pack is considered as capable of performing full charge-discharge cycles [77], while the SC pack is not expected to be depleted and a lower limit exists as $SOE_{min}$ ($SOE_{min}$ depends on DESS topology [77] and will be further explained in Section 6.3.1.3). Either battery SOC or SC SOE can be used as a state variable ($x$) to represent the EM states of the DESS, and this section adopts the later one, as (56). Where SC SOE is initialised and finalised as the same at 50%, following the "charge-sustaining" principle [13]. A state transfer function ($z$) can then be formulated along the timeline, as (33). Equation (33) is a function of both the SC pack's power and size, which links EM with sizing and enables the joint sizing-EM optimisation.

$$\begin{cases} 0 \le SOC \le 100\% \\ SOE_{min} \le SOE \le 100\% \end{cases} \tag{55}$$

$$\begin{cases} x(k) = SOE(k) \\ SOE(0) = SOE(t_{end}) = 50\% \end{cases} \tag{56}$$

$$z(k) = x(k) - x(k+1) = P_{SC}(k) / E_{SC} / 3.6 \tag{57}$$

5) Feed the objective function. With the traversed DESS size and EM strategy as well as the calculated electrical states of DESS components, the objective function (*O*) of DESS overall costs can be fulfilled as (34).

$$O = Min \sum_{k=1}^{t_{end}} J_{all}(k) \tag{58}$$

6) Export results. After completing the first five steps, the sizing-EM framework would find out the optimal combination of DESS size and EM to minimise the objective function, and the optimisation results would be exported. In summary, the brief pseudocodes of the sizing-EM framework are shown in Table XIV.

Table XXI Brief pseudocodes of the joint sizing-EM framework.

| |
|---|
| **% Import profiles %** |
| **for** $E_{BAT} = E_{BAT,min} : E_{BAT,max}$ **;** **% battery pack sizing** |
| **for** $E_{SC} = E_{SC,min} : E_{SC,max}$ **;** **% SC pack sizing** |
| **for** $k = 0 : t_{end}$ **;** **% timeline of EM** |
| **for** $SOE = SOE_{min} : 1$ **;** **% states of EM** |
| **% Calculate electrical states of DESS components %** |
| $O = \text{Min} \sum_{k=0}^{t_{end}} J_{all}(k)$ **;** **% objective function** |
| **end** |
| **end** |
| **end** |
| **end** |
| **% Export results %** |

### 6.2.3 Case study

With the proposed optimisation problems and solving methods, this section presents a case study's sizing results. The case study uses the US06 drive cycle (Figure 20) and SC/battery DESS topology (Figure 11), and the other inputs come from Tesla Model S P85 EV (Table VII, Table VIII), Panasonic NCR 18650B battery (Table IX), Maxwell BCAP3400 2.7V SC (Table IX) and a hypothetical DC/DC converter (Table X).

By varying the DESS size while ensuring that the EM is optimal, Figure 46 shows the overall costs with the size of the battery and SC pack. The overall costs vary within a large range between 75000 USD and 115000 USD, which indicates that DESS sizing efforts can significantly reduce the overall costs. The minimum allowable size of the battery pack, as constrained by (44), is 85 kWh, with 96 battery cells in series and 74 cells in parallel. A red dotted curve highlights the minimum allowable battery pack size. Beyond this curve, the overall costs grow as battery pack size increases. Therefore,

the optimal battery pack size is precisely the minimum allowable size. Besides, as SC pack size varies from 0 to 300 Wh, the corresponding overall costs witness a sharp drop firstly, followed by slow growth. Thus, the optimal SC pack size exists at an extreme point. By varying SC pack size while ensuring the EM and battery pack size optimal, the red dotted curve of overall costs is mapped from Figure 46 to Figure 47; four kinds of sub-costs are also plotted. As SC pack size increases, battery degradation costs decrease noticeably at first but finally maintain almost stationary. Therefore, a small SC pack can significantly reduce battery degradation, but a huge SC pack can hardly contribute more. The electricity costs witness a rather slow growth, which means that the electricity consumption of DESS is not significantly affected by SC pack size. SC purchase cost increases linearly with SC pack size, while DC/DC converter purchase cost has a nonlinear relation with SC pack size and it rises rapidly at first but slows down after. In the combination of all sub-costs, the overall costs show optimal at the extreme point of SC pack size being 138Wh, with 40 SC cells in series.

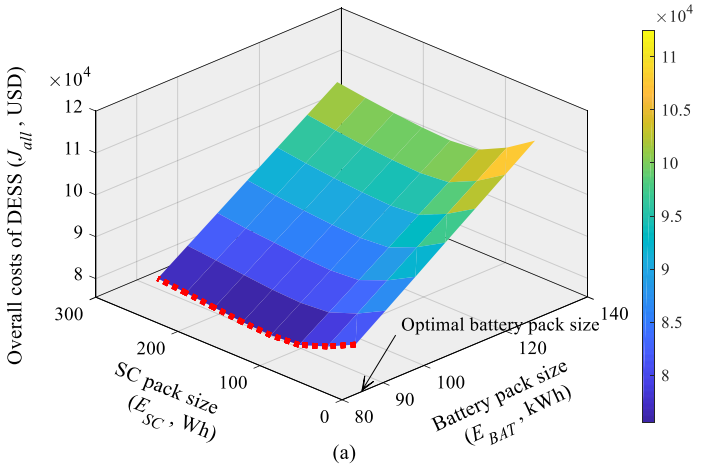


Figure 46 Case study: overall costs of DESS with the size of battery pack and SC pack when ensuring EM optimal.

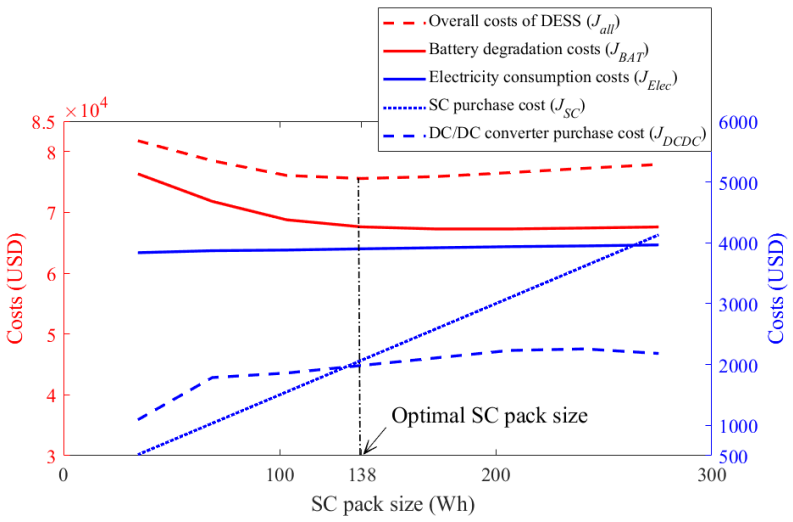


Figure 47 Case study: overall costs and four sub-costs with SC pack size when ensuring both EM and battery pack size optimal.

Figure 48 presents the proportions of sub-costs when both DESS size and EM are held optimal. Battery degradation costs represent 89% of overall costs, which implies that battery degradation is the dominating cause of financial costs and thus needs the most efforts from optimisation. DESS electricity consumption costs rank second with a 5% proportion. SC purchase cost and DC/DC converter purchase cost are the fixed costs of DESS, but each only makes up 3%, respectively. Thus, most of the overall costs attribute to the long-term costs that happen with DESS operation, while the fixed costs only represent a tiny proportion. Figure 49 checks the battery working power and SC working power in the time frame of one US06 drive cycle when both DESS size and EM are held optimal. In general, the battery pack experiences a mild discharging process since its working power mostly fluctuates above zero but is limited below 50kW. In contrast, the SC pack works as a power buffer since its working power fluctuates swiftly between -70kW and 100kW.

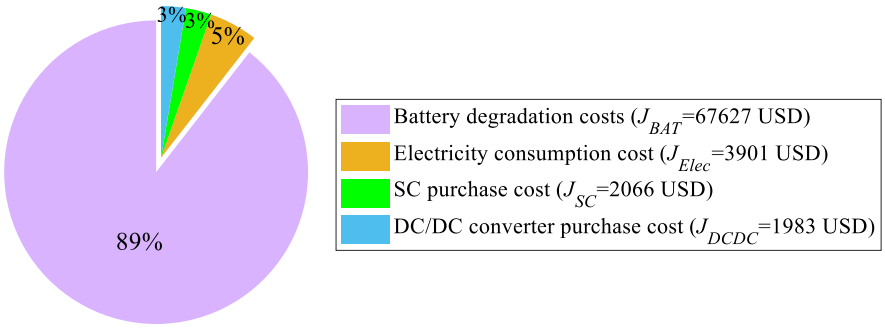


Figure 48 Case study: proportions of sub-costs when ensuring the EM, the size of battery and SC pack optimal.

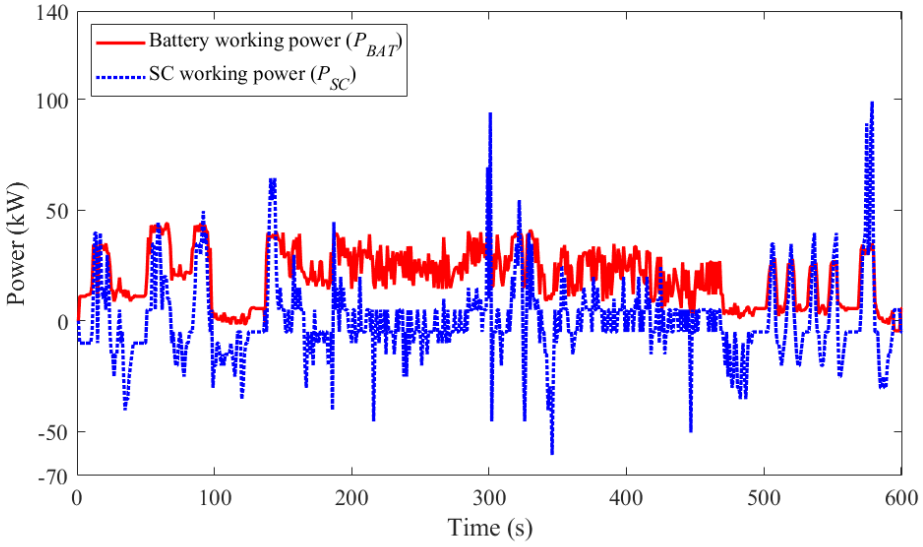


Figure 49 Case study: battery and SC working power in the time frame of one US06 drive cycle when ensuring the EM, the size of battery and SC pack optimal.

## 6.3 Sensitivity analysis

Section 6.2.3 presents the optimal sizing results of a base case using standard EV parameters as inputs. However, even a small change in one of the inputs can lead to very different sizing results. For example, previous research [44] indicates that DESS size and financial costs are quite sensitive to motor efficiency. In [136], the intensity of EV drive cycle is found to have a big impact on the optimal SC pack size. In [113], the battery unit price is shown to significantly impact the financial costs and thus influences the optimal sizing results. Therefore, it is necessary to investigate how the optimal sizing results evolve with different inputs, rather than merely offering results for a specific input set. Published articles rarely investigate the influences of different inputs on DESS sizing results; for those performing the investigations, there are limitations as summarised below. Firstly, the categories of investigated inputs are not adequate. In [44, 113, 136], only motor efficiency, EV drive cycle and battery unit price are investigated, respectively; however, other inputs such as EV driving range and DESS topology, which may have significant impacts on DESS sizing results [77], have not been taken into consideration. Secondly, although the impacts of investigated inputs are worked out, these articles lack discussion on the in-depth reasons for causing the impacts. It is still ambiguous why the sizing results are sensitive to the investigated inputs. Lastly, each article investigates specific inputs separately but fails to present a parallel comparison among different inputs. Therefore, the relative importance of different inputs is not clear, and each article only stresses the impacts of the specifically investigated inputs. Considering a comprehensive study on different inputs is still a missing part of DESS sizing research, this section performs sensitivity analysis towards eight categories of inputs (i.e. sensitive factors): EV drive cycle, EV driving range, DESS topology, nominal bus voltage, DC/DC conversion efficiency, component price (further divided into battery price, SC price and DC/DC converter price). The reasons for choosing these factors are due to their significance to vehicle dynamic performance, DESS architecture, component selection, and that they are usually considered at the early-stage EV development [3]. To understand why and how DESS sizing is sensitive to these factors, the trends of optimal DESS size and overall costs with varying sensitive factors, as well as the underlying causes of the trends, are discussed in Section 6.3.1. More than that, in Section 6.3.2, this project also tries to identify the impact degrees of sensitive factors so that the relative importance of each factor can be distinguished for guiding practical engineering; namely, the factors with high impact degrees need more consideration in practice while those with low impact degrees may be sacrificed since it is difficult to focus on every sensitive factor.

### 6.3.1 Sensitivity analysis of different factors

The eight sensitive factors are classified into different levels and assigned with different values, as Table XXII. The characteristics of different types of vehicles can be reflected by using different combinations of factor values. With these factors and their value sets, the sensitivity analysis adopts the one-at-a-time (OAT) technique [121], analysing the influence of one factor on DESS sizing

results at a time while keeping the other factors fixed at their base-case values. Each factor is analysed individually in the following subsections, with emphasis on 1) why can the factor cause sensitivity; 2) how is the evolution of optimal DESS size and overall costs with varying factor values.

Table XXII Eight sensitive factors and their value sets used in the sensitivity analysis (*: base-case values used in Section 6.2.3) [15, 24, 31, 32, 97, 104, 154, 165-170].

| **Sensitive factors** | | | **Value sets** |
|---|---|---|---|
| **Vehicle level** | Drive cycle | | UDDS, HWFET, US06* |
| | Driving range (km) | | 142, 284, 426* |
| **System level** | DESS topology | | SC/battery topology*, battery/SC |
| | Nominal bus voltage (V) | | 320, 350*, 380 |
| **Component level** | DC/DC conversion efficiency (%) | | 84, 88, 92*, 96, 100 |
| | Component price | Battery (USD/kWh) | 100, 200, 300*, 400, 500 |
| | | SC (USD/Wh) | 5, 10, 15*, 20, 25 |
| | | DC/DC converter | 10, 15, 20*, 25, 30 |

6.3.1.1 EV drive cycle

The drive cycle defines the longitudinal speed with time for the EV to follow; based on this, the EV further proposes the energy and power requests for the DESS to fulfil [166]. Standard drive cycles, such as UDDS, HWFET and US06, originate from real-life driving conditions and are typically used for testing the equivalent fuel consumption and the driving range of EV [135]. Therefore, this section adopts the UDDS, HWFET and US06 drive cycles (presented in Figure 20) to investigate the impacts of drive cycles on DESS sizing. However, these cycles have different durations and diverse statistic characteristics, making it difficult to distinguish which cycle is more intense than the other. In this case, the "intensity factor" is introduced to quantify the intensity of drive cycles. The intensity factor was proposed [136] specifically for the EV equipped with a DESS, and the method to recognise the intensity factor is described as follows. One drive cycle can be divided into a few micro-trips, which are excursions between two successive instants at which the vehicle speed is zero, e.g., the US06 cycle has five micro-trips. Each micro-trip's energy demand and peak power can be calculated and used to feed a fuzzy logic algorithm. Based on prescribed membership functions and rules, the fuzzy logic algorithm returns the recognised intensity factor of each micro-trip, and the maximum intensity factor of all micro-trips can be used as the intensity factor of the drive cycle. Details of the algorithm can be found in [136], while generally, the micro-trip with both high energy demand and high peak power tends to be the most intense, while the energy demand has a higher weight than the peak power in determining the intensity factor. With this method, the intensity factors of the UDDS, HWFET and US06 cycles are recognised as 0.257, 0.903 and 0.914, which means that the US06 cycle is the most intense drive cycle while the UDDS cycle is the least intense one for the studied Tesla EV.

With the three drive cycles, Figure 50 (a1) presents the results of optimal overall costs, the size of the battery pack and the SC pack. As the drive cycle becomes more intense, the optimal overall costs

turn increasingly higher, and the US06 cycle has the highest overall costs. The optimal battery pack size remains unchanged at the minimum allowable size since the drive cycle does not change the energy requests for covering vehicle driving range, while the optimal SC pack size gets increasingly larger. To understand how the drive cycles cause the above trends, Figure 50 (a2) presents the energy demand and peak power of the most intense micro-trip of each drive cycle. As mentioned previously, the most intense micro-trip is the one that determines the intensity factor of the whole drive cycle. Compared with the HWFET cycle, the US06 cycle has a slightly lower energy demand yet a much higher peak power, and the higher peak power results in that the US06 cycle generates more costs and requires a larger SC pack than the HWFET cycle. Compared with the UDDS cycle, the HWFET cycle has a slightly lower peak power yet a much higher energy demand, and the higher energy demand leads to the HWFET cycle having more costs and a larger SC pack. It can be seen that the drive cycle with higher peak power does not necessarily raise the overall costs and SC pack size; the energy demand caused by the drive cycle also has an impact, while the drive cycle with both high energy demand and high peak power would lift up the overall costs and SC pack size. Namely, DESS sizing is impacted by the drive cycle with the combined result of both peak power and energy demand.

#### 6.3.1.2 EV driving range

The EV driving range is an important EV design parameter and a technical specification related to the energy capacity of the onboard battery pack [32]. Normally, the EV driving range is designated under the standard test procedure. For example, the most widely accepted test procedure is the one issued by the US Environmental Protection Agency (EPA), which uses a combination of three standard drive cycles (UDDS, US06, HWFET) to designate the officially recognised driving range [135]. Namely, the driving range is confirmed by the prescribed, particular drive cycles so that it is unaffected by the drive cycles or driving styles adopted for vehicle operation. According to (44), a longer driving range requires equipping a battery pack with larger energy capacity, which is fulfilled by grouping more parallel branches of battery cells, while the number of serial branches is not affected since the serial voltage of the battery pack should maintain the same with that of the bus. The studied Tesla EV specifies the base-case driving range as 426km under the EPA test procedure [135]. This base-case driving range is very long because the studied Tesla EV is designed for long-distance driving. In contrast, the range of common EVs is normally much shorter at around 200km, but recent years have witnessed the EV driving range being prolonged with the development of new energy storage technologies and EV design standards [32]. Moreover, 142km and 284km, as one-third and two-thirds of the base-case driving range, are assigned into the value set.

The sizing results with different driving ranges are plotted in Figure 50 (b1). As the driving range increases, the optimal battery pack size experiences a linear growth because the minimum allowable battery pack size linearly grows. Meanwhile, the optimal SC pack size keeps unchanged since the driving range does not change the power demands for EV propulsion. The overall costs witness a rapid growth; to find out the reason, the four sub-costs are then checked. It is found that SC purchase

cost, DC/DC purchase cost and electricity consumption costs witness no much change with the growing driving range; however, battery degradation costs are found increasing noticeably. The increasing battery degradation costs can be explained as follows and validated by Figure 50 (b2). As mentioned above, the optimal battery pack size grows with the growing driving range, leading to more battery cells being added as parallel branches. In this case, each parallel branch and each battery cell would share smaller power demands and working current, which relieves the degradation of a single battery cell. In contrast, the entire battery pack, whose degradation accumulates that of every single battery cell, is shown to have an aggravated degradation.

#### 6.3.1.3 DESS topology

The DESS topology describes the electrical connections of DESS components. As reviewed in Section 2.2.3, the semi-active topology has a good balance between cost and functionality; therefore, it is the most popular engineering practice. The semi-active topology can be further divided into SC/battery and battery/SC topologies (Figure 11), and the two topologies are assigned in the value set, while the former topology is the base case because it is the most popular one in literature [77]. The battery/SC topology can be considered as transformed from the SC/battery topology by swapping places of battery and SC pack. However, this swap brings complex influences on the sizing and EM of DESS. Firstly, in the SC/battery topology, the nominal voltage of the battery pack has to be the same as the nominal bus voltage since the battery pack is directly connected to the bus, while no hard restriction is enforced to the nominal voltage of the SC pack [77]. In contrast, in the battery/SC topology, the SC pack's nominal voltage is required as the same as that of the bus; consequently, a large number of SCs need to be deployed in series to reach nominal bus voltage, which significantly increases SC purchase cost. Secondly, the SC pack's operating voltage in the SC/battery topology can vary within a broad scope since the DC/DC converter is capable of handling a certain degree of voltage fluctuation [77]. In contrast, in the battery/SC topology, the SC pack's operating voltage cannot vary too much because the voltage fluctuation needs to be handled by the bus; a broad voltage scope of SC pack would impose a challenge on the motor/inverter. To distinguish the voltage scope between SC/battery and battery/SC topologies, this project considers that the minimum allowable voltage of SC pack for each topology is 20% and 50% of the nominal voltage of SC pack, respectively, while the maximum allowable voltage of SC pack is 100% for both topologies [154]. Thirdly, the voltage scope of SC pack is also related to the ratio of usable energy in the SC pack. Under the voltage scope mentioned above and based on (2), the usable energy ratio of SC pack for the SC/battery and battery/SC topologies is 96% and 75% [154], respectively. Lastly, the DC/DC converter of SC/battery topology is usually lager than that of battery/SC topology because the maximum working power of SC pack is usually much higher than that of battery pack [3].

Figure 50 (c1) shows the sizing results with DESS topologies. As the DESS topology changes from SC/battery to battery/SC, the optimal battery pack size does not change, while the optimal SC pack

size increases; meanwhile, the usable energy capacity of the SC pack grows from 132Wh to 336Wh. The overall costs show mild growth. By checking the sub-costs, SC purchase cost and electricity consumption costs are found increasing while DC/DC converter purchase cost decreasing; however, as analysed in Figure 48, these sub-costs each only occupies a small part of overall costs and thus can hardly account for the growth of overall costs. The major reason should attribute to that battery degradation costs are found increasing. To explain the increasing battery degradation costs, the energy throughputs of the battery pack and SC pack for both topologies are presented in Figure 50 (c2). Configured with more usable energy capacity, the SC pack of battery/SC topology has doubled energy throughput than that of SC/battery topology, which contributes to reducing and stabilising battery power and, consequently, lowering battery degradation pack. However, Figure 50 (c2) indicates that the battery pack energy throughput of battery/SC topology is larger than that of SC/battery topology. This is because the battery pack of either topology is responsible for providing the energy required by EV propulsion, but in the battery/SC topology, the DC/DC converter interfaces the battery pack and thus, the battery pack needs to provide extra energy to cover the DC/DC conversion loss. In this case, the battery pack of battery/SC topology generates more energy throughput and higher battery degradation.

#### 6.3.1.4 Nominal bus voltage

The bus is an intermediary between the mechanical drivetrain and electrical energy storage, conveying power and energy flows between the motor/inverter and the DESS [3]. Practical applications require the nominal voltages of the motor, the DESS and the bus to be as same as possible so that fewer efforts are needed for voltage transformation [168]. For the SC/battery topology, a higher nominal bus voltage requires the battery pack to arrange more battery cells as serial branches but fewer cells as parallel branches. In this case, the battery pack's equivalent resistance would increase while the working current of the battery pack can be reduced to fulfil the same power demands. The change of resistance and current would influence battery degradation and electricity consumption, while the detailed outcomes need to be checked with results; due to this, the nominal bus voltage is treated as a sensitive factor. The studied Tesla EV specifies the base-case nominal bus voltage as 350V. Besides, 380V and 320V are assigned in the value set because they are common nominal voltages of EV motors [24].

Optimal DESS size and overall costs with nominal bus voltage are shown in Figure 50 (d1). Nominal bus voltage does not influence the optimal battery pack size or SC pack size because it does not change either energy or power demands from EV propulsion. The check of sub-costs shows that SC purchase cost, DC/DC converter purchase cost and electricity consumption costs do not change too much with increasing nominal bus voltage, but battery degradation costs are significantly reduced, resulting in decreasing overall costs. As analysed previously, a higher bus voltage is beneficial to lowering the working current of the whole battery pack; however, the working current of each battery cell is not necessarily reduced because a higher bus voltage leads to fewer parallel branches to be

arranged, which proposes a possibility to increase the working current of battery cells in each parallel branch. Figure 49 (d2) validated that a higher nominal bus voltage does not much influence the average cell current but can significantly reduce the variance of cell current, which means that cell current is stabilised within a narrower scope centred by the average cell current. In this case, the degradation of a single cell is relieved because of the lowered fluctuation of cell current [148]. Since the optimal battery pack size is unchanged with nominal bus voltage, the battery cells' total number in the battery pack is subsequently unchanged. Thus, the reduction of battery cell degradation would eventually lead to the reduction of battery pack degradation.

#### 6.3.1.5 DC/DC conversion efficiency

The DC/DC conversion efficiency is defined as the ratio between energy output and energy input [15]. Despite that SCs are commonly considered as energy-efficient storages [170], the effectiveness of SCs also relies on DC/DC conversion efficiency because a lower conversion efficiency results in more energy lost during DC/DC conversion and consequently increased electricity consumption. Besides, a lower conversion efficiency also leads to SC energy depleting faster; thus, the battery needs to operate more frequently instead of the SC, increasing battery use and aggravating battery degradation. In practical, DC/DC conversion efficiency varies with the input/output voltage and current of the DC/DC converter [31]. However, to find out the straight relationship between DC/DC conversion efficiency and DESS sizing, the conversion efficiency is assigned as constants from 84% to 100% with a 4% interval, while 92% is used in the base case.

Figure 51 (a1) presents the results with DC/DC conversion efficiency. As the efficiency grows, the overall costs witness a near-linear decline. This decline can be attributed to the reduction of electricity consumption and battery degradation, which can be validated in Figure 51 (a2). With increasing DC/DC conversion efficiency, the energy loss due to DC/DC conversion is greatly reduced; thus, the electricity consumption to fulfil EV propulsion is reduced. Figure 51 (a2) also indicates that more useful energy throughput arises via DC/DC converter. This means that the SC pack is better exploited by buffering more energy and power, which relieves the battery pack's workload so that battery degradation can be significantly lowered. Besides, the optimal SC pack size finds an increasing tendency with improving conversion efficiency. This can be explained as, with more efficient DC/DC conversion, more SCs are encouraged to be configured; despite the increasing SC purchase cost, the benefit of reducing battery degradation costs and electricity consumption cost outweighs the incremental SC purchase cost.

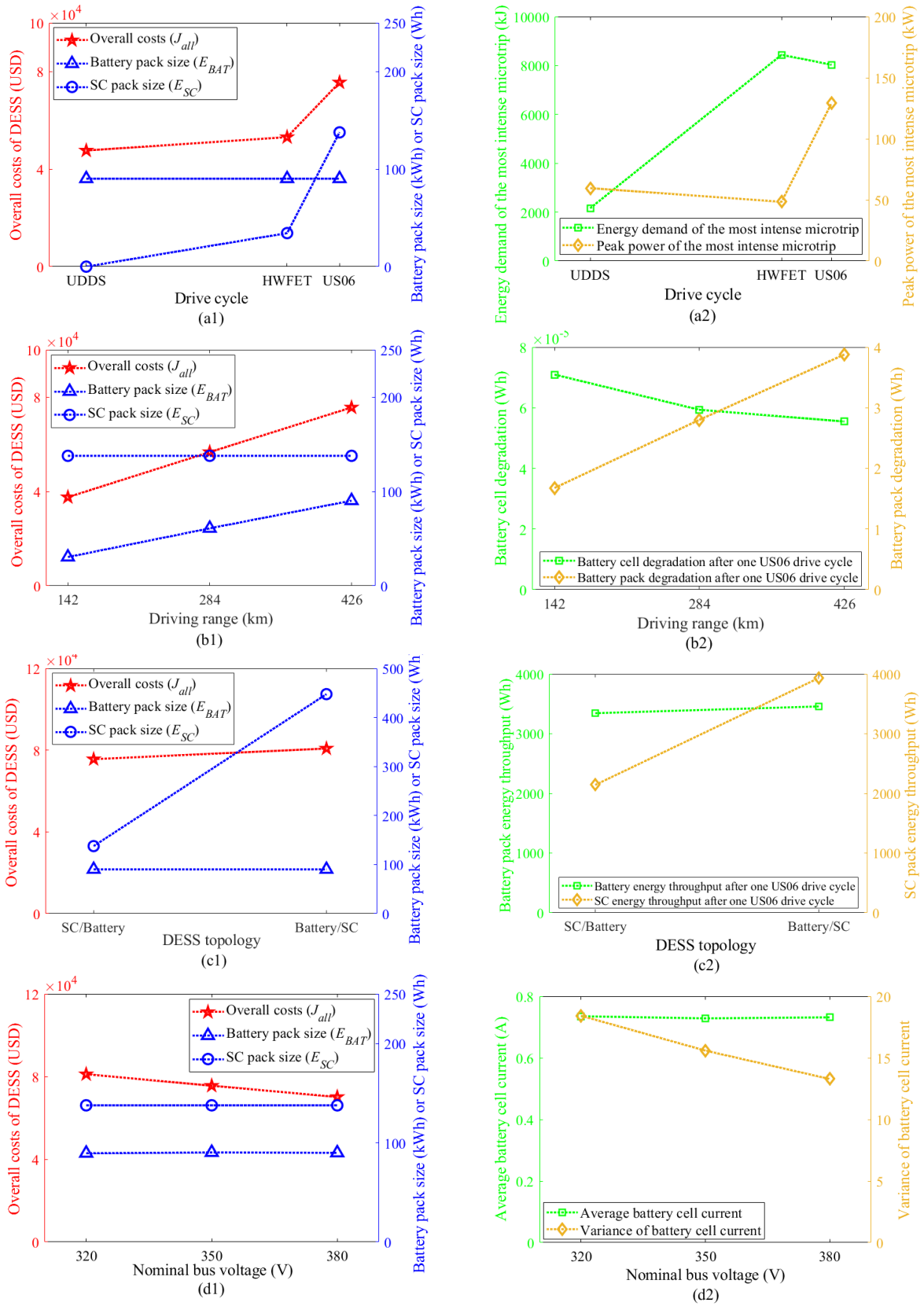


Figure 50 Optimal overall costs and the corresponding battery pack size and SC pack size with four sensitive factors: (a1) drive cycle; (b1) driving range; (c1) DESS topology; (d1) nominal bus voltage. Explanations for each sensitive factor: (a2) Average and peak power demands with drive cycle; (b2) degradation of battery cell and pack with driving range; (c2) energy throughputs of battery and SC pack with DESS topology; (d2) average and variance of cell current with nominal bus voltage.

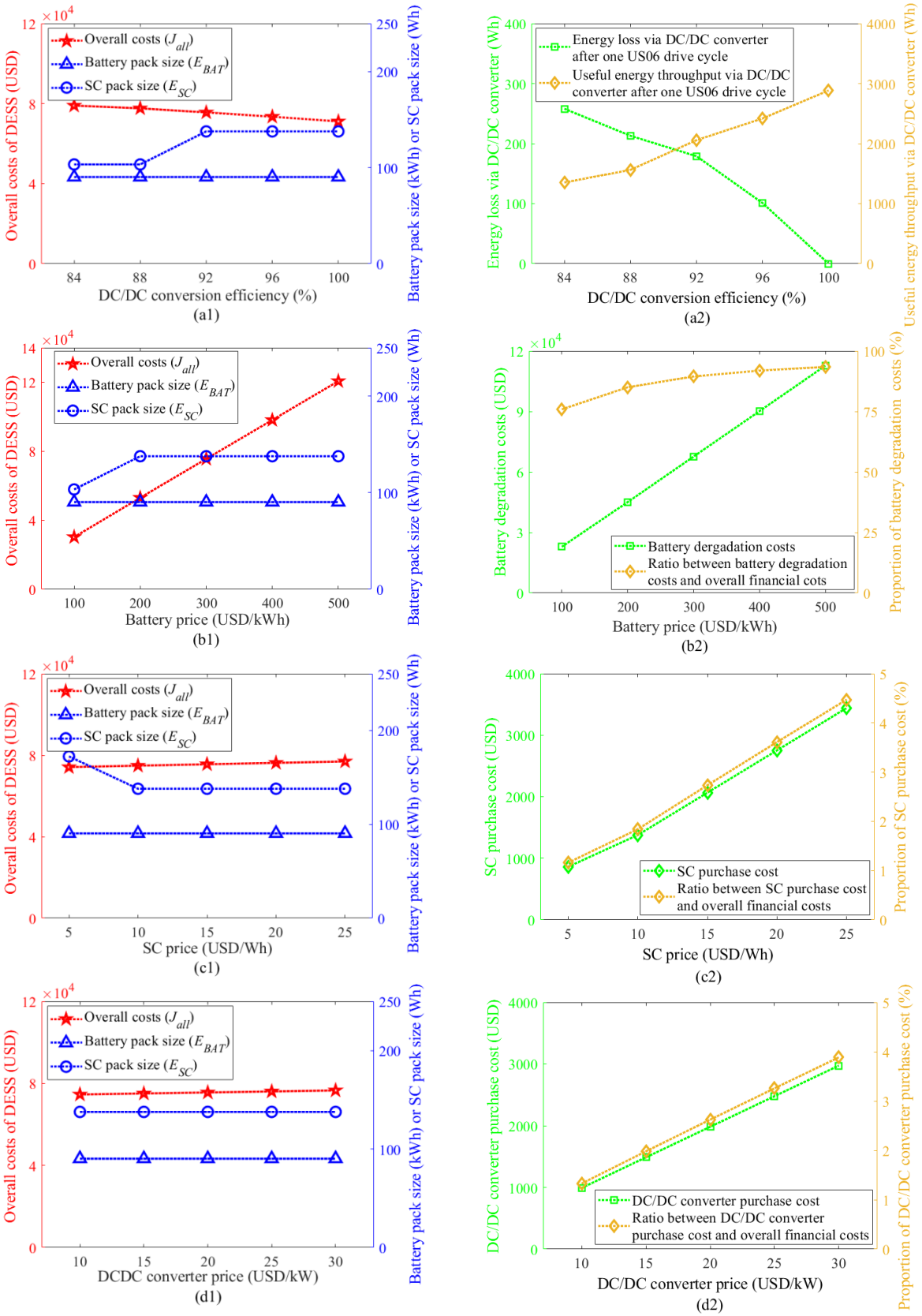


Figure 51 Optimal overall costs and the corresponding battery pack size and SC pack size with four sensitive factors: (a1) DC/DC conversion efficiency; (b1) battery price; (c1) SC price; (d1) DC/DC converter price. Explanations for each sensitive factor: (a2) energy loss and useful energy throughput via DC/DC converter with DC/DC conversion efficiency; (b2) battery degradation costs and their proportion to overall costs with battery price; (c2) SC purchase cost and its proportion to overall costs with SC price; (d2) DC/DC converter purchase cost and its proportion to overall costs with DC/DC converter price.

#### 6.3.1.6 Component price

It is easy to understand that as the component price increases, the overall costs would increase, and the component would be downsized. This project considers the battery, SC and DC/DC converter prices, and assigns their value sets in Table XXII. The results of overall costs and DESS size with battery price, SC price, DC/DC converter price are provided in Figure 51 (b1), (c1) and (d1); the corresponding explanations are offered in Figure 51 (b2), (c2) and (d2), respectively. Figure 51 (b1) shows that the increasing battery price leads to the overall costs growing dramatically, and battery degradation costs represent an increasingly high proportion of overall costs, and this proportion reaches 93% when battery price is 500 USD/kWh, as shown in Figure 51 (b2). Even if the battery price can be as low as 100 USD/kWh (which is less than half of the state-of-the-art price and can hardly be achieved in the next three years [7]), battery degradation still causes more than three quarters of overall costs. It can be inferred that the overall costs can be significantly reduced by battery degradation being reduced, and this is the motivation of Chapter 7, focusing on the optimisation of battery degradation. The increasing battery price also tends to raise the optimal SC pack size, as Figure 51 (b1). This can be explained as, with increasing battery price, reducing battery degradation costs becomes a more crucial matter; thus, more SCs are demanded to help reduce battery degradation. As SC price or DC/DC converter price increases, the overall costs witness a slow rise because either SC purchase cost or DC/DC converter purchase cost only represents around 3% of overall costs, as Figure 51 (c2) and (d2). Besides, the optimal SC pack size shows a decreasing tendency with SC price, in which case the incremental SC purchase cost outweighs the reduced battery degradation costs and thus discourages more SCs from being configured. In contrast, the DC/DC converter price has no evident influence on the optimal SC pack size.

### 6.3.2 Impact degrees of different factors

Following Section 6.3.1, this section quantifies the relative importance of each sensitive factor as an impact degree. The impact degrees of different factors are compared and discussed in terms of practical engineering.

By referring to the discipline of mathematical finance, this section firstly introduces the quantification of “sensitivity” [171], as (59). This equation calculates the percentage change of both output and input compared to the base case and obtains the sensitivity by dividing the former percentage change by the later one. In this chapter, the input is one of the factor values assigned in Table XXII, while the output is the corresponding overall costs. A nonzero sensitivity can be worked out for each value (except the base-case value) of one sensitive factor. Finally, the impact degree of that sensitive factor is quantified as the average of all nonzero sensitivities, as (60), where $n$ represents the number of non-base-case values. When calculating the impact degrees of drive cycle and DESS topology, (59) cannot be directly used because the value sets of the drive cycle and DESS topology are not numerical. For calculating the impact degree of drive cycle, the intensity factor of

the drive cycle is adopted as the input into (59); while for calculating the impact degree of DESS topology, SC pack energy capacity is adopted because it is the most remarkable difference between different DESS topologies in terms of DESS sizing [77].

$$Sensitivity = \left| \frac{\%\ Change\ in\ output}{\%\ Change\ in\ input} \right| \tag{59}$$

$$Impact\ degree = \frac{\sum_{i=1}^{n} Sensitivity_i}{n} \tag{60}$$

The impact degrees of eight sensitive factors are worked out as the radar plot in Figure 52. The drive cycle shows the largest impact degree - 1.243 and is considered to have a big impact on DESS overall costs. The drive cycle is not only a design parameter prescribing EV driving conditions but somewhat a reflection of driving habits [166]. From the driver's standpoint, less aggressive driving habits such as low-speed cruise and mild acceleration can significantly reduce the overall costs of DESS.

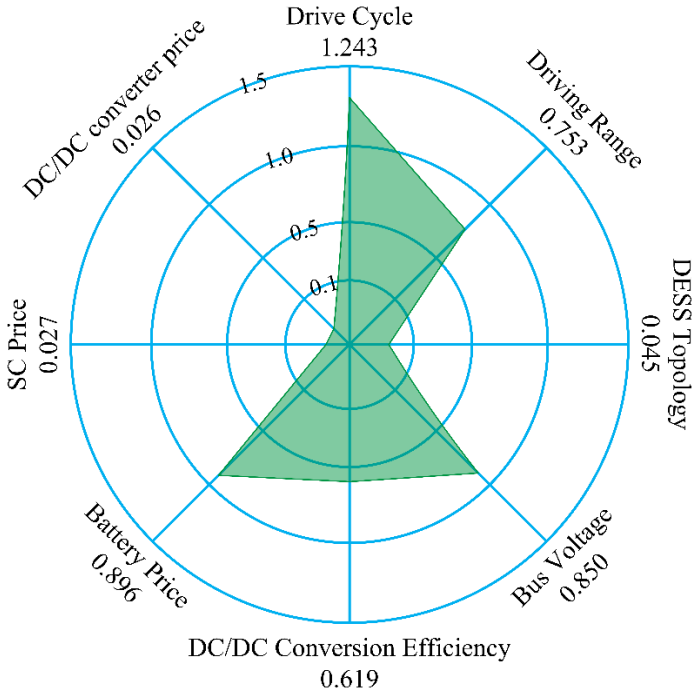


Figure 52 Radar plot of the impact degrees of eight sensitive factors. The number under each sensitive factor represents the corresponding impact degree.

The battery price, bus voltage, driving range and DC/DC conversion efficiency have descending impact degrees from 0.896 to 0.619, and they are considered to have medium impacts on DESS overall costs. Currently, the battery price is still high [14]; therefore, even a small percentage of battery degradation could bring a huge battery degradation cost, while the reduction of battery price relies on the breakthrough of economical battery manufacturing technology. The nominal bus voltage affects the overall costs by changing the battery pack's electrical configuration, while a higher bus

voltage can better reduce overall costs. As compared with lowering battery price, boosting nominal bus voltage is more practicable to achieve, but this relies on a good match with the motor and inverter [168]. The driving range is an EV design parameter related to the battery pack size. Nowadays, the concern of "range-anxiety" pushes EV manufacturers to deploy an increasingly larger battery pack to fulfil a longer driving range [32]. However, as the battery pack becomes larger with increasing driving range, the overall costs are found growing rapidly due to the fast-rising battery degradation costs. The DC/DC conversion efficiency determines not only the energy conversion loss but also the effectiveness of the SC pack, while the improvement of DC/DC conversion efficiency would require efforts on developing efficient topologies and power electronics [15].

The DESS topology, SC price and DC/DC converter price have descending impact degrees from 0.045 to 0.026, and they are considered to have little impacts on overall costs. Although DESS topology can change the electrical connections of DESS components, it is found to have no much impact on overall costs. The SC price is normally much higher than the battery price [3], but this does not mean that SC price has a bigger impact than battery price. This is because the optimal sizing results suggest configuring a small SC pack due to the fact that the efficacy of reducing battery degradation becomes increasingly less effective with more SCs being deployed. Therefore, the SC purchase cost only makes up around 3% of the overall costs. The DC/DC converter price has the least impact on overall costs; thus, it would be the last factor to consider when designing a DESS.

To offer general DESS sizing guides for EV applications, Table XXIII summaries the trends of optimal battery pack size, SC pack size and overall costs with eight sensitive factors, plus the impact degree of each factor.

Table XXIII Trends of optimal battery pack size, SC pack size and DESS overall costs with eight sensitive factors increasing, plus the impact degree of each factor.

(↑:increase, ↓:decrease, ─:unaffected)

| | Drive cycle | Driving range | DESS topology | Bus voltage | DC/DC efficiency | Battery price | SC price | DC/DC price |
|---|---|---|---|---|---|---|---|---|
| Battery size | ─ | ↑ | ─ | ─ | ─ | ─ | ─ | ─ |
| SC size | ↑ | ─ | ↑ | ─ | ↑ | ↑ | ↓ | ─ |
| Overall costs | ↑ | ↑ | ↑ | ↓ | ↓ | ↑ | ↑ | ↑ |
| Impact degree | High | medium | low | medium | medium | medium | low | low |

### 6.3.3 Summary

In summary, the significant findings from this chapter are listed as follows:

1) Size of battery pack and SC pack: The DESS should deploy as small as possible battery pack, as long as the EV driving range can be guaranteed. The SC pack size is a U-shape function of DESS costs so that there is an optimal SC pack size at which the DESS costs can be minimised.

2) Proportions of DESS costs: Battery degradation is the dominating cause (more than 75%) of DESS costs, so that it needs the most attention when sizing a DESS. In contrast, the energy consumption of DESS and the fixed costs to purchase the SC pack and DC/DC converter only represent a small part (around 11%) of DESS costs.

3) Impacts of sensitive factors: The EV drive cycle has the biggest impact on DESS costs since an intense drive cycle proposes both high peak power and high energy demand for the DESS to fulfil. When sizing a DESS for EVs designed with high acceleration capabilities or for drivers with aggressive driving styles, the SC pack needs to be significantly enlarged. Battery price, nominal bus voltage, EV driving range and DC/DC conversion efficiency have medium impacts on DESS costs. The currently high battery price determines that even a small percentage of battery degradation leads to a huge battery degradation cost, while the tendency of increasingly economical battery technologies would enable the SC pack to be downsized. The nominal bus voltage affects the electrical configuration and equivalent circuit parameters of the battery pack, and a high nominal bus voltage can lower the fluctuation of battery cell current and thus reduce battery degradation and DESS costs. Although boosting nominal bus voltage seems like a convenient, practicable approach to reduce DESS costs, the coordination of bus voltage with the motor and inverter must be settled simultaneously. EV driving range is directly related to the energy capacity of the battery pack. Demands of long driving range require to upsize the battery pack, but a large battery pack can generate more battery degradation cost and DESS costs. DC/DC conversion efficiency determines the effectiveness of the SC pack. As the conversion efficiency improves, the SC pack can become larger and thus better reduce battery degradation without increasing the total DESS costs. DESS topology, SC price and DC/DC converter price have little impacts on DESS costs, so that they should be considered with low priorities in practical engineering. Although DESS topology notably affects the SC pack size, the DESS costs are not obviously influenced by it. Compared with battery price, the prices of SC and DC/DC converter have much smaller impacts on DESS costs and size because the purchase costs of SC pack and DC/DC converter are much less than battery degradation cost.

# Chapter 7 Particular study: battery degradation with energy management and sizing

One important finding from Chapter 6 is that battery degradation costs occupy more than 75% of the overall costs of using a dual energy storage system (DESS) throughout electric vehicle (EV) lifetime, even if the battery price can be as low as 100 USD/kWh. Aiming at reducing DESS overall costs, the first priority is to optimise battery degradation. If battery degradation can be effectively relieved, the overall costs will be significantly reduced as a consequence. In this regard, this chapter targets the deep optimisation of battery degradation from two aspects - energy management (EM) and sizing, since battery degradation is a coupled result of both aspects [96].

As reviewed in Section 2.4.1, the optimisation of battery degradation has been widely studied in literature by means of the joint framework or multi-objective optimisation (MOP). However, these studies fail to induce the general rules of how to tune the EM or configure the size of DESS so as to reduce battery degradation, and their EM and sizing methodologies are usually confined to specific case studies and cannot be generalised. The three limitations of the previous studies are as follows:

(1) For the joint framework, it can optimise battery degradation by global, best-case EM and sizing, but the optimality is subject to the specific EM technique implemented. For example, in [44], the EM technique combing the wavelet transformation and power split ratio is implemented, using which the results of optimal battery degradation along with DESS component size are acquired. However, these results can only justify their optimality with the specifically implemented EM technique but cannot be proved optimal with another EM technique [121].

(2) MOP can work out a set of non-inferior solutions (i.e., Pareto Frontier) for multiple objectives from different metrics [110], while battery degradation is one of the objectives. However, its limitation is when generating an optimal solution, it needs to coordinate different metrics by manually weighting each. For example, in [112], a weight factor is specified to make a tradeoff between DESS mass and battery degradation; the optimal solution is thus enabled, but the weight factor's assignment is determined manually and thus has strong subjectivity. Besides, by assigning a high weight factor to the objective of battery degradation, the solutions can be much near-optimal to battery degradation. However, the solutions are still impacted by not only battery degradation but also the other objectives [111].

(3) For either joint framework or MOP, the solutions to battery degradation can only be worked out for specific case studies along with running a large number of algorithms that can take days [113], but it is not sure whether the solutions can be generalised from the case study to other scenarios using different EV parameters.

In contrast to the previous studies, this chapter deduces the general EM and sizing benchmarks for general cases to best reduce battery degradation, with the following novelties. 1) The EM benchmarks are not confined to any specific EM techniques, while the sizing benchmarks are not limited to any specific formulations of DESS component size. Namely, the EM and sizing benchmarks are independent of EM techniques and sizing formulations. 2) Targeted the pure relationship between battery degradation and optimal EM and sizing, battery degradation is the only objective to optimise without being weighted and interfered with any other objectives. 3) The EM and sizing benchmarks fit for wide cases using different parameters of EVs, batteries, SCs, rather than merely working for specific case studies. The remainder is structured as follows.

1) Section 7.1 illustrates four assessments of battery degradation – (1) battery degradation coefficient, (2) battery energy capacity loss, (3) battery replacement times and (4) DESS component costs. The first two assessments have been mentioned in the previous chapters and are complimented in this chapter with (3) and (4) for evaluating the engineering and financial impacts of battery degradation [89], respectively.

2) Section 7.2 investigates the EM benchmarks to optimise battery degradation. Targeted optimising battery degradation by EM efforts, the size of DESS components is considered as invariant in this section. The optimal EM scheme for a size-fixed DESS to minimise battery degradation is obtained by mathematical deductions, which benchmarks the best-case battery degradation that whatever EM technique can ever achieve.

3) Section 7.3 investigates the sizing benchmarks to optimise battery degradation from the aspect of sizing. Targeted optimising battery degradation by sizing efforts, the EM of DESS is held as optimal in this section. The general trends of battery degradation with DESS component size are assessed, which offers benchmarks for the DESS components to upsize or downsize so as to reduce battery degradation.

4) Since the EM and sizing benchmarks are obtained by deductions, their efficacy should be verified, and this is done by a case study in Section 7.4. The case study uses the high-performance Tesla EV running with the drastic S-US06 drive cycle. This chapter investigates the benchmarks for general EVs while emphasising the application in high-performance EVs. Compared with standard EVs, high-performance EVs feature long-distance, aggressive driving capabilities [47], which requires to deploy a large battery pack working at high power/current rates and thus poses a possibility of severe battery degradation.

## 7.1 Assessments of battery degradation

As formulated in Section 5.1.2, the battery degradation coefficient ($\alpha$) is used to calculate the percentage capacity loss, and the battery energy capacity loss ($E_{loss}$) equates to the Watt-hour

decrease caused by battery degradation. Besides, this chapter also uses the battery replacement times ($N$) and DESS component costs ($J_{compo}$) to evaluate the engineering and financial impacts of battery degradation, respectively, and are explained as follows.

Battery replacement times ($N$) are an assessment associated with the maintenance of the battery pack. As each time battery degradation coefficient $\alpha$ reaches 20%, the onboard battery pack is considered end-of-life (EOL) and needs to be replaced with a new one [44]. However, too many battery replacements are unwanted by EV users and manufacturers [12], as $N$ is expected to be as few as possible throughout the EV lifetime. The formulation of $N$ is expressed as (61). Where $Range_{EVlife}$ and $Range_{EVcycle}$ are the driving range of EV lifetime (considered 150000km [70]) and of one EV drive cycle, respectively. Namely, ($Range_{EVlife}/Range_{EVcycle}$) is the coefficient transferring the battery replacement times from one drive cycle to EV lifetime.

$$N = \frac{\alpha}{20\%} \cdot \frac{Range_{EVlife}}{Range_{EVcycle}} \tag{61}$$

The DESS component costs ($J_{compo}$) are defined as the financial costs to purchase and renew DESS components due to battery degradation. Based on Section 6.2.1, where the battery degradation costs ($J_{BAT}$), SC purchase cost ($J_{SC}$) and DC/DC converter purchase cost ($J_{DCDC}$) are formulated, $J_{compo}$ is formulated as the sum of $J_{BAT}$, $J_{SC}$ and $J_{DCDC}$, as (51). Even though $J_{BAT}$ is the direct result of battery degradation, $J_{compo}$ rather than $J_{BAT}$ is used to assess the financial impacts of battery degradation. This is because $J_{BAT}$ may be reduced by configuring a larger SC pack, but the corresponding $J_{SC}$ and $J_{DCDC}$ are simultaneously higher [91]. Therefore, it is unfair to only use $J_{BAT}$ to assess the financial impacts of battery degradation; in contrast, the comprehensive assessment should take into account all of $J_{BAT}$, $J_{SC}$ and $J_{DCDC}$.

$$J_{compo} = J_{BAT} + J_{SC} + J_{DCDC} \tag{62}$$

## 7.2 Battery degradation with energy management

This section deduces how the battery operating power ($P_{BAT}$) and SC operating power ($P_{SC}$) should perform to reduce battery degradation. As mentioned previously, the size of DESS components is considered fixed; therefore, minimising any of the four assessments is equivalent to minimising the other three, because the four assessments have positive correlations to each other. For convenience, battery energy capacity loss ($E_{loss}$) is used here as the factor to minimise. The deduction is divided into two parts: the first part disregards the SC pack's energy capacity and then deduces the ideal EM benchmarks if the SC pack can be infinitely large. The second part, evolving from the first part, considers that the SC pack usually has a small energy capacity [13] and then deduces the practical EM benchmarks.

### 7.2.1 Ideal EM benchmarks with infinite SC pack

Assume the battery pack operates following any given power demands, and the power demands change with time at a set time interval. Knowing that battery degradation, reflected by $E_{loss}$, grows sharply with increasing $P_{BAT}$ [49], the rate of $E_{loss}$ ($dE_{loss}/dt$, defined as battery energy capacity loss in the set time interval) can be expressed as an increasing convex function of $P_{BAT}$ [57], as Figure 53, and (63) is workable. Where $P_{BAT,1}$, $P_{BAT,2}$, …, $P_{BAT,n}$ are the battery operating power at time point 1, 2, …, n. $\bar{P}_{BAT}$ is the mean battery operating power.

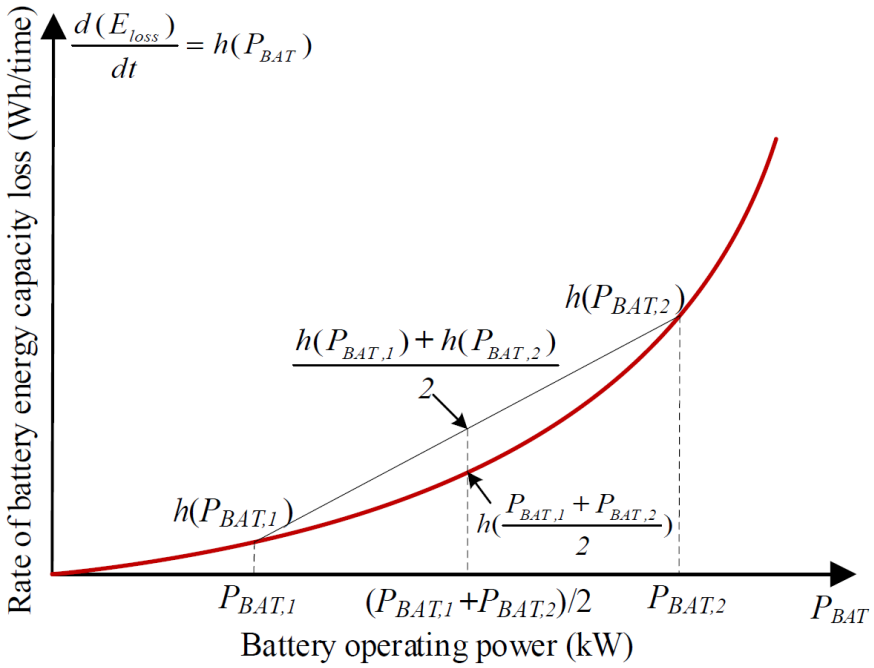


Figure 53 Rate of battery energy capacity loss as an increasing convex function of battery operating power.

$$\begin{cases} dE_{loss}/dt = h(P_{BAT}) \\ \dfrac{h(P_{BAT,1}) + h(P_{BAT,2}) + \ldots + h(P_{BAT,n})}{n} \geq h\left(\dfrac{P_{BAT,1} + P_{BAT,2} + \ldots + P_{BAT,n}}{n}\right) = h(\bar{P}_{BAT}) \end{cases} \quad (63)$$

Assume the DESS operates following any given bus power profile ($P_{bus}$) from time zero to time $t_n$. At each time point ($t_i$, $i$= 1, 2, …, $n$), the battery operating power ($P_{BAT,i}$, $i$= 1, 2, …, $n$) is specifically allocated by the EM scheme. Based on Figure 53 and (63), the $E_{loss}$ over this period can be expressed as (64).

$$\begin{aligned} E_{loss} &= \int_0^{t_n} \frac{dE_{loss}}{dt} dt = \int_0^{t_n} h\left(P_{BAT}\right) dt = \lim_{n\to\infty}\left[\sum_{i=1}^{n} h\left(P_{BAT,i}\right)\right] \cdot \frac{t_n}{n} \\ &\geq \lim_{n\to\infty} h\left[\sum_{i=1}^{n}\left(P_{BAT,i}\right) \cdot \frac{1}{n}\right] \cdot t_n = h(\bar{P}_{BAT}) \cdot t_n \end{aligned} \quad (64)$$

Equation (64) implies that $E_{loss}$ can get its minimum value $h(\bar{P}_{BAT})t_n$ by making $P_{BAT}$ constant at $\bar{P}_{BAT}$. According to the "charge-sustaining principle" indicating that $\bar{P}_{BAT}$ approximately equals the mean bus power ($\bar{P}_{bus}$) [13], (64) can be transformed into (65).

$$E_{loss} \geq h(\overline{P}_{BAT}) \cdot t_n \approx h(\overline{P}_{bus}) \cdot t_n \tag{65}$$

Equation (65) implies that the minimum value of $E_{loss}$ approximately equals $h(\bar{P}_{bus})t_n$ and this value can be achieved by the optimal EM scheme allocating $P_{BAT}$ constant at $\bar{P}_{bus}$. However, to maintain $P_{BAT}$ constant at $\bar{P}_{bus}$, the optimal EM scheme must ensure that the residual power demands ($P_{bus}$ - $\bar{P}_{bus}$) can be continuously compensated by the SC pack, which calls for configuring an ideal SC pack with excessively large energy capacity (this will be demonstrated in Section 7.4.2 by Figure 56). In practice, a much smaller SC pack would be configured, but consequently, $P_{BAT}$ cannot stay constant and would fluctuate around $\bar{P}_{bus}$ [172]. Towards practical application, Section 7.2.2 adjusts the optimal EM scheme by deducing how $P_{BAT}$ variation impacts $E_{loss}$ and raises the requirement for the energy capacity of SC pack.

### 7.2.2 Practical EM benchmarks with non-infinite SC pack

Assume a bus power profile with only two points ($P_{bus,1}$ at $t_1$ and $P_{bus,2}$ at $t_2$), and the mean bus power is confirmed as $\bar{P}_{bus}$. To fulfil this profile, three imaginary EM schemes are numbered as ⓐ, ⓑ and ⓒ in Figure 54. The difference among the EM schemes can be reflected by any subplot of Figure 2. The $P_{BAT}$ allocated by the three EM schemes, which is presented in Figure 54 (I) and designed according to (66), have different scales of fluctuation: ⓐ represents that $P_{BAT}$ follows the bus power like a battery-only ESS and has large fluctuation; ⓒ represents that $P_{BAT}$ stays constant at $\bar{P}_{bus}$ and has no fluctuation; ⓑ is a compromise between ⓐ and ⓒ, representing that $P_{BAT}$ has medium fluctuation. The $P_{BAT}$ of three EM schemes are then mapped to Figure 54 (II), where the rate of $E_{loss}$ is an increasing convex function of $P_{BAT}$, like Figure 53; however, for the convenience of mapping, Figure 54 (II) uses $P_{BAT}$ as Y-axis. Based on Figure 54 (II), the $E_{loss}$ resulting from each EM scheme ($E_{loss,a}$, $E_{loss,b}$ and $E_{loss,c}$) can be expressed as (67) and (68).

$$\overline{P}_{bus} = \frac{P_{bus,1} + P_{bus,2}}{2} = \frac{P_{BAT,1} + P_{BAT,2}}{2} = \overline{P}_{BAT} \tag{66}$$

$$\begin{cases} E_{loss,a} = \left[ h\left(P_{bus,1}\right) + h\left(P_{bus,2}\right) \right] dt \\ E_{loss,b} = \left[ h\left(P_{BAT,1}\right) + h\left(P_{BAT,2}\right) \right] dt \\ E_{loss,c} = 2h\left(\overline{P}_{bus}\right) dt \end{cases} \tag{67}$$

$$E_{loss,a} = E_{loss,b} + (m+n)\,dt > E_{loss,b} > E_{loss,c} \tag{68}$$

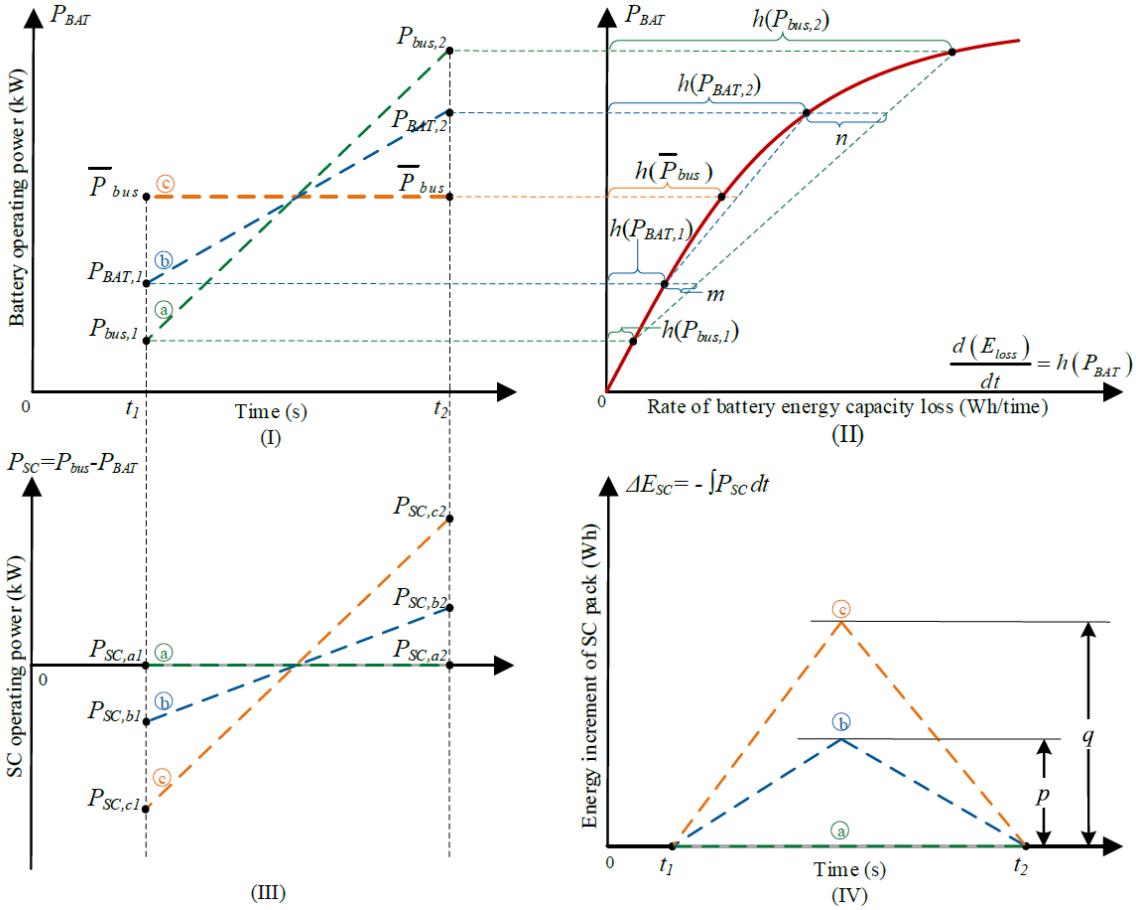


Figure 54 Three alternative EM schemes and their: (I) battery operating power; (II) rate of battery energy capacity loss as a function of battery operating power; (III) SC operating power; (IV) energy increment of SC pack (*a*, *b*, *c* represent subscripts of three EM schemes; *1*, *2* represent subscripts of two time points; *m*, *n*, *p*, *q* represent the algebraic length).

Equation (68) indicates that the EM scheme with larger $P_{BAT}$ fluctuation generates larger $E_{loss}$. Therefore, to reduce battery degradation, the EM scheme should aim at reducing $P_{BAT}$ fluctuation, which requires assistance from the SC pack. Figure 54 (III) presents the $P_{SC}$ allocated by the three EM schemes, which follows (69) due to the charge-sustaining principle [87].

$$P_{SC,a1}=P_{SC,a2} = \frac{P_{SC,b1}+P_{SC,b2}}{2} = \frac{P_{SC,c1}+P_{SC,c2}}{2} = 0 \tag{69}$$

Based on Figure 54 (III), the energy increment of SC pack ($\Delta E_{SC}$, defined as the time integral of $P_{SC}$) are worked out in Figure 54 (IV). As the range of $\Delta E_{SC}$ equals the usable energy capacity of SC pack ($E_{SC}$), the $E_{SC}$ required by each EM scheme ($E_{SC,a}$, $E_{SC,b}$ and $E_{SC,c}$) can be compared as (70), which indicates that $E_{SC}$ is required to increase with smaller $P_{BAT}$ fluctuation. If a SC pack is configured according to the energy capacity required by EM scheme ⓑ, this SC pack can also fulfill ⓐ but cannot fulfill ⓒ. Thus, the potential for the EM to reduce $P_{BAT}$ fluctuation is subject to the configured

$E_{SC}$: as $E_{SC}$ becomes larger, the EM scheme would have more flexibility to reduce $P_{BAT}$ fluctuation, and as a result, reduce $E_{loss}$. Based on Figure 54 (I) to (IV), reducing the fluctuation of battery operating power can decrease battery degradation but simultaneously increases the fluctuation of SC operating power and thus proposes the requirement for a larger SC pack to secure the larger range of energy increment.

$$E_{SC,c} = q > E_{SC,b} = p > E_{SC,a} = 0 \tag{70}$$

Combining Sections 7.2.1 and 7.2.2, the EM benchmark for a DESS to minimise battery degradation can be redefined as: the optimal EM scheme should aim at reducing the fluctuation of battery operating power; the smaller the fluctuation, the smaller the battery degradation. However, the potential for the EM scheme to reduce battery degradation is subject to the size of SC pack; the optimal EM scheme would be the same for DESSs with the same size SC packs. In the ideal situation where the SC pack is large enough to maintain the battery working power constant at the mean bus power demand, battery degradation can be a minimum. The deduction of the EM benchmark does not include any specific EM techniques or parameters of the EV, battery or SC; therefore, the EM benchmark is independent of these factors and thus can apply to wide cases.

## 7.3 Battery degradation with sizing

This section deduces how the battery pack size (represented by $E_{BAT}$) and SC pack size (represented by $E_{SC}$) influence the battery degradation (represented by each of $\alpha$, $E_{loss}$, $J_{compo}$ and $N$). The general trends of battery degradation with DESS component size are obtained as the sizing benchmarks. As mentioned previously, the EM of DESS is held optimal by following the EM benchmarks deduced in Section 7.2.

### 7.3.1 Battery degradation with SC pack size

This section regards $E_{BAT}$ as fixed and investigates how $\alpha$, $E_{loss}$, $J_{compo}$ and $N$ vary with $E_{SC}$. Section 7.2 points out that $E_{loss}$ decreases with growing $E_{SC}$; according to (27), $\alpha$ also decreases as $E_{SC}$ grows; according to (61), $N$ also decreases. According to (51), $J_{compo}$ comprises $J_{BAT}$, $J_{SC}$ and $J_{DCDC}$. As $E_{SC}$ grows, $J_{BAT}$ would decrease because $E_{loss}$ can be reduced, while $J_{SC}$ and $J_{DCDC}$ would increase. In combination, $J_{compo}$ would depend on not only battery degradation but also the prices of battery, SC and DC/ DC converter [109]. However, it can be inferred as a general trend independent of component prices that $J_{compo}$ would initially drop but finally upswing in a U-shape change with growing $E_{SC}$. This is because $J_{compo}$ can be initially reduced with $J_{BAT}$ being effectively reduced by a lager $E_{SC}$; while the capability of enlarging $E_{SC}$ to reduce $J_{BAT}$ would be increasingly less effective and finally reach a limit after which $J_{BAT}$ along with battery degradation can hardly be further reduced but $J_{SC}$ and $J_{DCDC}$ would keep increasing as $E_{SC}$ becomes larger. In the combination of $J_{BAT}$, $J_{SC}$ and $J_{DCDC}$, there would be an extreme point of $E_{SC}$ at which $J_{compo}$ can be minimised.

### 7.3.2 Battery degradation with battery pack size

This section regards $E_{SC}$ as fixed and deduces how $\alpha$, $E_{loss}$, $J_{compo}$ and $N$ vary with $E_{BAT}$. The battery degradation model expressed by (27) in Section 5.1.2 is reused to calculate $\alpha$ (battery degradation coefficient). $\alpha$ can be expressed as a function of $E_{BAT}$, as (71). Where $I_{BAT}$ is battery operating current. $U_{BAT,nom}$ is battery nominal voltage and is a constant subject to the bus voltage. Since $E_{BAT}$ is a variable representing battery pack size and independent of $I_{BAT}$, $U_{BAT,nom}$ and $t$, the partial derivative of $\alpha$ to $E_{BAT}$ be expressed as (72). The sign of (72) is always below zero so that $\alpha$ monotonously decreases with growing $E_{BAT}$. According to (61), $N$ also decreases with growing $E_{BAT}$.

$$\alpha = f\left(E_{BAT}\right) = 4.23 \cdot 10^{-4} exp\left(0.396 \frac{\left|I_{BAT}\right| U_{BAT,nom}}{E_{BAT}}\right) \left|I_{BAT}\right| t \tag{71}$$

$$\frac{\partial(\alpha)}{\partial(E_{BAT})} = f'\left(E_{BAT}\right) = -1.68 \cdot 10^{-4} exp\left(0.396 \frac{\left|I_{BAT}\right| U_{BAT,nom}}{E_{BAT}}\right) \frac{I_{BAT}^2 U_{BAT,nom}}{E_{BAT}^2} t < 0 \tag{72}$$

Combining (27) and (71), $E_{loss}$ can be expressed as a function of $E_{BAT}$, as (73). The partial derivative of $E_{loss}$ to $E_{BAT}$ can be expressed as (74). The sign of (74) depends on the battery current rate ($I_{rate}$): if $I_{rate}$ is less than 2.5C, (74) would be above zero. This work considers $I_{rate}$ as less than 2.5C, because the batteries deployed in a DESS tend to be energy-intense batteries whose $I_{rate}$ is usually smaller than 2C; moreover, with the help of SCs, the $I_{rate}$ in practical operations can be secured far below 2.5C [58]. Therefore, $E_{loss}$ monotonously increases with growing $E_{BAT}$, and this trend can be explained from the engineering aspect, as follows. As $E_{BAT}$ grows, more battery cells would be added as parallel branches into the battery pack, while the number of serial branches would maintain unchanged because the nominal voltage of the battery pack is subject to the nominal bus voltage. Given the same operating power of battery pack, the battery cell in a larger battery pack would take on smaller operating power and current; therefore, each battery cell's degradation can be lowered as represented by smaller energy capacity loss of each cell. However, the energy capacity loss of the whole battery pack ($E_{loss}$), which is the energy capacity loss of each battery cell added up, would increase. Finally, according to (51), $J_{compo}$ also increases with growing $E_{BAT}$.

$$E_{loss} = E_{BAT}\alpha = g\left(E_{BAT}\right) = 4.23 \cdot 10^{-4} exp\left(0.396 \frac{\left|I_{BAT}\right| U_{BAT,nom}}{E_{BAT}}\right) \left|I_{BAT}\right| E_{BAT} t \tag{73}$$

$$\begin{aligned} \frac{\partial(E_{loss})}{\partial(E_{BAT})} &= g'\left(E_{BAT}\right) \\ &= 4.23 \cdot 10^{-4} exp\left(0.396 \frac{\left|I_{BAT}\right| U_{BAT,nom}}{E_{BAT}}\right) \left(1 - \frac{0.396 \left|I_{BAT}\right| U_{BAT,nom}}{E_{BAT}}\right) \left|I_{BAT}\right| t \\ &= 4.23 \cdot 10^{-4} exp\left(0.396 I_{rate}\right) \left(1 - 0.396 I_{rate}\right) \left|I_{BAT}\right| t \end{aligned} \tag{74}$$

In summary of the above deductions, Table XXIV collects the general trends of battery degradation with increasing DESS component size, which are independent of EM techniques or parameters of the EV, battery and SC. From an engineering point of view, the combination of a large battery pack and a large SC pack is preferred to reduce the battery replacement times over EV lifetime. To reduce the DESS component costs over EV lifetime, a small battery pack is definitely preferred, while the determination of SC pack size needs to consider component prices, but it can be sure that the DESS component costs would experience a U-shape change with enlarging SC pack size.

Table XXIV General trends of battery degradation with increasing DESS component size

| | Battery degradation coefficient ($\alpha$) | Battery energy capacity loss ($E_{loss}$) | Battery replacement times ($N$) | DESS component costs ($J_{compo}$) |
|---|---|---|---|---|
| Battery pack size ($E_{BAT}$) | Negative | Positive | Negative | Positive |
| SC pack size ($E_{SC}$) | Negative | Negative | Negative | Initially negative, finally positive |

## 7.4 Case study

This section verifies the deduced EM and sizing benchmarks by a case study. The case study uses the S-US06 drive cycle (Figure 21) and SC/battery DESS topology (Figure 11), and the other inputs come from Tesla Model S P85 EV (Table VII, Table VIII), Panasonic NCR 18650B battery (Table IX), Maxwell BCAP3400 2.7V SC (Table IX) and a hypothetical DC/DC converter (Table X). The verification follows the following process:

1) The feasible set constraining DESS component size ($E_{BAT}$ and $E_{SC}$) is obtained based on Section 6.1. Within the feasible set, five DESS designs, which differ from each other by either battery pack size or SC pack size, are selected as samples for comparison.

2) The optimal EM scheme and the power split strategy for each DESS design are obtained based on Section 5.2.1. The battery and SC operating power of each DESS design are compared, and as such, the EM benchmarks are verified.

3) The battery degradation coefficient ($\alpha$) and energy capacity loss ($E_{loss}$) for each DESS design are also obtained. By comparing the $\alpha$ and $E_{loss}$ of each DESS design, the general trends of $\alpha$ and $E_{loss}$ with $E_{BAT}$ and $E_{SC}$ are verified.

4) The battery replacement times ($N$) and DESS component costs ($J_{compo}$) are obtained for the whole feasible set instead of only for the five DESS designs. The general trends of $N$ and $J_{compo}$ with $E_{BAT}$ and $E_{SC}$ are then verified. With an emphasis on the financial impacts of battery degradation, the

optimal DESS design is worked out in terms of minimum $J_{compo}$. Specifically, the underlying reasons for the impacts of DESS component size on DESS component costs are discussed.

### 7.4.1 Feasible set and sample selection

Using (44) and (45), the feasible set of DESS component size is constrained as Figure 55. The battery pack energy capacity ($E_{BAT}$) is the X-axis to represent battery pack size, and the SC pack energy capacity ($E_{SC}$) is the Y-axis to represent SC pack size. Following (46) and (47), the mass and volume of DESS are also presented in Figure 55. Any point within the feasible set can be a workable DESS design that meets the prescribed EV driving range and S-US06 drive cycle operations.

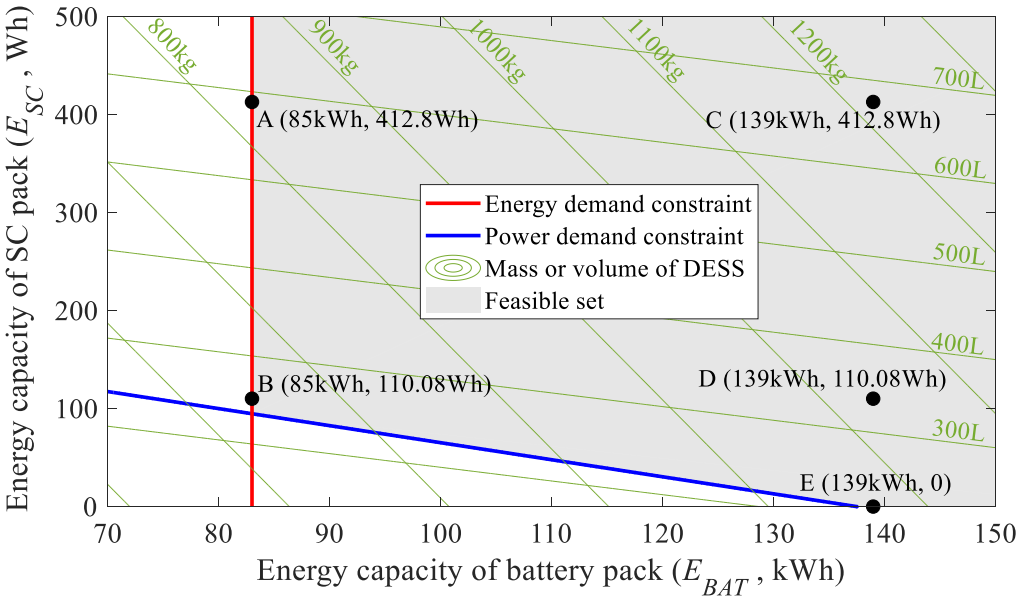


Figure 55 Feasible set of DESS component size and five DESS samples to compare.

Five DESS designs and their component size are labelled in Figure 55, as points A, B, C, D and E, and their electrical configurations are compared in Table XXV. Points A and C are selected with the consideration of DC/DC conversion efficiency: in SC/battery DESS topology, the higher conversion efficiency can be achieved with the narrower voltage gap between the SC pack and bus [15]. In this case, points A and C apply 120 SCs in series, respectively, reaching a voltage level (324V) very close to the bus voltage (350V). In comparison, point A deploys the minimum allowable battery pack, while point C deploys a larger battery pack same as point E. Point B is selected near the joint of the power and energy constraints (rather than exactly on the joint, because in terms of battery packaging, the number of battery cells must be an integer while the joint is not the case), representing a DESS with a small battery pack and a small SC pack. Point D has the same battery pack as E, and the same SC pack as B. Point E is a battery-only ESS. It can be seen that point B has the minimum mass among all designs, while point E has the minimum volume. The five designs are compared in the following sections.

Table XXV Electrical configurations of the five designs

| | A (small battery & large SC) | B (small battery & small SC) | C (large battery & large SC) | D (large battery & small SC) | E (large battery-only) |
|---|---|---|---|---|---|
| Battery pack configuration | 96 serial 74 parallel | 96 serial 74 parallel | 96 serial 124 parallel | 96 serial 124 parallel | 96 serial 124 parallel |
| SC pack configuration | 120 serial | 32 serial | 120 serial | 32 serial | 0 |

### 7.4.2 Verification of EM benchmarks

The ideal EM benchmarks indicate that battery degradation can be minimised by maintaining battery operating power constant at the mean bus power ($\bar{P}_{bus}$), but in this case, the SC pack would be excessively large. To verify this, a DESS with an 85 kWh battery pack (same as the DESS designs A and B) and a theoretically infinite SC pack is simulated with the objective of minimising battery energy capacity loss. The simulated bus power demand $P_{bus}$, battery operating power $P_{BAT}$ and SC operating power $P_{SC}$ are plotted in Figure 56 (a). With the infinite SC pack, $P_{BAT}$ stays constant, near but a bit above $\bar{P}_{bus}$. This is because the battery pack delivers extra power to compensate for the DC/DC conversion loss. Based on Figure 56 (a), the energy increment of SC pack ($\Delta E_{SC}$), which is the time integral of $P_{SC}$, is plotted in Figure 56 (b). It can be seen that the range of $\Delta E_{SC}$ is 2488Wh, which means that to make $P_{BAT}$ constant, the energy capacity of the SC pack does not have to be infinite but must be no less than 2488Wh. However, this SC pack is still too large to be mounted in practical application because of its huge mass and volume (calculated as 1174kg and 2571L).

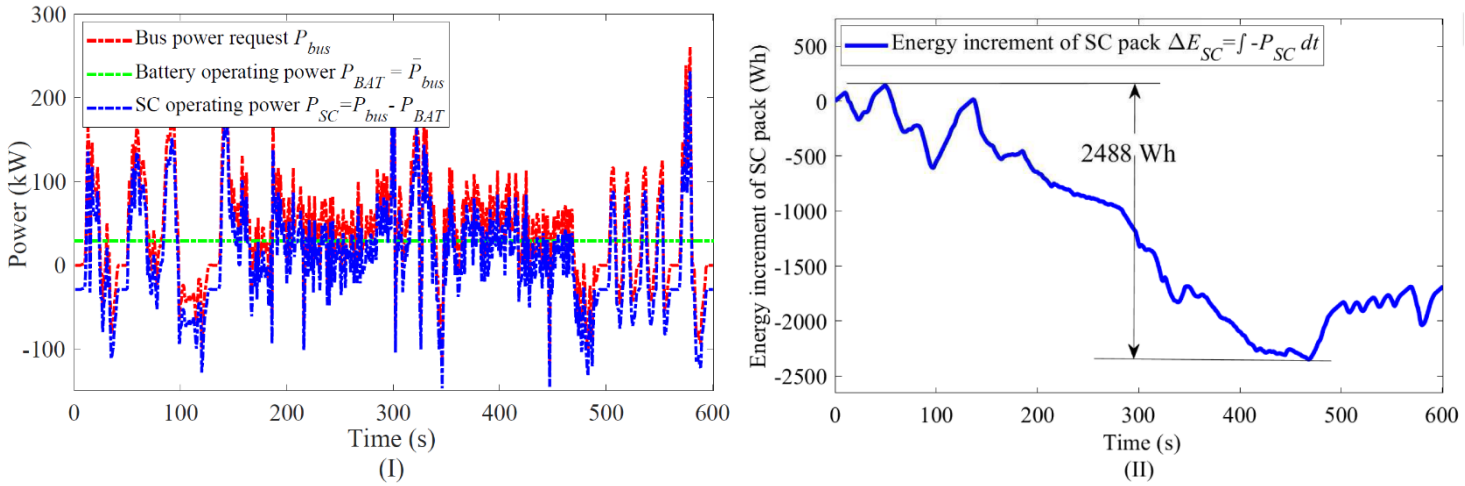


Figure 56 Verification of the ideal EM benchmarks with infinite SC pack: (a) bus power demand, battery operating power and SC operating power; (b) energy increment of SC pack. Both subfigures are in the time frame of one S-US06 drive cycle.

The practical EM benchmarks indicate that the optimal EM scheme is dependent on the SC pack size, and a larger SC pack can enable the EM scheme to better reduce the fluctuation of battery operating

power. To verify this, the simulated battery operating power ($P_{BAT}$) and SC operating power ($P_{SC}$) curves of the DESS designs A to D are compared in Figure 57 (a) and (b), respectively; the variance of each curve, which is a sign of fluctuation, is also presented in the legends. Figure 57 (a) shows that DESSs A and C have almost overlapped $P_{BAT}$ curves and very close variances (so do DESSs B and D). This is because they have the same size SC packs, which offers them the same optimal EM schemes. The fluctuation of A or C is smaller than that of B or D because A or C has a SC pack larger than that of B or D, which offers the EM scheme more flexibility to reduce the $P_{BAT}$ fluctuation. Figure 57 (b) compares the SC operating power ($P_{SC}$) curves. Similarly, DESSs A and C have almost overlapped $P_{SC}$ curves (so do DESSs B and D). However, as the expense of reducing $P_{BAT}$ fluctuation, the $P_{SC}$ fluctuation of A or C is larger than that of B or D. By Figure 57, it is verified that the DESS design with a larger SC pack has more stabilised battery operating power; the DESS designs with the same size SC packs have almost the same optimal EM scheme, while the size of battery pack only has a very limited impact on optimal EM scheme.

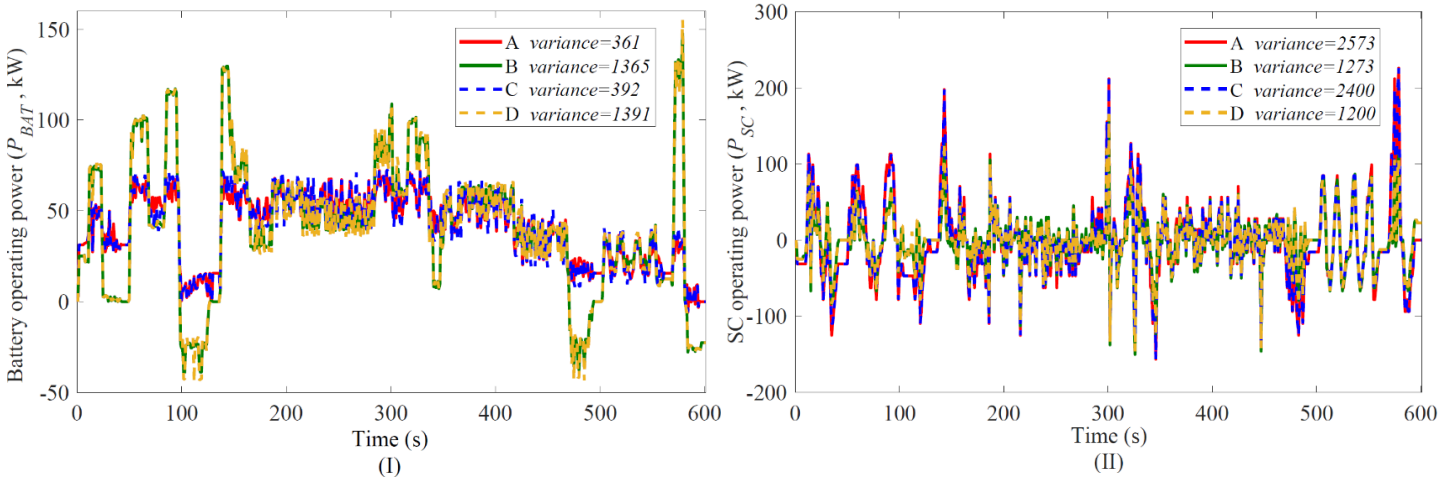


Figure 57 Verification of the practical EM benchmarks by comparing the power curves of four DESS designs: (a) battery operating power; (b) SC operating power. Both subfigures are in the time frame of one S-US06 drive cycle.

### 7.4.3 Verification of battery degradation coefficient and energy capacity loss with DESS component size

As Table XXIV, the sizing benchmarks indicate that battery degradation coefficient ($\alpha$) is a negative correlation of both battery pack size and SC pack size, while battery energy capacity loss ($E_{loss}$) is a positive correlation of battery pack size and a negative correlation of SC pack size. To verify this, Figure 58 (a) and (b) compare the $\alpha$ and $E_{loss}$ curves of the five designs, respectively; each curve's final value is also presented in the legends. Figure 58 (a) shows that DESS C has the smallest $\alpha$ among all designs because C has both the largest battery pack and the largest SC pack; DESS B has the largest $\alpha$ among the four DESS designs because B has both the smallest battery pack and the smallest SC pack. The $\alpha$ curve of A or D lies in the middle between B and C because the battery pack and SC pack of A or D are smaller than those of C but larger than those of B. Figure 58 (a) shows

that DESS A has the smallest $E_{loss}$ among all designs because A has both the smallest battery pack and the largest SC pack; DESS D has the largest $E_{loss}$ among the four DESS designs because D has both the largest battery pack and the smallest SC pack. Compared to DESS B, DESS C has a larger $E_{loss}$ because the battery pack of C is larger than that of B, even though the SC pack of C is larger than that of B. The battery-only ESS E has the largest $\alpha$ and the largest $E_{loss}$ because E has no SC pack.

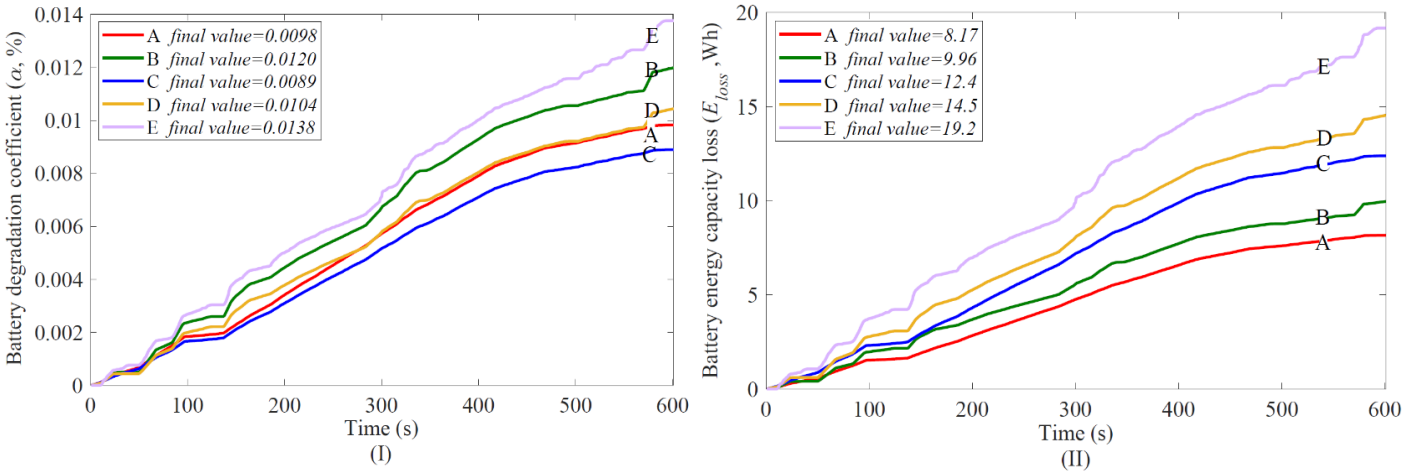


Figure 58 Verification of the sizing benchmarks by comparing the battery degradation of five designs: (a) battery degradation coefficient, (b) battery energy capacity loss. Both subfigures are in the time frame of one S-US06 drive cycle.

### 7.4.4 Verification and discussion of battery replacement times and DESS component costs with DESS component size

As Table XXIV, the sizing benchmarks indicate that battery replacement times ($N$) are a negative correlation of both battery pack size and SC pack size, while DESS component costs ($J_{compo}$) are a positive correlation of battery pack size but has a U-shape relationship with SC pack size. To verify this, Figure 59 (a) and (b) work out the $N$ and $J_{compo}$, respectively, as battery pack size varies from 80 to 170 kWh and SC pack size varies from 100 to 450 Wh. Discussion follows.

Figure 59 (a) indicates that the battery replacement times are three to five times over EV lifetime, which is more than the normal situation in which the battery pack only needs one or even no replacement [57]. This is because the case study uses a high-performance EV running at the drastic S-US06 drive cycle, which leads to the battery degrading much faster than normal. Besides, battery replacement times see a monotonous decline with increasing battery pack size and SC pack size. However, deploying a large battery pack and a large SC pack would require considering their mass and volume in case of the inconvenience to DESS packaging and chassis layout. To reduce the battery replacement times over EV lifetime, the DESS would better deploy an as larger battery pack and an as lager SC pack as possible, but the mass and volume of the DESS need to be considered.

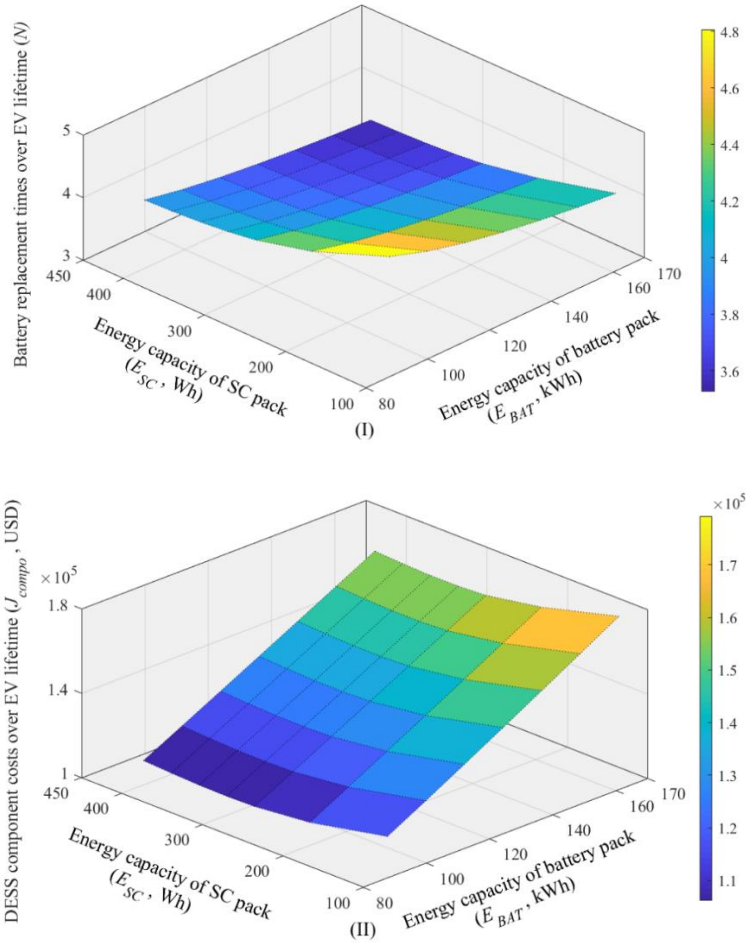


Figure 59 Verification of the sizing benchmarks by investigating the engineering and financial impacts of battery degradation: (a) battery replacement times; (b) DESS component costs. Both subfigures are in the time frame of EV lifetime.

Figure 59 (b) shows that the DESS component costs vary with DESS size widely from 11000 to 18000 USD, which implies that a carefully sized DESS can significantly reduce its financial costs in future use. Furthermore, the DESS component costs witness a monotonous growth with increasing battery pack size. Thus, deploying as smaller a battery pack as possible is necessary to reduce DESS component costs, while the feasible set constrains the minimum allowable battery pack size. According to Figure 55, the minimum allowable battery pack (i.e., the optimal battery pack) for the case study is 85 kWh. As SC pack size increases, the DESS component costs first drop and then rise, and the extreme point (i.e., the optimal SC pack) is 309.8 Wh. For the case study to minimise costs, the optimal DESS design is to deploy an 85 kWh battery pack and a 309.8 Wh SC pack. The corresponding electrical configuration of the optimal DESS is 96 serial 74 parallel for the battery pack and 90 serial 1 parallel for the SC pack plus a 342 kW DC/DC converter. As compared with the other feasible DESS designs in Figure 59 (b), the optimal DESS can save costs by up to 39%. To reduce the DESS component costs over EV lifetime, the DESS would better deploy the minimum allowable battery pack constrained by the feasible set, while the optimal SC pack size exists at an extreme point that is relevant to component prices.

To better understand the influence of DESS component size on DESS component costs, Figure 60 (a) and (b) further discuss the underlying reasons for the trends in Figure 59 (b). Figure 60 (a) presents the DESS component costs and sub-costs over EV lifetime, as SC pack size varies while battery pack size is held optimal at 85 kWh. Battery degradation costs ($J_{BAT}$) are the dominating part (around 90%) of DESS component costs ($J_{compo}$), while SC and DC/DC converter purchase costs ($J_{SC}$ and $J_{DCDC}$) only represent a small part. As SC pack size grows, $J_{BAT}$ witnesses a decelerating downtrend, which means that the efforts to reduce battery degradation by enlarging the SC pack become increasingly less effective. Meanwhile, $J_{SC}$ and $J_{DCDC}$ experience a near-linear uptrend. The overall $J_{compo}$, as the sum of $J_{BAT}$, $J_{SC}$ and $J_{DCDC}$, initially decreases because $J_{BAT}$ can be significantly reduced, but finally rises up because $J_{BAT}$ is less effectively reduced with more SCs being deployed while $J_{SC}$ and $J_{DCDC}$ still increase rapidly. Therefore, an over large SC pack cannot contribute more to lowering DESS component costs.

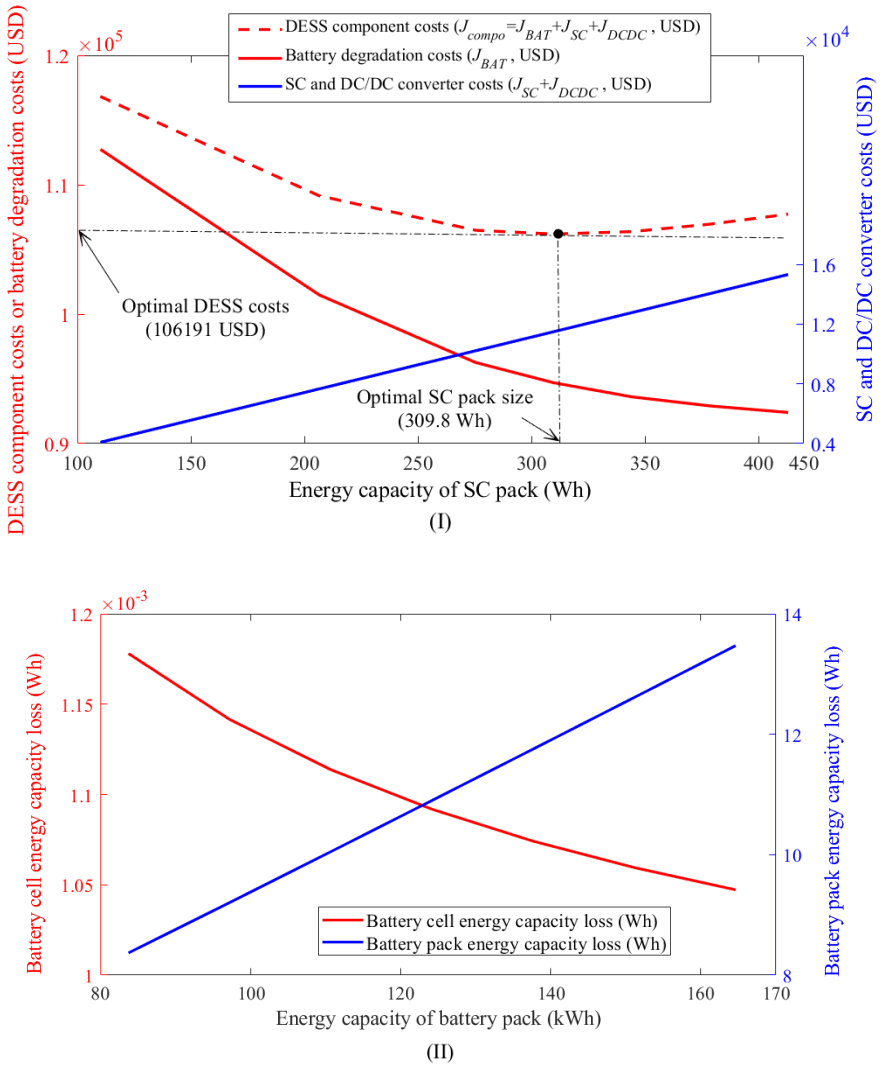


Figure 60 Discussion on DESS component costs with DESS component size: (a) DESS component costs and sub-costs over EV lifetime, when SC pack size varies and battery pack size maintains optimal at 85 kWh; (b) energy capacity loss of battery cell/pack after one S-US06 drive cycle operation, when battery pack size varies and SC pack size maintains optimal at 309.8 Wh.

Figure 60 (b) presents the energy capacity loss of battery cell and battery pack after the EV completes one S-US06 drive cycle, as battery pack size varies while SC pack size is held optimal at 309.8 Wh. As battery pack size grows, each battery cell's energy capacity loss can be reduced because more parallel branches in the battery pack lead to each cell sharing a smaller current and subsequently relieved degradation. However, with all the cells in combination, the whole battery pack has increasing energy capacity loss with battery size increasing. Considering the battery degradation costs ($J_{BAT}$) resulting from energy capacity loss is the primary part of DESS component costs ($J_{compo}$), a larger battery pack with more energy capacity loss would have higher DESS component costs.

### 7.4.5 Summary

In summary of Chapter 7, the significant findings are listed as follows:

1) EM benchmarks to optimise battery degradation: the optimal EM scheme to reduce battery degradation is revealed in Section 7.2, which indicates that the essence of reducing battery degradation exists in reducing the fluctuation of battery operating power. The optimal EM scheme is significantly affected by the size of the SC pack but inapparently affected by the battery pack size.

2) Sizing benchmarks to optimise battery degradation: the general trends of battery degradation with DESS component size are deduced as Table XXIV, which can be generalised to wide cases using different EM techniques, EVs, batteries and SCs.

3) General guides for reducing the engineering and financial impacts of battery degradation: the DESS with a larger battery pack and a larger SC pack can have fewer battery replacement times. DESS component costs grow with increasing battery pack size, while first drop and then rise with increasing SC pack size. As a general guide to save financial costs over EV lifetime, it is suggested to deploy a DESS with a small battery pack as constrained by the feasible set and a medium SC pack that can be found optimal at an extreme point.

# Chapter 8 Particular study: aluminium dual energy storage system

The previous chapters have investigated the modelling, sizing and energy management (EM) methodology of the dual energy storage system (DESS) composed of Li-ion batteries (LIBs) and supercapacitors (SCs). Despite the long existence of LIB and SC technologies, increasing attentions are paid to their limitations. For the LIB, there have been concerns about lithium's future availability, safety issues associated with thermal runaway, environmental impact, and rapid degradation [43]. For the SC, although it is capable of peaking bursts of power, its excessively low energy density requires mass deployment in practical applications [9]. These limitations are motivating the efforts to develop alternative energy storage (ES) technologies [173]. The Al-ion battery (AIB) is being developed as alternatives to existing ES technologies as it uses more abundant materials in nature and suffers from fewer safety risks. It has other benefits such as the comparatively low cost, ease of handling and the ability to transfer three electrons [174]. Recent publications report that the ionic liquid Al-ion battery (ILAIB) has high specific energy (0.12 kWh/kg) and a longer cycle life as compared to the LIB [175], while the aqueous electrolyte Al-ion battery (AEAIB) has high specific power (30 kW/kg) and a higher energy density as compared to the SC [176]. Besides, both batteries have very low manufacturing costs [177]. The above facts indicate that the ILAIB is likely to be a candidate to replace the LIB, while the AEAIB may be a substitute for the SC.

As the ILAIB and AEAIB show themselves potential future substitutes of the LIB or SC, further attempts arise of applying the ILAIB and AEAIB in a DESS for electric vehicle (EV) propulsion. With the curiosity of assessing the novel Aluminium chemistries, this section adapts the modelling methodology presented in Chapter 4 and thus models DESSs applying ILAIB and AEAIB. Using the AIB data from published work [174-180], the ILAIB and AEAIB are substituted for one or both of the components of the benchmark LIB-SC DESS, and thus the hypothetical ILAIB-SC, LIB-AEAIB and ILAIB-AEAIB DESSs are proposed (schematics of the DESSs are presented in Figure 61 in Section 8.2.2). These Aluminium DESSs along with the conventional LIB-SC DESS are modelled, simulated and compared with the optimisation problems (OPs) of mass, volume, initial cost and overall financial costs. To formulate and solve the OPs for the Aluminium DESSs, the methodology for the LIB-SC DESS can be significantly reused. However, the ILAIB and AEAIB use different chemistries from the LIB or SC. Therefore, the methodology needs to be modified to fit for the characteristics of ILAIB and AEAIB. By solving the OPs for each DESS, results show that the ILAIB-based DESSs surpass the LIB-based DESSs in terms of overall costs by a 16% reduction, but the ILAIB-based DESSs are heavier and especially bulkier, for which reason the volumetric parameters of ILAIB need to be modified in future work. The AEAIB-based DESSs surpass the SC-based DESSs in all aspects of mass, volume, initial cost and overall costs, which indicates that the

AEAIB can be a promising substitute for the SC. These results imply the viability of using novel AIB technologies to replace the conventional LIB and SC technologies, which is believed, can offer more options for DESS component selection and motivate DESS applications in EVs. The remainder of this chapter is structured as follows.

1) The characteristics of ILAIB and AEAIB are collected from published data and compared with the LIB and SC. The reasons for the acceptance of ILAIB and AEAIB are analysed.

2) Using data of ILAIB and AEAIB, the Aluminum DESSs are modelled with the Tesla EV.

3) To evaluate the DESSs, the performance metrics of DESS are formulated as OPs in terms of the mass, volume, initial cost and overall costs. The methods to optimise these OPs are also demonstrated.

4) The performance results of different DESSs are compared and discussed. The LIB-AEAIB DESS is proved to be the most viable DESS among all and thus is case-studied in particular.

## 8.1 Characteristics of Al-ion batteries

Based on published work [17, 178-183], Table XXIV collects ILAIB and AEAIB parameters at 20℃ and 1C current rate. These parameters have been scaled up from initially reported values to equivalent values of a 18650 cell. Besides, Panasonic NCR18650B LIB and Maxwell BCAP 3400F 2.7V SC are chosen as the representative LIB and SC for EV propulsion [153], and their parameters are also presented in Table XXIV for comparison purpose.

The comparison between ILAIB and LIB shows that the ILAIB has a lower voltage; in terms of battery packaging, more ILAIBs need to be arranged in series to reach the given bus voltage imposes an extra burden to the battery management system [6]. The maximum power and power density of ILAIB are much lower than those of LIB; however, both ILAIB and LIB are positioned as mainly responsible for delivering energy than power. From the perspectives of capacity and energy, ILAIB seems inferior to LIB; however, considering the mass of ILAIB is less than one-tenth that of LIB, ILAIB still has an energy density close to LIB. The two kinds of batteries witness slight differences in coulombic efficiency and unit price, while the resistance of ILAIB is much higher than that of LIB. The most significant advantage of ILAIB is its cycle life, which is five times that of LIB. Compared with LIB, the reason for acceptance of ILAIB is the comparable energy density and unit price but a much longer cycle life.

Table XXVI Parameters of the ILAIB, AEAIB and typical LIB, SC [17, 147, 178-184].

| | Main ES | | Second ES | |
|---|---|---|---|---|
| | ILAIB | LIB | AEAIB | SC |
| Type | Equivalent 18650 | Panasonic NCR 18650B | Equivalent 18650 | Maxwell BCAP 3400F 2.7V |
| Nominal voltage (V) | 2.2 | 3.6 | 2.4 | 2.7 |
| Voltage range (V) | 1.7 – 2.4 | 2.5 – 4.2 | 0.2 – 2.4 | 0 – 2.7 |
| Maximum current (A) | 0.22 | 6.50 | 126.2 | 2600 |
| Maximum power (W) | 0.48 | 23.40 | 302.88 | 3800 |
| Capacity (Ah) | 0.31 | 3.25 | 0.06 | 1.27 |
| Energy (Wh) | 0.69 | 11.70 | 0.15 | 3.44 |
| Mass (g) | 5.6 | 76 | 10 | 513 |
| Volume (mL) | 13.67 | 16.54 | 13.34 | 390 |
| Power density (kW/kg) | 0.09 | 0.31 | 30.29 | 7.41 |
| Energy density (kWh/kg) | 0.122 | 0.150 | 0.015 | 0.007 |
| Coulombic efficiency (%) | 93 | 95 | 80 | 99 |
| Resistance (Ohm) | 2.273 | 0.036 | 0.017 | $2.2*10^{-4}$ |
| Unit price * | 330 USD/kWh | 300 USD/kWh | 1.63 USD/kW | 14.17 USD/kW |
| Projected cycle life (cycles) | 10000 | 2000 | 100000 | 1000000 |

*: The unit price of ILAIB and LIB is presented in USD/kWh since ILAIB and LIB are energy-intense storages for delivering energy; while that of AEAIB and SC is presented in USD/kW since AEAIB and SC are power-intense storages for delivering power.

The comparison between AEAIB and SC shows that both ESs have little difference in voltage, but SC has extremely higher power capability. However, considering the mass of AEAIB is less than one-fiftieth that of SC, the power density of AEAIB is more than four times that of SC and ten times that of LIB. In terms of energy density, AEAIB is two times higher than SC and nearly one-tenth of LIB, which shows that AEAIB has an energy capability much better than SC. The AEAIB has a lower coulombic efficiency and a higher resistance than SC, while AEAIB has a significantly lower unit price as compared with the SC. The cycle life of AEAIB is very long at 100000 cycles, which is fifty times that of LIB; however, SC's cycle life is even longer and is ten times that of AEAIB. Compared with SC, the reason for acceptance of AEAIB is the much lower unit price but four times higher power density as well as a better balance between energy and power density.

## 8.2 Modelling

With the parameters of AIBs, the Aluminium DESSs can be modelled by significantly reusing yet slightly adjusting the modelling methodology in Chapter 4. The modelling of AIBs and Aluminium DESSs are described below.

### 8.2.1 Modelling of Al-ion batteries

Like LIB modelling, the ILAIB and AEAIB are modelled to reflect both the electrical and degradation characteristics. In terms of electrical modelling, the LIB modelling methodology, as presented in Section 4.1.1.1, can be reused for the ILAIB and AEAIB, respectively. The acceptance of such reuse is because the battery with either Lithium or Aluminium chemistry can always be treated as an equivalent circuit.

In terms of degradation modelling, the LIB methodology, as presented in Section 4.1.1.2, cannot be reused for the ILAIB and AEAIB, because the degradation mechanism of AIB is still under investigation may be different from that of LIB [181]. In this case, the projected cycle life of ILAIB and AEAIB, as presented in Table XXIV, is utilised to enable the degradation modelling. Consequently, the degradation coefficient ($\alpha$, defined as the ratio between the degraded capacity and original capacity [149]) of ILAIB or AEAIB is formulated as (75), and explanations follow. Where $Ah_{put}$ is the ampere-hour throughput of battery. $Ah_{BAT}$ is the nominal ampere-hour capacity of the battery. $Cycle_{life}$ is the projected cycle life (cycles) of the battery. Equation (75) regards that the total usable ampere-hour throughput over battery lifetime is directly proportional to battery cycle life and is calculated as ($Ah_{BAT} \cdot Cycle_{life} \cdot 2$). Therefore, battery degradation coefficient can be expressed as the ratio between the used ampere-hour throughput and total usable ampere-hour throughput. In Chapter 8, (75) is not only used for calculating the degradation of ILAIB and AEAIB but also for that of LIB and SC, which aims to make a fair comparison among LIB, SC, ILAIB and AEAIB.

$$\alpha = \frac{Ah_{put}}{Ah_{BAT} \cdot Cycle_{life} \cdot 2} \tag{75}$$

It should be noted that battery cycle life $Cycle_{life}$ is characterised under constant battery temperature and current rate, as presented in Table XXIV. However, battery cycle life is usually affected by its temperature and current rate [55], but no literature has so far specified the detailed influences of different temperatures and current rates on the cycle life of ILAIB and AEAIB. Therefore, (16) formulates the battery degradation coefficient by assuming that battery cycle life would not change too much with battery temperature and current rate.

### 8.2.2 Modelling of Aluminium DESSs

Using the conventional LIB-SC DESS as a benchmark, the ILAIB-SC, LIB-AEAIB and ILAIB-AEAIB DESSs are designed to compare and contrast DESSs comprising combinations of LIB, SC, ILAIB and AEAIB, as shown in Figure 61. The four DESSs are modelled by grouping the models of two of LIB, SC, ILAIB and AEAIB, plus a DC/DC converter. The LIB and SC models have been presented in Sections 4.1.1 and 4.1.2, respectively; the modelling methodology for the ILAIB and AEAIB is presented in Section 8.2.1; the model of DC/DC converter has been presented in Section 4.1.3. The four DESSs adopt the same semi-active SC/battery topology with the following features. Firstly, the ES with high specific energy (either LIB or ILAIB) is used as the main ES for mostly delivering energy, while the one with high specific power (either SC or AEAIB) is used as the second ES for mostly delivering power [3]. Secondly, the main ES is directly connected to the power bus; therefore, its voltage cannot vary significantly and should maintain close to the bus's voltage [77]. Thirdly, the second ES is connected via a bi-directional DC/DC converter; therefore, its voltage can vary within a wide range since the DC/DC converter can handle a certain degree of voltage fluctuation. It is considered that the voltage of the second ES can be as low as one quarter of its maximum voltage (i.e, full-charge voltage) [154]. Lastly, the power capability of DC/DC converter is subject to that of the second ES.

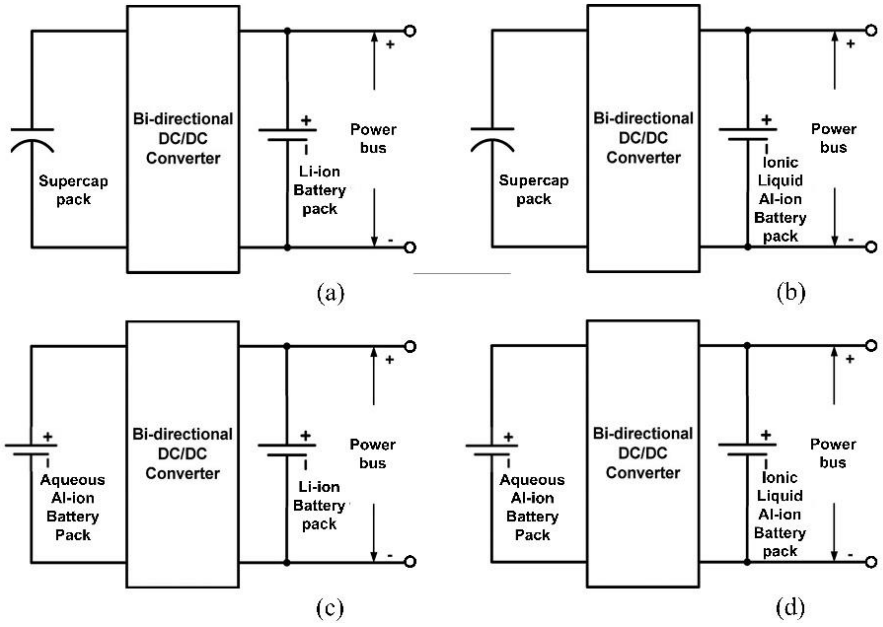


Figure 61 Architecture of four DESSs: (a) LIB-SC; (b) ILAIB-SC; (c) LIB-AEAIB; (d) ILAIB-AEAIB.

Each of the four DESSs is respectively embedded into the EV model developed in Section 4.2 so that the DESS performance with EV operations can be simulated. The integrated EV model is shown in Figure 62. The inputs for the integrated EV model include the S-US06 drive cycle (Figure 21), parameters of Tesla Model S P85 EV (Table VII, Table VIII), ESs (Table XXIV) and DC/DC converter (Table X).

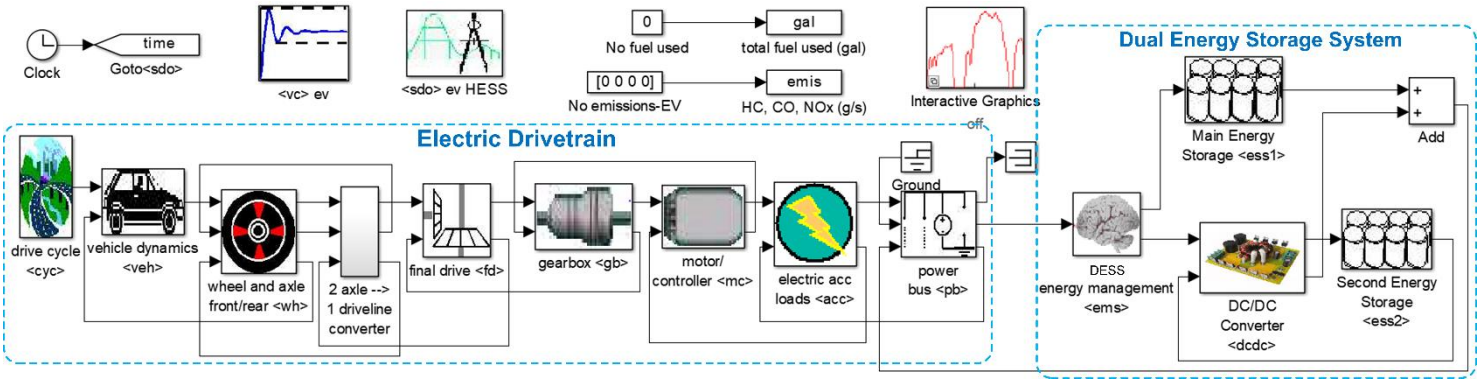


Figure 62 Integrated EV model with Aluminium DESS.

## 8.3 Performance metrics and optimisation methods

To compare the performance of the four DESSs, this section formulates the performance metrics as the mass, volume, initial cost and overall costs of DESS; moreover, the methods to optimise these metrics are also demonstrated. The optimisation of metrics is very necessary because, for example, a DESS can have different overall costs, which depends on its design and operating conditions [136]. The optimisation aims at working out the minimum overall costs, which reflects the greatest potential of the DESS under best-case design and operating conditions. Namely, the four DESSs are compared by their greatest potentials of minimising mass, volume, initial cost and overall costs. Before formulating and optimising the performance metrics, this section firstly introduces the energy and power constraints for the DESS. These constraints are raised by EV propulsion, which must be satisfied so that the DESS can fulfil its fundamental duty of powering the EV [16]. The constraints, performance metrics and optimisation methods can significantly reuse the methodology presented in Chapter 6 with minor adjustments, and the details follow.

### 8.3.1 Constraints of energy and power

The energy and power constraints for the four DESSs can mostly reuse those for the LIB-SC DESS presented in Section 6.1.1, while the only change for Aluminium DESSs is to substitute the LIB with ILAIB and the SC with AEAIB. After this change, the general constraints for the four DESSs can be expressed as (76) and (77). Equation (76) describes that the total energy capacity of the main and second ESs should satisfy the energy demands over the EV driving range. Where $E_{main}$ and $E_{second}$ are the energy capacity of the main and second ES, respectively. $\eta_{DCDC}$ is DC/DC conversion efficiency. $E_{EV}$ is EV energy demands over driving range. Equation (77) describes that the total power capability of main and second ESs should satisfy the maximum EV power demand. Where $P_{main,max}$ and $P_{second,max}$ are the maximum power capability of the main and second ES, respectively. $\rho_{main,P/E}$ and $\rho_{second,P/E}$ are the power to energy density of the main and second ES, respectively. $P_{EV,max}$ is the maximum EV power demand. Combining (76) and (77), a feasible set of $E_{main}$ and $E_{second}$ can be constrained, and DESS performance is assessed within this feasible set.

$$E_{main} + E_{second} \cdot \eta_{DCDC} \geq E_{EV} \tag{76}$$

$$P_{main,max} + P_{second,max} \cdot \eta_{DCDC} = E_{main}\rho_{main,P/E} + E_{second}\rho_{second,P/E} \cdot \eta_{DCDC} \geq P_{EV,max} \tag{77}$$

### 8.3.2 Metric and optimisation of mass, volume and initial cost

The formulations of mass ($M_{DESS}$), volume ($V_{DESS}$) and initial cost ($J_{initial}$) for the four DESSs can mostly reuse those for the LIB-SC DESS presented in Section 6.1.2, while the only change for Aluminium DESSs is to substitute the LIB with ILAIB and the SC with AEAIB. After this change, the general formulations for the four DESSs can be expressed as (78), (79) and (80). These equations consider the total mass, volume and initial cost of the DESS as the accumulation of each DESS component. Where $\rho_{main,E/M}$, $\rho_{main,E/V}$, $\rho_{main,E/C}$ are the energy to mass, to volume, to costs density of the main ES, respectively. $\rho_{second,E/M}$, $\rho_{second,E/V}$, $\rho_{second,E/C}$ are the energy to mass, to volume, to costs density of the second ES, respectively. $\rho_{DCDC,P/M}$, $\rho_{DCDC,P/V}$, $\rho_{DCDC,P/C}$ are the power to mass, to volume, to costs density of the DC/DC converter, respectively. $P_{DCDC,max}$ is the maximum power capability of the DC/DC converter and can be further expressed as (81), where $P_{second,max}$ is the second ES's maximum power capability.

$$M_{DESS} = M_{main} + M_{second} + M_{DCDC} = \frac{E_{main}}{\rho_{main,E/M}} + \frac{E_{second}}{\rho_{second,E/M}} + \frac{P_{DCDC,max}}{\rho_{DCDC,P/M}} \tag{78}$$

$$V_{DESS} = V_{main} + V_{second} + V_{DCDC} = \frac{E_{main}}{\rho_{main,E/V}} + \frac{E_{second}}{\rho_{second,E/V}} + \frac{P_{DCDC,max}}{\rho_{DCDC,P/V}} \tag{79}$$

$$J_{initial} = J_{main} + J_{second} + J_{DCDC} = \frac{E_{main}}{\rho_{main,E/C}} + \frac{E_{second}}{\rho_{second,E/C}} + \frac{P_{DCDC,max}}{\rho_{DCDC,P/C}} \tag{80}$$

$$P_{DCDC,max} = P_{second,max} = E_{second}\rho_{second,P/E} \tag{81}$$

It can be seen from (78), (79), (80) and (81) that $M_{DESS}$, $V_{DESS}$ and $J_{initial}$ are linear functions of $E_{main}$ and $E_{second}$. Therefore, the linear programming (LP) approach is capable of solving the optimal (i.e., minimum) mass, volume and initial cost by finding the optimal $E_{main}$ and $E_{second}$ within the feasible set. The LP approach presented in [161] is adopted as the optimisation method.

### 8.3.3 Metric and optimisation of overall costs

Similar to the overall costs of LIB-SC DESS presented in Section 6.2.1, the overall costs ($J_{all}$) of Aluminium DESSs are considered as the sum of initial cost ($J_{initial}$) and long-term costs ($J_{long}$). $J_{initial}$ has been formulated as (80), while $J_{long}$ is composed of the electricity consumption cost ($J_{Elec}$) and

ES degradation cost ($J_{Degrad}$), as (82). The formulations of $J_{Elec}$ and $J_{Degrad}$ are described in the following subsections, while the method to optimise $J_{all}$ is illustrated in the end.

$$J_{all} = J_{initial} + J_{long} = J_{initial} + J_{Elec} + J_{Degrad} \tag{82}$$

8.3.3.1 Formulation of electricity consumption cost

The formulation of electricity consumption cost ($J_{Elec}$) for the four DESSs can mostly reuse that for the LIB-SC DESS presented in Section 5.1.2, while the only change for Aluminium DESSs is to substitute the LIB with ILAIB and the SC with AEAIB. After this change, the general formulation for the four DESSs can be expressed as (83). Where $Q_{DESS}$, $Q_{main}$ and $Q_{second}$ are the electricity consumption of the whole DESS, main ES and second ES, respectively. 0.1 USD/kWh is the electricity price [148]. $Range_{EVlife}$ and $Range_{S\text{-}US06}$ are the driving range of EV lifetime (considered 150000km [70]) and of one S-US06 drive cycle, respectively. Namely, ($Range_{EVlife}/Range_{S\text{-}US06}$) is the coefficient transferring the electricity consumption cost from one S-US06 drive cycle to EV lifetime. $\Delta SOC_{main}$ and $\Delta SOC_{second}$ are the delta state-of-charge of the main and second ES, respectively, while $\Delta SOE_{second}$ is the second ES's delta state-of-energy. If the second ES of DESS is AEAIB, $\Delta SOC_{second}$ will be used in (83); if it is SC, $\Delta SOE_{second}$ will be used in (83). $\Delta SOC_{second}$ can be calculated using (14) presented in Section 4.1.1.1, while $\Delta SOE_{second}$ can use (23) in Section 4.1.2.

$$\begin{cases} J_{Elec} = Q_{DESS} \cdot 0.1\ USD/kWh \cdot \dfrac{Range_{EVlife}}{Range_{S-US06}} \\ Q_{DESS} = Q_{main} + Q_{second} = E_{main}\Delta SOC_{main} + \begin{cases} E_{second}\Delta SOC_{second} \\ or \\ E_{second}\Delta SOE_{second} \end{cases} \end{cases} \tag{83}$$

8.3.3.2 Formulation of ES degradation cost

The ES degradation cost ($J_{Degrad}$) for the four DESSs is formulated as (84). Where $J_{Degrad,main}$ and $J_{Degrad,second}$ are the degradation cost of the main and second ES under one S-US06 drive cycle, respectively. The coefficient ($Range_{EVlife}/Range_{S\text{-}US06}$) is used to transfer the ES degradation cost from one S-US06 drive cycle to EV lifetime. $\alpha_{main}$ and $\alpha_{second}$ are the degradation coefficient of the main and second ES, respectively, and they can be calculated by (75). $Price_{main}$ and $Price_{second}$ are the unit price of the main and second ES, respectively. A coefficient of 20% is divided by because the ES is commonly considered as end-of-life when its degradation coefficient reaches 20%, at which time the ES loses all its values [43]. It can be seen from (84) that $J_{Degrad}$ includes the degradation cost of not only the main ES but also the second ES. This is different from Chapter 6, where the ES degradation cost of LIB-SC DESS only considers the battery (main ES) degradation cost but neglects SC (second ES) degradation cost. The reason for Chapter 6 not considering the SC degradation cost is because the lifespan of SC is assumed even longer than that of EV [9], so that SC degradation can be neglected

over EV lifetime. In contrast, this chapter aims at comparing the AEAIB and SC, with each of them being the second ES, in which case, the degradation cost of the second ES should be counted to make a fair comparison. As shown in Table XXIV, although both AEAIB and SC have a very long cycle life, the cycle life of AEAIB is only one-tenth that of SC, which indicates that the AEAIB and SC have a big difference in terms of degradation. This difference may further result in that AEAIB and SC have very different degradation cost. Therefore, the degradation cost of second ES cannot be neglected but considered into $J_{Degrad}$.

$$\begin{cases} J_{Degrad} = \left( J_{Degrad,main} + J_{Degrad,second} \right) \cdot \dfrac{Range_{EVlife}}{Range_{S-US06}} \\ J_{Degrad,main} = \alpha_{main} \cdot E_{main} \cdot Price_{main} / 20\% \\ J_{Degrad,second} = \alpha_{second} \cdot E_{second} \cdot Price_{second} / 20\% \end{cases} \tag{84}$$

8.3.3.3 Optimisation method for overall costs

Combining (80) to (84), it can be seen that the overall costs ($J_{all}$) are a nonlinear function of the current, voltage and energy capacity of ESs. As mentioned previously in Section 6.2.2, solving such a cost function requires a joint sizing-EM optimisation. The joint optimisation framework proposed for the LIB-SC DESS can be significantly resued for the Aluminium DESSs, while the only change is to substitute the LIB with ILAIB and the SC with AEAIB. After this change, the joint optimisation framework, which solves the optimal DESS size and EM strategy to minimise $J_{all}$ for each of the four DESSs, can be expressed as a six-step process in the following.

1) Import profiles. The optimisation framework accepts the parameters of the EV and DESS components as inputs.

2) Traverse DESS size within the feasible set. The DESS size is represented by the combination of $E_{main}$ and $E_{second}$, and is constrained by the energy and power constraints in Section 8.3.1. Each feasible $E_{main}$ and $E_{second}$ within constraints will be traversed in ascending order.

3) Traverse EM strategy with time. The optimisation process further traverses the possible EM strategy of DESS. Given that the duration of the used S-US06 drive cycle is 600 seconds, the EM strategy can be regulated to perform every one second; thus, the timeline ($k$) of the EM strategy can be expressed as (85). At each time point of $k$, the EM strategy determines the $P_{main}$ and $P_{second}$, based on the constraints in (86) and the correlation in (87).

$$k = 0,1,2,...,600 \tag{85}$$

$$\begin{cases} \left|P_{main}(k)\right| \le P_{main,max} \\ \left|P_{second}(k)\right| \le P_{second,max} \end{cases} \tag{86}$$

$$P_{main}(k) = \begin{cases} P_{EV}(k) - P_{second}(k)\eta_{DCDC}, & P_{second}(k) > 0 \\ P_{EV}(k) - P_{second}(k)/\eta_{DCDC}, & P_{second}(k) \le 0 \end{cases} \tag{87}$$

4) Calculate the electrical states of ESs. The equivalent circuit model described in Section 8.2.1 accounts for the electrical states. Specifically, the SOC or SOE range of the main and second ES is constrained as (88). Where the main ES is considered capable of performing full charge-discharge cycles [54], while the second ES is not expected to be depleted and a lower limit exists as 20% [77]. The SOC or SOE of the second ES is used as a state variable ($x$) to represent the EM states of the whole DESS, as (89). Where $x$ is initialised and finalised as the same at 50%, following the "charge-sustaining" principle [13]. A state transfer function ($z$) can be formulated along the timeline, as (90).

$$\begin{cases} 0 \le SOC_{main} \le 100\% \\ \begin{cases} 20\% \le SOC_{second} \le 100\% \\ or \\ 20\% \le SOE_{second} \le 100\% \end{cases} \end{cases} \tag{88}$$

$$\begin{cases} x(k) = \begin{cases} SOC_{second}(k) \\ SOE_{second}(k) \end{cases} \\ x(0) = x(600) = 50\% \end{cases} \tag{89}$$

$$z(k) = x(k) - x(k+1) = P_{second}(k) / E_{second} / 3.6 \tag{90}$$

5) Feed the objective function. With the traversed DESS size and EM strategy as well as the calculated electrical states of ESs, the objective function ($O$) of overall costs can be fulfilled as (91).

$$O = Min \sum_{k=1}^{600} J_{all}(k) \tag{91}$$

6) Export results. The sizing-EM framework would find out and export the optimal combination of DESS size and EM to minimise the objective function based on dynamic programming. In summary, the brief pseudocodes of the optimisation framework are shown in Table XXVII.

Table XXVII Brief pseudocodes of the sizing-EM optimisation framework.

| |
|---|
| **% Import profiles %** |
| **for** $E_{main} = E_{main,min} : E_{main,max}$ **;** **% main ES sizing** |
| **for** $E_{second} = E_{second,min} : E_{second,max}$ **;** **% second ES sizing** |
| **for** $k = 0 : 600$ **;** **% timeline of EM** |
| **for** $\begin{cases} SOC_{second} = SOC_{second,min} : 1; \\ \text{or} \\ SOE_{second} = SOE_{second,min} : 1; \end{cases}$ **% states of EM** |
| **% Calculate electrical states of ESs %** |
| $O = \text{Min} \sum_{k=0}^{600} \{J_{all}(k)\}$ **;** **% objective function** |
| **end** |
| **end** |
| **end** |
| **end** |
| **% Export results %** |

## 8.4 Comparison and case study

With the performance metrics and optimisation methods, this section compares the four DESSs in terms of the feasible set, mass, volume, initial cost and overall costs. By comparison, the LIB-AEAIB DESS is regarded as the most suitable one for EV application; therefore, it is specifically case-studied.

### 8.4.1 Feasible set

Combining the energy and power constraints expressed by (76) and (77), as Figure 63, each of the four DESSs obtains a feasible set, in which any point ($E_{main}$, $E_{second}$) can be a workable DESS design that meets the prescribed EV driving range and S-US06 drive cycle operations. The energy constraint line is the same for all four DESSs, while the power constraint line is different because the axes of Figure 63 are represented by energy rather than power. The feasible set for each DESS has a different magnitude, and it tends to be larger if the main ES has a higher energy density or the second ES has a higher power density. In general, for all four DESSs, the main ES is constrained as more than 80 kWh, while the second ES can be much smaller with only hundreds of Wh capacity. The intersections of constraint lines are highlighted as points A to E, while the five points will be discussed later in terms of the optimal mass, volume and initial cost.

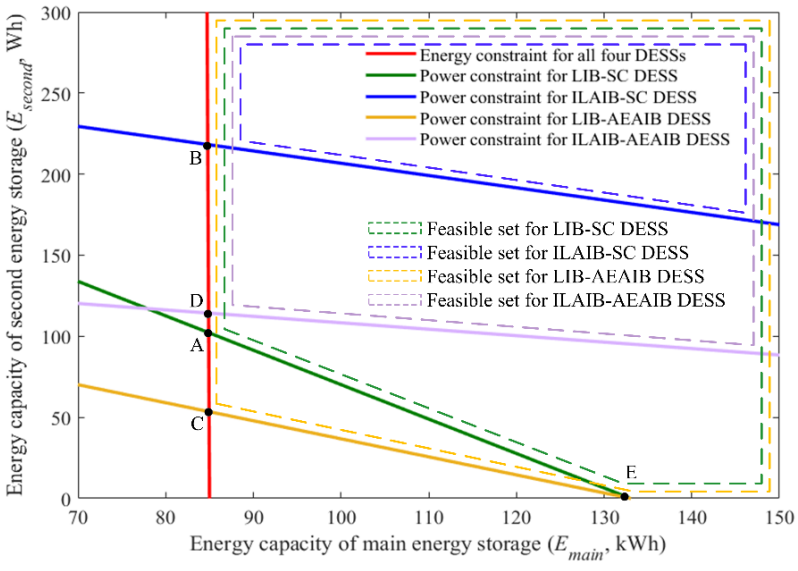


Figure 63 Feasible sets for four DESSs.

### 8.4.2 Mass, volume and initial cost

Using (78) to (81) and the LP approach, the optimal mass, volume and initial cost of each DESS are worked out, as Figure 64 (a) (b) (c). The total mass, volume and initial cost are significantly impacted by the main ES technology but less influenced by the second ES technology, which can be inferred from the following observations. Firstly, the main ES occupies a vast majority of DESS mass, volume and initial cost. Lastly, the two DESSs with the same main ESs yet different second ESs witness no much differences in mass, volume and initial cost, while the two DESSs with different main ESs yet the same second ESs have much larger differences. For the ILAIB-SC DESS, its optimal mass, volume and initial cost are achieved at the same point B, while for the LIB-AEAIB and ILAIB-AEAIB DESS, it is the same point C and D, respectively. However, for the LIB-SC DESS, its optimal mass and initial cost are achieved at point A, but its optimal volume is achieved at point E. Back to Figure 63, it can be seen that point E is in fact a LIB-only ESS with no second ES and no DC/DC converter. Therefore, when using the LIB as the main ES, deploying the SC as the second ES will inevitably add extra volume to the whole DESS. In contrast, deploying the AEAIB as second ES with the LIB can enable the DESS to achieve a small volume comparable to that of the LIB-only ESS and a small mass and low initial cost compared with the LIB-SC DESS. In this regard, the AEAIB proves itself to be a competitive second ES that surpasses the SC in terms of mass, volume and initial cost. When using the ILAIB as the main ES, the ILAIB-SC and ILAIB-AEAIB DESSs are noticeably heavier, bulkier, and more expensive than the LIB-based DESSs. In particular, the volume of ILAIB-based DESSs is nearly ten times that of LIB-based DESSs, which makes the ILAIB-based DESSs difficult to be deployed in practical engineering. Therefore, the ILAIB, mainly due to its inferior volumetric characteristics, can hardly replace the LIB as the main ES in the present stage.

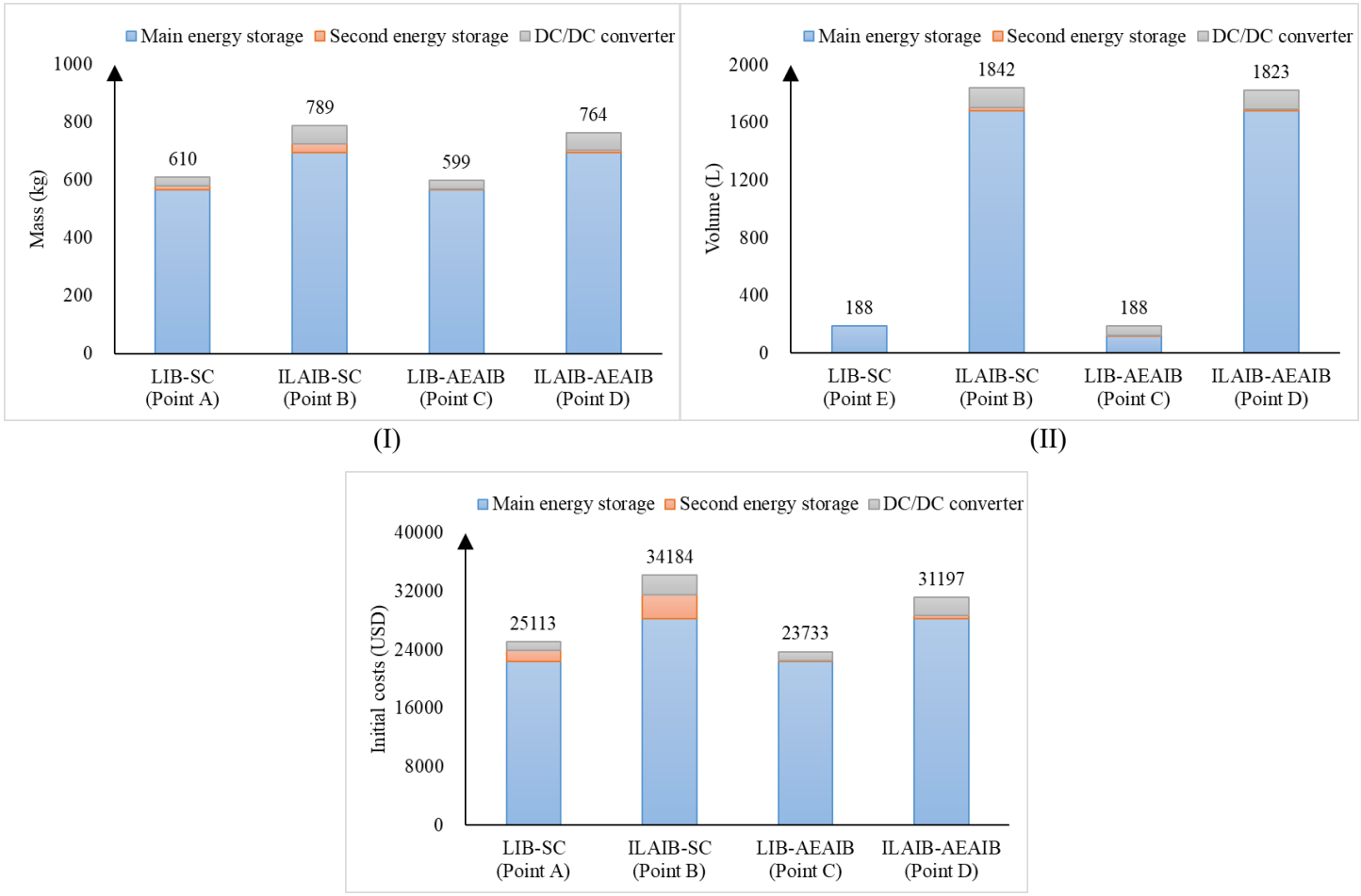


Figure 64 Optimal (a) mass, (b) volume and (c) initial cost, for four DESSs. Points A to E, which correspond to the highlighted points in Figure 63, represent the optimal DESS designs to achieve the corresponding mass, volume and initial cost.

### 8.4.3 Overall costs

Using (82) to (84) and the sizing-EM framework, the optimal overall costs ($J_{all}$) and the corresponding configurations of each DESS are worked out, as in Table XXVIII. The LIB-SC DESS has the largest $J_{all}$, followed by the LIB-AEAIB, ILAIB-SC and ILAIB-AEAIB DESS. It can be inferred that $J_{all}$ is greatly subject to the main ES technology, based on the observations that the LIB-SC and LIB-AEAIB DESSs have very close $J_{all}$, while the ILAIB-SC and ILAIB-AEAIB DESSs as well. As mentioned previously, $J_{all}$ is composed of initial cost ($J_{initial}$), electricity consumption costs ($J_{Elec}$) and ES degradation costs ($J_{Degrad}$). It is found in Table XXVIII that although the $J_{initial}$ of ILAIB-based DESSs is higher than that of LIB-based DESSs, the $J_{Degrad}$ of ILAIB-based DESSs is significantly lower than that of LIB-based DESSs, while the $J_{Elec}$ of either DESSs only occupies a small proportion (<12%) of $J_{all}$ and thus has a limited influence on $J_{all}$. Combining $J_{initial}$, $J_{Ele}$ and $J_{Degrad}$, the $J_{all}$ of ILAIB-based DESSs is approximately 16% less than that of LIB-based DESSs, verifying that the ILAIB technology surpasses the LIB technology in terms of financial costs.

Table XXVIII Optimal overall costs and the corresponding configurations of four DESSs.

| | | LIB-SC | ILAIB-SC | LIB-AEAIB | ILAIB-AEAIB |
|---|---|---|---|---|---|
| **DESS costs** | Overall costs ($J_{all}$, USD) | 51427 | 43170 | 50395 | 42216 |
| | Initial cost ($J_{initial}$, USD) | 24539 | 33429 | 22363 | 28335 |
| | Electricity consumption costs ($J_{Elec}$, USD) | 5586 | 1292 | 5712 | 5039 |
| | ES degradation costs ($J_{Degrad}$, USD) | 21303 | 8448 | 22320 | 8842 |
| **ES energy capacity** | Main ES capacity ($E_{main}$, kWh) | 85 | 85 | 85 | 85 |
| | Second ES capacity ($E_{second}$, Wh) | 102 | 240 | 108 | 144 |
| **ES packaging** | Main ES configuration | 96s74p* | 158s764p | 96s74p | 158s764p |
| | Second ES configuration | 30s1p | 70s1p | 120s6p | 120s8p |

*: 96s74p means that the ES is packed with 96 cells in series and 74 cells in parallel.

However, looking at the main ES configuration presented in Table XXVIII, the ILAIB pack has 158 cells in series and 764 cells in parallel, resulting in 120712 cells to be deployed in total. This huge number of cells cannot be arranged in practical engineering, because of not only the numerous workloads imposed on the battery management system, but also the massive volume of the ILAIB pack, which has been discussed in Figure 64 (b). Therefore, despite the economical feature, the volumetric deficiency of ILAIB prevents itself to be a competitive substitute for LIB, and efforts are needed in future work specifically regarding improving the volumetric energy density of ILAIB. Besides, Table XXVIII indicates that using either LIB or ILAIB as the main ES, the main ES's capacity is the same at around 85 kWh. In contrast, the capacity of the second ES is noticeably affected by the main ES technology. Compared with the LIB-based DESSs, the ILAIB-based DESSs require the second ES to have a larger capacity, because the power density of ILAIB is lower than that of LIB, and a larger second ES can make up the power capability of the whole DESS. From the second ES technology perspective, Table XXVI shows that the AEAIB-based DESSs can save overall costs by around 2% compared with the SC-based DESSs. This verifies that the AEAIB technology surpasses the SC technology in terms of financial costs, and the reason can be attributed to the reduced initial cost.

### 8.4.4 Case study of LIB-AEAIB DESS

Based on the above analysis of the four DESSs, the LIB-AEAIB DESS shows reduced initial cost and overall costs compared with the conventional LIB-SC DESS, as well as a reasonable mass and

volume to be fulfilled in practical engineering. Therefore, the LIB-AEAIB DESS is considered the most suitable DESS for high-performance EV propulsion and is thus case-studied in particular. Using the configuration of LIB-AEAIB DESS presented in Table XXVIII and the models in Section 8.2, Figure 65 (a) (b) (c) shows the simulated power, SOC and degradation coefficient of the main and second ESs with one S-US06 drive cycle.

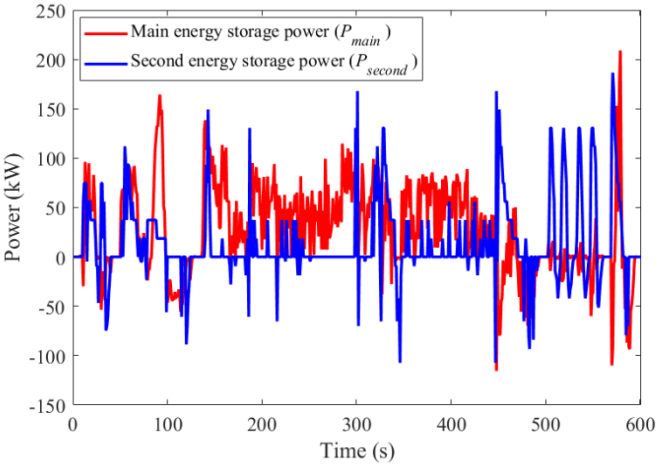


(I)

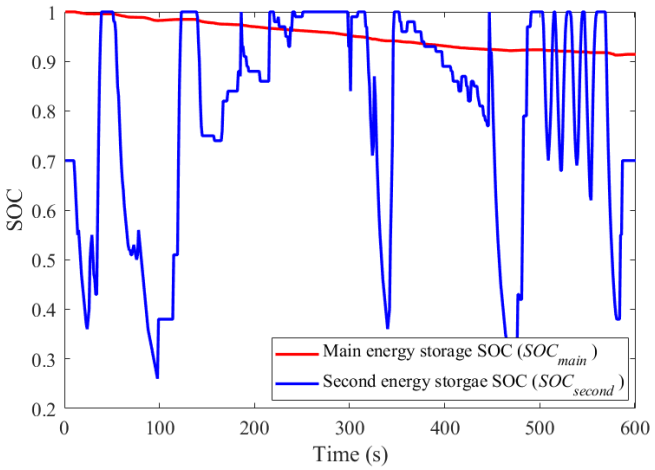


(II)

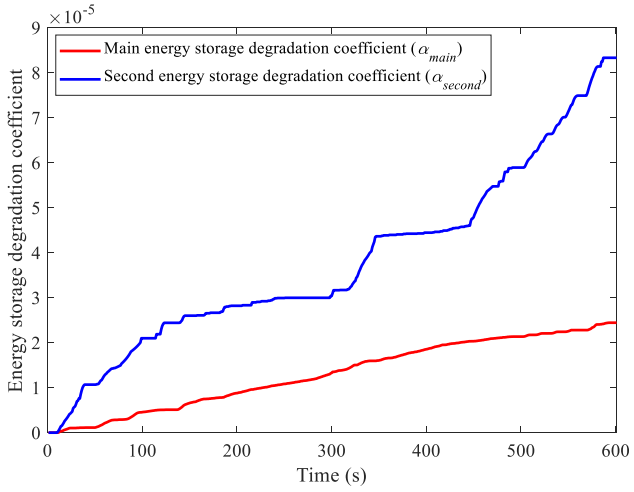


(III)

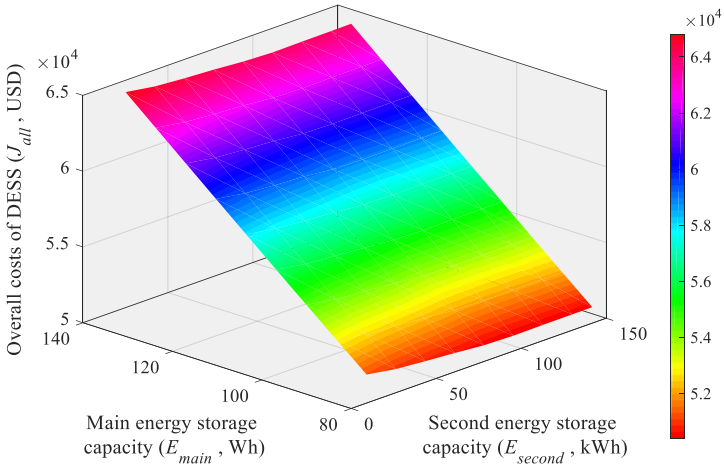


(IV)

Figure 65 Optimal trajectory of (a) power, (b) SOC, (c) degradation coefficient, for the main and second ESs in the LIB-AEAIB DESS with the optimal configuration presented in Table XXVIII. (IV) optimal overall costs of the LIB-AEAIB DESS with different configurations of the main and second ESs.

In Figure 65 (a), the main and second ESs have a similar power amplitude, but the second ES has sharper power fluctuations, especially during the period from 500 to 600 second, where the second ES boosts 100 kW within seconds for five times. This observation verifies that the second ES fulfils its duty as a power peaking unit.

In Figure 65 (b), the main ES witnesses a slowly declining SOC, which implies that the main ES generally experiences a discharging process and fulfils its primary role of delivering energy. In

contrast, the SOC of the second ES fluctuates dramatically between 20% and 100% due to the fast-changing peaking power.

In Figure 65 (c), the main ES sees a steadily rising degradation, while the second ES has a more checkered degradation process because of its more fluctuating power. The second ES generates a higher degradation coefficient in the end, compared with the main ES. This is because the main ES is much more expensive than the second (this can be reflected by Figure 64 (c)); thus, the optimal EM strategy sacrifices more the second ES so that overall costs can be minimised. Combining Figure 65 (a) (b) (c), the LIB-AEAIB DESS proves itself capable of dealing with the aggressive driving conditions of high-performance EVs.

Lastly, to find out how overall costs change with LIB-AEAIB DESS configurations, Figure 65 (d) configures the main and second ESs with different energy capacity and obtain the corresponding optimal overall costs. It can be seen that overall costs keep rising with the enlarging main ES, but first decline and then upswing with the enlarging second ES. Therefore, for deploying the LIB-AEAIB DESS in practical engineering, the LIB pack only needs to meet the minimum allowable energy capacity, while the AEAIB pack has an optimal energy capacity to minimise overall costs.

### 8.4.5 Summary

In summary of Chapter 8, the significant findings are listed as follows:

1) Using the ILAIB-based DESSs can benefit from 16% less overall costs than the LIB-based DESSs, due to the noticeably reduced ES degradation. However, the ILAIB-based DESSs are volumetrically ten times larger than the LIB-based DESSs, which prevents the ILAIB from being applied in practical engineering.

2) From the second ES technology perspective, the AEAIB-based DESSs surpass the SC-based DESSs with 3% less mass, a small volume comparable to the LIB-only ESS and 2% less overall costs. This indicates that the AEAIB can be a strong competitor of the SC in DESS applications.

3) The case study of the LIB-AEAIB DESS further confirms that the LIB-AEAIB DESS is capable of handling the power and energy requests from high-performance EV propulsion and is the most viable hybrid combination of lithium-ion, aluminium-ion and SC technologies for future development.

4) Although the modelling methodology is applied to the Aluminium DESSs, it can also be applied to potential future chemistries. This is because the methodology is based on the equivalent circuits for modelling the general main and second energy storages.

# Chapter 9 Conclusion

## 9.1 Summary and key findings

Recent years have witnessed a boom in the development of electric vehicles (EVs), with global sales of 27 million units projected by 2030 [7]. Energy storage system (ESS), as the heart of an EV, is expected to have a high energy capacity to sustain long-distance driving and a high power capability to boost sharp accelerations. However, a single energy storage technology may not be optimal for both power and energy, which obliges the EV designers to compromise EV driving range and dynamic performance. In this regard, a dual energy storage system (DESS) comprising two energy storage components is an option for compensating any shortcoming of single energy storage technology by pairing it with a complementary option. Combining Li-ion batteries (LIBs) and supercapacitors (SCs) into a DESS is the most popular practice and has long been studied. This work starts with modelling the LIB-SC DESS and then focuses on two research problems: energy management (EM) and sizing. The EM is to split the power and energy demands of EV propulsion for each energy storage component to undertake. The sizing is to design the physical, electrical, financial parameters of each energy storage component. Considering the inter-related connections between EM and sizing, in this work, EM and sizing are decoupled and studied, respectively, and then combined jointly with application to the optimisation of battery degradation. Furthermore, the modelling, EM and sizing methodologies are generalised from the LIB-SC DESS to general DESS using any two kinds of energy storage components. Specifically, a particular study is performed with DESSs using ionic liquid and aqueous electrolyte Al-ion batteries (AIBs). This work is expected to provide systematic, general EM and sizing guides for various DESSs in EV applications. The research problem-specific investigations presented in this work are concluded as follows.

(1) The development of EV and DESS models is the starting point of this work. An EV model with DESS is developed in ADVISOR to simulate EV operations and DESS performance as a function of drive cycles. Each component within the EV model is modelled and explained in terms of hypothesis and input/output relationships. The component models are then packaged into the drivetrain module and DESS module, and finally into the overall EV model. The adaptation of ADVISOR to match and run the overall model is also presented. Experimental validation is performed specifically with the component models of the battery and SC, while simulation validation is performed with the drivetrain module and DESS module by analysing the simulation results from a case-study EV. The modelling methodology is developed and tested for the LIB-SC DESS and then generalised to a variety of DESS with a main and a second energy storage. The modelling of Aluminum DESS is an example of how the modelling methodology can be applied to the DESS using novel Aluminum chemistries.

(2) The investigation of EM proposes an online energy management strategy (EMS) that optimises the operating costs of DESS and can be adaptive to real-time EV driving conditions. The dynamic programming (DP) algorithm is tailored to solve the optimal offline EMS, which is then analysed to inspire online EMS design. The designed online EMS has three components: the variable perception horizon to capture consistent driving behaviour, the neural network to predict the threshold for battery-SC power splitting, and the rule-based strategy to imitate the optimal offline EMS. Compared with existing studies, the proposed EMS has the following advantages. Benefiting from the advantages, the proposed online EMS shows high control effectiveness, with the cost optimisation rate being more than 97%.

- Rather than perceiving mixed driving behaviours, the proposed variable perception horizon accurately recognise the consistent driving behaviour within each micro-trip.
- Rather than burdening the neural network with many unsubstantiated inputs, the proposed neural network only accepts necessary inputs that are refined based on analytical deductions and regression analysis.
- Rather than using a complicated framework to integrate the whole EMS, the proposed online EMS is integrated with low complexity using the proposed rule-based strategy, designed based on careful analysis of optimal offline EMS.

(3) The investigation of sizing proposes a sizing method with sensitivity analysis for the DESS to minimise financial costs over EV lifetime. After configuring the constraints for sizing, an optimisation framework is proposed based on the DP algorithm to solve both the size and EMS of DESS. Eight parameters of the EV, DESS and components are sorted out as sensitive factors of DESS sizing. The trends of optimal DESS size and costs with varying factor values are analysed to explain why DESS sizing is sensitive to each factor. Each factor's relative importance is quantified as an impact degree and discussed in terms of practical engineering. The key findings are:

- The optimal battery pack size is precisely the minimum allowable size to guarantee EV driving range, while the SC pack size is a U-shape function of DESS costs so that there is an optimal SC pack size to minimise DESS costs.
- Battery degradation is the dominating cause (more than 75%) of DESS costs so that it needs the most attention when sizing a DESS.
- The EV drive cycle has the biggest impact on DESS costs as a drastic drive cycle can dramatically raise the power demands of EV propulsion. Battery price, nominal bus voltage, EV driving range and DC/DC conversion efficiency have medium impacts. In contrast, DESS topology, SC price and DC/DC converter price have little impacts on DESS costs, and they should be considered with descending priorities in practical engineering.

(4) The investigation of battery degradation proposes both EM and sizing benchmarks for the DESS to optimise battery degradation and its engineering impacts. The benchmarks are independent of EM

techniques and sizing formulations and can be generalised to wide cases using different EVs, batteries and SCs. The efficacy of the proposed EM and sizing benchmarks is tested by a case study using a high-performance EV. The key findings are:

- In terms of EM, the essence of reducing battery degradation exists in reducing the fluctuation of battery operating power; the optimal EM benchmarks are significantly affected by the size of the SC pack but less significantly affected by the size of the battery pack.
- In terms of sizing, the general trends of battery degradation with DESS size are deduced. Specifically, the DESS with a larger battery pack and a larger SC pack can have fewer battery replacements; DESS component costs grow with increasing battery pack size, while first drop and then rise with increasing SC pack size.

(5) The investigation of Aluminium DESS proposes DESSs composed of ionic liquid Al-ion batteries (ILAIBs) and aqueous Al-ion batteries (AAIBs) for EV propulsion. The Al-ion batteries are substituted for one or both of the LIBs and SCs of the conventional LIB-SC DESS. Thus the ILAIB-SC, LIB-AAIB and ILAIB-AAIB DESSs are modelled and simulated compared to the LIB-SC DESS in terms of mass, volume, initial cost and overall financial costs. The key findings are:

- Using the ILAIB as the main energy storage in the DESS can reduce overall financial costs by 16% compared with the LIB-based DESSs, but the volume of ILAIB-based DESSs is ten times that of LIB-based DESSs, which prevents the ILAIB from being applied in practical engineering.
- Using the AAIB as the second energy storage can reduce overall financial costs by 2% and benefit from 2% less mass and 1% less volume than the SC-based DESSs, which proves the AAIB a strong competitor of the SC in DESS applications.
- Considering both financial costs and deployment feasibility, the LIB-AAIB DESS is the most viable combination of Li-ion, Al-ion and SC technologies for future development.

Oriented real-life engineering, suggestions are provided for DESS configuration in EVs. Assume the EV design parameters are all known, and sufficient batteries and SCs are available for deploying the DESS. The only remaining question is to configure a DESS with a determined size and online implementable EMS. It is suggested first to work out the optimal size of DESS using the sizing method presented in Section 6.2. It should be noted that an input drive cycle is needed for using the sizing method, and DESS sizing results are subject to the input drive cycle. In this case, the input drive cycle should be carefully selected and typical of the EV's expected, common driving conditions. After confirming the size of DESS, the EMS of DESS can be worked out using the EM methods presented in Sections 5.2 and 5.3. Using the method in Section 5.2, the optimal offline EMS of DESS can be obtained and analysed so as to guide the design of online EMS. Finally, using the method in Section 5.3, the adaptive online EMS can be designed and implemented as the combination of variable perception horizon, neural network and rule-based strategy.

## 9.2 Future work

The research area of DESS for EVs is complex; hence, the presented work cannot be exhaustive in discussing every research problem and methodology relating to the DESS study. The following provides alternative directions for improvement in future work.

(1) In terms of DESS topology, this work mainly focuses on the SC/battery DESS, while the battery/SC DESS is merely discussed in Section 6.3.1.3. Future work may adapt the modelling, EM and sizing methodologies of the SC/battery DESS to make them fit the battery/SC DESS. The preliminary discussion in Section 6.3.1.3 has indicated that the adaptation will not be very complicated since the methodologies of the SC/battery DESS can be significantly reused for the battery/SC DESS.

(2) In terms of energy storage device selection, this work only considers the LIB, SC and AIB. In addition, the hydrogen fuel cells, whose energy density is even higher than LIBs, have found plenty of applications as the main energy storage in an ESS. Future work may try the combination of hydrogen fuel cell and one of LIB, SC and AIB to form a DESS for EV propulsion and compare it with the other hybrid combinations presented in this work.

(3) In terms of energy storage device modelling, this work does not consider the thermal issues and assumes that energy storage devices' temperature can be maintained at 20°C constantly. In practical engineering, the temperature is usually controlled by specifically designed thermal management systems (TMSs). Future work may consider implementing TMSs and investigating the influence of temperature on energy storage devices' degradation and efficiency. Besides, the depth-of-discharge (DOD), which is known to have an impact on the energy storage degradation rate, has not been taken into account in this work. Future work may also consider DOD as a variable in modelling energy storage degradation.

(4) In terms of EM, the variable perception horizon proposed in Section 5.3.1 can be improved by optimising the maximum horizon length. This work uses 200 seconds as the maximum horizon length, while optimisation approaches can be applied to determine the best-case value. Besides, more samples can be tailored to train the neural network proposed in Section 5.3.2 so that the prediction accuracy can be further improved.

(5) In terms of sizing, more factors can be considered in the sensitivity analysis in Section 6.3, such as ambient temperature and coulombic efficiency of energy storage. Besides, this work considers the factors listed in Table XXII as independent of each other, while some factors, such as DC/DC converter price and efficiency, have a certain degree of interdependence. Future work can also investigate DESS sizing and perform sensitivity analysis with the interdependence between factors.

# List of References


[1] H. A. Bonges III and A. C. Lusk, "Addressing electric vehicle (EV) sales and range anxiety through parking layout, policy and regulation," *Transportation Research Part A: Policy and Practice*, vol. 83, pp. 63-73, 2016. doi: https://doi.org/10.1016/j.tra.2015.09.011

[2] C. Mi and M. A. Masrur, *Hybrid electric vehicles: principles and applications with practical perspectives*. John Wiley & Sons, 2017. ISBN: 111897056X

[3] M. Ehsani, Y. Gao, S. Longo, and K. Ebrahimi, *Modern electric, hybrid electric, and fuel cell vehicles*. CRC press, 2018. ISBN: 0429998244

[4] S. M. Lukic, J. Cao, R. C. Bansal, F. Rodriguez, and A. Emadi, "Energy Storage Systems for Automotive Applications," *IEEE Transactions on Industrial Electronics*, vol. 55, no. 6, pp. 2258-2267, 2008. doi: https://doi.org/10.1109/TIE.2008.918390

[5] A. Khaligh and Z. Li, "Battery, Ultracapacitor, Fuel Cell, and Hybrid Energy Storage Systems for Electric, Hybrid Electric, Fuel Cell, and Plug-In Hybrid Electric Vehicles: State of the Art," *IEEE Transactions on Vehicular Technology*, vol. 59, no. 6, pp. 2806-2814, 2010. doi: https://doi.org/10.1109/TVT.2010.2047877

[6] L. Lu, X. Han, J. Li, J. Hua, and M. Ouyang, "A review on the key issues for lithium-ion battery management in electric vehicles," *Journal of Power Sources*, vol. 226, pp. 272-288, 2013. doi: https://doi.org/10.1016/j.jpowsour.2012.10.060

[7] G. Berckmans, M. Messagie, J. Smekens, N. Omar, L. Vanhaverbeke, and J. Van Mierlo, "Cost projection of state of the art lithium-ion batteries for electric vehicles up to 2030," *Energies*, vol. 10, no. 9, p. 1314, 2017. doi: https://doi.org/10.3390/en10091314

[8] B. Yang *et al.*, "Design and implementation of Battery/SMES hybrid energy storage systems used in electric vehicles: A nonlinear robust fractional-order control approach," *Energy*, p. 116510, 2019. doi: https://doi.org/10.1016/j.energy.2019.116510

[9] L. Zhang, X. Hu, Z. Wang, F. Sun, and D. G. Dorrell, "A review of supercapacitor modeling, estimation, and applications: A control/management perspective," *Renewable and Sustainable Energy Reviews*, vol. 81, pp. 1868-1878, 2018. doi: https://doi.org/10.1016/j.rser.2017.05.283

[10] S. Shili, A. Hijazi, A. Sari, X. Lin-Shi, and P. Venet, "Balancing Circuit New Control for Supercapacitor Storage System Lifetime Maximization," *IEEE Transactions on Power Electronics*, vol. 32, no. 6, pp. 4939-4948, 2017. doi: https://doi.org/10.1109/TPEL.2016.2602393

[11] C. Wu, R. Fu, Z. Xu, and Y. Chen, "Improved State of Charge Estimation for High Power Lithium Ion Batteries Considering Current Dependence of Internal Resistance," *Energies*, vol. 10, no. 10, p. 1486, 2017. doi: https://doi.org/10.3390/en10101486

[12] J. Li, A. M. Gee, M. Zhang, and W. Yuan, "Analysis of battery lifetime extension in a SMES-battery hybrid energy storage system using a novel battery lifetime model," *Energy*, vol. 86, pp. 175-185, 2015. doi: https://doi.org/10.1016/j.energy.2015.03.132

[13] Z. Song, H. Hofmann, J. Li, X. Han, and M. Ouyang, "Optimization for a hybrid energy storage system in electric vehicles using dynamic programing approach," *Applied Energy*, vol. 139, pp. 151-162, 2015. doi: https://doi.org/10.1016/j.apenergy.2014.11.020

[14] J. Ruan, Q. Song, and W. Yang, "The application of hybrid energy storage system with electrified continuously variable transmission in battery electric vehicle," *Energy*, vol. 183, pp. 315-330, 2019. doi: https://doi.org/10.1016/j.energy.2019.06.095

[15] C. Lai, Y. Cheng, M. Hsieh, and Y. Lin, "Development of a Bidirectional DC/DC Converter With Dual-Battery Energy Storage for Hybrid Electric Vehicle System," *IEEE Transactions on Vehicular Technology*, vol. 67, no. 2, pp. 1036-1052, 2018. doi: https://doi.org/10.1109/TVT.2017.2763157

[16] J. Du, J. Chen, Z. Song, M. Gao, and M. Ouyang, "Design method of a power management strategy for variable battery capacities range-extended electric vehicles to improve energy efficiency and cost-effectiveness," *Energy*, vol. 121, pp. 32-42, 2017. doi: https://doi.org/10.1016/j.energy.2016.12.120

[17] B. D. Smith, R. G. A. Wills, and A. J. Cruden, "Aqueous Al-ion cells and supercapacitors — A comparison," *Energy Reports*, vol. 6, pp. 166-173, 2020. doi: https://doi.org/10.1016/j.egyr.2020.03.021

[18] G. Offer, D. Howey, M. Contestabile, R. Clague, and N. Brandon, "Comparative analysis of battery electric, hydrogen fuel cell and hybrid vehicles in a future sustainable road transport system," *Energy policy*, vol. 38, no. 1, pp. 24-29, 2010. doi: https://doi.org/10.1016/j.enpol.2009.08.040

[19] M. Dawei, Z. Yu, Z. Meilan, and N. Risha, "Intelligent fuzzy energy management research for a uniaxial parallel hybrid electric vehicle," *Computers & Electrical Engineering*, vol. 58, pp. 447-464, 2017. doi: https://doi.org/10.1016/j.compeleceng.2016.03.014

[20] R. Lot and S. A. Evangelou, "Green driving optimization of a series hybrid electric vehicle," in *52nd IEEE Conference on Decision and Control*, 2013, pp. 2200-2207.

[21] R. Bishop, *Intelligent vehicle technology and trends*. 2005. ISBN: 1580539114

[22] K. Çağatay Bayindir, M. A. Gözüküçük, and A. Teke, "A comprehensive overview of hybrid electric vehicle: Powertrain configurations, powertrain control techniques and electronic control units," *Energy Conversion and Management*, vol. 52, no. 2, pp. 1305-1313, 2011. doi: https://doi.org/10.1016/j.enconman.2010.09.028

[23] L. Chen, F. Zhu, M. Zhang, Y. Huo, C. Yin, and H. Peng, "Design and Analysis of an Electrical Variable Transmission for a Series Parallel Hybrid Electric Vehicle," *IEEE Transactions on Vehicular Technology*, vol. 60, no. 5, pp. 2354-2363, 2011. doi: https://doi.org/10.1109/TVT.2011.2134876

[24] G. Pellegrino, A. Vagati, B. Boazzo, and P. Guglielmi, "Comparison of Induction and PM Synchronous Motor Drives for EV Application Including Design Examples," *IEEE Transactions on Industry Applications*, vol. 48, no. 6, pp. 2322-2332, 2012. doi: https://doi.org/10.1109/TIA.2012.2227092

[25] (17 Jan 2018). *BMW i3*. Available: https://en.wikipedia.org/wiki/BMW_i3#Range_extender_option

[26] M. Ehsani, Y. Gao, and A. Emadi, *Modern Electric, Hybrid Electric, and Fuel Cell Vehicles: Fundamentals, Theory, and Design, Second Edition*. Taylor & Francis, 2009. ISBN: 9781420053982

[27] (11 May 2018). *Recommendation of HEVs for Sale in China*. Available: http://newcar.xcar.com.cn/200911/news_73600_1.html

[28] (29 Oct 2017). *How many speeds make sense for EV transmissions? Probably one*. Available: https://www.autoblog.com/2015/07/21/how-many-speeds-make-sense-for-ev-transmissions-probably-one/?guccounter=1

[29] (11 May 2018). *Do electric vehicles actually reduce carbon emissions?* Available: https://www.drax.com/technology/electric-vehicles-actually-reduce-carbon-emissions/

[30] (23 Apr 2018). *Cleaner Cars from Cradle to Grave (2015)*. Available: https://www.ucsusa.org/clean-vehicles/electric-vehicles/life-cycle-ev-emissions#.WvrIW6iPKUl

[31] W. Zhao, G. Wu, C. Wang, L. Yu, and Y. Li, "Energy transfer and utilization efficiency of regenerative braking with hybrid energy storage system," *Journal of Power Sources*, vol. 427, pp. 174-183, 2019. doi: https://doi.org/10.1016/j.jpowsour.2019.04.083

[32] A. Patzak, F. Bachheibl, A. Baumgardt, G. Dajaku, O. Moros, and D. Gerling, "Driving range evaluation of a multi-phase drive for low voltage high power electric vehicles," in *International Conference on Sustainable Mobility Applications, Renewables and Technology*, 2015, pp. 1-7.

[33] G. A. Putrus, P. Suwanapingkarl, D. Johnston, E. C. Bentley, and M. Narayana, "Impact of electric vehicles on power distribution networks," in *2009 IEEE Vehicle Power and Propulsion Conference*, 2009, pp. 827-831.

[34] J. F. Peters, M. Baumann, B. Zimmermann, J. Braun, and M. Weil, "The environmental impact of Li-Ion batteries and the role of key parameters – A review," *Renewable and Sustainable Energy Reviews*, vol. 67, pp. 491-506, 2017. doi: https://doi.org/10.1016/j.rser.2016.08.039

[35] (15 May 2018). *Automotive Battery Market Size Worth $95.57 Billion By 2025*. Available: https://www.grandviewresearch.com/press-release/global-automotive-battery-market

[36] (2017, Jul 10,2019). *How Does a Lithium-ion Battery Work?* Available: https://www.energy.gov/eere/articles/how-does-lithium-ion-battery-work

[37] B. Wang, J. Xu, B. Cao, and B. Ning, "Adaptive mode switch strategy based on simulated annealing optimization of a multi-mode hybrid energy storage system for electric vehicles," *Applied Energy*, vol. 194, pp. 596-608, 2017. doi: https://doi.org/10.1016/j.apenergy.2016.05.030

[38] C. Lin, S. Xu, Z. Li, B. Li, G. Chang, and J. Liu, "Thermal analysis of large-capacity LiFePO4 power batteries for electric vehicles," *Journal of Power Sources*, vol. 294, pp. 633-642, 2015. doi: https://doi.org/10.1016/j.jpowsour.2015.06.129

[39] N. Damay, C. Forgez, M.-P. Bichat, and G. Friedrich, "Thermal modeling of large prismatic LiFePO4/graphite battery. Coupled thermal and heat generation models for characterization and simulation," *Journal of Power Sources*, vol. 283, pp. 37-45, 2015. doi: https://doi.org/10.1016/j.jpowsour.2015.02.091

[40] E. Samadani *et al.*, "Empirical Modeling of Lithium-ion Batteries Based on Electrochemical Impedance Spectroscopy Tests," *Electrochimica Acta*, vol. 160, pp. 169-177, 2015. doi: https://doi.org/10.1016/j.electacta.2015.02.021

[41] R. Rao, S. Vrudhula, and D. N. Rakhmatov, "Battery modeling for energy aware system design," *Computer*, vol. 36, no. 12, pp. 77-87, 2003. doi: https://doi.org/10.1109/MC.2003.1250886

[42] Y. Li, L. Wang, C. Liao, L. Wu, J. Li, and Y. Guo, "Effects of temperature on dynamic characteristics of li-ion batteries in electric vehicle applications," in *2014 IEEE Conference and Expo Transportation Electrification Asia-Pacific*, 2014, pp. 1-6.

[43] E. Samadani, M. Mastali, S. Farhad, R. A. Fraser, and M. Fowler, "Li-ion battery performance and degradation in electric vehicles under different usage scenarios," *International Journal of Energy Research*, vol. 40, no. 3, pp. 379-392, 2016. doi: https://doi.org/10.1002/er.3378

[44] H. H. Eldeeb, A. T. Elsayed, C. R. Lashway, and O. Mohammed, "Hybrid energy storage sizing and power splitting optimization for plug-in electric vehicles," *IEEE Transactions on Industry Applications*, vol. 55, no. 3, pp. 2252-2262, 2019. doi: https://doi.org/10.1109/TIA.2019.2898839

[45] Z. Song, H. Hofmann, J. Li, J. Hou, X. Zhang, and M. Ouyang, "The optimization of a hybrid energy storage system at subzero temperatures: Energy management strategy design and battery heating requirement analysis," *Applied Energy*, vol. 159, pp. 576-588, 2015. doi: https://doi.org/10.1016/j.apenergy.2015.08.120

[46] Q. Zhang, F. Ju, S. Zhang, W. Deng, J. Wu, and C. Gao, "Power Management for Hybrid Energy Storage System of Electric Vehicles Considering Inaccurate Terrain Information," *IEEE Transactions on Automation Science and Engineering*, vol. 14, no. 2, pp. 608-618, 2017. doi: https://doi.org/10.1109/TASE.2016.2645780

[47] M. Wieczorek and M. Lewandowski, "A mathematical representation of an energy management strategy for hybrid energy storage system in electric vehicle and real time optimization using a genetic algorithm," *Applied Energy*, vol. 192, pp. 222-233, 2017. doi: https://doi.org/10.1016/j.apenergy.2017.02.022

[48] P. Golchoubian and N. L. Azad, "Real-Time Nonlinear Model Predictive Control of a Battery/Supercapacitor Hybrid Energy Storage System in Electric Vehicles," *IEEE Transactions on Vehicular Technology*, vol. 66, no. 11, pp. 9678-9688, 2017. doi: https://doi.org/10.1109/TVT.2017.2725307

[49] J. Jaguemont, L. Boulon, P. Venet, Y. Dubé, and A. Sari, "Lithium-Ion Battery Aging Experiments at Subzero Temperatures and Model Development for Capacity Fade Estimation," *IEEE Transactions on Vehicular Technology*, vol. 65, no. 6, pp. 4328-4343, 2016. doi: https://doi.org/10.1109/TVT.2015.2473841

[50] R. Bhattacharyya, B. Key, H. Chen, A. S. Best, A. F. Hollenkamp, and C. P. Grey, "In situ NMR observation of the formation of metallic lithium microstructures in lithium batteries," *Nature Materials*, Article vol. 9, p. 504, 2010. doi: https://doi.org/10.1038/nmat2764

[51] S. Saxena, C. Le Floch, J. MacDonald, and S. Moura, "Quantifying EV battery end-of-life through analysis of travel needs with vehicle powertrain models," *Journal of Power Sources*, vol. 282, pp. 265-276, 2015. doi: https://doi.org/10.1016/j.jpowsour.2015.01.072

[52] E. Sarasketa-Zabala, I. Gandiaga, E. Martinez-Laserna, L. M. Rodriguez-Martinez, and I. Villarreal, "Cycle ageing analysis of a LiFePO4/graphite cell with dynamic model validations: Towards realistic lifetime predictions," *Journal of Power Sources*, vol. 275, pp. 573-587, 2015. doi: https://doi.org/10.1016/j.jpowsour.2014.10.153

[53] M. Ouyang *et al.*, "Low temperature aging mechanism identification and lithium deposition in a large format lithium iron phosphate battery for different charge profiles," *Journal of Power Sources*, vol. 286, pp. 309-320, 2015. doi: https://doi.org/10.1016/j.jpowsour.2015.03.178

[54] J. Groot, M. Swierczynski, A. I. Stan, and S. K. Kær, "On the complex ageing characteristics of high-power LiFePO4/graphite battery cells cycled with high charge and discharge currents," *Journal of Power Sources*, vol. 286, pp. 475-487, 2015. doi: https://doi.org/10.1016/j.jpowsour.2015.04.001

[55] J. Wang *et al.*, "Degradation of lithium ion batteries employing graphite negatives and nickel–cobalt–manganese oxide + spinel manganese oxide positives: Part 1, aging mechanisms and life estimation," *Journal of Power Sources*, vol. 269, pp. 937-948, 2014. doi: https://doi.org/10.1016/j.jpowsour.2014.07.030

[56] J. Wang *et al.*, "Cycle-life model for graphite-LiFePO4 cells," *Journal of Power Sources*, vol. 196, no. 8, pp. 3942-3948, 2011. doi: https://doi.org/10.1016/j.jpowsour.2010.11.134

[57] C. Zhang *et al.*, "Using CPE Function to Size Capacitor Storage for Electric Vehicles and Quantifying Battery Degradation during Different Driving Cycles," *Energies*, vol. 9, no. 11, p. 903, 2016. doi: https://doi.org/10.3390/en9110903

[58] L. Kouchachvili, W. Yaïci, and E. Entchev, "Hybrid battery/supercapacitor energy storage system for the electric vehicles," *Journal of Power Sources*, vol. 374, pp. 237-248, 2018. doi: https://doi.org/10.1016/j.jpowsour.2017.11.040

[59] Maxwell Technologies, "Product Guide – Maxwell Technologies BOOSTCAP Ultracapacitors", Available: https://www.maxwell.com/images/documents/PG_boostcap_product_guide.pdf, Accessed on: Oct 18, 2018.

[60] Maxwell Technologies, "DESIGN CONSIDERATIONS FOR ULTRACAPACITORS", Available: https://www.maxwell.com/images/documents/https://www.maxwell.com/images/documents/technote_designinguide.pdf.pdf, Accessed on: Oct 25, 2018.

[61] C. Xiang, F. Ding, W. Wang, and W. He, "Energy management of a dual-mode power-split hybrid electric vehicle based on velocity prediction and nonlinear model predictive control," *Applied Energy*, vol. 189, pp. 640-653, 2017. doi: https://doi.org/10.1016/j.apenergy.2016.12.056

[62] MaxwellTechnologies, "DATASHEET OF K2 ULTRACAPACITORS - 2.7V SERIES", Available: https://www.maxwell.com/images/documents/K2Series_DS_1015370_5_20141104.pdf, Accessed on: Oct 17, 2018.

[63] Maxwell Technologies, "ULTRACAPACITOR ASSISTED ELECTRIC DRIVES FOR TRANSPORTATION", Available: https://www.maxwell.com/images/documents/whitepaper_electricdrives.pdf, Accessed on: Nov 5, 2018.

[64] (15 Mar 2018). *Supercapacitor*. Available: https://en.wikipedia.org/wiki/Supercapacitor

[65] Maxwell Technologies, "Top 10 Reasons for using Ultracapacitors in your system designs", Available: https://www.maxwell.com/images/documents/whitepaper_top_10_reasons_for_ultracaps.pdf, Accessed on: Nov 13, 2018.

[66] A. Oukaour *et al.*, "Supercapacitors aging diagnosis using least square algorithm," *Microelectronics Reliability*, vol. 53, no. 9-11, pp. 1638-1642, 2013. doi: https://doi.org/10.1016/j.microrel.2013.07.032

[67] Maxwell Technologies, "Energy Storage Modules Life Duration Estimation", Available: https://www.maxwell.com/images/documents/applicationnote_1012839_1.pdf, Accessed on: Nov 18, 2018.

[68] M. Marracci, B. Tellini, M. Catelani, and L. Ciani, "Ultracapacitor Degradation State Diagnosis via Electrochemical Impedance Spectroscopy," *IEEE Trans. Instrumentation and Measurement*, vol. 64, no. 7, pp. 1916-1921, 2015. doi: https://doi.org/10.1109/TIM.2014.2367772

[69] T. Kovaltchouk, B. Multon, H. B. Ahmed, J. Aubry, and P. Venet, "Enhanced aging model for supercapacitors taking into account power cycling: Application to the sizing of an energy storage system in a direct wave energy converter," *IEEE Transactions on Industry Applications*, vol. 51, no. 3, pp. 2405-2414, 2015. doi: https://doi.org/10.1109/TIA.2014.2369817

[70] E. Weymar and M. Finkbeiner, "Statistical analysis of empirical lifetime mileage data for automotive LCA," *The International Journal of Life Cycle Assessment*, vol. 21, no. 2, pp. 215-223, 2016. doi: https://doi.org/10.1007/s11367-015-1020-6

[71] V. Sedlakova *et al.*, "Supercapacitor degradation assesment by power cycling and calendar life tests," *Metrology and Measurement Systems*, vol. 23, no. 3, pp. 345-358, 2016. doi: https://doi.org/10.1515/mms-2016-0038

[72] S. M. Lukic, S. G. Wirasingha, F. Rodriguez, J. Cao, and A. Emadi, "Power management of an ultracapacitor/battery hybrid energy storage system in an HEV," in *Vehicle Power and Propulsion Conference*, 2006, pp. 1-6: IEEE.

[73] I. Aharon and A. Kuperman, "Topological Overview of Powertrains for Battery-Powered Vehicles With Range Extenders," *IEEE Transactions on Power Electronics*, vol. 26, no. 3, pp. 868-876, 2011. doi: https://doi.org/10.1109/TPEL.2011.2107037

[74] A. Sripakagorn and N. Limwuthigraijirat, "Experimental assessment of fuel cell/supercapacitor hybrid system for scooters," *International journal of hydrogen energy*, vol. 34, no. 15, pp. 6036-6044, 2009. doi: https://doi.org/10.1016/j.ijhydene.2009.04.059

[75] R. M. Schupbach, J. C. Balda, M. Zolot, and B. Kramer, "Design methodology of a combined battery-ultracapacitor energy storage unit for vehicle power management," in *Power Electronics Specialist Conference*, 2003, vol. 1, pp. 88-93 vol.1.

[76] L. Gao, R. A. Dougal, and S. Liu, "Power enhancement of an actively controlled battery/ultracapacitor hybrid," *IEEE transactions on power electronics*, vol. 20, no. 1, pp. 236-243, 2005. doi: https://doi.org/10.1109/TPEL.2004.839784

[77] J. Cao and A. Emadi, "A New Battery/UltraCapacitor Hybrid Energy Storage System for Electric, Hybrid, and Plug-In Hybrid Electric Vehicles," *IEEE Transactions on Power Electronics*, vol. 27, no. 1, pp. 122-132, 2012. doi: https://doi.org/10.1109/TPEL.2011.2151206

[78] A. Emadi, K. Rajashekara, S. S. Williamson, and S. M. Lukic, "Topological overview of hybrid electric and fuel cell vehicular power system architectures and configurations," *IEEE Transactions on Vehicular Technology*, vol. 54, no. 3, pp. 763-770, 2005. doi: https://doi.org/10.1109/TVT.2005.847445

[79] A. Emadi, S. S. Williamson, and A. Khaligh, "Power electronics intensive solutions for advanced electric, hybrid electric, and fuel cell vehicular power systems," *IEEE Transactions on Power Electronics*, vol. 21, no. 3, pp. 567-577, 2006. doi: https://doi.org/10.1109/TPEL.2006.872378

[80] J. Cao, N. Schofield, and A. Emadi, "Battery balancing methods: A comprehensive review," in *2008 IEEE Vehicle Power and Propulsion Conference*, 2008, pp. 1-6: IEEE.

[81] A. Di Napoli, F. Crescimbini, F. G. Capponi, and L. Solero, "Control strategy for multiple input DC-DC power converters devoted to hybrid vehicle propulsion systems," in *Proc. IEEE Int. Symp. Ind. Electron*, 2002, vol. 3, pp. 1036-1041.

[82] A. Di Napoli, F. Crescimbini, S. Rodo, and L. Solero, "Multiple input DC-DC power converter for fuel-cell powered hybrid vehicles," in *2002 IEEE 33rd Annual IEEE Power Electronics Specialists Conference*, 2002, vol. 4, pp. 1685-1690: IEEE.

[83] S. Chung and O. Trescases, "Hybrid lead-acid/lithium-ion energy storage system with power-mix control for light electric vehicles," in *2016 18th European Conference on Power Electronics and Applications*, 2016, pp. 1-10.

[84] G. Lijun, R. A. Dougal, and L. Shengyi, "Power enhancement of an actively controlled battery/ultracapacitor hybrid," *IEEE Transactions on Power Electronics*, vol. 20, no. 1, pp. 236-243, 2005. doi: https://doi.org/10.1109/TPEL.2004.839784

[85] Z. Fu, B. Wang, X. Song, L. Liu, and X. Wang, "Power-split hybrid electric vehicle energy management based on improved logic threshold approach," *Mathematical Problems in Engineering*, vol. 2013, 2013. doi: https://doi.org/10.1155/2013/840648

[86] R. M. Schupbach and J. C. Balda, "Comparing DC-DC converters for power management in hybrid electric vehicles," in *IEEE International Electric Machines and Drives Conference*, 2003, vol. 3, pp. 1369-1374: IEEE.

[87] S. Onori, L. Serrao, and G. Rizzoni, *Hybrid electric vehicles: energy management strategies*. Springer, 2016. ISBN: 1447167813

[88] L. Zhang, X. Hu, Z. Wang, F. Sun, J. Deng, and D. G. Dorrell, "Multiobjective optimal sizing of hybrid energy storage system for electric vehicles," *IEEE Transactions on Vehicular Technology*, vol. 67, no. 2, pp. 1027-1035, 2017. doi: https://doi.org/10.1109/TVT.2017.2762368

[89] J. Du *et al.*, "Battery degradation minimization oriented energy management strategy for plug-in hybrid electric bus with multi-energy storage system," *Energy*, vol. 165, pp. 153-163, 2018. doi: https://doi.org/10.1016/j.energy.2018.09.084

[90] H. Ruan *et al.*, "Compound self-heating strategies and multi-objective optimization for lithium-ion batteries at low temperature," *Applied Thermal Engineering*, p. 116158, 2020. doi: https://doi.org/10.1016/j.applthermaleng.2020.116158

[91] Z. Song, X. Zhang, J. Li, H. Hofmann, M. Ouyang, and J. Du, "Component sizing optimization of plug-in hybrid electric vehicles with the hybrid energy storage system," *Energy*, vol. 144, pp. 393-403, 2018. doi: https://doi.org/10.1016/j.energy.2017.12.009

[92] R. Xiong, H. Chen, C. Wang, and F. Sun, "Towards a smarter hybrid energy storage system based on battery and ultracapacitor-A critical review on topology and energy management," *Journal of cleaner production*, vol. 202, pp. 1228-1240, 2018. doi: https://doi.org/10.1016/j.jclepro.2018.08.134

[93] J. Peng, H. He, and R. Xiong, "Rule based energy management strategy for a series–parallel plug-in hybrid electric bus optimized by dynamic programming," *Applied Energy*, vol. 185, pp. 1633-1643, 2017. doi: https://doi.org/10.1016/j.apenergy.2015.12.031

[94] L. Zhang *et al.*, "Hybrid electrochemical energy storage systems: An overview for smart grid and electrified vehicle applications," *Renewable and Sustainable Energy Reviews*, p. 110581, 2020. doi: https://doi.org/10.1016/j.rser.2020.110581

[95] C. Liu, Y. Wang, L. Wang, and Z. Chen, "Load-adaptive real-time energy management strategy for battery/ultracapacitor hybrid energy storage system using dynamic programming optimization," *Journal of Power Sources*, vol. 438, p. 227024, 2019. doi: https://doi.org/10.1016/j.jpowsour.2019.227024

[96] Z. Song, H. Hofmann, J. Li, J. Hou, X. Han, and M. Ouyang, "Energy management strategies comparison for electric vehicles with hybrid energy storage system," *Applied Energy*, vol. 134, pp. 321-331, 2014. doi: https://doi.org/10.1016/j.apenergy.2014.08.035

[97] Z. Chen, R. Xiong, C. Wang, and J. Cao, "An on-line predictive energy management strategy for plug-in hybrid electric vehicles to counter the uncertain prediction of the driving cycle," *Applied Energy*, vol. 185, pp. 1663-1672, 2017. doi: https://doi.org/10.1016/j.apenergy.2016.01.071

[98] L. Wang, Y. Wang, C. Liu, D. Yang, and Z. Chen, "A power distribution strategy for hybrid energy storage system using adaptive model predictive control," *IEEE Transactions on Power Electronics*, vol. 35, no. 6, pp. 5897-5906, 2019. doi: https://doi.org/10.1016/10.1109/TPEL.2019.2953050

[99] S. Zhang, R. Xiong, and F. Sun, "Model predictive control for power management in a plug-in hybrid electric vehicle with a hybrid energy storage system," *Applied Energy*, vol. 185, pp. 1654-1662, 2017. doi: https://doi.org/10.1016/j.apenergy.2015.12.035

[100] G. Du, Y. Zou, X. Zhang, T. Liu, J. Wu, and D. He, "Deep reinforcement learning based energy management for a hybrid electric vehicle," *Energy*, vol. 201, p. 117591, 2020. doi: https://doi.org/10.1016/j.energy.2020.117591

[101] B. Xu *et al.*, "Parametric study on reinforcement learning optimized energy management strategy for a hybrid electric vehicle," *Applied Energy*, vol. 259, p. 114200, 2020. doi: https://doi.org/10.1016/j.apenergy.2019.114200

[102] Y. Wang, L. Wang, M. Li, and Z. Chen, "A review of key issues for control and management in battery and ultra-capacitor hybrid energy storage systems," *eTransportation*, p. 100064, 2020. doi: https://doi.org/10.1016/j.etran.2020.100064

[103] R. Xiong, J. Cao, and Q. Yu, "Reinforcement learning-based real-time power management for hybrid energy storage system in the plug-in hybrid electric vehicle," *Applied Energy*, vol. 211, pp. 538-548, 2018. doi: https://doi.org/10.1016/j.apenergy.2017.11.072

[104] S. Zhang and R. Xiong, "Adaptive energy management of a plug-in hybrid electric vehicle based on driving pattern recognition and dynamic programming," *Applied Energy*, vol. 155, pp. 68-78, 2015. doi: https://doi.org/10.1016/j.apenergy.2015.06.003

[105] J. P. Trovão, P. G. Pereirinha, H. M. Jorge, and C. H. Antunes, "A multi-level energy management system for multi-source electric vehicles – An integrated rule-based meta-heuristic approach," *Applied Energy*, vol. 105, pp. 304-318, 2013. doi: https://doi.org/10.1016/j.apenergy.2012.12.081

[106] Y. Yang, X. Hu, H. Pei, and Z. Peng, "Comparison of power-split and parallel hybrid powertrain architectures with a single electric machine: dynamic programming approach," *Applied Energy*, vol. 168, pp. 683-690, 2016. doi: https://doi.org/10.1016/j.apenergy.2016.02.023

[107] Z. Song *et al.*, "Simultaneous identification and control for hybrid energy storage system using model predictive control and active signal injection," *IEEE Transactions on Industrial Electronics*, 2019. doi: https://doi.org/10.1109/TIE.2019.2952825

[108] A. Al-Mamun, Z. Liu, D. Rizzo, and S. Onori, "An Integrated Design and Control Optimization Framework for Hybrid Military Vehicle Using Lithium-ion Battery and Supercapacitor as Energy Storage Devices," *IEEE Transactions on Transportation Electrification*, 2018. doi: https://doi.org/10.1109/TTE.2018.2869038

[109] M. Masih-Tehrani, M.-R. Ha'iri-Yazdi, V. Esfahanian, and A. Safaei, "Optimum sizing and optimum energy management of a hybrid energy storage system for lithium battery life improvement," *Journal of Power Sources*, vol. 244, pp. 2-10, 2013. doi: https://doi.org/10.1016/j.jpowsour.2013.04.154

[110] Z. Song *et al.*, "Multi-objective optimization of a semi-active battery/supercapacitor energy storage system for electric vehicles," *Applied Energy*, vol. 135, pp. 212-224, 2014. doi: https://doi.org/10.1016/j.apenergy.2014.06.087

[111] L. Zhang, X. Hu, Z. Wang, F. Sun, J. Deng, and D. G. Dorrell, "Multiobjective Optimal Sizing of Hybrid Energy Storage System for Electric Vehicles," *IEEE Transactions on*

*Vehicular Technology*, vol. 67, no. 2, pp. 1027-1035, 2018. doi: https://doi.org/10.1109/TVT.2017.2762368

[112] J. Shen, S. Dusmez, and A. Khaligh, "Optimization of Sizing and Battery Cycle Life in Battery/Ultracapacitor Hybrid Energy Storage Systems for Electric Vehicle Applications," *IEEE Transactions on Industrial Informatics*, vol. 10, no. 4, pp. 2112-2121, 2014. doi: https://doi.org/10.1109/TII.2014.2334233

[113] Z. Song, J. Li, J. Hou, H. Hofmann, M. Ouyang, and J. Du, "The battery-supercapacitor hybrid energy storage system in electric vehicle applications: A case study," *Energy*, vol. 154, pp. 433-441, 2018. doi: https://doi.org/10.1016/j.energy.2018.04.148

[114] Q. Xiaodong, W. Qingnian, and Y. YuanBin, "Power Demand Analysis and Performance Estimation for Active-Combination Energy Storage System Used in Hybrid Electric Vehicles," *IEEE Transactions on Vehicular Technology*, vol. 63, no. 7, pp. 3128-3136, 2014. doi: https://doi.org/10.1109/TVT.2014.2302017

[115] C. Zhang, H. Min, Y. Yu, Q. Wang, and H. Sun, "A New Method to Optimize Semiactive Hybrid Energy Storage System for Hybrid Electrical Vehicle by Using PE Function," *Mathematical Problems in Engineering*, vol. 2015, p. 14, 2015, Art. no. 457303. doi: https://doi.org/10.1155/2015/457303

[116] A. Ostadi and M. Kazerani, "A comparative analysis of optimal sizing of battery-only, ultracapacitor-only, and battery–ultracapacitor hybrid energy storage systems for a city bus," *IEEE Transactions on Vehicular Technology*, vol. 64, no. 10, pp. 4449-4460, 2015. doi: https://doi.org/10.1109/TVT.2014.2371912

[117] F. J. Jimenez-Espadafor, J. J. R. Marín, J. A. B. Villanueva, M. T. García, E. C. Trujillo, and F. J. F. Ojeda, "Infantry mobility hybrid electric vehicle performance analysis and design," *Applied energy*, vol. 88, no. 8, pp. 2641-2652, 2011. doi: https://doi.org/10.1016/j.apenergy.2011.02.010

[118] L. Deng, H. Huang, L. Lu, and F. Yang, "Experimental study and modelling of supercapacitors," *Vehicle Engine*, no. 1, pp. 28-32, 2010.

[119] (2014, Nov 12). *SLM—Shape Language Modeling, MATLAB central file exchange*. Available: https://www.mathworks.com/matlabcentral/fileexchange/24443-slm-shape-language-modeling

[120] T. Yi, Z. Xin, Z. Liang, and Z. Xinn, "Intelligent energy management based on driving cycle identification using fuzzy neural network," in *2009 Second International Symposium on Computational Intelligence and Design*, 2009, vol. 2, pp. 501-504: IEEE.

[121] D. N. Luta and A. K. Raji, "Optimal sizing of hybrid fuel cell-supercapacitor storage system for off-grid renewable applications," *Energy*, vol. 166, pp. 530-540, 2019. doi: https://doi.org/10.1016/j.energy.2018.10.070

[122] T. Huria, M. Ceraolo, J. Gazzarri, and R. Jackey, "High fidelity electrical model with thermal dependence for characterization and simulation of high power lithium battery cells," in *2012 IEEE International Electric Vehicle Conference*, 2012, pp. 1-8.

[123] İ. A. Bayram küçük, Cetin Elmas, "Simulation of a Hybrid Compressed Air/Li-Ion Battery Energy Storage System for Electric Vehicles," in *The Third International Symposium on Innovative Technologies in Engineering and Science*, 2015. pp. 319-328.

[124] T. Markel *et al.*, "ADVISOR: a systems analysis tool for advanced vehicle modeling," *Journal of Power Sources*, vol. 110, no. 2, pp. 255-266, 2002. doi: https://doi.org/10.1016/S0378-7753(02)00189-1

[125] X. Peng, Q. Shuhai, and X. Changjun, "A New Supercapacitor and Li-ion Battery Hybrid System for Electric Vehicle in ADVISOR," *Journal of Physics: Conference Series*, 2017, vol. 806, no. 1, p. 012015. doi: https://doi.org/10.1088/1742-6596/806/1/012015

[126] L. H. Saw, Y. Ye, and A. A. O. Tay, "Electro-thermal analysis and integration issues of lithium ion battery for electric vehicles," *Applied Energy*, vol. 131, pp. 97-107, 2014. doi: https://doi.org/10.1016/j.apenergy.2014.06.016

[127] Z. Song, J. Hou, H. Hofmann, J. Li, and M. Ouyang, "Sliding-mode and Lyapunov function-based control for battery/supercapacitor hybrid energy storage system used in electric vehicles," *Energy*, vol. 122, pp. 601-612, 2017. doi: https://doi.org/10.1016/j.energy.2017.01.098

[128] Q. Zhang, W. Deng, and G. Li, "Stochastic Control of Predictive Power Management for Battery/Supercapacitor Hybrid Energy Storage Systems of Electric Vehicles," *IEEE Transactions on Industrial Informatics*, vol. 14, no. 7, pp. 3023-3030, 2018. doi: https://doi.org/10.1109/TII.2017.2766095

[129] A. Swingler and W. Dunford, "Development of a bi-directional DC/DC converter for inverter/charger applications with consideration paid to large signal operation and quasi-linear digital control," in *Power Electronics Specialists Conference*, 2002, vol. 2, pp. 961-966: IEEE.

[130] M. Carignano, V. Roda, R. Costa-Castelló, L. Valiño, A. Lozano, and F. Barreras, "Assessment of energy management in a fuel cell/battery hybrid vehicle," *IEEE access*, vol. 7, pp. 16110-16122, 2019. doi: https://doi.org/10.1109/ACCESS.2018.2889738

[131] M. Kardasz and M. Kazerani, "Systematic electric vehicle scaling for test bed simulation," in *2016 IEEE Transportation Electrification Conference and Expo*, 2016, pp. 1-6: IEEE.

[132] E. Bongermino, F. Mastrorocco, M. Tomaselli, V. G. Monopoli, and D. Naso, "Model and energy management system for a parallel hybrid electric unmanned aerial vehicle," in *2017 IEEE 26th International Symposium on Industrial Electronics*, 2017, pp. 1868-1873.

[133] O. Vynakov, E. Savolova, and A. Skrynnyk, "Modern electric cars of Tesla Motors company," *Automation of technological and business-processes*, no. 8, pp. 9-18, 2016. doi: https://doi.org/10.15673/atbp.v8i2.162

[134] J. G. Hayes and K. Davis, "Simplified electric vehicle powertrain model for range and energy consumption based on EPA coast-down parameters and test validation by Argonne National Lab data on the Nissan Leaf," in *2014 IEEE Transportation Electrification Conference and Expo*, 2014, pp. 1-6.

[135] S. L. T J Barlow, I S McCrae and PG Boulter, "A reference book of driving cycles for use in the measurement of road vehicle emissions", 2009, Available: https://trl.co.uk/reports/PPR354.

[136] Z. Song, J. Hou, S. Xu, M. Ouyang, and J. Li, "The influence of driving cycle characteristics on the integrated optimization of hybrid energy storage system for electric city buses," *Energy*, vol. 135, pp. 91-100, 2017. doi: https://doi.org/10.1016/j.energy.2017.06.096

[137] J. Ruan, P. D. Walker, N. Zhang, and J. Wu, "An investigation of hybrid energy storage system in multi-speed electric vehicle," *Energy*, vol. 140, pp. 291-306, 2017. doi: https://doi.org/10.1016/j.energy.2017.08.119

[138] L. Piris-Botalla, G. G. Oggier, A. M. Airabella, and G. O. García, "Power losses evaluation of a bidirectional three-port DC–DC converter for hybrid electric system," *International Journal of Electrical Power & Energy Systems*, vol. 58, pp. 1-8, 2014. doi: https://doi.org/10.1016/j.ijepes.2013.12.021

[139] V. Johnson, "Battery performance models in ADVISOR," *Journal of power sources*, vol. 110, no. 2, pp. 321-329, 2002. doi: https://doi.org/10.1016/S0378-7753(02)00194-5

[140] (2018, Oct 11). *EV Model Issues when switch to front-wheel drive*. Available: https://sourceforge.net/p/adv-vehicle-sim/tickets/41/

[141] G. Chen, L. Wu, and L. Wu, "Redevelopment of ADVISOR for Design and Simulation of Plug-in Hybrid Electric Vehicle," in *2015 AASRI International Conference on Circuits and Systems*, 2015.

[142] S. Nejad, D. T. Gladwin, and D. A. Stone, "A hybrid battery parameter identification concept for lithium-ion energy storage applications," in *42nd Annual Conference of the IEEE Industrial Electronics Society*, 2016, pp. 1980-1985.

[143] D. H. Doughty and C. C. Crafts, "Freedom CAR: electrical energy storage system abuse test manual for electric and hybrid electric vehicle applications," Available: https://core.ac.uk/download/pdf/207830229.pdf, Accessed on: Oct 18, 2018.

[144] (2019, 23 Nov). *Efest IMR18650 3500mAh 20A flat top battery*. Available: http://www.efestpower.com/index.php?ac=article&at=read&did=543

[145] Maxwell Technologies, "DATASHEET OF 2.7V 3400F ULTRACAPACITOR CELL" , 2018, Available: https://www.maxwell.com/images/documents/3V_3400F_datasheet.pdf, Accessed on: Oct 26, 2018.

[146] D. Wang, Y. Bao, and J. Shi, "Online Lithium-Ion Battery Internal Resistance Measurement Application in State-of-Charge Estimation Using the Extended Kalman Filter," *Energies*, vol. 10, no. 9, p. 1284, 2017. doi: https://doi.org/10.3390/en10091284

[147] S. Kamalisiahroudi, J. Huang, Z. Li, and J. Zhang, "Study of temperature difference and current distribution in parallel-connected cells at low temperature," *Int. J. Electr. Comput. Energ. Electron. Commun. Eng*, vol. 8, no. 10, pp. 1471-1474, 2014. doi: https://doi.org/10.5281/zenodo.1096459

[148] T. Zhu *et al.*, "An Optimized Energy Management Strategy for Preheating Vehicle-Mounted Li-ion Batteries at Subzero Temperatures," *Energies*, vol. 10, no. 2, p. 243, 2017. doi: https://doi.org/10.3390/en10020243

[149] A.-A. Mamun, Z. Liu, D. M. Rizzo, and S. Onori, "An integrated design and control optimization framework for hybrid military vehicle using lithium-ion battery and supercapacitor as energy storage devices," *IEEE Transactions on Transportation Electrification*, vol. 5, no. 1, pp. 239-251, 2018. doi: https://doi.org/10.1109/TTE.2018.2869038

[150] R. Wang and S. M. Lukic, "Review of driving conditions prediction and driving style recognition based control algorithms for hybrid electric vehicles," in *2011 IEEE Vehicle Power and Propulsion Conference*, 2011, pp. 1-7: IEEE.

[151] M. Montazeri-Gh, A. Ahmadi, and M. Asadi, "Driving condition recognition for genetic-fuzzy HEV control," in *3rd International Workshop on Genetic and Evolving Systems*, 2008, pp. 65-70: IEEE.

[152] Z. Song, H. Hofmann, J. Li, X. Han, X. Zhang, and M. Ouyang, "A comparison study of different semi-active hybrid energy storage system topologies for electric vehicles," *Journal of Power Sources*, vol. 274, pp. 400-411, 2015. doi: https://doi.org/10.1016/j.jpowsour.2014.10.061

[153] T. Zhu, R. Lot, R. G. A. Wills, and X. Yan, "Sizing a battery-supercapacitor energy storage system with battery degradation consideration for high-performance electric vehicles," *Energy*, vol. 208, p. 118336, 2020. doi: https://doi.org/10.1016/j.energy.2020.118336

[154] H. Min, C. Lai, Y. Yu, T. Zhu, and C. Zhang, "Comparison Study of Two Semi-Active Hybrid Energy Storage Systems for Hybrid Electric Vehicle Applications and Their Experimental Validation," *Energies*, vol. 10, no. 3, p. 279, 2017. doi: https://doi.org/10.3390/en10030279

[155] Z. Yuan, L. Teng, S. Fengchun, and H. Peng, "Comparative Study of Dynamic Programming and Pontryagin's Minimum Principle on Energy Management for a Parallel Hybrid Electric Vehicle," *Energies*, vol. 6, no. 4, p. 2305, 2013. doi: https://doi.org/10.3390/en6042305

[156] X. Li, L. Han, H. Liu, W. Wang, and C. Xiang, "Real-time optimal energy management strategy for a dual-mode power-split hybrid electric vehicle based on an explicit model predictive control algorithm," *Energy*, vol. 172, pp. 1161-1178, 2019. doi: https://doi.org/10.1016/j.energy.2019.01.052

[157] X. Huang, Y. Tan, and X. He, "An intelligent multifeature statistical approach for the discrimination of driving conditions of a hybrid electric vehicle," *IEEE Transactions on Intelligent Transportation Systems*, vol. 12, no. 2, pp. 453-465, 2010. doi: https://doi.org/10.1109/TITS.2010.2093129

[158] C.-C. Lin, S. Jeon, H. Peng, and J. Moo Lee, "Driving pattern recognition for control of hybrid electric trucks," *Vehicle System Dynamics*, vol. 42, no. 1-2, pp. 41-58, 2004. doi: https://doi.org/10.1080/00423110412331291553

[159] S. Attaway, *Matlab: a practical introduction to programming and problem solving*. Butterworth-Heinemann, 2013. ISBN: 0124058930

[160] Z. Song, J. Hou, H. F. Hofmann, X. Lin, and J. Sun, "Parameter identification and maximum power estimation of battery/supercapacitor hybrid energy storage system based on Cramer–Rao bound analysis," *IEEE Transactions on Power Electronics*, vol. 34, no. 5, pp. 4831-4843, 2018. doi: https://doi.org/10.1109/TPEL.2018.2859317

[161] T. Zhu, R. Lot, and R. G. Wills, "Optimization of Dual Energy Storage System for High-Performance Electric Vehicles," in *2018 IEEE Vehicle Power and Propulsion Conference*, 2018, pp. 1-6: IEEE.

[162] Z. Song, J. Hou, H. Hofmann, X. Lin, and J. Sun, "Parameter identification and maximum power estimation of battery/supercapacitor hybrid energy storage system based on Cramer-Rao bound analysis," *IEEE Transactions on Power Electronics*, vol. 34, no. 5, pp. 4831-4843, 2018. doi: https://doi.org/10.1109/TPEL.2018.2859317

[163] B. Kantharaj, S. Garvey, and A. Pimm, "Compressed air energy storage with liquid air capacity extension," *Applied Energy*, vol. 157, pp. 152-164, 2015. doi: https://doi.org/10.1016/j.apenergy.2015.07.076

[164] H. Yu, D. Tarsitano, X. Hu, and F. Cheli, "Real time energy management strategy for a fast charging electric urban bus powered by hybrid energy storage system," *Energy*, vol. 112, pp. 322-331, 2016. doi: https://doi.org/10.1016/j.energy.2016.06.084

[165] X. Yan, J. Fleming, C. Allison, and R. Lot, "Portable Automobile Data Acquisition Module (ADAM) for naturalistic driving study," in *15th European Automotive Congress*, 2017.

[166] X. Huang, Y. Tan, and X. He, "An intelligent multifeature statistical approach for the discrimination of driving conditions of a hybrid electric vehicle," *IEEE Transactions on Intelligent Transportation Systems*, vol. 12, no. 2, pp. 453-465, 2011. doi: https://doi.org/10.1109/TITS.2010.2093129

[167] Q. Xu, J. Xiao, X. Hu, P. Wang, and M. Y. Lee, "A Decentralized Power Management Strategy for Hybrid Energy Storage System With Autonomous Bus Voltage Restoration and State-of-Charge Recovery," *IEEE Transactions on Industrial Electronics*, vol. 64, no. 9, pp. 7098-7108, 2017. doi: https://doi.org/10.1109/TIE.2017.2686303

[168] Y. Ma, H. Lin, Z. Wang, and T. Wang, "Capacitor voltage balancing control of modular multilevel converters with energy storage system by using carrier phase-shifted modulation," in *2017 IEEE Applied Power Electronics Conference and Exposition*, 2017, pp. 1821-1828.

[169] Y. Zhang, X.-F. Cheng, C. Yin, and S. Cheng, "A Soft-switching Bidirectional DC-DC Converter for the Battery Super-capacitor Hybrid Energy Storage System," *IEEE Transactions on Industrial Electronics*, vol. 65, no. 10, pp. 7856 - 7865, 2018. doi: https://doi.org/10.1109/TIE.2018.2798608

[170] V. Lystianingrum, V. G. Agelidis, and B. Hredzak, "State of health and life estimation methods for supercapacitors," in *2013 Australasian Universities Power Engineering Conference*, 2013, pp. 1-7: IEEE.

[171] E. Borgonovo, S. Gatti, and L. Peccati, "What drives value creation in investment projects? An application of sensitivity analysis to project finance transactions," *European Journal of Operational Research*, vol. 205, no. 1, pp. 227-236, 2010. doi: https://doi.org/10.1016/j.ejor.2009.12.006

[172] T. Liu, H. Yu, H. Guo, Y. Qin, and Y. Zou, "Online Energy Management for Multimode Plug-in Hybrid Electric Vehicles," *IEEE Transactions on Industrial Informatics*, vol. 15, no. 7, pp. 4352 - 4361, 2019. doi: https://doi.org/10.1109/TII.2018.2880897

[173] A. Ostadi and M. Kazerani, "A comparative analysis of optimal sizing of battery-only, ultracapacitor-only, and battery–ultracapacitor hybrid energy storage systems for a city bus," *IEEE Transactions on Vehicular Technology*, vol. 64, no. 10, pp. 4449-4460, 2014. doi: https://doi.org/10.1109/TVT.2014.2371912

[174] B. Smith, R. Wills, and A. Cruden, "Aqueous Al-ion cells and supercapacitors—A comparison," *Energy Reports*, vol. 6, pp. 166-173, 2020. doi: https://doi.org/10.1016/j.egyr.2020.03.021

[175] R. Mckerracher, A. Holland, A. Cruden, and R. Wills, "Comparison of carbon materials as cathodes for the aluminium-ion battery," *Carbon*, vol. 144, pp. 333-341, 2019. doi: https://doi.org/10.1016/j.carbon.2018.12.021

[176] A. Holland, A. Cruden, A. Zerey, A. Hector, and R. Wills, "Electrochemical study of TiO2 in aqueous AlCl3 electrolyte via vacuum impregnation for superior high-rate electrode performance," *BMC Energy*, vol. 1, no. 1, pp. 1-7, 2019. doi: https://doi.org/10.1186/s42500-019-0010-9

[177] L. A.-W. Ellingsen *et al.*, "Environmental screening of electrode materials for a rechargeable aluminum battery with an AlCl3/EMIMCl electrolyte," *Materials*, vol. 11, no. 6, p. 936, 2018. doi: https://doi.org/10.3390/ma11060936

[178] A. W. Holland, R. McKerracher, A. Cruden, and R. G. A. Wills, "TiO2 nanopowder as a high rate, long cycle life electrode in aqueous aluminium electrolyte," *Materials Today Energy*, vol. 10, pp. 208-213, 2018. doi: https://doi.org/10.1016/j.mtener.2018.09.009

[179] A. Holland, R. McKerracher, A. Cruden, and R. Wills, "Electrochemically Treated TiO2 for Enhanced Performance in Aqueous Al-Ion Batteries," *Materials*, vol. 11, no. 11, p. 2090, 2018. doi: https://doi.org/10.3390/ma11112090

[180] A. Holland, H. Kimpton, A. Cruden, and R. Wills, "CuHCF as an electrode material in an aqueous dual-ion Al3+/K+ ion battery," *Energy Procedia*, vol. 151, pp. 69-73, 2018. doi: https://doi.org/10.1016/j.egypro.2018.09.029

[181] R. D. McKerracher, A. Holland, A. Cruden, and R. G. A. Wills, "Comparison of carbon materials as cathodes for the aluminium-ion battery," *Carbon*, vol. 144, pp. 333-341, 2019. doi: https://doi.org/10.1016/j.carbon.2018.12.021

[182] A. W. Holland, A. Cruden, A. Zerey, A. Hector, and R. G. A. Wills, "Electrochemical study of TiO2 in aqueous AlCl3 electrolyte via vacuum impregnation for superior high-rate electrode performance," *BMC Energy*, vol. 1, no. 1, p. 10, 2019. doi: https://doi.org/10.1186/s42500-019-0010-9

[183] L. A.-W. Ellingsen *et al.*, "Environmental Screening of Electrode Materials for a Rechargeable Aluminum Battery with an AlCl3/EMIMCl Electrolyte," *Materials*, vol. 11, no. 6, p. 936, 2018. doi: https://doi.org/10.1016/j.mtener.2018.09.009

[184] Maxwell Technologies, "Datasheet of 2.7V 3400F Ultracapacitor Cell", Available: https://www.maxwell.com/images/documents/3V_3400F_datasheet.pdf, Accessed on: Oct 26, 2018.